Functional consequences of RyR1 variants

A thesis presented in partial fulfilment of the requirements for the degree of

Doctor of Philosophy

in

Biochemistry

at Massey University, Manawatū, New Zealand.

Remai Parker

2019

Abstract

Malignant hyperthermia (MH) is an uncommon pharmacogenetic disorder that is asymptomatic until triggered by volatile anaesthetics or depolarising muscle relaxants. Exposure to such a trigger can result in a potentially fatal hypermetabolic crisis in an MH-susceptible individual. With prior diagnosis, MH episodes can be avoided by using alternative anaesthesia. Diagnostic testing requires a morbidly invasive muscle biopsy for those considered at risk based on family history. Linkage of MH-susceptibility to variants in the skeletal muscle calcium release channel ryanodine receptor 1 (RyR1) has provided an opportunity for DNA testing as an alternative to the muscle biopsy. DNA-based diagnosis is severely limited by the number of diagnostic mutations identified—only 50 mutations have been established as MH-causative from over 300 genetic variants associated with the disorder. Moreover, DNA testing may only diagnose an individual as MH-susceptible; a negative DNA test is insufficient under current guidelines for a negative MH diagnosis. The purpose of this study was to develop molecular tools to investigate the hypothesis that RyR1 variants associated with MH-susceptibility cause dysregulation of calcium release from intracellular stores. Two experimental approaches were followed with the objective of expanding the capabilities of DNA-based diagnosis for MH. The first technique was the generation of mammalian cell lines stably expressing recombinant RyR1 variants by use of the Flp-In™ T-REx™ system from Invitrogen, followed by functional analysis. Four of five genetic variants associated with MH or myopathy had altered sensitivities to an RyR1 agonist and therefore meet the criteria for use as diagnostic variants for MH-susceptibility. The second molecular technique explored was gene editing, with the aim of showing that a single nucleotide change was both necessary and sufficient to cause MH-susceptibility. This was developed by introducing a well-characterised MH-causative variant into the genome of a human skeletal muscle cell line. Preliminary results indicated that gene editing was successful.

Acknowledgements

Firstly, I would like to express my sincere gratitude to Prof. Kathryn Stowell for her continuous support, motivation, and immense knowledge. The door to Kathryn's office was always open whenever I had a question about my studies or encountered an issue in the lab. She consistently allowed this research to be my own work, but also steered me in the right the direction when I asked for guidance. Kathryn's patience during the writing of this thesis was endless, and I could not have imagined having a better advisor for my PhD research.

I would like to express my special appreciation and thanks to my co-supervisor, Dr. Anja Schiemann, for her insightful comments and encouragement, but also for the hard questions that ensured this research was of a high calibre. She has been a tremendous mentor for me, allowing me to grow as an independent researcher.

Besides my supervisors, I would like to acknowledge the biomedical research group for their social attitude to science, and most importantly, my officemates Jeremy, Sam, Sean, Sophie, and Shannon for the fun we had between experiments.

My sincere thanks go to The Duncan Trust for the Sir Thomas and Lady Duncan Scholarship in Neuromuscular Research, the Institute of Fundamental Sciences for their financial support, and the New Zealand Society for Biochemistry and Molecular Biology and the Claude McCarthy Fellowship for travel funding.

I would like to acknowledge my friend Johanna Poole for her valuable comments that greatly improved this thesis. My thanks also to Dr. Anja Schiemann and Jeremy Stephens for providing the full-length *RYR1* constructs for this research.

Finally, I must thank my parents, my sisters and their growing families, and my partner Joshua. You all provided me with unfailing encouragement throughout my years of study and through the process of researching and writing this thesis. It would not have been possible without your support.

Table of Contents

List of Figures

List of Tables

List of Abbreviations

4-c*m*c	4-chloro-*m*-cresol
APS	ammonium persulfate
ATP	adenosine triphosphate
BSA	bovine serum albumin
BSS	buffered salt solution
C-terminal	carboxyl-terminal
CACNA1S	gene for the DHPR α1 subunit
CACNB1	gene for the DHPR β subunit
CaM	calmodulin
Cas9	CRISPR-associated protein 9
Casq1	skeletal muscle calsequestrin isoform
Casq2	cardiac muscle calsequestrin isoform
CCD	central core disease
cDNA	complementary DNA
CMV	Cytomegalovirus
CPVT	catecholaminergic polymorphic ventricular tachycardia
CRISPR	clustered regularly interspaced short palindromic repeats
DAPI	4',6-diamidino-2-phenylindole
DHPR	dihydropyridine receptor
DMEM	Dulbecco's Modified Eagle's Medium
DNA	deoxyribonucleic acid
DSB	double-strand break
E. coli	Escherichia coli

EC	excitation-contraction
EC_{50}	half maximal effective concentration
EDTA	ethylenediaminetetraacetic acid
EHI	exertional heat illness
EIR	exercise-induced rhabdomyolysis
ER	endoplasmic reticulum
EVS	Exome Variant Server
ExAC	Exome Aggregation Consortium
FBS	foetal bovine serum
FATHMM	Functional Analysis Through Hidden Markov Models
FITC	fluorescein isothiocyanate
FKBP12	FK506-binding protein 12
Flp	flippase
FRT	flippase recombination target
FT-293	Flp-In™ T-REx™ 293 cell line
gDNA	genomic DNA
gRNA	guide RNA
GFP	green fluorescent protein
HDR	homology-directed repair
HEK-293	human embryonic kidney 293
HEK-293T	HEK-293 with the SV40 large T-antigen
HMCL-7304	human myoblast cell line 7304
HRC	histidine-rich Ca^{2+} binding protein
HRM	high resolution amplicon melting
indel	insertion or deletion

IVCT	*in vitro* contracture test
JSRP1	junctional sarcoplasmic reticulum protein 1
kb	kilobase
LB	Luria Bertani
MAF	minor allele frequency
MCS	multiple cloning site
MH	malignant hyperthermia
MHN	malignant hyperthermia negative diagnosis
MHS	malignant hyperthermia susceptible diagnosis
N-terminal	amino-terminal
NEB	New England Biolabs
NHEJ	non-homologous end-joining
NTC	no template control
PAM	protospacer-adjacent motif
PBS	phosphate-buffered saline
PCR	polymerase chain reaction
PDI	protein disulphide isomerase
PROVEAN	Protein Variant Effect Analyser
PVDF	polyvinylidene difluoride
RNA	ribonucleic acid
RT	room temperature
RT-qPCR	quantitative reverse transcription PCR
RYR1	ryanodine receptor 1 gene
RyR1	ryanodine receptor 1 protein
RyR2	ryanodine receptor 2 protein

RyR3	ryanodine receptor 3 protein
S100A1	S100 Ca^{2+} binding protein A1
SDS	sodium dodecyl sulfate
SDS-PAGE	SDS polyacrylamide gel electrophoresis
SEM	standard error of the mean
SERCA	sarco/endoplasmic reticulum Ca^{2+} ATPase
SOCE	store-operated Ca^{2+} entry
SOICR	store overload-induced Ca^{2+} release
SpCas9	Cas9 derived from *Streptococcus pyogenes*
SR	sarcoplasmic reticulum
Stac3	SH3 and cysteine-rich domain 3
Stim1	stromal interaction molecule 1
T7E1	T7 Endonuclease I
TAE	tris-acetate-EDTA
TALEN	transcription activator-like effector nuclease
TBE	tris-borate-EDTA
TBST	tris-buffered saline with Tween 20
TEMED	tetramethylethylenediamine
TRITC	tetramethylrhodamine isothiocyanate
t-tubule	transverse tubule
WT	wild type
ZFN	zinc finger nuclease

1 Introduction

1.1 Malignant hyperthermia

1.1.1 Manifestation

Malignant hyperthermia (MH) is a life-threatening pharmacogenetic disorder that is clinically asymptomatic in susceptible individuals until exposure to potent volatile anaesthetics or the depolarising muscle relaxant succinylcholine—either alone or in combination.[1] An MH crisis can develop rapidly with a wide variety of clinical symptoms including increased end-tidal carbon dioxide, elevated core body temperature, tachycardia, increased oxygen consumption, rigid muscles, metabolic acidosis, and rhabdomyolysis.[2,3] A potentially fatal crisis may occur immediately upon administration of the triggering agent or in the period following. If not identified and treated quickly, MH may cause widespread organ failure and cardiac arrest.

An MH episode is caused by the action of a hyperactive calcium (Ca^{2+}) channel in the sarcoplasmic reticulum (SR), the primary Ca^{2+} storage organelle in skeletal muscle. During an MH crisis, the hyperactive channel, ryanodine receptor 1 (RyR1), inappropriately releases a large volume of Ca^{2+} into the cytosol, causing the sustained and uncontrolled contraction of skeletal muscles and other hypermetabolic effects. A fulminant crisis can be treated by the immediate removal of triggering agents, lowering the core body temperature, and the intravenous administration of dantrolene. Dantrolene is a skeletal muscle relaxant that reduces the Ca^{2+} release from the SR. Although the exact mechanism remains unclear, it has been suggested that dantrolene binds RyR1 in the cytoplasm, greatly enhancing the inhibitory effect of magnesium ions (Mg^{2+}) on RyR1.[4,5] Since its introduction in 1979, dantrolene has reduced the worldwide MH mortality rate from 80% to below 5%, in combination with improved patient monitoring.[6-8] Dantrolene remains the only treatment for MH and, although it has been largely successful, approximately a third of patients that survive an MH reaction may suffer considerable morbidity.[9] Although no long-term effects from short-term exposure to dantrolene have been observed, treatment for longer than one month can cause serious liver damage.[10,11] As a consequence, the prevention of fulminant MH events through complete avoidance of triggering agents is the only sustainable option for those suspected to be MH-susceptible.

1.1.2 Diagnosis

A standard grading system of clinical signs is used to determine the probability of an event being an MH crisis; this is to reduce the likelihood of misdiagnosis.[12] Because of its variable expressivity, symptoms of MH can be vague, inconsistent, and often similar to those observed from common complications of anaesthesia and surgery.[13] The diagnosis of MH-susceptibility by histopathological examination is not feasible because there are no observable differences between the muscle tissue of MH-susceptible individuals and normal individuals.[14] Definitive diagnosis of MH-susceptibility requires testing of a muscle biopsy specimen in a procedure known as the *in vitro* contracture test (IVCT).[15] In this procedure, the force exerted by an electrically stimulated muscle strip is measured in the presence of incremental doses of two agonists, caffeine and halothane, applied individually. An abnormal result is judged to be sustained contracture with concentrations of caffeine or halothane below the thresholds of 2.0 mmol L^{-1} and 0.44 mmol L^{-1}, respectively.[16] A patient with normal results for both drugs is characterised as MH-negative (MHN) whereas a patient with an abnormal result is MH-susceptible (MHS). Within the MHS group, laboratory classifications of MHS_h, MHS_c, and MHS_{hc} are given to patients with an abnormal response respectively to halothane, caffeine, or both drugs.[16] The IVCT is the gold-standard presently as it has a reported 99% sensitivity and 94% specificity.[15] However, in addition to being an expensive and invasive form of diagnosis, the IVCT has been found to produce both false-positive and false-negative results.[17] Although all false results are problematic, a false-negative diagnosis can be fatal.

Susceptibility to MH is inherited in an autosomal dominant manner with high genetic heterogeneity. Six genomic *loci* have thus far been identified as potentially associated with MH-susceptibility, although this list is not exhaustive: MHS1 (19q13.1), MHS2 (17q11.2–q24), MHS3 (7q21–q22), MHS4 (3q13.1), MHS5 (1q32), and MHS6 (5p).[18-22] An estimated 70% of MH-susceptibility cases arise from variants at *locus* MHS1 in *RYR1*, the gene encoding RyR1.[23] Up to 1% of MH-susceptibility cases have been linked to variants at *locus* MHS5 in *CACNA1S*, the gene for the α1 subunit of the dihydropyridine receptor (DHPR), the skeletal muscle voltage sensor.[23] A novel variant associated with MH-susceptibility was identified at *locus* MHS2 in *CACNB1*, the gene for the DHPR β subunit.[24] Functional assessment of

this *CACNB1* variant indicated that it may affect Ca^{2+} handling, although it is unlikely to independently cause MH-susceptibility.

A small number of individuals with mutations in the *STAC3* gene encoding the SH3 and cysteine-rich domain 3 (Stac3) protein have experienced adverse reactions to anaesthesia.[25] These are suspected to be MH-susceptible, although no instances have been confirmed by IVCT. It was recently reported that two mutations in the gene encoding the transient receptor potential vanilloid 1 channel in the SR were identified in two patients that were diagnosed as MHS_h by IVCT.[26] The authors found those mutations to alter the activity of that channel in the presence of the volatile anaesthetic isoflurane in mouse muscle fibres and indicated a link to MH, but this result is as yet unconfirmed. The genetic cause of up to 30% of patients diagnosed with MH-susceptibility remains undetermined.

1.1.3 Epidemiology

MH is thought to be an uncommon disease with estimations of incidence in the population ranging widely from 1 in 2,000 to 1 in 250,000 individuals.[27,28] This discrepancy is because of the incomplete penetrance of the disease; it is common for those diagnosed as MH-susceptible to have had previous exposures to triggering agents without incident.[29] It has been estimated that on average one out of every three anaesthetics may trigger a crisis in someone with MH-susceptibility.[30]

MH-susceptibility was first described in an Australian family with ten deaths attributed to the use of general anaesthetics in surgery.[31] Since then, it has been found in numerous families throughout the world and several species of animal such as cats, pigs, horses, and dogs.[32,33] The fulminant MH phenotype in pigs, porcine stress syndrome, has many similarities to that observed in humans and has therefore contributed to the research into causes and possible treatments of MH. Like MH in humans, porcine stress syndrome is caused by a point variant in *RYR1*. It differs slightly in its manifestation, however, because it is inherited in an autosomal recessive manner and is susceptible to be triggered by stress.[34,35]

1.2 Calcium homeostasis in skeletal muscle

1.2.1 Skeletal muscle organisation

Skeletal muscle is a form of striated muscle and comprises long, cylindrical cells known as muscle fibres bundled together by collagen and attached to the nervous system through a network of motor neurons. Fibres are large and multinucleated because they form after the fusion and development of several immature myoblast cells. Each fibre has a vast network of membrane invaginations known as transverse tubules (t-tubules) in which DHPR channels reside across the sarcolemma (Figure 1.1).[36]

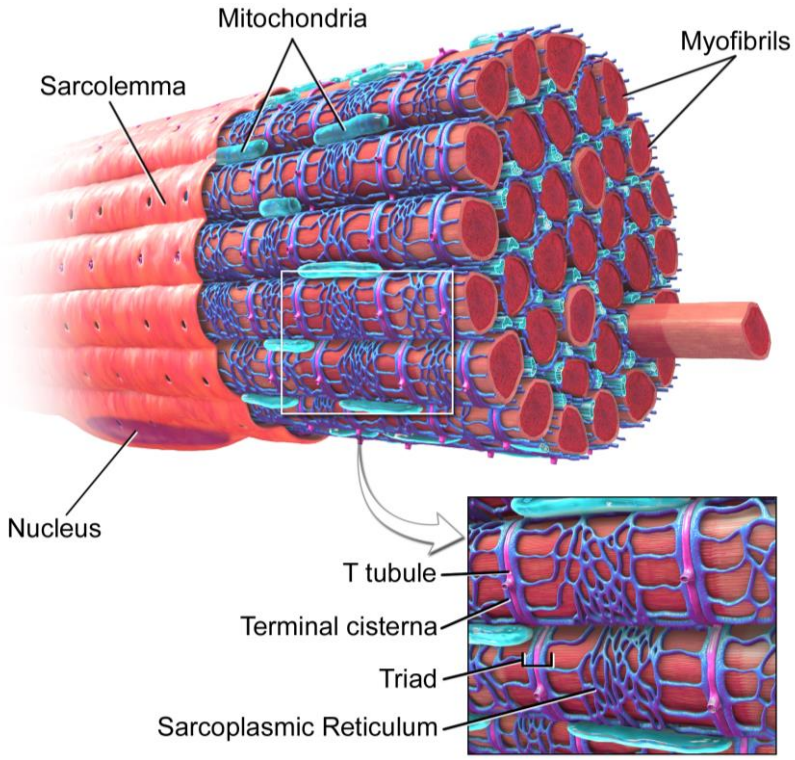

Figure 1.1 Fibre organisation in skeletal muscle

Three-dimensional rendering of the major structures in a single skeletal muscle fibre. Surrounding the myofibrils (red) is the sarcoplasmic reticulum network (dark blue) which associates with the transverse (T) tubule system (pink). Also shown are mitochondria in light blue, a nucleus in purple, and the main body of the plasma membrane, the sarcolemma (light red*). Image reproduced with permission from the rightsholder, Blausen Medical.*[37]

In the cytosol, DHPR channels physically interact with RyR1 channels located across the SR membrane. RyR1 channels reside in enlarged regions of the SR known as terminal cisternae and these surround the t-tubules to make large amounts of Ca^{2+} available for release (Figure 1.1). The SR maintains low cytosolic Ca^{2+} concentrations (approximately 50 nM at rest) and surrounds bundles of myofilaments known as myofibrils.[38] Clustered around the SR are mitochondria which are present in varying numbers, depending on fibre type.[39] Mitochondria have been implicated in the upregulation of dehydrogenases in skeletal muscle to fine-tune the ATP supply of the cell in response to energy requirements, such as that during muscle contraction.[40-42] These organelles are known to act as a buffer, taking up free Ca^{2+} at particular locations in the cytoplasm to prevent their diffusion through the cell and the subsequent inhibition of extracellular Ca^{2+} entry.[43,44]

The buffering capacity of mitochondria has an important function in muscle fibre performance. For example, the muscle fibres of mice with the neuromuscular disorder amyotrophic lateral sclerosis have reduced mitochondrial Ca^{2+} uptake, resulting in a large and uncontrolled increase in cytoplasmic Ca^{2+} levels.[45] Type I—or 'slow-twitch'—fibres have a high mitochondrial content because they rely on aerobic respiration for slow contraction that is resistant to fatigue.[46] Type II—or 'fast-twitch'—fibres have a smaller mitochondrial content because they use anaerobic respiration for rapid contraction, and thus are easily fatigued.[46] The composition of the muscle fibre is not believed to influence the MH phenotype because distinct muscle groups, comprising either mostly type 1 or mostly type 2 fibres, have no difference in the opening of RyR1 in the porcine MH model.[47]

1.2.2 Calcium as a second messenger

Although the specific physiological cause of MH-susceptibility is unknown, it is theorised that one or more genetic abnormalities result in altered Ca^{2+} homeostasis in skeletal muscle. Ca^{2+} transport is a potent cellular signal that has a vital function as a second messenger in several cellular functions. The movement of free Ca^{2+} participates in a broad spectrum of processes and therefore its transmission is both tightly regulated and tissue specific. Elevated cytoplasmic Ca^{2+} levels signal for the ATP supply to increase by indirectly increasing the enzymatic rates in glycolysis, the citric acid cycle, and the electron transport

chain. Changes in Ca^{2+} homeostasis also modify the rate of protein synthesis in the cell; for example, it can cause muscle fibre type shifting through altered gene expression.[48] The composition of fibres in skeletal muscle governs how that muscle functions, so fibre type switching allows the body to adapt to environmental cues. Its most notable role in skeletal muscle is the strict control of muscle contraction and relaxation through a process known as excitation-contraction (EC) coupling—in which the excitation of a somatic motor neuron is coupled to the contraction of a skeletal muscle fibre.

1.2.3 Excitation-contraction coupling

EC coupling is initiated when a somatic motor neuron fires, releasing the skeletal muscle neurotransmitter, acetylcholine, into the synaptic cleft. Acetylcholine then diffuses across the cleft where its binding to specific receptors on the muscle surface elicits the depolarisation of the sarcolemma. An action potential is then created that is rapidly conducted through the t-tubule network and is recognised by the DHPR as a voltage signal. This causes the DHPR channels to undergo structural changes that, in turn, promote conformational changes in the RyR1 channels to which they are mechanically coupled (Figure 1.2).[49] Only half of all RyR1 channels are thought to open through direct interaction with DHPR channels; the remaining channels are simultaneously activated by adjacent RyR1 channels through cooperative gating.[50] The coordinated gating of channel clusters enables the large conductance of Ca^{2+} and likely results from physical interaction because it is independent of Ca^{2+} concentration.[51]

Opening of the RyR1 channel causes the rapid efflux of Ca^{2+} from the SR, temporarily elevating local Ca^{2+} levels around the myofibrils approximately 100-fold.[38] Ca^{2+} then binds troponin, causing the sarcomeres to shorten and therefore resulting in muscle contraction at the expense of ATP hydrolysis. Muscle relaxation is achieved by the removal of Ca^{2+} from the myofibrils, thereby depriving the troponin complex of Ca^{2+} and reversing the force generated by this interaction. Ca^{2+} localised around the myofibrils is pumped back into the SR by the sarco/endoplasmic reticulum Ca^{2+} ATPase (SERCA), another Ca^{2+} channel across the SR membrane.[52] Elevated cytoplasmic Ca^{2+} levels activate SERCA, which then replenishes the SR stores in an ATP-dependent manner both during and after

EC coupling events, eventually reducing cytosolic Ca^{2+} levels to that at rest. The increased cytoplasmic Ca^{2+} levels cause increased cellular respiration to replace the ATP consumed during both contraction and relaxation, and meet the energy needs of the cell.[53]

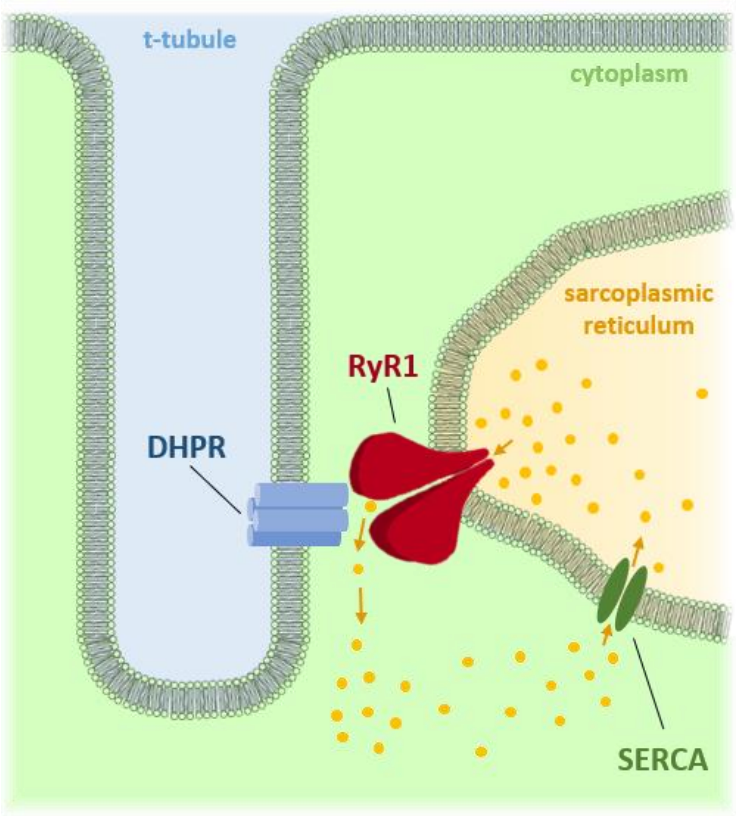

Figure 1.2 Calcium release in skeletal muscle

Dihydropyridine receptor channels (DHPR; blue) in the transverse tubules (t-tubules) physically interact with ryanodine receptor channels (RyR1; red) in the terminal cisternae of the sarcoplasmic reticulum (orange) to facilitate movement of Ca^{2+} (orange circles) through RyR1 into the cytoplasm (light green). Ca^{2+} is pumped back into the sarcoplasmic reticulum by the sarco/endoplasmic reticulum Ca^{2+} ATPase channel (SERCA; dark green). *Figure created by the Author.*

1.2.4 Extracellular calcium entry

Complementing the internal Ca^{2+} release from the SR, extracellular Ca^{2+} can enter the cell in response to different physiological changes through the action of several distinct pathways. One such pathway arises by the co-activation of DHPR and RyR1 channels with conformational changes in RyR1 leading to the movement of Ca^{2+} through the DHPR Ca^{2+}

channel.[54] Another extracellular Ca^{2+} entry pathway is store-operated Ca^{2+} entry (SOCE)—independent of the EC coupling machinery. This process does not contribute to contraction, but is essential for replenishing SR stores and preventing fatigue.[55,56] Low Ca^{2+} levels in the SR lumen are detected by the amino-terminal (N-terminal) domain of a transmembrane protein stromal interaction molecule 1 (Stim1).[57] Upon depletion of Ca^{2+} stores in the SR, three Stim1 dimers physically interact with and subsequently activate a Ca^{2+} channel in the sarcolemma, Orai1, to oligomerise.[55] This activated Orai1 channel comprises six subunits arranged around an ion-conducting pore through which extracellular Ca^{2+} may enter the cell.[58] This Ca^{2+} entry is enhanced by the action of two muscle-specific transmembrane proteins, mitsugumin23 and mitsugumin53. These proteins co-localise with Orai1 channels in the sarcolemma to activate SOCE and are critical for preventing fatigue over long periods of EC coupling.[59,60]

Another Ca^{2+} influx pathway activated by SR store depletion involves the transient receptor potential cation family of channels that reside in the sarcolemma. Although this Ca^{2+} entry is thought to be independent of Stim1 and Orai1 function, three transient receptor potential cation channels are implicated in SOCE, although the associated mechanism is unknown.[61,62] Influx of extracellular Ca^{2+} can also be caused by prolonged periods of sarcolemma depolarisation through the excitation-coupled Ca^{2+} entry pathway.[63] Excitation-coupled Ca^{2+} entry is independent of the SOCE pathway and requires the interaction of the DHPR and RyR1, although the identity of the channel concerned is unknown.[64,65]

1.2.5 Store overload-induced calcium release

Extracellular Ca^{2+} entry occurs at a near constant rate in muscle fibres to ensure adequate supply for Ca^{2+} homeostasis, most of which is subsequently pumped into the SR for storage. This movement of Ca^{2+} into the cell is then balanced by efflux which may be mediated by luminal Ca^{2+} levels monitored by RyR1.[66] When Ca^{2+} stores in the SR reach a critical level, the spontaneous release of Ca^{2+} through RyR1 occurs by store overload-induced Ca^{2+} release (SOICR).[67] The resulting Ca^{2+} oscillations usually have no downstream effect because they occur at different intervals between terminal cisternae.

However, recent evidence has revealed that certain conditions, including the exposure of MH-triggering agents, may activate SOICR inappropriately.[68,69]

1.2.5.1 Calcium dysregulation and cardiac arrhythmia

SOICR was originally associated with disease in cardiac muscle in which mutations in the cardiac ryanodine receptor (RyR2) caused an increased sensitivity of the channel to luminal Ca^{2+} levels.[70,71] It was then determined that the inappropriate Ca^{2+} release linked to the familial cardiac disease catecholaminergic polymorphic ventricular tachycardia (CPVT) was the result of a lowered threshold for SOICR.[72,73] The enhanced propensity for cardiac SOICR has been linked to mutations in both RyR2 and the cardiac SR Ca^{2+} buffering protein, calsequestrin 2 (Casq2). These connections indicate a common cause of disease—either an inability of RyR2 to tolerate luminal Ca^{2+} level increases, or a reduced Ca^{2+} buffering capacity of Casq2 in the SR. With CPVT under normal resting conditions, the lowered SOICR threshold is tolerated; however, conditions that result in greater Ca^{2+} loading, such as stress, exercise, or the introduction of catecholamines, reduce this threshold substantially (schematic in Figure 1.3).[69] Evidence showing shared characteristics between the cause of CPVT in cardiac muscle and the MH phenotype in skeletal muscle indicates a possible common cause. For example, caffeine lowers the cardiac SOICR threshold and consequently reduces luminal Ca^{2+} levels whereas RyR2 inhibition produced the opposite effect.[68,70]

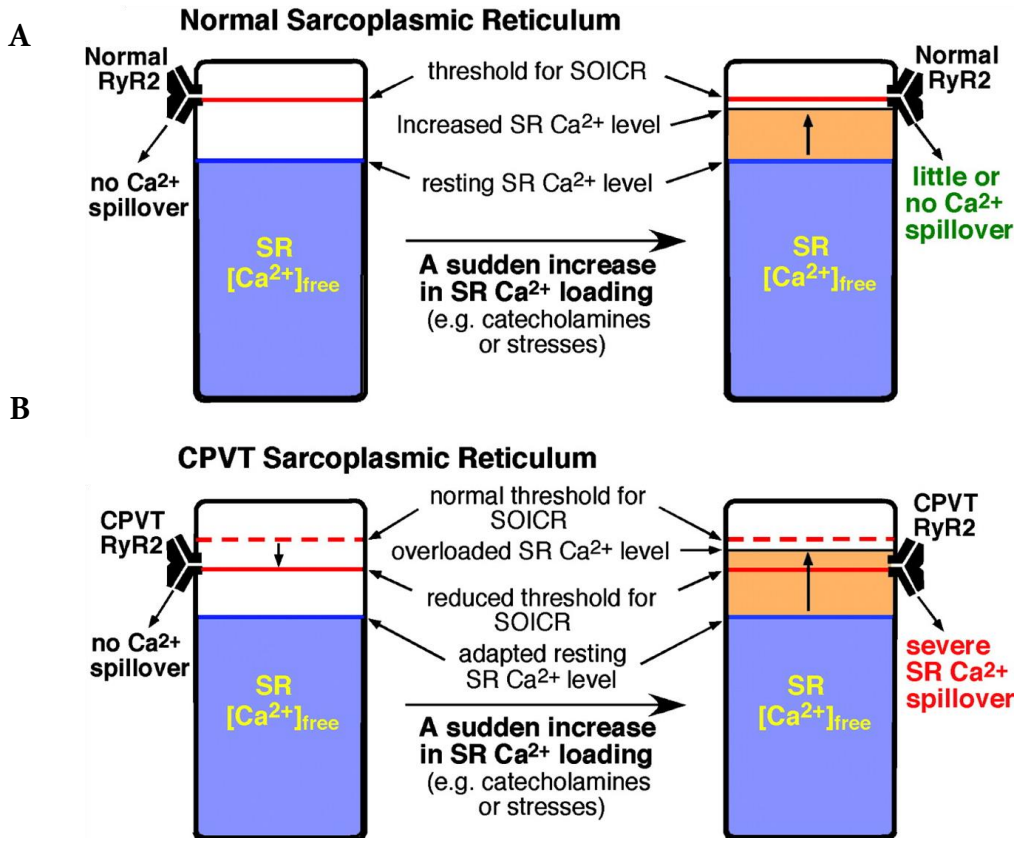

Figure 1.3 Altered response to luminal calcium in cardiac muscle

Model of store overload-induced Ca^{2+} release (SOICR) in cardiac muscle from a reduced $[Ca^{2+}]$ threshold in the sarcoplasmic reticulum (SR). **A** In normal muscle, resting luminal $[Ca^{2+}]$ (blue) is lower than the SOICR threshold. Under stress, luminal $[Ca^{2+}]$ increases (orange) but does not induce SOICR through ryanodine receptor 2 (RyR2). **B** In catecholaminergic polymorphic ventricular tachycardia (CPVT) muscle, the SOICR threshold and luminal $[Ca^{2+}]$ is lower. Under stress, $[Ca^{2+}]$ exceeds the reduced threshold and causes release of Ca^{2+} through SOICR. *Copyright 2004 National Academy of Sciences (DOI: 10.1073/pnas.0402388101).*[70]

1.2.5.2 Calcium dysregulation in skeletal muscle

SOICR was initially linked to MH-susceptibility in mice when a reduced buffering capacity of the SR caused an MH-like phenotype upon exposure to halothane or heat stress.[74,75] As with the cardiac channel, both halothane and caffeine reduce the threshold for SOICR in skeletal muscle by binding the RyR1.[76,77] It is now believed that MH-linked variants—either within *RYR1* or in the genes of other players in the EC coupling machinery—may lower

this threshold further (see schematic in Figure 1.4).[75] MH-causative variants in *RYR1* cause enhanced SOICR *in vitro*; this is increased further upon exposure to RyR1 agonists and subsequently rescued by dantrolene.[69,78]

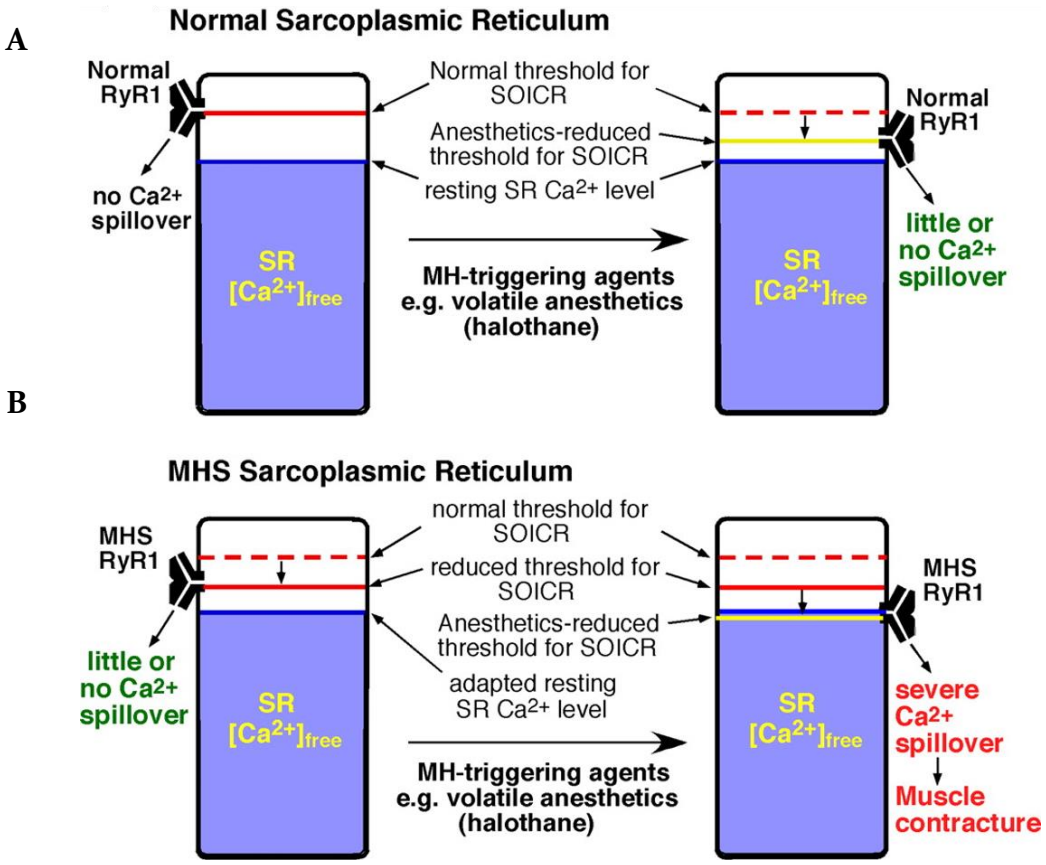

Figure 1.4 Calcium dysregulation in malignant hyperthermia

Model of inappropriate Ca^{2+} leak in skeletal muscle from a reduced $[Ca^{2+}]$ threshold in the sarcoplasmic reticulum (SR). **A** In normal muscle, resting luminal $[Ca^{2+}]$ (blue) is below the threshold (red line) for store overload-induced Ca^{2+} release (SOICR). Upon exposure to an agonist, the SOICR threshold is reduced (yellow) but causes no SOICR through ryanodine receptor 1 (RyR1). **B** In malignant hyperthermia (MH) muscle, the SOICR threshold at rest is reduced (red line). Upon exposure to a trigger, the threshold is further reduced, causing release of Ca^{2+} by SOICR. *Republished with permission of The American Society for Biochemistry and Molecular Biology, Inc.; permission conveyed through Copyright Clearance Centre, Inc. (DOI: 10.1074/jbc.M801944200).*[69]

1.3 The ryanodine receptor

The ryanodine receptor family of Ca^{2+} channels is named after ryanodine, a plant alkaloid to which the channels bind with high specificity and affinity. There are three mammalian isoforms: RyR1, found primarily in skeletal muscle; RyR2, in cardiac muscle; and RyR3, known as the brain isoform but expressed at low levels in many cell types.[79-82] The type 3 ryanodine receptor is also expressed in skeletal muscle and, although little is known about its function, it has been observed to have no noticeable effect on Ca^{2+} homeostasis in this tissue.[83,84] All three isoforms share a large amount of sequence identity and contain divergent regions that are likely related to their specialised functions.[81] In contrast to the mechanical control of RyR1 by the DHPR, the opening of RyR2 and RyR3 channels is indirectly initiated by activation of DHPR channels in a process known as Ca^{2+}-induced Ca^{2+} release. Upon activation, the DHPR produces a small local Ca^{2+} influx which subsequently binds to and activates RyR2 or RyR3.[85,86]

1.3.1 Ryanodine receptor 1 structure

RyR1 is a large homotetramer encoded by the gene *RYR1,* which consists of 106 exons and comprises 160 kilobases of DNA. The tetramer, 2.2 MDa in size, is mushroom-shaped with 80% of the protein located in the cytoplasm (Figure 1.5). The relatively small carboxyl-terminal (C-terminal) region is located in the SR lumen and spans the SR membrane. RyR1 is organised into three distinct regions: the central tower, the corona, and the peripheral domains. The central tower contains the core of the channel with three layers: N-terminal, central, and channel domains. Surrounding the central tower are domains that compose the corona and the peripheral domains that increase the surface area of the channel.[87]

The N-terminal domains from each protomer interact with each other and the central domains to surround a cytoplasmic vestibule (Figure 1.5). Several interactions within the N-terminal region combine to form a robust structure in the closed state; these are disrupted upon channel opening for which extensive conformational changes are facilitated by association with adjacent domains.[88] The central domains are vital for the transmission of allosteric signals through the tetramer because they are the only

connection between the cytoplasmic and transmembrane regions.[89] The central tower extends through the entire tetramer, forming a pore through which Ca^{2+} ions may flow (Figure 1.5).[90]

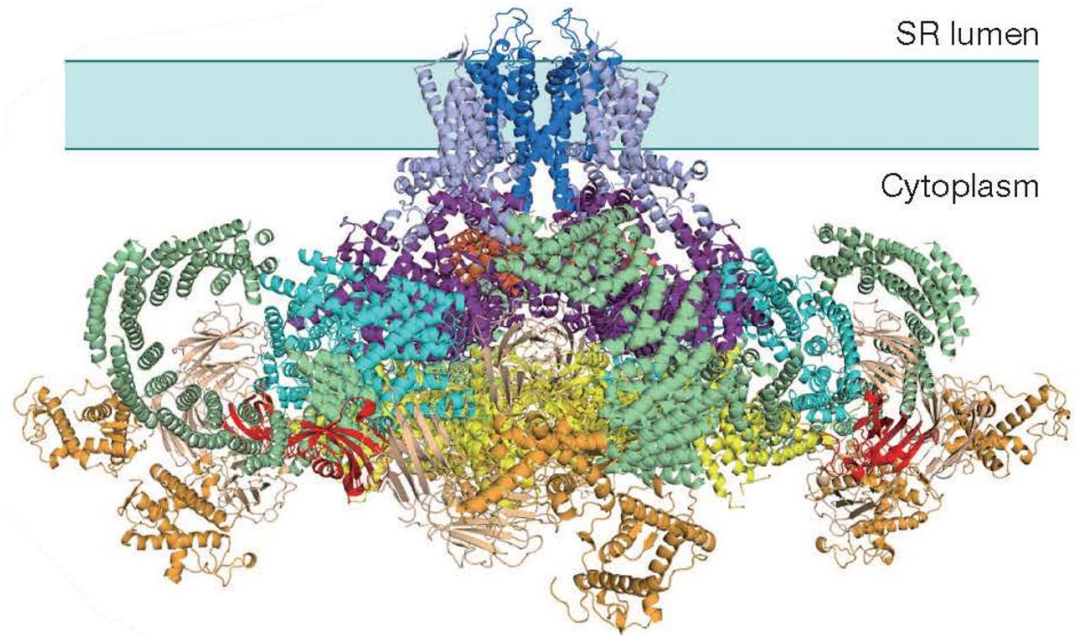

Figure 1.5 The RyR1 homotetramer

The structure of the ryanodine receptor 1 (RyR1) across the sarcoplasmic reticulum (SR) membrane, as determined by cryogenic electron microscopy in complex with the FK506 binding protein 12 (FKBP12, red). N-terminal (yellow), central (dark orange, purple), and transmembrane regions (light and dark blue) compose the central tower. The corona comprises two helical domains (green) and the handle domain (teal). Peripheral regions are shown in brown and orange. *Reprinted by permission from Macmillan Publishers Limited: Springer Nature (DOI: 10.1038/nature14063).*[87]

Six helices cross the SR membrane, with regions on either side of the membrane involved in interactions that fine-tune overall Ca^{2+} release. A large number of electronegative amino acids are found in the loops on the luminal side of the channel, indicating a role in the attraction of the positively charged Ca^{2+} ions to the entrance of the pore.[91] The selectivity filter near the luminal side has the smallest diameter throughout the pore when in an open state; this filter restricts movement to Ca^{2+} ions only.[92] Beyond the selectivity filter is the hydrophobic cavity lined by a large proportion of electronegative residues which may assist with the rapid transmission of ions to the constriction point that follows.[87] This is

located at the cytoplasmic edge of the membrane and, when RyR1 is in its closed state, the entire channel is permeable to Ca^{2+} with the exception of this constriction point.

The corona comprises two helical domains and the handle domain and is believed to be involved in several structural roles facilitating allosteric changes.[93] Its core function is the long-range transmission of signals between the peripheral domains in the cytoplasm and the central tower which contains the Ca^{2+} conducting pore. The corona also associates with DHPR channels in the cytoplasm and neighbouring RyR1 channels.[94,95]

The peripheral domains are extremely dynamic and have the most dramatic change in conformation between the open and closed states of the channel.[96] Within this region is a residue specifically targeted for phosphorylation by protein kinases; phosphorylation of this residue can strongly promote the opening of RyR1.[97,98] Also contained within these domains are sites of interdomain interactions, the binding site for the FK506-binding protein of skeletal muscle (FKBP12; red structures in Figure 1.5), and the predicted location of the mechanical association with the DHPR.[99-101] It is likely these domains are directly involved in the coupling with the DHPR in which long-range allosteric changes induce the opening of the Ca^{2+} channel.[89,102]

1.3.2 Ryanodine receptor 1 regulation

The gating of RyR1 is under the regulation of several small, diffusible molecules. The binding sites of Ca^{2+} and ATP were resolved in the interface between the central and channel domains.[103] Low levels of Ca^{2+} and high levels of ATP in the cytoplasm rearrange the structure of the channel core, placing it in a stimulated state ready for opening.[104] There are believed to be three of these high-affinity binding sites in a cluster that bind Ca^{2+} cooperatively.[93,105] During periods of high cytoplasmic Ca^{2+} levels, the binding of Ca^{2+} to two putative low-affinity sites (also in the interface between the central and channel domains) inhibits opening of the channel.[105-107] Mg^{2+} also inhibits opening of the channel by binding RyR1 in the same locations as Ca^{2+}, although with much lower affinity. Mg^{2+} augments the Ca^{2+}-dependent inhibition of RyR1 at the low-affinity binding site and competes with Ca^{2+} that activates RyR1 at the high-affinity Ca^{2+} binding site.[108-110] In

addition to the cytoplasmic regulation, high levels of Ca^{2+} in the SR may result in channel opening through binding to a low-affinity site on the luminal side of the membrane.[111,112]

The RyR-specific antagonist ryanodine binds within the transmembrane cavity on the cytoplasmic side.[113] Ryanodine binding inhibits movement of ions through the channel due to steric interference, and high levels of ryanodine block the channel completely.[114] This is believed to be why low levels of ryanodine hold the channel in an open state with reduced Ca^{2+} conductance. The other RyR1 agonists, caffeine and 4-chloro-*m*-cresol (4-c*m*c), bind the cytoplasmic portion of the C-terminal region where it may interact with the central domains to initiate robust opening of the channel.[103,115,116]

1.3.3 Ryanodine receptor 1 accessory proteins

There are numerous proteins that interact with and modulate RyR1 activity, each with specific roles in normal muscle function. The *in vitro* heterologous expression of RyR1, two DHPR subunits, Stac3, and junctophilin2, can produce a complex that is sufficient for functional EC coupling.[117] The full protein complement, however, is believed to be required for the precise regulation of skeletal muscle contraction.[118]

1.3.3.1 The dihydropyridine receptor

In the process of excitation-contraction coupling, the DHPR is the physical link between the extracellular signal and the flood of Ca^{2+} into the cell from stores. The 430 kDa channel is a heteromultimer expressed exclusively in skeletal muscle and comprises a core alpha 1 (α1) subunit in complex with four auxiliary subunits: alpha 2 (α2), beta (β), delta (δ), and gamma (γ; Figure 1.6).[119] The DHPR α1 subunit comprises six transmembrane helices that form the Ca^{2+}-conducting pore and voltage sensing domains.[120] The II–III and III–IV cytoplasmic loops (between domains 2 and 3 and domains 3 and 4, respectively) of this core subunit have strong interactions with RyR1 in the cytoplasm that are essential for EC coupling.[121,122] Upon association with RyR1, the II–III cytoplasmic loop of the DHPR α1 subunit is rearranged, allowing transmission of signals between the two channels.[123] Several mutations in the *CACNA1S* gene have been linked to MH;[124,125] only one of these,

however, is located in a region that directly interacts with RyR1—the p.Arg1086His variant (GenBank NP_000531.2) in the III–IV cytoplasmic loop of the DHPR α1 subunit.[126]

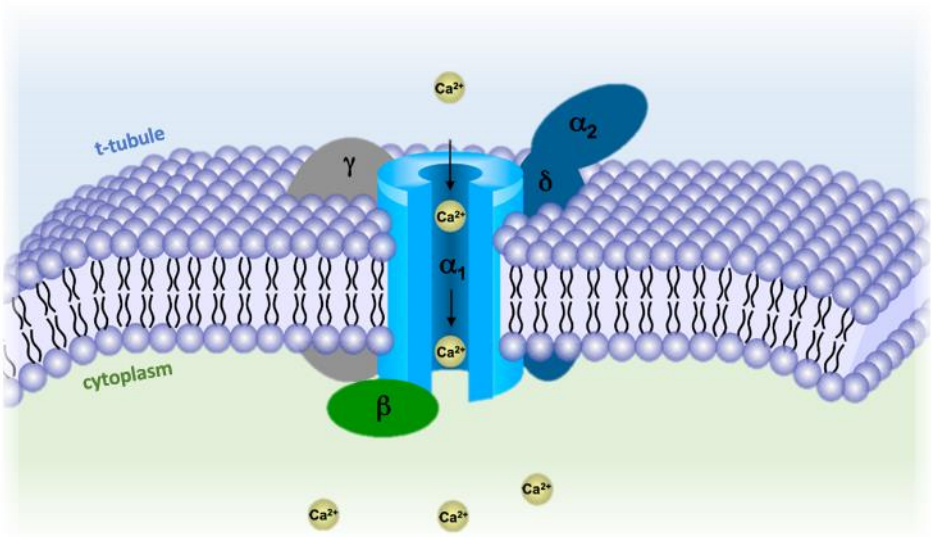

Figure 1.6 The subunits that compose the dihydropyridine receptor

Five subunits, alpha 1 (α1), alpha 2 (α2), beta (β), delta (δ), and gamma (γ), form the dihydropyridine receptor (DHPR). Three subunits—α1, δ, and γ—are located across the plasma membrane (purple) with the α1 subunit forming the Ca^{2+} conducting pore. The α2 subunit is located extracellularly whereas the β subunit is in the cytoplasm. *Image adapted under the Creative Commons licence 4.0 (DOI: 10.3390/genes8120344).*[127]

The cytoplasmic DHPR β subunit is required for the correct targeting of DHPR channels to t-tubules. Its main role, however, seems to be in the interaction between RyR1 and the α1 subunit of the DHPR.[122,128] The facilitation of this interaction by the DHPR β subunit is essential because it facilitates Ca^{2+} release from the SR. Ablation of the *CACNB1* gene in mice completely disrupts EC coupling, and a *CACNB1* variant has been implicated in MH-susceptibility, although there is insufficient evidence to date for a definitive link to MH.[129-132] The physiological functions of the other auxiliary subunits are unclear; however, the only DHPR subunit with genetic variants linked to MH-susceptibility thus far is the α1 subunit.

1.3.3.2 FK506 binding proteins

FKBP12 is a 12 kDa cytoplasmic protein that binds RyR1 at a ratio of four molecules per channel (Figure 1.7).[133] Its role is thought to be in the stabilisation of the closed state of the RyR1 tetramer and facilitation of gating of the channel.[134,135] This is posited to occur through the binding of FKBP12 at the interface between the peripheral regions and handle domains of RyR1, stabilising these dynamic regions and the central tower in the state of the closed channel.[136,137] This is corroborated by *in vitro* studies in which FKBP12 deficiency has resulted in increased RyR1 sensitivity to agonists and partial conductance states that are reversed upon reintroduction of FKBP12.[138] The cardiac muscle isoform (FKBP12.6) binds RyR2 preferentially; however, its role in the modulation of RyR1 activity is unclear because it competes for the same binding site as FKBP12 to activate the RyR1 channel *in vitro*.[135,139]

1.3.3.3 Stac3

Stac3 is a 41.5 kDa cytoplasmic protein found exclusively around the t-tubules of skeletal muscle cells. It is a requirement of functional EC coupling that has been demonstrated in both zebrafish and mouse models.[140-142] Stac3 strongly associates with the DHPR to enhance the targeting of the DHPR to t-tubules and the stability and functionality of those DHPR channels (Figure 1.7).[143-145] Its likely role in EC coupling is the facilitation of the interaction between the DHPR and RyR1 because Stac3 binds the cytoplasmic loops of DHPR required for RyR1 binding.[146] This was observed in Stac3-deficient zebrafish that had a phenotype of reduced EC coupling. The direct activation of RyR1 by the RyR-agonist 4-chloro-*m*-cresol, bypassing the DHPR-mediated activation, rescued the loss of contraction observed.[147]

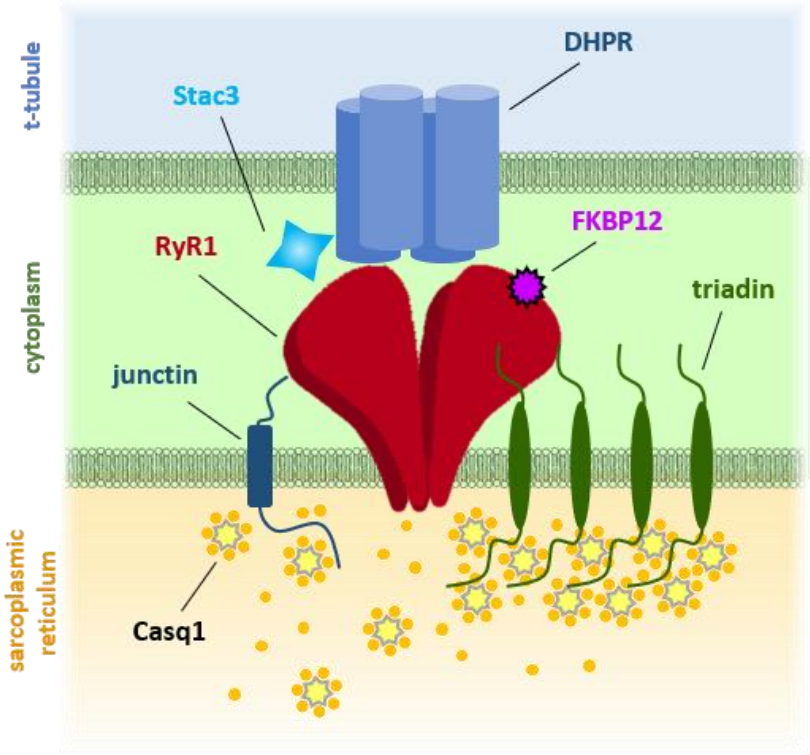

Figure 1.7 Protein complement involved in EC coupling

The major components of the excitation-contraction coupling process in skeletal muscle are shown at a terminal cisterna. The dihydropyridine receptor (DHPR; medium blue) is across the plasma membrane and associates with Stac3 (light blue) and ryanodine receptor 1 (RyR1; red) in the cytoplasm. Across the sarcoplasmic reticulum membrane are RyR1, junctin (dark blue), and aggregated triadin (green). FK506 binding protein 12 (FKBP12; purple star) is bound to RyR1 in the cytoplasm and calsequestrin 1 (Casq1; yellow) associates with free Ca^{2+} (orange) in the sarcoplasmic reticulum lumen. *Figure created by the Author.*

1.3.3.4 Calsequestrin 1

Calsequestrin 1 (Casq1) is a 41.8 kDa skeletal muscle specific protein located in the SR lumen and participates in the sequestration of Ca^{2+} that prevents swelling of the organelle due to osmotic pressure (Figure 1.7). It has a large Ca^{2+} buffering capacity with a highly charged C-terminal tail able to bind up to sixty Ca^{2+} ions.[148] Casq1 is enriched at the terminal cisternae where it makes Ca^{2+} available for release through RyR1. A secondary function of Casq1 is as a sensor of SR store depletion in cardiac muscle. It is suggested to be essential for the closing of the channel in response to depleted Ca^{2+} stores in both

cardiac and skeletal muscle and therefore support channel stability.[149-151] An MH-like phenotype is observed in mice with a loss of Casq1 upon exposure to halothane and heat stress.[74,152] This is likely because these mice release substantially more Ca^{2+} from stores—93% contrasted with the 65% observed in wild-type (WT) mice—after continuous membrane depolarisation.[153] Although no Casq1 mutations have been definitively associated with MH-susceptibility, mutations in the cardiac muscle isoform, Casq2, contribute to CPVT *in vivo*.[154] CPVT is a disorder that is also linked to mutations in the cardiac muscle ryanodine receptor isoform.

1.3.3.5 Triadin and junctin

Triadin and junctin are transmembrane proteins located across the SR membrane. Each protein comprises a small, N-terminal domain in the cytoplasm and a large, highly charged C-terminal domain in the SR lumen that physically interacts with each other, Casq1, and the negatively charged luminal loops of RyR1.[91,155] Triadin is a 95 kDa protein expressed in muscle tissue that localises exclusively to DHPR-coupled RyR1 channels and can self-oligomerise to increase binding capacity.[156] Junctin is a 26 kDa protein expressed in many tissues; it remains as a monomer and is not restricted to terminal cisternae. Triadin and junctin share high sequence similarity but are thought to interact with RyR1 at different locations because their binding is non-competitive.[157] Although they each have greater and more specific roles individually, both proteins localise around RyR1 channels and serve as anchor points for Casq1 to bind (Figure 1.7).[158]

The C-terminal domain of triadin binds the luminal region of RyR1 at a single site to enhances the degree to which RyR1 opens, independent of luminal Ca^{2+} levels; [159,160] in contrast, the C-terminal domain of junctin interacts with several sites in the luminal loops of the channel to inhibit RyR1 activity.[161] In the cytoplasm, the N-terminal domain of triadin interacts with RyR1 to prevent channel opening whereas the N-terminal domain of junctin binds with and activates RyR1.[157,161,162] Triadin is thought to be critical for EC coupling because a loss of triadin disrupts this process.[159,163,164] Analogous to Casq2, mutations in the cardiac muscle isoform of triadin have been linked to CPVT, although no mutations in the skeletal muscle isoform have been observed to contribute to MH-

susceptibility.[165] Although junctin is structurally similar to triadin, it is not thought to be essential because the ablation of junctin in mice has little effect on EC coupling.[158] Little is known about the exact function of junctin; however, it is believed to inhibit RyR1 gating independent of Ca^{2+} levels in the SR lumen and therefore promote closing of the channel.[157]

1.3.3.6 Calmodulin and S100A1

Calmodulin (CaM) and S100 Ca^{2+} binding protein A1 (S100A1) are small, cytoplasmic messenger proteins that bind RyR1. CaM is a 16.7 kDa protein with ubiquitous expression whereas S100A1 forms a 20.8 kDa homodimer highly expressed in muscle tissue. The binding of Ca^{2+} to these proteins causes large conformational changes that alter their ability to bind and regulate RyR1 activity. Additionally, S100A1 binds the cardiac isoform of SERCA to enable reuptake of Ca^{2+} into the SR during and after Ca^{2+} release in cardiac muscle.[166]

A model has been proposed in which, at rest, low cytoplasmic Ca^{2+} levels result in a predominance of the unbound forms of these two proteins, enabling the weak activation of RyR1 through CaM binding.[167,168] During muscle stimulation, Ca^{2+} levels increase in the cytoplasm, a process enhanced by the association of Ca^{2+}-bound S100A1 with RyR1.[169] After sustained stimulation, the elevated cytoplasmic Ca^{2+} results in Ca^{2+}-bound CaM which subsequently binds and strongly inactivates the channel.[168] CaM and S100A1 are thought to share a single binding site on RyR1, between the handle and peripheral domains, and therefore are posited to interact with the channel in a competitive and Ca^{2+}-dependent manner.[169-172] An *in vitro* study showed that binding of S100A1 indirectly alters the conformation of the RyR1-bound CaM because no competitive binding could be observed.[173] Although the exact mechanism is still unclear, these two proteins precisely regulate channel gating in response to cytoplasmic Ca^{2+} concentrations.

1.3.3.7 Junctophilins

Junctophilins are structural proteins involved in the organisation of terminal cisternae.[174] There are two isoforms expressed in skeletal muscle that share similar roles: junctophilin

1 (90 kDa) and junctophilin 2 (74 kDa). They both have a large cytoplasmic region that associates with phospholipids in the t-tubule membrane and a transmembrane C-terminal domain that anchors the protein in the SR membrane.[175] In this way, junctophilins span the distance between the two membrane systems, facilitating their close positioning and therefore the contact between DHPR and RyR1 channels. Silencing of junctophilin genes impairs the organisation of this contact and disrupts EC coupling.[176,177] Junctophilins also associate with RyR1 and DHPR channels directly, substantiating the proposed role for junctophilins in stabilising the localisation of all EC coupling components.[178-180]

1.3.3.8 Histidine-rich calcium binding protein

The histidine-rich Ca^{2+} binding protein (HRC) is a 165 kDa protein expressed predominantly in muscle tissue and localised to the lumen of the SR. The behaviour of HRC is analogous to Casq1 because it undergoes conformational changes upon the binding of Ca^{2+} ions which bind with low affinity and high capacity.[181] Whether this occurs in a regulatory role or HRC acts as an auxiliary Ca^{2+} buffer has not been determined. It has been hypothesised, however, that HRC acts as a Ca^{2+} sensor, fine-tuning channel gating in response to changing store levels.[182] When luminal Ca^{2+} levels are high, HRC activates channel opening indirectly through an association with triadin; this is supported by evidence that changes in HRC activity modulate channel gating.[183-185] During periods of low Ca^{2+} levels in the SR, HRC interacts with SERCA to promote reuptake of cytoplasmic Ca^{2+} and restore SR levels to that of rest.[186]

1.3.3.9 Junctional sarcoplasmic reticulum protein 1

Junctional sarcoplasmic reticulum protein 1 (JSRP1) is a 45 kDa transmembrane protein found mainly in the SR membrane of skeletal muscle. It is localised around RyR1 channels where its cytoplasmic regions interact with the α1 subunit of the DHPR and its positively charged luminal tail associates with Casq1 in the SR.[187,188] JSRP1 modulates Ca^{2+} release from stores which may be through its regulation of functional expression of DHPR channels into the t-tubule network.[189,190] Its importance in correct muscle function has been observed in mice in which the ablation of JSRP1 causes reduced muscle strength.[191]

Moreover, two missense variants in the gene for JSRP1 were identified in the general population as possible modifiers of EC coupling in skeletal muscle; both variants were found to decrease the sensitivity of the DHPR to voltage depolarisation signals in transgenic mice.[192,193] These results may support a model of MH in which modifier variants contribute to the complexity of neuromuscular disorders and have the potential to phenotypically modulate RyR1 activity.

1.4 Related muscular disorders

There are several neuromuscular disorders with links to MH, most notably central core disease (CCD), multiminicore disease, King-Denborough syndrome, Native American myopathy, exertional heat illness (EHI), and exercise-induced rhabdomyolysis (EIR).

1.4.1 Central core disease

Central core disease (CCD) is a congenital myopathy that may present as muscle weakness and underdeveloped motor skills from an early age. Notable differences in the severity of the disease are common, even within the same family; some people have no obvious symptoms whereas others can have skeletal abnormalities, low muscle development, and respiratory problems.[194,195] Diagnosis of CCD is simple with a histological examination of a small muscle biopsy in which unusual organisation of muscle fibres and a predominance of type 1 fibres would be evident.[196,197] The most obvious phenotype for diagnosis of CCD is the presence of large 'cores' of low mitochondrial activity in the centre of type 1 muscle fibres that usually extend down the length of the fibre (Figure 1.8).

CCD is a disorder that usually has an autosomal dominant mode of inheritance, most commonly caused by dominant variants in *RYR1*; however, recessive *RYR1* variants have also been linked to CCD.[198-201] To date, no genes other than *RYR1* have been found to segregate with instances of CCD. CCD sufferers are treated as though they are MH-susceptible and, when anaesthetic is required, precautions are taken that reflect this. This is because some, but not all, of those diagnosed with CCD have also been diagnosed as MHS by IVCT.[202]

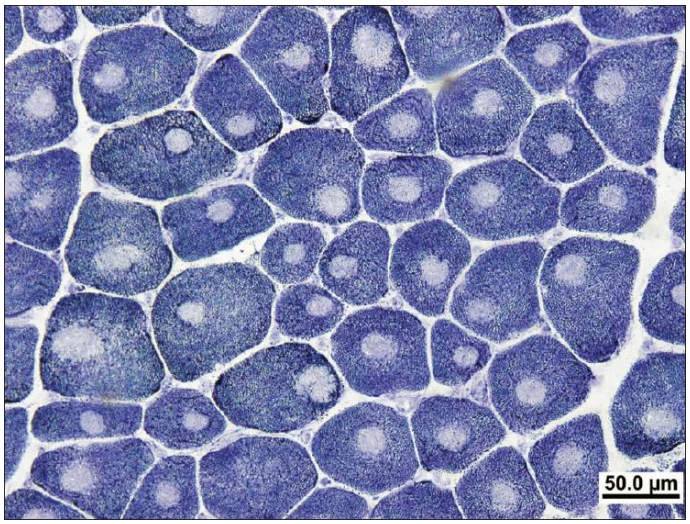

Figure 1.8 Histological diagnosis of central core disease

A transverse section of skeletal muscle stained with nicotinamide adenine dinucleotide tetrazolium reductase reveals a predominance of type 1 fibres (dark stain) that contain large, centrally located 'cores' of low or no oxidative activity. *Image reproduced with permission from Neurology India (DOI: 10.4103/0028–3886.43451).*[203]

1.4.2 Multiminicore disease

Multiminicore disease is a myopathy that bears similarities with CCD. As with CCD, it is characterised by hypotonia and muscle weakness, although clinical symptoms such as scoliosis and respiratory issues distinguish it as a distinct disease.[204] A predominance of type 1 fibres is common, and regions of low mitochondrial activity are observed on a histological stain of muscle fibres similar to CCD. These 'cores' differ from those observed in CCD in several ways—there are multiple cores distributed randomly through the fibre, they are generally found in both type 1 and 2 fibres, they are small in diameter, and they do not extend far down the length of the fibre.[204,205]

Multiminicore disease is an autosomal recessive disease that is genetically heterogeneous and has been linked to both homozygous and compound heterozygous variants.[206] A small number of instances are associated with *RYR1* variants, although the majority are caused by variants in the gene for selenoprotein 1, a glycoprotein in the endoplasmic reticulum (ER) with numerous roles including the redox regulation of Ca^{2+} homeostasis.[200,207-209]

There is no consensus on the relationship between multiminicore disease and MH; however, those diagnosed with the disease may have an increased risk for MH-susceptibility because there have been instances diagnosed MHS by IVCT.[210,211]

1.4.3 *King-Denborough syndrome*

A small subset of the MH-susceptible population suffers from King-Denborough syndrome. This is a rare myopathy characterised by skeletal abnormalities, muscle weakness, and dysmorphic facial features.[212] It is inherited in an autosomal dominant manner with *RYR1* variants implicated as the likely cause.[213-215] Given the strong association between the two disorders, MH triggering agents are avoided when those diagnosed with King-Denborough syndrome undergo surgery.[215,216]

1.4.4 *Native American myopathy*

Native American myopathy is a debilitating skeletal disease originally found in the Lumbee Native American population; however, this disease has since been diagnosed in several different ethnicities.[217,218] Present from birth, Native American myopathy is characterised by symptoms such as general weakness, skeletal abnormalities, cleft palate, and suspected MH-susceptibility.[217,219] The genetic cause of this disorder has been identified as a recessive missense variant in *STAC3*, resulting in an amino acid change in the Stac3 protein.[140] This variant causes decreased EC coupling and an increase in the Ca^{2+} released in the presence of caffeine in zebrafish which is in agreement with the MH phenotype.[25] The loss of Stac3 in the mouse model resulted in substantially reduced muscle contraction related to defective EC coupling.[142]

1.4.5 *'Awake' malignant hyperthermia episodes*

MH-susceptibility has also been linked to two related syndromes in which environmental stressors such as extreme heat or strenuous exercise induce a hypermetabolic state resembling an MH crisis.[220,221] These syndromes are exertional heat illness (EHI) and exercise-induced rhabdomyolysis (EIR). It is thought that, although extreme exertion or heat stress can trigger a response in anyone, individuals may have a greater susceptibility

to EHI or EIR that is related to genetic factors such as those that cause MH.[222] Exertional heat illness is a clinical emergency described as an elevated core temperature, generally above 40 °C. Several patients with a known history of EHI episodes have been diagnosed as MH-susceptible, with a few instances specifically linked to *RYR1* variants.[223-226] It is not uncommon for the EHI phenotype to include rhabdomyolysis—a life-threatening condition for which the extensive necrosis of muscle tissue leads to the release of intracellular muscle components into the bloodstream. Exercise-induced rhabdomyolysis differs from EHI in that it may occur in moderate climates and usually arises during or immediately following strenuous exercise. The strong link between EIR and MH-susceptibility is well documented and *RYR1* variants have been found in several individuals with a history of EIR.[227-229] Generally, there is no need for those diagnosed as or suspected to be MH-susceptible to avoid hot climates or strenuous activity because non-anaesthetic MH events known as 'awake' episodes are extremely rare. Conversely, a history of EHI or EIR must be considered when individuals are to be exposed to MH triggering agents.

1.6 Characterisation of genetic variants

The European malignant hyperthermia group was established in 1983 to improve diagnostic standards between laboratories, advance scientific research into MH, and provide a universal database of MH-causative variants. Although over 300 variants of unknown significance have been found in MH-susceptible individuals, only 48 *RYR1* variants and two *CACNA1S* variants have been accepted as diagnostic thus far.[30] Classification of a variant as being causal for MH-susceptibility requires three criteria be met according to the guidelines established by the European malignant hyperthermia group: co-segregation of the variant and MH-susceptibility in the family, a minor allele frequency (MAF) below 0.1%, and the functional analysis of the variant in an appropriate system must show an altered phenotype consistent with MH pathology.[230] When these criteria are met, the variant can then be used for DNA-based diagnosis as MH-susceptible along with the other 50 variants currently known to contribute to MH-susceptibility. This form of testing is simple and inexpensive, and thus is the preferred alternative to the IVCT.

Only a positive DNA test, however, can be used diagnostically because the absence of a sequence variant that affects function does not necessarily indicate the absence of disease.

1.6.1 Identification of variants

There are several methods for the identification of variants that may have a role in MH-susceptibility, and these are selected based on the funds available and the coverage and accuracy needed. Amplicon sequencing of *CACNA1S* and *RYR1* is a suitable first step because these are the genes most likely to harbour variants and the costs are relatively small. Because the 160 kilobase *RYR1* gene is considerable, with some regions having high GC content that are difficult to sequence, three variant 'hotspots' are sometimes preferentially screened which may lead to some variants being missed.[198,231] If no variants are found with these methods, then the set of candidate genes can be expanded to those known to be involved in Ca^{2+} homeostasis such as the remaining DHPR subunits, Casq1, and SERCA.[232]

Targeted sequence capture or whole exome sequencing may also be used for variant discovery because these methods are cost-effective, efficient, and are successful for variant screening of diseases with locus heterogeneity.[233] The quality of the DNA and the abundance of GC content and repeat elements can affect sequencing coverage; therefore, additional sequencing may be required for 100% coverage and false-negatives may arise with these approaches.[234] Yet with high-throughput screening of this nature comes the potential for the misidentification of benign variants as those that affect function, highlighting the need for functional analysis of any variant identified.[235]

1.6.2 In silico analysis of potential variants

Variants that affect function are likely to be rare, so a list of potential variants of interest found with sequence capture screening may be filtered to those with a low MAF as determined from an appropriate human genetic database. Then, prediction software may be used to extrapolate the change in protein function from the genetic change. This bioinformatics approach uses information such as evolutionary conservation, domain architecture, and the amino acid sequence to model the impact of a variant on protein

structure and function. However, this method is reliant on current knowledge about each protein, and thus its use in prediction of disease is limited.[236] In a study of the ability of commonly used bioinformatics programmes to predict the outcomes of over 40,000 known neutral and variants that affect function, many did not perform well—the best software had a success rate of only 82%.[237] The usefulness of *in silico* analysis for prediction of functional consequences of a genetic change is therefore limited and functional characterisation of variants remains a vital step toward expanding the DNA-based diagnosis of MH.

1.6.3 Functional analysis

1.6.3.1 Detection of RyR1 activity

The abnormal activity of RyR1 observed in the MH phenotype can be measured by several means for comparison with that of the WT channel. A hyperactive RyR1 channel—thought to be the cause of MH-susceptibility—should open and release Ca^{2+} with greater sensitivity than normally functioning channels. RyR1 channel opening can be induced by agonists such as caffeine, halothane, 4-c*mc*, electrical stimuli, or K^+; although, the use of electrical stimuli and K^+ is limited for use with depolarisable cells. The activity of RyR1 may be measured indirectly in living cells by use of intracellular fluorescent Ca^{2+} indicators; these are specific for Ca^{2+} and have little background interference.

Channel conductance can also be measured by a voltage signal transduced through RyR1 by use of patch-clamp techniques.[238] This system requires the use of vesicles and cannot be used in live cells because RyR1 is located on the SR membrane within the cell; however, it can be used to directly determine the opening of the channel. The binding affinity of radiolabelled ligands such as ryanodine is another method to determine channel gating, although the cost and availability of radioisotopes is a major limitation.[239,240] The degree to which RyR1 opens under different conditions can be determined by the size of the radioactive signal because ryanodine preferentially binds RyR1 in the open state; although, this method may only be used *in vitro* with isolated protein samples.

1.6.3.2 Ex vivo testing

The simplest functional studies use tissue taken from the patient that can be analysed *ex vivo*. A variant studied in this way requires that patients from two independent pedigrees be analysed to eliminate contributing factors from the genetic background—this is rarely possible. B-lymphoblastoid cells can be extracted from a blood sample and are easily immortalised and analysed in the laboratory. In contrast, SR microsomes and primary myoblasts must be prepared from muscle biopsy tissue such as that used for the IVCT. SR microsomes are versatile because they can be used in patch-clamp experiments, but they do not show RyR1 channels in their intracellular environment. Although difficult to work with, only myotubes produced from primary myoblasts can attempt to replicate the physiological state of the muscle. Myotubes are immature skeletal muscle fibres that express the most muscle proteins in an almost physiological muscle environment; but even these do not have equivalent behaviour to an innervated muscle.[241]

1.6.3.3 In vitro testing

A standardised testing system is the heterologous expression of rabbit or human recombinant *RYR1* complementary DNA (cDNA) in mammalian cells such as the human embryonic kidney 293 (HEK-293) cell line.[242,243] This approach requires the construction of mutant cDNAs for subsequent transfection of these cell lines which is not a trivial exercise because of the size of the *RYR1* cDNA. HEK-293 is a non-muscle cell type that has been widely used in scientific research and, although the karyotype and phenotype of this cell line are thought to vary between laboratories, it has proven useful in the study of *RYR1* variants associated with MH.

Ca^{2+} homeostasis in these model cell systems is different from muscle cells; for example, the Ca^{2+} storage organelle is the ER. The system is easy to use and interpret, but only simple results that reflect the activity of the isolated RyR1 channel can be expected.[244] Divergent results have been observed between muscle and non-muscle cell systems on rare occasions and, however seldom, these findings make evident the advantage of utilising a muscle cellular background for analysis of variants.[245] A homologous system would include the

expression of *RYR1* cDNA in *RYR1*-null myotubes. This is a far more technically challenging system than in HEK-293 cells, but it is a more physiologically relevant *in vitro* system to study *RYR1* variants when resources allow because myotubes may be closer in function to mature muscle.[246] They also provide a system to express many different *RYR1* variants in an identical genetic background.

1.6.3.4 In vivo testing

The most complex and technically demanding system for testing *RYR1* variants is the use of knock-in mice. Knock-in mice are created in an *RYR1*-null mouse by introducing *RYR1* with the variant into the genome by targeted mutagenesis. This is a valuable means of analysis because the variant *RYR1* allele is targeted to the location of endogenous *RYR1* and therefore its expression levels and patterns should be the same as the WT allele it replaced. Dose-dependent phenotypes can also be examined by use of this method because mice both heterozygous and homozygous for the variant *RYR1* allele can be created; this is important because MH variants are generally heterozygous. MH-linked variants have been successfully introduced into mice to produce the classical MH phenotype in response to pharmacological stimuli or heat stress that can be rescued by dantrolene treatment.[247,248] These studies show that the mouse model is currently the most physiologically relevant system when investigating the effects of a single genetic change on disease progression.

The requirements of testing in the mouse model are substantially different to that of cellular systems and therefore precludes most researchers from these studies—only six genetic variants have been investigated in this way to date.[248-253] The use of mouse systems is also prohibitively expensive. In addition, the phenotypes of some knock-in mice may have notable differences to that of people with the equivalent variant.[250,251] This could be attributed to differences between mouse and human muscle or it could be highlighting the incomplete penetrance and variable expressivity of MH-susceptibility and its related neuromuscular diseases.[248]

1.7 Project outline

1.7.1 Significance of project

The current options for diagnosis of MH are either the morbidly invasive and expensive contracture testing with use of tissue from a muscle biopsy or the minimally invasive and simple DNA-based diagnosis. Most genetic variants linked to MH-susceptibility have been found in the genes encoding the two major components of the skeletal muscle EC coupling pathway, but the phenotypic variability of MH-susceptibility and related disorders may be because of the action of secondary alleles that modify the phenotype.[233,254] This heterogeneity may be the source of the discordance between genotype and phenotype reported in 2.6% of families tested for MH-susceptibility.[255-257] The existence of several instances in which a family member was diagnosed as MHS by IVCT but did not test positive for the familial MH variant is a major obstruction of DNA-based diagnosis. Much is unknown regarding this complex disease and the list of known MH-causative variants is not comprehensive; therefore, the IVCT will continue to be the gold-standard of diagnosis until this is achieved.

Two major bottlenecks exist in DNA-based diagnosis for MH-susceptibility. These are the lack of functionally characterised variants and the inability to make an MHN diagnosis with DNA. Ideally, variants linked to MH-susceptibility would be examined in a physiologically relevant system that contains all components of the complex network that controls Ca^{2+} homeostasis in skeletal muscle. Unfortunately, the current methods for functional analysis of variants are either oversimplified, technically difficult, or too expensive to be achievable in a realistic timeframe. The overarching theme of this study was to develop novel molecular techniques for the generation of cells expressing MH-causative genetic variants and then demonstrate their effectiveness in the study of the functional causes of MH-susceptibility.

1.7.2 Hypothesis

RyR1 variants associated with MH-susceptibility cause dysregulation of calcium release from intracellular stores.

1.7.3 Aims of project

1.7.3.1 Stable expression lines

The aim of the first part of this research was to introduce *RYR1* cDNAs to the Flp-In™ T-REx™ 293 host cell line for inducible stable expression of RyR1 channels for functional studies. This recombinase system enables the generation of stable mammalian expression cell lines by site-specific recombination of a gene of interest into a transcriptionally active genomic locus.

The key objectives were as follows:

- Introduce full-length *RYR1* cDNAs with and without variants to the Flp-In™ system expression vector.
- Create monoclonal Flp-In™ T-REx™ 293 cell lines by stable transfection with *RYR1* cDNAs with the Flp-In system.
- Confirm inducible expression of RyR1 with microscopy and immunoblotting.
- Compare Ca^{2+} release of mutated RyR1 with that of wild type using stable expression in Flp-In™ T-REx™ 293 cells.

1.7.3.2 Direct editing of the genome

The final aim of this project was to develop the CRISPR/Cas9 gene editing system to directly introduce genetic variants linked to MH-susceptibility into immortalised human myoblasts. This system could then be used in the future in patient-derived myoblasts to

investigate if a single *RYR1* variant is both necessary and sufficient to cause the MH phenotype.

The key objectives were as follows:

- Design a strategy and prepare components for CRISPR/Cas9 gene editing of an immortalised human myoblast cell line.
- Introduce a *RYR1* variant into the human myoblast cell line by gene editing.
- Confirm the presence of the variant and the lack of off-target effects by Sanger sequencing of genomic DNA.
- Compare Ca^{2+} release of myotubes from the original cell line and monoclonal cell lines with the variant.

2 Materials and Methods

2.1 Materials

Table 2.1 List of materials used and their suppliers

Supplier	Material
Addgene, Massachusetts, USA	pCMV-VSV-G was a gift from Bob Weinberg (Cat. No. 8454), lentiCRISPR v2 was a gift from Feng Zhang (Cat. No. 52961), psPAX2-D64V was a gift from David Rawlings and Andrew Scharenberg (Cat. No. 63586), pLJM1-EGFP was a gift from David Sabatini (Cat. No. 19319).
Anchor, New Zealand	Trim milk powder.
Applied Biological Materials, British Colombia, Canada	qPCR lentivirus titration kit (Cat. No. LV900).
Applied Biosystems, California, USA	ExoSAP-IT® PCR Product Cleanup Reagent (Cat. No. 78201.1.ml)
Bio-Rad Laboratories, California, USA	40% Acrylamide/Bis solution 29:1, Mini PROTEAN® 3 System, Precision Plus Protein™ Dual Colour Standards, SsoFast™ EvaGreen® Supermix.
Corning® Life Sciences, New York, USA	T-200-Y pipette tips, T-1000-B pipette tips, T-300 pipette tips, 1.7 mL micro-centrifuge tubes, 0.6 mL micro-centrifuge tubes.
Gold Biotechnology, Missouri, USA	Tris base (Cat. No. T-400-500).

(continued)

Supplier	Material
Greiner Bio-One, Frickenhausen, Germany	CELLSTAR® 50 mL Falcon tubes, CELLSTAR® 15 mL falcon tubes, Cryo-S™ cryotubes, seriological pipettes, UV-Star® 96-well plates.
Integrated DNA Technologies, Iowa, USA	Custom DNA oligonucleotides.
Invitrogen™, California, USA	TRIzol® Reagent (Cat. No. 15596026), Opti-MEM® (Cat. No. 22600050), ChargeSwitch®-Pro Plasmid Miniprep kit (Cat. No. CS30050), 1 Kb Plus DNA Ladder, T4 DNA Ligase (Cat. No. 15224025), Foetal Bovine Serum, PureLink™ HiPure Plasmid Filter Midiprep kit (Cat. No. K210014), ProLong® Gold antifade mountant with DAPI (Cat. No. P36941), Trypsin-EDTA (Cat. No. 25200056), Flp-In™ T-REx™ core kit (Cat. No. K650001), TURBO™ DNA-free kit (Cat. No. AM2238).
Jackson ImmunoResearch, Pennsylvania, USA	Rhodamine (TRITC)-AffiniPure Goat Anti-Rabbit IgG (Cat. No. 111-025-045).
Kapa Biosystems, Massachusetts, USA	2× KAPA HiFi HotStart ReadyMix (Cat. No. KK2601).
Lonza, Basel, Switzerland	P5 Primary Cell 4D-Nucleofector™ X kit (Cat. No. V4XP-5032).

(continued)

Supplier	Material
New England Biolabs (NEB), Massachusetts, USA	Restriction endonucleases, restriction endonuclease buffers, Antarctic Phosphatase (Cat. No. M0289S), T7 Endonuclease I (Cat. No. M0302S), Low Molecular Weight DNA Ladder (Cat. No. N3233G), 6× gel loading dye.
OfficeMax, New Zealand	Overhead Projector Transparency Film, A4 (Cat. No. 1219839).
Pall Corporation, New York, USA	BioTrace™ PVDF transfer membrane (Cat. No. 66543), AcroCap™ Filter Unit.
Promega, Wisconsin, USA	FuGENE® HD Transfection Reagent (Cat. No. E2311), Wizard® SV Gel and PCR Clean-Up System (Cat. No. A9282), pGEM®-T Easy vector system (Cat. No. A1360), Wizard® Genomic DNA Purification kit (Cat. No. A1125), anti-mouse horseradish peroxidase-conjugated antibody (Cat. No. W402B), FuGENE® 6 Transfection Reagent (Cat. No. E2691).
Promocell GmbH, Heidelberg, Germany	Skeletal muscle cell growth medium (Cat. No. 23060), skeletal muscle cell differentiation medium (Cat. No. 23061).
Roche, Basel, Switzerland	BM Chemiluminescence Blotting Substrate, cOmplete™ Mini EDTA-free protease inhibitor cocktail tablets, LightCycler® 480 High Resolution Melting Master (Cat. No. 04909631001), Transcriptor High Fidelity cDNA Synthesis kit (Cat. No. 5081955001).

(continued)

Supplier	Material
Sigma-Aldrich®, Missouri, USA	Dulbecco's Modified Eagle's Medium (Cat. No. D7777), 34C anti-ryanodine receptor antibody produced in mouse (Cat. No. R129), anti-PDI produced in rabbit (Cat. No. P7496), anti-tubulin antibody produced in mouse (Cat. No. T9026), anti-mouse FITC antibody produced in goat (Cat. No. F8521), R-250 Coomassie Brilliant Blue, Glucose, KCl, SDS, chloroquine, APS, ampicillin, $CaCl_2$, Pluronic F-127, Tween 20, Trypan blue solution, dimethyl sulfoxide, bromophenol blue, $MgCl_2$, β-mercaptoethanol, TEMED, BSA, Triton X-100, paraformaldehyde, Poly-D-lysine hydrobromide, tetracycline hydrochloride.
Thermo Fisher Scientific, Massachusetts, USA	T25 Nunc™ flasks, T75 Nunc™ flasks, EDTA, ethanol, methanol, petri dishes, bacteriological agar, agarose, glycine, glass cloning rings, penicillin/streptomycin, GeneRuler™ Ultra Low Range DNA Ladder (Cat. No. SM1211), Nunc™ Lab-Tek™ Chamber Slide System™, Fura-2 AM (Cat. No. F-1221), LB broth base, DAPI solution (Cat. No. 62248), Whatman® 3MM filter paper.
UK Biobank, Greater Manchester, UK	HMCL-7304 cell line (RRID: CVCL_T053).
VWR International, Pennsylvania, USA	4-chloro-*m*-cresol, ethidium bromide, 0.2 mL PCR tubes.

2.2 DNA manipulation

2.2.1 Transformation of chemically competent bacteria

DH5 alpha *Escherichia coli* (*E. coli*) were grown in 100 mL Luria-Bertani (LB) broth (1% peptone, 0.5% yeast extract, 0.5% NaCl) supplemented with 0.1 mg mL^{-1} ampicillin. When the culture reached an optical density of 0.6 measured at 600 nm in a spectrophotometer, cells were collected by centrifugation at 12,000 g for one minute at room temperature (RT). These were gently resuspended in 10 mL ice-cold 0.1 M $CaCl_2$, collected by centrifugation at 3,000 g at 4 °C and then made competent by incubation in 3.2 mL ice-cold, 0.1 M $CaCl_2$ overnight. Ice-cold glycerol was added to a final concentration of 10% glycerol and 80 mM $CaCl_2$ and competent cells were stored at –80 °C.

One nanogram of plasmid DNA was added to 100 µL competent cells thawed on ice and incubated for 20 minutes, before being subjected to heat-shock at 42 °C for 30 seconds. After a brief period on ice to recover, the cells were incubated with 1 mL LB broth for 1½ hours at 30 °C with agitation at 220 rpm. Cells were then collected by centrifugation at 2,000 g for one minute and spread onto a LB Agar plate containing 0.1 mg mL^{-1} ampicillin to grow at 30 °C overnight. All plasmids used in this study conferred resistance to ampicillin.

2.2.2 Plasmid DNA isolation

E. coli were grown in either 5 mL or 100 mL LB broth containing 0.1 mg mL^{-1} ampicillin at 30 °C with agitation at 220 rpm for 20 hours for the extraction of either less than or greater than 10 µg of plasmid, respectively. Plasmid DNA was prepared with an ion exchange procedure from either a 5 mL culture with the ChargeSwitch®-Pro Plasmid Miniprep kit (Invitrogen™) or 100 mL culture with the PureLink™ HiPure Plasmid Filter Midiprep kit (Invitrogen™) according to the instructions of the manufacturer. The DNA was then quantified visually by comparison with a loading standard after gel electrophoresis.

2.2.3 *Horizontal electrophoresis of DNA fragments*

DNA fragments were subjected to electrophoresis in differing concentrations of 25 mL agarose (5.7 × 8.3 × 0.05 cm) in a horizontal electrophoresis tank (15.2 × 24 × 7 cm) in TAE buffer (40 mM Tris-acetate, 1 mM EDTA, pH 8.0) containing ethidium bromide (0.2 μg mL^{-1}) depending on the length of the DNA (see Table 2.2). DNA samples were loaded onto the agarose gel with loading dye alongside 4 μL of 0.25 μg μL^{-1} DNA marker as a size control.

Table 2.2 Percentage of agarose used in gel electrophoresis

DNA fragment size	Percentage agarose
Less than 100 bp	3%
Between 100 bp and 1 kb	2%
Between 1 kb and 6 kb	1%
Over 6 kb	0.8%

For most gels, 1 Kb Plus DNA Ladder (Invitrogen™) was used, whereas GeneRuler™ Ultra Low Range DNA Ladder (Thermo Fisher) and Low Molecular Weight DNA Ladder (NEB) were used where indicated. Electrophoresis was always performed at 90 V with the agarose gel immersed in 1× TAE buffer and the DNA was visualised under UV light. When non-specific PCR products were unavoidable, the DNA was excised from the gel and purified with the Wizard® SV Gel and PCR Clean-Up System (Promega) according to the instructions of the manufacturer.

2.2.4 *Restriction endonuclease digestion*

For both sub-cloning purposes and characterisation of plasmids, DNA was digested with restriction endonucleases (NEB) according to the instructions of the manufacturer. This was usually performed with 300 ng plasmid DNA, 10 units of each endonuclease, and 2 μL

10× buffer in a volume of 20 µL for one hour at 37 °C. When required for cloning, vector fragments were then treated with 5 units of Antarctic Phosphatase (NEB) with 3 µL 10× buffer in a volume of 30 µL for one hour at 37 °C. Vector and insert fragments were subjected to electrophoresis, excised from the agarose gel while under UV light, and then purified with the Wizard® SV gel and PCR Clean-up system (Promega) according to the instructions of the manufacturer.

2.2.5 Ligation of DNA fragments

Each cloning step that required an insert to be ligated into a vector was performed with directional cloning. The molar ratio of insert DNA to vector DNA was between 3:1 and 6:1. Usually a total of 100 ng DNA was ligated together with 1 unit of T4 DNA ligase (Invitrogen™) and 4 µL 5× ligase buffer in a total volume of 20 µL according to the instructions of the manufacturer for four hours to overnight at 18 °C.

2.2.6 Polymerase chain reaction

Polymerase chain reaction (PCR) was performed on complementary DNA (cDNA) or genomic DNA (gDNA) with the Kapa HiFi HotStart Readymix (Kapa Biosystems) according to the instructions of the manufacturer with primer pairs from Integrated DNA Technologies (listed in Appendix A.1). Primers were removed from PCR reactions used in downstream applications enzymatically with the ExoSAP-IT® PCR Product Cleanup Reagent (Applied Biosystems) according to the instructions of the manufacturer.

2.2.7 Sanger sequencing of DNA

DNA sequencing was used to confirm the identity of PCR products or plasmids. Sanger sequencing was performed with specific primers from Integrated DNA Technologies with a capillary ABI3730 Genetic Analyzer with BigDye® Terminator Version 3.1 chemistry (Applied Biosystems) at the Massey Genome Service in Palmerston North, New Zealand (listed in Appendix A.2).

2.2.8 *Genomic DNA extraction*

Genomic DNA was extracted from mammalian cells grown in 96-well plates or T25 flasks with the Wizard® Genomic DNA Purification kit (Promega) according to the instructions of the manufacturer. The volumes of solutions used were modified for optimisation of the extraction according to Table 2.3.

Table 2.3 Volumes of Wizard® kit solutions used in gDNA extraction.

Solution	T25 flask	96-well plate
Nuclei lysis buffer (µL)	600	60
Protein precipitation buffer (µL)	200	20
Isopropanol (µL)	600	60
70% ethanol (µL)	600	60
Resuspension buffer (µL)	50	10

2.2.9 *RNA extraction and synthesis of cDNA*

Cells were grown to 25% confluence in a T25 flask, after which they were removed by treatment with 0.25% Trypsin ethylenediaminetetraacetic acid (Trypsin-EDTA; Invitrogen™) for four minutes at 37 °C. Cells were then resuspended in 1 mL 1× PBS and collected by centrifugation at 12,000 g for one minute and resuspended in 750 µL TRIzol® reagent (Invitrogen™) at RT. This was incubated for five minutes before 200 µL chloroform was added and incubated for a further two minutes. The upper, colourless phase was collected after centrifugation at 12,000 g for 15 minutes at 4 °C after which it was mixed with 500 µL isopropanol and incubated for 10 minutes at RT. RNA was then collected by centrifugation at 12,000 g for 10 minutes at 4 °C, washed with 70% ethanol, and resuspended in 50 µL water.

The RNA concentration was measured as the absorbance at 260 nm and purity was determined as acceptable within the range of a 1.6–1.8 absorbance ratio of 260/280 nm with the UV spectrophotometry with a DeNovix DS-11 FX+. DNA was removed with the TURBO™ DNA-free kit (Invitrogen™) according to the instructions of the manufacturer. Synthesis of cDNA was performed on RNA samples with the Transcriptor High Fidelity cDNA Synthesis kit (Roche) with the random hexamer priming method according to the instructions of the manufacturer.

2.2.10 T7 Endonuclease I assay

A region of the genome comprising the proposed locus for gene editing was amplified by PCR from gDNA extracted from mammalian cells. PCR products were cleaned up with ExoSAP-IT® PCR Product Cleanup reagent (Applied Biosystems) according to the instructions of the manufacturer after which 250 ng of the product was denatured and re-annealed with 2 µL 10× NEBuffer 2 (NEB) in a total volume of 19 µL. Initial denaturation was performed at 95 °C for 5 minutes followed by two annealing steps: the first reduced the temperature to 85 °C at a rate of –2 °C/second and the second step reduced the temperature to 25 °C at a rate of –0.1 °C/second.

Digestion with 10 units T7 Endonuclease I (NEB) was then performed at 37 °C for 15 minutes before the products were analysed by gel electrophoresis. DNA fragments were subjected to electrophoresis either in a 3% agarose gel as in Section 2.2.3 or a 15% native polyacrylamide gel (15% acrylamide, 89 mM Tris, 89 mM boric acid, 2 mM EDTA, 0.15% APS, 0.1% TEMED) immersed in Tris-borate-EDTA (TBE) buffer (89 mM Tris, 89 mM boric acid, 2 mM EDTA). DNA samples were loaded onto the polyacrylamide gel with 6× loading dye (NEB) alongside the Low Molecular Weight DNA Ladder (NEB) as a size control and then subjected to electrophoresis for 1.5 hours at 100 V with the Mini PROTEAN® 3 electrophoresis system (Bio-Rad). The gel was then stained in TBE buffer containing 0.5 µg mL^{-1} ethidium bromide for 15 minutes and then destained in TBE buffer for 5 minutes before being visualised under UV light with a transilluminator.

2.2.11 High resolution amplicon melting analysis

Genomic DNA extracted from mammalian cells was amplified by PCR to detect the c.14477C>T (RyR1 p.Thr4826Ile) *RYR1* variant by high resolution amplicon melting (HRM) analysis. PCR was performed with LightCycler® 480 High Resolution Melting Master (Roche) supplemented with 3 mM $MgCl_2$, 0.3 µM each primer (Appendix A.1), and 25 ng gDNA template in a total volume of 10 µL. The region with the variant was amplified by PCR with the following cycling conditions: 95 °C for 10 minutes (4.4 °C/s), 95 °C for 10 seconds (4.4 °C/s), 65 °C for 10 seconds (2.2 °C/s), 72 °C for 4 seconds (4.4 °C/s) and steps 2–4 were repeated 39 times. Amplicons were then heated to 95 °C for one minute (4.4 °C/s), cooled to 40 °C for one minute (1.5 °C/s), and heated to 76 °C (4.4 °C/s). Then, in the presence of a fluorescent dye (as supplied in the master mix), amplicons were heated incrementally from 76 °C to 92 °C at 0.02 °C per second. The decrease in fluorescence as the DNA melted was measured in the LightCycler® 480 instrument II (Roche) with LightCycler® 480 Gene Scanning software version 1.5.

2.3 Mammalian cell culture

2.3.1 Cell maintenance

Mammalian cells were cultured in specific media dependent on their cell type and stage of growth (cell culture components listed in Table 2.4). Human embryonic kidney 293 cells with the SV40 large T-antigen (HEK-293T; RRID: CVCL_0063) and Flp-In™ T-REx™ 293 (FT-293) cells (RRID: CVCL_U427; Invitrogen™) were grown in 6 mL of their specific growth medium in a T25 flask placed horizontally at 37 °C in a humidified atmosphere containing 5% CO_2. The base solution of these media was Dulbecco's Modified Eagle's Medium (DMEM; Sigma-Aldrich®) with 10% foetal bovine serum (FBS; Invitrogen™).

Table 2.4 Components of cell culture media

Component	HEK-293T Growth medium	FT-293 Growth medium	FT-293 Transfection medium	FT-293 Selection medium	HMCL-7304 Growth medium
Basal medium	DMEM	DMEM	DMEM	DMEM	SkMC growth medium
FBS (%)	10	10	10	10	10
Penicillin (U L^{-1})	0.1				
Streptomycin (U L^{-1})	0.1				
Blasticidin (µg mL^{-1})		15	15	15	
Zeocin (µg mL^{-1})		100			
Hygromycin (µg mL^{-1})				30	
GlutaMAX (mM)					3
Gentamicin (µg mL^{-1})					6

Immortalised human myoblasts (HMCL-7304; RRID: CVCL_T053) from the UK Biobank were grown in either 6 mL or 15 mL of growth medium in a T25 or T75 flask, respectively, with Promocell skeletal muscle cell (SkMC) growth medium as a base. Flasks were placed horizontally at 37 °C in a humidified atmosphere containing 5% CO_2 and 10% O_2. Differentiation into myotubes was initiated by replacing the growth media on myoblasts

with Promocell skeletal muscle cell differentiation media and monitoring by visualisation with an Olympus CKX41 inverted light microscope.

2.3.2 *Cryopreservation and reanimation of cells*

Cells grown in a T25 flask were removed by brief washing with 2 mL 0.25% Trypsin-EDTA (Invitrogen™) which was repeated once, followed by trypsin removal and incubation for four minutes at 37 °C in a humidified atmosphere containing 5% CO_2. Cells were resuspended in 1 mL FBS (Invitrogen™) containing 10% dimethyl sulfoxide and then dispensed into a cryotube. These were cooled slowly to –80 °C in a CoolCell™ (Corning®) before being stored long-term in liquid nitrogen (gas phase). Cells stored in liquid nitrogen were thawed quickly at 37 °C, resuspended in 5 mL growth medium, and then collected by centrifugation at 200 g for five minutes at RT. Cell pellets were resuspended in 7 mL growth medium and grown in a T25 flask placed horizontally at 37 °C in a humidified atmosphere containing 5% CO_2 (and 10% O_2 for myoblasts).

2.3.3 *Transfection for transient gene expression*

Cells were grown to 80% confluence in growth medium. Two hours prior to the transfection, the medium on the cells was replaced with either 3 mL or 100 µL of grown medium in a T25 flask or 96-well plate, respectively. A transfection mixture of 6 µg plasmid DNA, 24 µL FuGENE® HD (Promega) and incomplete DMEM (Sigma-Aldrich®) to a total volume of 300 µL was added to the T25 flask after incubation at room temperature (RT) for 30 minutes. For the 96-well plate, the transfection mixture was 300 ng plasmid DNA, 1 µL FuGENE® HD (Promega), and incomplete DMEM (Sigma-Aldrich®) to a total volume of 10 µL. These cells were incubated at 37 °C in a humidified atmosphere containing 5% CO_2 for 24 hours after which 3 mL growth medium was added to the flask or 100 µL to each well of the 96-well plate. Forty-eight hours after transfection, the medium on the cells was replaced with 6 mL growth medium in the flask or 200 µL in the 96-well plate. The cells were ready for use 72 hours after transfection.

2.3.4 *Generation of stable expression cells*

FT-293 cells (Invitrogen™) were grown in a T25 flask to 80% confluence in growth medium. Two hours prior to the transfection, the medium on the cells was replaced with 3 mL transfection medium. A transfection mixture of 6 µg plasmid DNA, 24 µL FuGENE® HD (Promega), and incomplete DMEM (Sigma-Aldrich®) to a total volume of 300 µL was added to the cells after incubation at RT for 30 minutes and then incubated at 37 °C in a humidified atmosphere containing 5% CO_2. Twenty-four hours after transfection, 3 mL of transfection medium was added to the flask which was replaced after 48 hours with 6 mL of selection medium. The cells were removed from the flask by treatment with 0.25% Trypsin-EDTA (Invitrogen™; see Section 2.3.2 for method) and 10% of the cells were seeded onto a 15-cm^2 tissue culture plate in 15 mL selection medium.

Single colonies were identified visually with an Olympus CKX41 inverted light microscope and isolated with cloning rings (Thermo Fisher) in which they were removed to individual wells of a 96-well plate after treatment with 0.25% Trypsin-EDTA (Invitrogen™; see Section 2.3.2 for method). Ryanodine receptor 1 (RyR1) expression was induced by addition of tetracycline (Sigma-Aldrich®) to the growth medium to a final concentration of 1 µg mL^{-1} for at least 72 hours before use.

2.3.5 *Nucleofection*

Plasmids were introduced into human myoblasts by an electroporation-based method called Nucleofection. The number of viable myoblasts was quantified by trypan blue exclusion after following treatment with 0.25% Trypsin-EDTA (Invitrogen™; see Section 2.3.2) and resuspension in 5 mL growth media. A volume of 10 µL from a mixture of 50 µL trypan blue (Sigma-Aldrich®) and 50 µL resuspended cells was loaded into a haemocytometer.

After counting, 2×10^5 cells were collected by centrifugation at 200 g for 6 minutes. These were gently resuspended in a premixed solution containing 16.4 µL P5 primary cell Nucleofector® solution and 3.6 µL supplement 3 (both proprietary reagents from the P5 Primary Cell 4D-Nucleofector® Kit from Lonza) supplemented with 400 ng plasmid DNA.

This was then pipetted into a well of the 16-well Nucleocuvette™ strip from the P5 Primary Cell 4D-Nucleofector Kit and immediately transfected in the X unit of the Nucleofector™ with a specific Nucleofection programme (see the list of Lonza programmes used in Table 2.5). The cells were first allowed to recover in 80 µL growth medium in the Nucleocuvette™ strip at 37 °C in a humidified atmosphere containing 5% CO_2 and 10% O_2 for ten minutes before transfer into a T25 flask with 6 mL growth medium, placed horizontally at 37 °C in a humidified atmosphere containing 5% CO_2 and 10% O_2.

Table 2.5 Lonza Nucleofection programs

Programme identifier	Proprietary name
A	EO-100
B	CA-137
C	FG-113
D	CM-137
E	EH-106
F	CM-158
G	CM-189
H	CU-137
I	DG-137

2.3.6 Lentivirus production

Twenty-four hours prior to transfection, HEK-293T cells were seeded in 6 mL DMEM supplemented with 10% FBS in a T25 flask at 80% confluence and incubated in a humidified atmosphere containing 5% CO_2 to recover overnight. Two hours prior to transfection, the medium on the cells was replaced with 4 mL Opti-MEM® (Invitrogen™) supplemented with 25 µM chloroquine (Sigma-Aldrich®). A transfection mixture

containing 5 µg total DNA, 12 µL FuGENE® HD (Promega), and Opti-MEM® (Invitrogen™) to a total volume of 1 mL was incubated at RT for 30 minutes before being added dropwise to the medium on the cells and agitated to distribute. The ratios of transfer plasmid, packaging plasmid, and envelope plasmid used differed between the green fluorescent protein (GFP) control, Cas9-expressing plasmids, and repair template plasmids. The total amount of DNA used remained the same (Addgene; see the ratio of plasmids used in Table 2.6).

Table 2.6 Ratio of plasmids used in lentivirus production

Lentivirus		**Transfer plasmid**	**Packaging plasmid**	**Envelope plasmid**
GFP control	vector ratio	pLJM1-EGFP 2	psPAX2-D64V 3	pCMV-VSV-G 1
Cas9/Guides	vector ratio	LentiGuide 4	psPAX2-D64V 3	pCMV-VSV-G 1
Repair templates	vector ratio	Lenti-RT 2.5	psPAX2-D64V 3	pCMV-VSV-G 1

After a six-hour incubation at 37 °C in a humidified atmosphere containing 5% CO_2, the medium was replaced with fresh growth medium. Viruses were harvested from the medium 48 hours after the media change by centrifugation at 3,000 g for 10 minutes at 4 °C before filtration through a 0.45 µM filter and then stored at -80 °C. Titration of lentiviruses was performed by quantitative reverse transcription PCR (RT-qPCR) with the qPCR lentivirus titration kit (Applied Biological Materials) with SsoFast™ EvaGreen® Supermix (Bio-Rad) according to the instructions of the manufacturer.

2.3.7 *Lentivirus transduction*

To determine the efficiency of the lentiviral transduction, myoblasts were transduced with viral particles made with GFP control DNA (pLJM1-EGFP). The number of viable myoblasts was quantified by trypan blue exclusion with a haemocytometer (see method in Section 2.3.5), seeded in a 96-well plate at 70% confluence in growth medium and allowed to recover for 24 hours at 37 °C in a humidified atmosphere containing 5% CO_2 and 10% O_2. Viral particles were diluted in myoblast growth medium and placed on the cells at a multiplicity of infection of 20. After 20 hours, the viral particles were removed and replaced with fresh growth medium. After a further 24 hours, the medium was removed, and the cells were briefly fixed with phosphate-buffered saline (PBS) containing 2% paraformaldehyde (Sigma-Aldrich®), permeabilised with PBS containing 0.1% Triton-X-100 (Sigma-Aldrich®), and blocked with PBS containing 5% bovine serum albumin (BSA; Sigma-Aldrich®) and 0.5% Tween 20 (Sigma-Aldrich®). This was then followed by a five-minute incubation with PBS containing 1 μg mL^{-1} DAPI (Thermo Fisher) for visualisation of nuclei. The cells were then covered with PBS and visualised with the Olympus IX83 inverted fluorescence microscope.

2.3.8 *Total protein extraction*

Extraction of protein was performed on cells grown in a T25 flask. Cells were by removed by treatment with 0.25% Trypsin-EDTA (Invitrogen™; see Section 2.3.2), transferred to a 15 mL tube, collected by centrifugation at 200 g, and then the pellet was resuspended in cOmplete™, Mini, EDTA-free protease inhibitor (Roche) in 150 μL cell lysis buffer (0.1 M Tris-HCl pH 7.8, 0.5% Triton X-100). The proteins were isolated by centrifugation at 16,000 g at 4 °C for 30 minutes and the supernatant was collected in a new micro-centrifuge tube. The proteins were further isolated by centrifugation at 16,000 g at 4 °C for one hour. The supernatant was placed in a fresh tube, the concentration of protein was determined by UV spectrophotometry (A280) with a DeNovix DS-11 FX+, and the sample was kept at –80 °C until use.

2.3.9 SDS polyacrylamide gel electrophoresis

Total protein (140 µg) extracted from mammalian cells was subjected to SDS polyacrylamide gel electrophoresis (SDS-PAGE). Each protein sample was mixed at 4:1 ratio with 5× sample buffer (0.3 M Tris-HCl pH 6.8, 50% glycerol, 10% SDS, 0.5% bromophenol blue, 25% β-mercaptoethanol) and loaded alongside Precision Plus Protein™ Dual Colour Standard (Bio-Rad) on a 4% SDS-PAGE stacking gel (4% acrylamide, 0.125 M Tris-HCl pH 6.8, 0.1% SDS, 0.1% APS, 0.4% TEMED). Proteins were resolved with a 7.5% SDS-PAGE separating gel (7.5% acrylamide, 0.37 M Tris-HCl pH 8.8, 0.1% SDS, 0.1% APS, 0.1% TEMED). The protein gel apparatus was filled with running buffer (25 mM Tris, 0.19 M glycine, 0.1% SDS) and samples separated by electrophoresis for two hours at 120 V with the Mini PROTEAN® electrophoresis system (Bio-Rad).

2.3.10 Western blotting

A BioTrace™ polyvinylidene difluoride (PVDF) membrane (0.45 µM; Pall Corp.) trimmed to size was activated by immersion in methanol (Thermo Fisher) for 30 seconds and then rinsed in water for one minute. The PVDF membrane and an SDS polyacrylamide gel with protein samples separated by electrophoresis were soaked in transfer buffer (15.6 mM Tris, 0.12 M Glycine, 10% MeOH) for ten minutes. The membrane was placed on top of the gel and both were sandwiched between Whatman® 3MM filter paper (two on each side; Thermo Fisher) trimmed to size, sponges (one on each side) in the blotting cassette, and then immersed in ice-cold transfer buffer. The proteins contained within the SDS polyacrylamide gel were transferred to the PVDF membrane in transfer buffer at 70 mA for 20 hours at 4 °C.

After the transfer, the membrane was blocked in 10 mL 5% trim milk (Anchor) in TBST (50 mM Tris, 0.15 M NaCl, 0.1% Tween 20, pH 7.6) for three hours at RT with gentle agitation before being cut in half crosswise. The membrane section with the higher molecular weight proteins was incubated with mouse 34C (anti-RyR1) primary antibody (Sigma-Aldrich®) diluted 1:1000 in 5 mL 2.5% trim milk in TBST for detection of RyR1. The membrane section with the lower molecular weight proteins was incubated with mouse

anti-α-tubulin primary antibody (Sigma-Aldrich®) diluted 1:5000 in 5 mL 2.5% trim milk in TBST for detection of α-tubulin as a protein loading control. These were incubated for 16 hours at 4 °C with gentle agitation and then a further twenty minutes at RT before being washed in 10 mL TBST. They were then incubated with horseradish peroxidase-conjugated anti-mouse secondary antibody (Promega) diluted 1:5000 in 5 mL 2.5% trim milk in TBST for one hour at RT with gentle agitation before being washed in 10 mL TBST.

BM Chemiluminescence Western Blotting Substrate (Roche) was prepared according to the instructions of the manufacturer and applied to both membranes for one minute before being removed and the membrane held between two transparency films (OfficeMax) cut to size. The proteins were visualised by chemiluminescent detection with the Azure™ Biosystems c600 imaging system with standard sensitivity settings and adjusting exposure time for each individual membrane.

2.3.11 Immunofluorescence

Cells grown in a four-chamber slide were washed with 0.25 mL PBS and then fixed with 0.25 mL PBS containing 2% paraformaldehyde (Sigma-Aldrich®) for 15 minutes. Cells were then briefly washed with 0.25 mL PBS. This step was repeated twice before permeabilisation with 0.25 mL PBS containing 0.1% Triton-X-100 (Sigma-Aldrich®) for five minutes. Cells were again briefly washed with 0.25 mL PBS. This step was repeated twice before the cells were blocked with 0.25 mL PBS containing 5% BSA (Sigma-Aldrich®) and 0.5% Tween 20 (Sigma-Aldrich®) for 30 minutes with gentle agitation. This was then followed by an overnight incubation with 0.25 mL PBS containing primary antibodies at 4 °C for 16 hours. Each chamber was incubated with both mouse 34C antibody (Sigma-Aldrich®) and mouse anti-protein disulphide isomerase (anti-PDI) antibody (Sigma-Aldrich®) for detection of RyR1 and the endoplasmic reticulum (ER), respectively. Antibodies were each diluted either 1:1000 for Flp-In™ T-REx™ 293 or HEK-293T cells or diluted 1:500 for myoblasts.

The cells were briefly washed with 0.25 mL PBS which was repeated twice. The cells were then incubated with 0.25 mL PBS containing goat anti-mouse fluorescein isothiocyanate

(FITC) secondary antibody (diluted 1:200, Sigma-Aldrich®) for detection of RyR1 and goat anti-rabbit tetramethylrhodamine isothiocyanate (TRITC) secondary antibody (diluted 1:200, Jackson ImmunoResearch) for detection of the ER. The cells were briefly washed with 0.25 mL PBS which was repeated twice. The chambers were removed from the slide and a coverslip applied with ProLong® Gold AntiFade mountant containing the fluorescent DNA stain 4′,6-diamidino-2-phenylindole (DAPI) for detection of nuclei (Invitrogen™). This was cured for 24 hours in the dark before the coverslip was sealed with transparent nail polish and the cells visualised with a Leica SP5 DM6000B Scanning Confocal Microscope at 1260× magnification.

2.3.12 Calcium release assays

Cells were grown in a UV-transparent 96-well plate (Greiner) coated with 0.1 mg mL^{-1} poly-D-lysine (reusable up to five times; Sigma-Aldrich®) to 90% confluence in a humidified atmosphere containing 5% CO_2 (and 10% O_2 for myoblasts). Myoblasts were differentiated into myotubes by incubation in differentiation media. The medium on the cells was replaced with 100 µL balanced salt solution (BSS) buffer (1 mM $MgCl_2$, 0.14 M NaCl, 2.8 mM KCl, 10 mM HEPES pH 7.3) containing 2 mM $CaCl_2$ at 37 °C. These were then incubated in 100 µL premixed loading solution per well for one hour at 37 °C in the dark. This loading solution comprised BSS buffer, 2 mM $CaCl_2$, 2 µM Fura-2 AM (Thermo Fisher), and 0.01% Pluronic F-127 to increase solubility of the dye (Sigma-Aldrich®). Cells were then briefly washed with 100 µL BSS buffer warmed to 37 °C and then 100 µL fresh BSS buffer warmed to 37 °C was placed on the cells. These steps were conducted with minimal exposure to light. Cells were assayed immediately, and assays were concluded within 40 minutes of Fura-2 loading.

Activation of the RyR1 with 4-chloro-*m*-cresol (4-c*m*c; VWR) as a specific agonist was measured by the change in the fluorescence emission ratio at 510 nm when excited by wavelengths 340 nm and 380 nm with an Olympus IX81 inverted fluorescence microscope. Each well was assayed individually by measuring either a representative region of the well with several hundred FT-293 cells at 100× magnification or several individual myotubes at 600× magnification. A fluorescence ratio baseline was first established in 100 µL BSS

Ca^{2+}-free buffer before measuring the change in fluorescence after the addition of 100 µL Ca^{2+}-free BSS buffer containing 4-c*m*c. The final concentrations of 4-c*m*c used with FT-293 and HEK-293T were 0, 200, 300, 400, 600, 800, 1000, 1200 µM whereas those used with HMCL-7304 cells were 0, 200, 300, 400, 600, 800, 900, 1000 µM.

2.4 Data analysis

2.4.1 DNA sequence nomenclature

The description of genetic variants in the ryanodine receptor 1 gene (*RYR1)* coding DNA is according to the sequence with GenBank accession NM_000540.2 whereas variants in RyR1 protein is according to the sequence with GenBank accession NP_000531.2. The genomic sequence of the *RYR1* gene is based on the sequence with GenBank accession NG_008866.1.

2.4.2 Microscopic images

ImageJ software was used to process and merge microscopic images and to add scale bars.[258]

2.4.3 Statistical analysis

Ca^{2+} release assays to establish the responsiveness of RyR1 to the specific agonist 4-c*m*c were performed on mammalian cells. The amount of Ca^{2+} release at each concentration of 4-c*m*c was normalised to account for any differences between assays and calculated as a percentage of the total Ca^{2+} released with 1000 µM 4-c*m*c. A minimum of five biological replicates was performed for each value of 4-c*m*c used. The data were pooled, and a sigmoidal curve fitted for each dataset with CurveExpert software (Hyams Development).

Results were presented as the mean ± standard error of the mean (SEM) for each value of 4-c*m*c used. The half maximal effective concentration (EC_{50}) values were calculated from individual sigmoidal curves and then used to calculate the mean EC_{50} ± SEM for each dataset. *P*-values were calculated for each dataset with an unpaired Student's *t*-test and analysed for statistical significance with 99% confidence. The original α-value of 0.01 for

statistical significance was adjusted for multiple comparisons by the Bonferroni correction. An α-value of 2×10^{-3} was used for data from the stable expression lines and 3.3×10^{-3} for data after transient expression of *RYR1* cDNA.

3 Stable expression lines

3.1 Heterologous expression of RyR1

According to the American College of Medical Genetics and Genomics, the classification of allelic variants as being the underlying cause of disease relies on several criteria that may include segregation analysis, frequency of the variant in the general population, *in silico* analysis, and functional studies.[259] The main criterion used for classifying variants in the ryanodine receptor 1 gene (*RYR1*) as being causal for malignant hyperthermia (MH) is the functional characterisation of each variant. According to the European malignant hyperthermia group, this establishes variants of unknown significance as diagnostic variants for MH.[16] The purpose of this research was to use new experimental techniques to show that genetic variants alter the function of the ryanodine receptor 1 (RyR1) Ca^{2+} channel in such a way that would contribute to the MH phenotype.

Currently, the simplest method of assessing whether a genetic variant may cause the altered phenotype associated with MH-susceptibility is to introduce complementary DNA (cDNA) with that variant into a host cell line such as human embryonic kidney 293 (HEK-293). Mutant and wild-type (WT) RyR1 channels are expected to respond differently in the presence of agonist; accordingly, by way of comparison with that of the WT and an appropriate MH positive control, the phenotypes of variants can be deduced. This analysis is performed by transfection of HEK-293 cells with *RYR1* cDNA with variants for their transient expression. HEK-293 cells are ideal for functional characterisation of *RYR1* variants because they provide a reliable platform for the analysis of protein function with high transfection efficiency and robust protein production.[260] However, this method is disadvantaged by variable transfection efficiency because multiple biological replicates—and therefore transfection events—are required to reach statistical significance.[261]

3.1.1 The Flp-In™ T-REx™ system

In this study, mammalian cell lines were transfected with *RYR1* cDNA by use of the Flp-In™ T-REx™ system from Invitrogen™ for stable integration into the genome. These stable expression lines were used to analyse the function of variants in *RYR1* as a heterologous system. The method used flippase (Flp) recombinase to enable the stable introduction of

cDNA into an integrated Flp recombination target (FRT) site located in a transcriptionally active location of the genome of the host cell.[262,263] Potential positional effects were eliminated with the use of selection markers in the form of antibiotic resistance, ensuring that introduced cDNAs always integrated at the same genomic locus. Additionally, *RYR1* transcription was under the control of dual operator sites upstream of the *Cytomegalovirus* (CMV) promoter. The binding of repressor molecules to these operators caused repression of the promoter that could only be reversed in the presence of tetracycline.

The host cell line used in this research was the Flp-In™ T-REx™ 293 (FT-293; RRID: CVCL_U427) cell line sourced from Invitrogen™. It was originally created by the random introduction of two sets of genetic elements into the genome of the HEK-293 cell line as shown in Figure 3.1A. The first genetic element contained a zeocin resistance gene under the control of an SV40 promoter with an FRT site placed directly downstream of the start codon. The second genetic element contained a tetracycline repressor gene under the control of a CMV promoter and a blasticidin resistance gene under control of an SV40 promoter. These combined to make the host cell line resistant to two antibiotics, blasticidin and zeocin. The expression vector that was used with this system was the pcDNA™5/FRT/TO vector (plasmid map in Appendix B.1). The *RYR1* cDNA was subcloned into pcDNA™5/FRT/TO such that it was under the control of a CMV promoter and two tetracycline operator sequences upstream of an FRT site; this was renamed the ftRYR1 expression vector (schematic in Figure 3.1A; plasmid map in Appendix B.2). Directly downstream of this FRT site was a hygromycin antibiotic resistance gene lacking both a promoter and start codon.

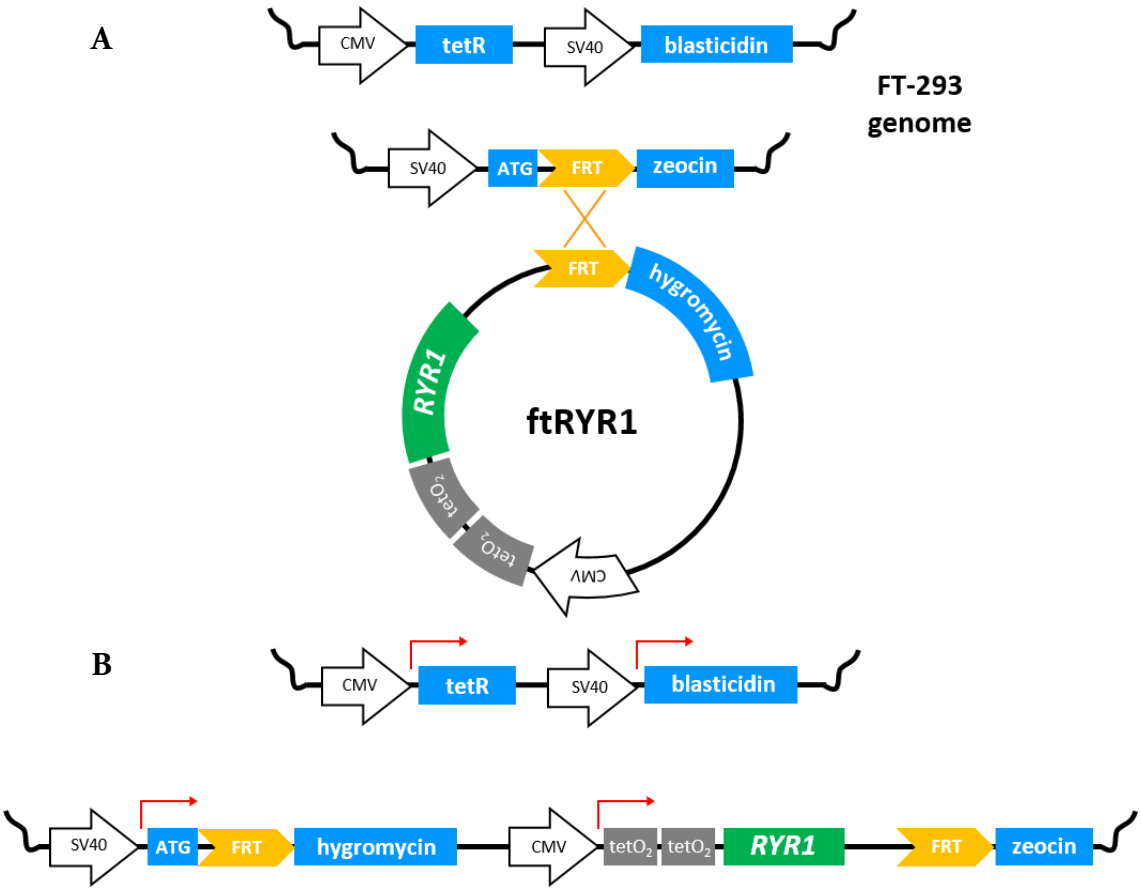

Figure 3.1 Schematic of the Flp-In™ T-REx™ system

A Genetic elements contained in the FT-293 host cell line genome are shown. Flp recombinase-mediated integration of the ftRYR1 expression vector with ryanodine receptor 1 (*RYR1*) cDNA (green) occurred between Flp recombinase target (FRT) sites (yellow) into the genome of the FT-293 host cell line. **B** Orientation of genetic elements introduced into the genome of FT-293 by use of FRT sites. Expression of genes are indicated by red arrows. *Figure created by the Author.*

The creation of stable expression lines was achieved by the co-transfection of the host cell line with ftRYR1 and the pOG44 plasmid that constitutively expresses Flp recombinase under the control of a CMV promoter (plasmid map in Appendix B.3). This transfection enabled the recombination of the FRT sites and therefore the integration of *RYR1* cDNA into this transcriptionally active region (schematic in Figure 3.1B). Correct integration placed the hygromycin resistance gene directly downstream of the zeocin promoter and start codon; thus, enabling transcription of the hygromycin resistance gene and preventing transcription of the zeocin resistance gene (schematic in Figure 3.1B). The resulting FT-293 expression cell line would become resistant to hygromycin and sensitive

to zeocin (and remain resistant to blasticidin); accordingly, successful integration of *RYR1* cDNA into the genome was monitored by selecting for these traits. Finally, addition of tetracycline to the cells enabled de-repression of the promoter controlling *RYR1* transcription.

3.2 *Analysis of ryanodine receptor 1 variants*

The genetic backgrounds of five individuals who presented with a disease phenotype typical of abnormal RyR1 function were examined. Four of those individuals (from Families A, B, C, and E) were identified with a susceptibility to MH after they experienced an adverse reaction during anaesthesia, one of whom also presented with a myopathy (Table 3.1). A single *RYR1* variant was identified in all four individuals; these variants were subsequently predicted to be disease-causing by *in silico* analysis (described in Section 3.2.6). The fifth individual (from Family D) presented with a non-specific myopathy; this individual was subsequently found to have two *RYR1* allelic variants—one variant was of unknown significance whereas the other was known to affect function.[264,265] Where possible, segregation analyses were performed for each pedigree to assess the likelihood of these variants being the cause of MH-susceptibility.

Table 3.1 Overview of ryanodine receptor 1 variants examined

Pedigree	Phenotype	Ryanodine receptor variant/s
Family A	MH	c.38T>G, p.Leu13Arg
Family B	MH / myopathy	c.1390C>A, p.Gln464Lys
Family C	MH	c.1615T>C, p.Phe539Leu
Family D	myopathy	c.5119C>T, p.Arg1707Cys c.14545G>A, p.Val4849Ile
Family E	MH	c.8378C>T, p.Pro2793Leu

3.2.1 *Segregation analysis of RyR1 variants*

Family A

The *RYR1* c.38T>G variant (p.Leu13Arg in RyR1) was identified in the proband (individual II-2) of Family A after a fulminant MH reaction whilst undergoing surgery. The MH phenotype of the proband was confirmed by *in vitro* contracture testing (IVCT) after which he was diagnosed as MH-susceptible (MHS_{hc}). Segregation analysis in the pedigree was not definitive because only one other family member was tested by IVCT (Figure 3.2). The mother of the proband (individual I-1) was diagnosed as MH-negative (MHN) by IVCT and sequencing confirmed the absence of the *RYR1* c.38T>G (RyR1 p.Leu13Arg) variant whereas the father tested positive for the familial variant but was not tested by IVCT.

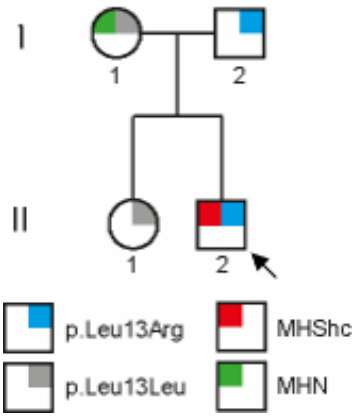

Figure 3.2 Pedigree chart of Family A

Segregation analysis of Family A. Top left corner denotes malignant hyperthermia (MH) diagnosis and top right corner denotes presence or absence of the *RYR1* c.38T>G (RyR1 p.Leu13Arg) variant. Absence of colour indicates this information is not known. The proband is labelled with an arrow.

Family B

The *RYR1* c.1390C>A variant (RyR1 p.Gln464Lys) was identified in the proband (individual III-8) of Family B after they died following anaesthesia (Figure 3.3). Although the proband was not tested for genetic variants, several family members underwent genetic testing and IVCT which enabled segregation analysis in this pedigree (Figure 3.3). Five individuals

(II-3, III-1, III-5, III-6, and IV-1) were diagnosed as MHS_{hc} by IVCT and were positive for the RyR1 p.Gln464Lys variant. Four of those family members were also diagnosed with a non-specific myopathy. One individual, III-2, was diagnosed as MHN by IVCT and they were subsequently confirmed as negative for the RyR1 p.Gln464Lys variant by genetic testing.

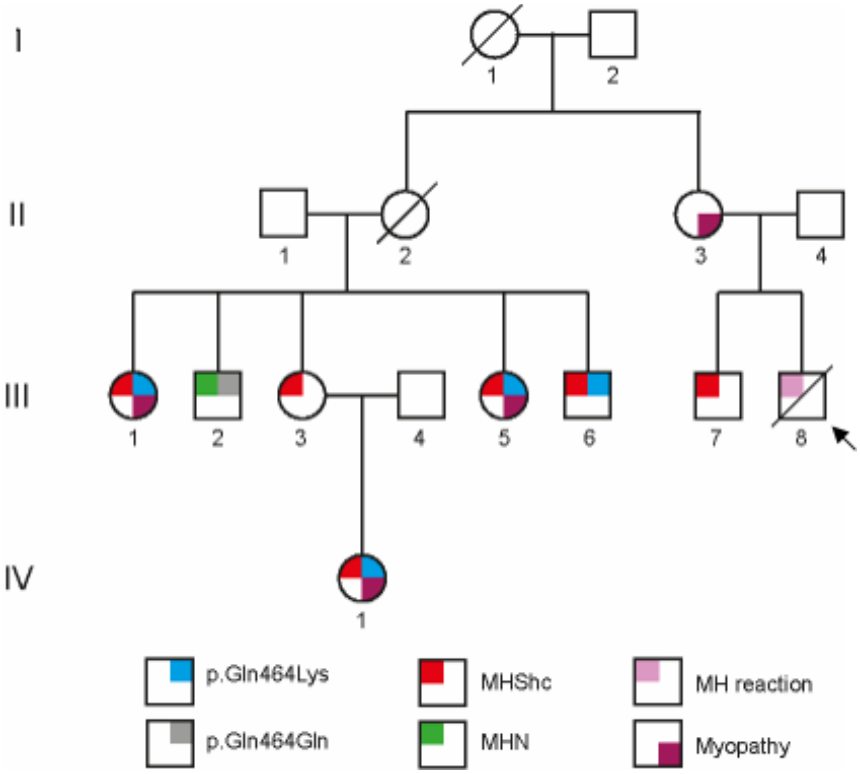

Figure 3.3 Pedigree chart of Family B

Segregation analysis in Family B. Top left corner denotes malignant hyperthermia (MH) diagnosis, bottom right corner indicates the myopathy diagnosis and top right corner denotes presence or absence of the *RYR1* c.1390C>A (RyR1 p.Gln464Lys) variant. Absence of colour indicates this information is not known. The proband is labelled with an arrow.

Family C

The *RYR1* c.1615T>C variant (p.Phe539Leu in RyR1) was identified in the proband (individual III-3) of Family C following a fatal MH reaction whilst undergoing surgery for a fractured jaw (Figure 3.4). Because the proband was unable to be tested for genetic

variants, several members of the family were available for segregation analysis by IVCT and genetic testing (Figure 3.4). The RyR1 p.Phe539Leu variant was identified in several family members and, where comparisons between genotype and phenotype were possible, the variant segregated with the IVCT result. The RyR1 p.Phe539Leu variant was found in all individuals diagnosed as MHS (n = 4) whereas those diagnosed as MHN did not have the genetic variant (n = 5).

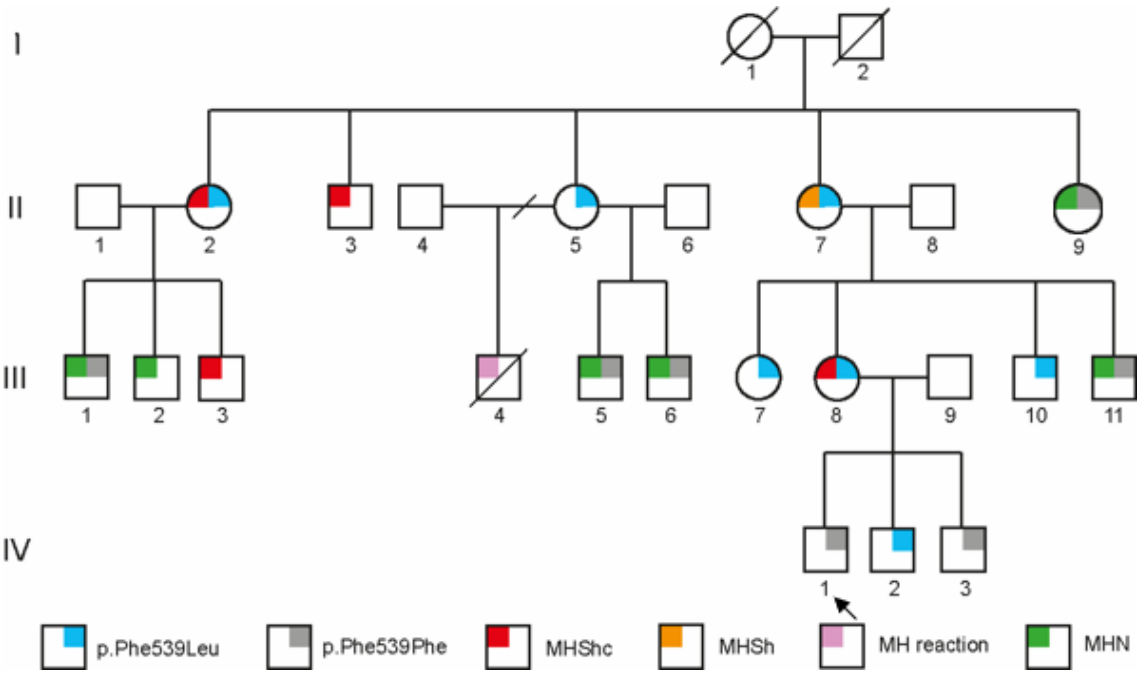

Figure 3.4 Pedigree chart of Family C

Segregation analysis in Family C. Top left corner denotes malignant hyperthermia (MH) diagnosis and top right corner denotes presence or absence of the *RYR1* c.1615T>C (RyR1 p.Phe539Leu) variant. Absence of colour indicates this information is not known. The proband is labelled with an arrow.

Family D

The proband (individual II-1) of Family D presented with a non-specific myopathy and, upon subsequent genetic testing, two *RYR1* variants were identified: c.5119C>T (RyR1 p.Arg1707Cys) and c.14515G>A (RyR1 p.Val4849Ile; Figure 3.5). Genetic screening of the parents determined that the mother of the proband possessed the RyR1 p.Arg1707Cys variant and the father had the RyR1 p.Val4849Ile variant; however, both were

asymptomatic for the myopathy. Although the RyR1 p.Arg1707Cys variant was a novel genetic change, the RyR1 p.Val4849Ile variant has been linked to both CCD and MH-susceptibility as a homozygous allele in several families.[201,266-269] In instances for which only one copy of the RyR1 p.Val4849Ile allele is present, there are generally no symptoms of disease, unless the other allele contains a null mutation.[264,266,270] This leaves room for the possibility that the RyR1 p.Val4849Ile variant may be a recessive allele and requires the presence of another variant such as RyR1 p.Arg1707Cys to produce a disease phenotype.

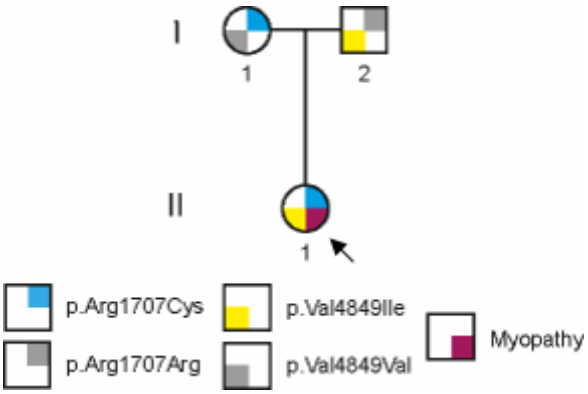

Figure 3.5 Pedigree chart of Family D

Segregation analysis in Family D. Bottom right corner indicates diagnosis of myopathy, top right corner denotes presence or absence of the *RYR1* c.5119C>T (RyR1 p.Arg1707Cys) variant and bottom right corner denotes presence or absence of the *RYR1* c.14545G>A (RyR1 p.Val4849Ile) variant. Absence of colour indicates this information is not known. The proband is labelled with an arrow.

Family E

The *RYR1* c.8378C>T variant (p.Pro2793Leu in RyR1) was identified in the proband (individual II-2) of Family C after he experienced a fulminant reaction while undergoing anaesthetic for surgery (Figure 3.6). No other information was available about this family except for a sibling of the proband who was found also to have the variant.

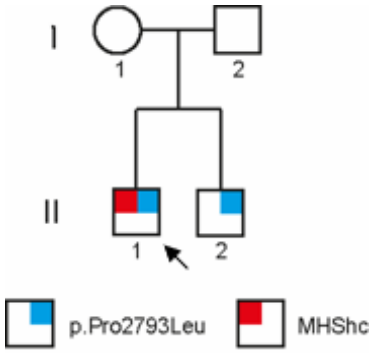

Figure 3.6 Pedigree chart of Family E

Segregation analysis in Family E. Top left corner denotes malignant hyperthermia (MH) diagnosis and top right corner denotes presence or absence of the *RYR1* c.8378C>T (RyR1 p.Pro2793Leu) variant. Absence of colour indicates this information is not known. The proband is labelled (arrow).

3.2.2 Conservation of the wild-type alleles

When analysing a genetic variant predicted to be disease-causing, the first criterion used is a low incidence of the variant in the general population, known as the minor allele frequency (MAF). A MAF of less than 1×10^{-3} (or 0.1%) in two genetic databases, Exome Variant Server (EVS) and Exome Aggregation Consortium (ExAC), is one criterion for a variant to affect function in the instance of MH-susceptibility because this disorder is rare.

None of the five genetic variants in this study were included in the EVS database whereas the only variant found in ExAC was RyR1 p.Pro2793Leu with a low MAF of 9.9×10^{-6} (Table 3.2). This indicated that all five RyR1 variants were rare, as would be expected for MH. The p.Pro2793 residue also had an alternative substitution in RyR1, p.Pro2793Ser, which had a low MAF in both databases (Table 3.2). The other residue with an alternative substitution in RyR1 was p.Arg1707. The p.Arg1707His substitution was found in both databases with low MAF values of 7.7×10^{-5} (EVS) and 1.7×10^{-5} (ExAC). All substitutions at these residues were uncommon and therefore confirm that these residues are generally conserved.

Differences in the MAFs between databases can be explained by the difference in the populations sampled, the number of samples and the data collection methods used. In short, the EVS contains data of over 6,000 exomes from a predominantly African American

and European American population whereas the ExAC database contains data from over 60,000 exomes from a diverse population.

Table 3.2 Minor allele frequency values for ryanodine receptor variants

Ryanodine receptor 1 residue	Alternative residue	Minor allele frequency	
		Exome Variant Server	Exome Aggregation Consortium
p.Leu13	Arg	–	–
p.Gln464	Lys	–	–
p.Phe539	Leu	–	–
p.Arg1707	Cys	–	–
	His	7.7×10^{-5}	1.7×10^{-5}
p.Pro2793	Leu	–	9.9×10^{-6}
	Ser	1.5×10^{-4}	2.0×10^{-5}

As variants that affect function are expected to involve conserved residues, the evolutionary conservation of the amino acids affected by the *RYR1* variants was investigated. All five amino acids were conserved in the three human ryanodine receptor isoforms in addition to that of zebrafish and several mammalian species (Table 3.3). This indicated that a substitution of these residues may not be tolerated within the protein.

Table 3.3 Comparison of ryanodine receptor alleles between species

Ryanodine receptor	GenBank accession	Amino acid residue				
		13	464	539	1707	2793
Human RyR1	NP_000531.2	Leu	Gln	Phe	Arg	Pro
Human RyR2	NP_001026.2	Leu	Gln	Phe	Arg	Pro
Human RyR3	NP_001027.3	Leu	Gln	Phe	Arg	Pro
Pig RyR1	NP_001001534.1	Leu	Gln	Phe	Arg	Pro
Rabbit RyR1	NP_001095188.1	Leu	Gln	Phe	Arg	Pro
Mouse RyR1	NP_033135.2	Leu	Gln	Phe	Arg	Pro
Zebrafish RyR1b	NP_001096041.1	Leu	Gln	Phe	Arg	Pro

3.2.3 In silico analysis RyR1 variants

Three different prediction algorithms were used to analyse the amino acid substitutions in this study (results in Table 3.4). They were MutPred2, Protein Variant Effect Analyser (PROVEAN), and the weighted form of Functional Analysis Through Hidden Markov Models (FATHMM). These were chosen based on a study which compared the predictive power of 17 *in silico* analysis programs by use of a data set with reliably designated, autosomal dominant, gain-of-function variants—both pathogenic and benign—analogous to MH.[271] In this study, MutPred2, PROVEAN, and weighted FATHMM were found to have accuracy rates of 83%, 74%, and 81%, respectively. Indeed, those three performed substantially better than the commonly used prediction programs PolyPhen2, SIFT, and Mutation Taster, which had reported accuracies of 66%, 63%, and 59%, respectively.[271]

MutPred2 categorises variants as benign if the score is below the threshold of 0.5, possibly pathogenic if it is between 0.5 and 0.75, and pathogenic if the score is above the threshold of 0.75.[271,272] PROVEAN defines a variant as neutral if the PROVEAN score is above the

threshold of –2.5, possibly damaging if it is between –2.5 and –4.1, and damaging if the score is below the threshold of –4.1.[271,273] Weighted FATHMM produces a prediction of an amino acid substitution as being either tolerated or damaging, based on the score being above or below the threshold of –1.5, respectively.[271,274]

Table 3.4 Results from pathogenicity prediction software

Ryanodine receptor 1 variant	MutPred2		PROVEAN		FATHMM	
	Score	Prediction	Score	Prediction	Score	Prediction
p.Leu13Arg	0.95	pathogenic	–3.58	possibly deleterious	–5.83	damaging
p.Gln464Lys	0.51	possibly pathogenic	–3.57	possibly deleterious	–3.79	damaging
p.Phe539Leu	0.89	pathogenic	–5.21	deleterious	–3.39	damaging
p.Arg1707Cys	0.88	pathogenic	–7.81	deleterious	–0.88	tolerated
p.Pro2793Leu	0.80	pathogenic	–8.74	deleterious	–3.06	damaging

Of the five RyR1 variants analysed in this way, only RyR1 p.Phe539Leu and RyR1 p.Pro2793Leu yielded a consensus (disease-causing) when predicted by all three programmes. The RyR1 p.Leu13Arg variant had high scores for two of the applications whereas its PROVEAN score almost reached the threshold, and thus was likely to affect function. Two of the variants were classed as being likely to affect function by two programmes whereas the third result was not concordant. The RyR1 p.Gln464Lys variant narrowly reached the MutPred2 threshold for pathogenicity whereas the RyR1 p.Arg1707Cys substitution was predicted to be tolerated by FATHMM. This reinforces the

need to use more than one bioinformatic algorithm to evaluate potential genetic variants of interest. The use of one programme may eliminate one or more variants, whereas these results, when taken together, provide evidence that all five should be investigated further. Bioinformatic predictions should also be accepted with caution because this is only one of many criteria that can be used to analyse genetic variants.

3.3 *Construction of expression vectors*

To create the expression vectors used to make the stable expression lines, human *RYR1* cDNAs were cloned into the pcDNA™5/FRT/TO vector as shown in the schematic in Figure 3.8A (plasmid map in Appendix B.1). The cDNAs were sourced from plasmids with the full-length human *RYR1* cDNA in a pcDNA™3.1+ vector (pcRYR1; map in Appendix B.4).[240] The immense size of the *RYR1* cDNA meant that there were few unique restriction endonuclease recognition sites flanking *RYR1* that were not present within the cDNA sequence or the pcDNA™5/FRT/TO vector backbone; therefore, the design of a suitable cloning strategy was not trivial.

The approach required the introduction of three additional restriction endonuclease recognition sites (NheI, KpnI, and AvrII) within the multiple cloning site (MCS) of the pcDNA™5/FRT/TO vector. These were used in two steps to subclone the two halves of the WT *RYR1* cDNA into this vector. This full-length clone was then used to create full-length plasmids with the five *RYR1* variants to be studied: *RYR1* c.38T>G (RyR1 p.Leu13Arg), *RYR1* c.1390C>A (RyR1 p.Gln464Lys), *RYR1* c.1615T>C (RyR1 p.Phe539Leu), *RYR1* c.5119C>T (RyR1 p.Arg1707Cys), and *RYR1* c.8378C>T (RyR1 p.Pro2793Leu). A full-length clone was also created for the *RYR1* c.14477C>T (RyR1 p.Thr4826Ile) variant as an MH positive control (Figure 3.7).[246]

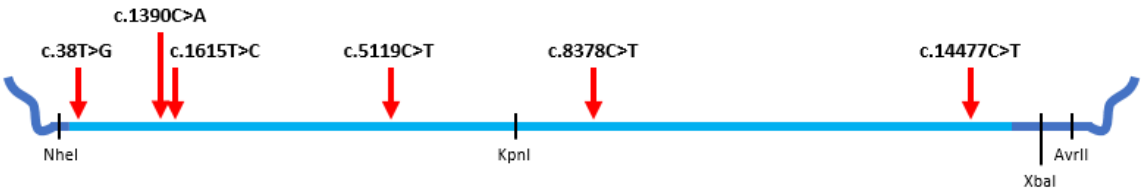

Figure 3.7 Relative locations of variants in ryanodine receptor 1 cDNA

Schematic of ryanodine receptor 1 cDNA (light blue) in the ftRYR1 vector (dark blue) with the relative locations of restriction endonuclease recognition sites labelled. Locations of variants within the ryanodine receptor cDNA are indicated with arrows: *RYR1* c.38T>G (RyR1 p.Leu13Arg), *RYR1* c.1390C>A (RyR1 p.Gln464Lys), *RYR1* c.1615T>C (RyR1 p.Phe539Leu), *RYR1* c.5119C>T (RyR1 p.Arg1707Cys), *RYR1* c.8378C>T (RyR1 p.Pro2793Leu), and *RYR1* c.14477C>T (RyR1 p.Thr4826Ile).

3.3.1 Creation of the pcFT cloning vector

To alter the MCS of the original pcDNA™5/FRT/TO vector, two complementary oligonucleotides were designed that, when annealed together, contained the three restriction endonuclease recognition sites for subsequent use (NheI, KpnI, and AvrII) in an appropriate order (plasmid map in Appendix A.3). The oligonucleotides had 5' overhangs to allow for direct ligation into the existing MCS of pcDNA™5/FRT/TO with the BamHI and HindIII restriction endonuclease sites, creating the new cloning vector, pcFT (schematic in Figure 3.8A; plasmid map in Appendix B.5). The identity of the newly created 5.2 kb pcFT vector was confirmed by restriction endonuclease digestion with KpnI and SphI enzymes. These were estimated to give DNA fragments of 324 bp and 4.8 kb (Figure 3.8B). Correct ligation was further confirmed by Sanger sequencing across the new multiple cloning site (Figure 3.8C).

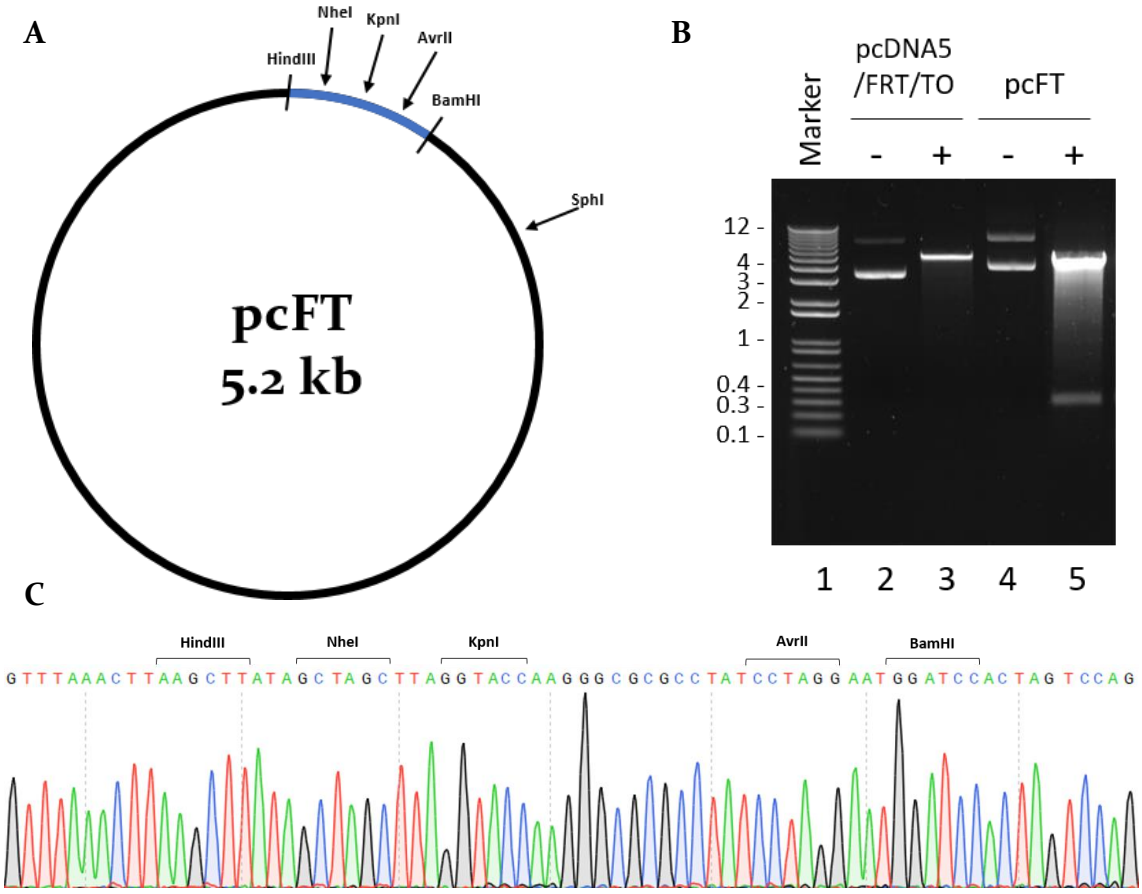

Figure 3.8 Creation of the pcFT cloning vector

A Plasmid map of the pcFT vector after alteration of the multiple cloning site in the pcDNA™5/FRT/TO plasmid. Shown are vector DNA (black), insert DNA (blue), and restriction endonuclease recognition sites. **B** Restriction endonuclease double digestion (+) of the pcDNA™5/FRT/TO and pcFT plasmids with KpnI and SphI enzymes and undigested (–) controls (Section 2.2.4). Samples were subjected to electrophoresis in a 1% agarose gel containing ethidium bromide and immersed in buffer (Section 2.2.3). Lane 1 contains 1 Kb Plus DNA Ladder with the fragment lengths indicated in kb. **C** Chromatogram of Sanger sequencing results of the new multiple cloning site in the pcFT vector with restriction endonuclease recognition sites indicated.

3.3.2 *Creation of the pcFTN cloning vector*

The first step in subcloning the full-length *RYR1* cDNA into the newly created pcFT vector was to insert the 5' half of the cDNA from pcRYR1 (corresponding to the N-terminal half of the gene product) into pcFT by use of directional cloning. The 5.2 kb vector and 7.0 kb insert sequences were prepared by restriction endonuclease digestion with NheI and KpnI

enzymes. These were subsequently ligated together, producing the pcFTN plasmid comprising the pcFT vector backbone and the 5' half of *RYR1* cDNA (Figure 3.9A; plasmid map in Appendix B.6). The identity of the newly created 12.2 kb pcFTN vector was confirmed by digestion with the restriction endonucleases HindIII and EcoRV. These were predicted to give two DNA fragments of 5.1 kb and 7.1 kb (Figure 3.9B). Correct ligation was further confirmed by Sanger sequencing across the ligation sites (Figure 3.9C).

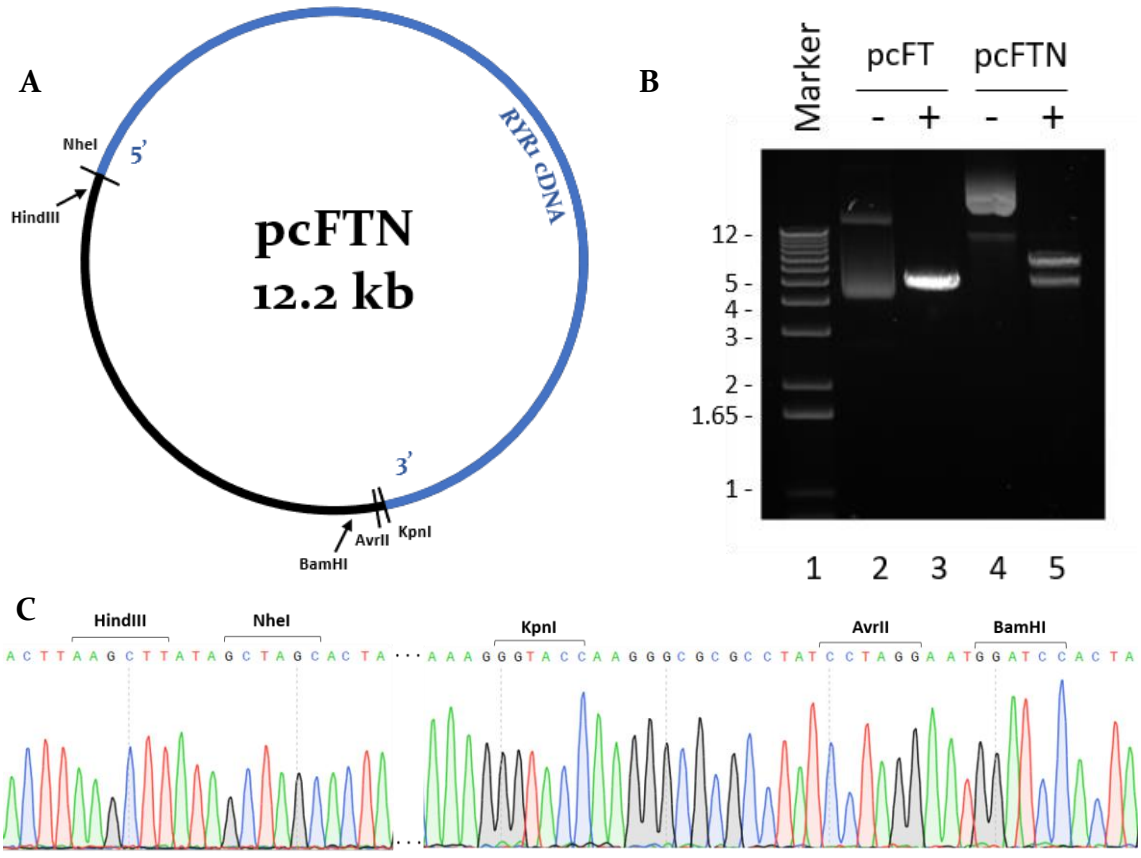

Figure 3.9 Creation of the pcFTN plasmid

A Plasmid map of the 12.1 kb pcFTN plasmid after cloning of the 7 kb *RYR1* insert (blue) into the 5.2 kb pcFT vector (black). Relative locations of relevant restriction endonuclease recognition sites are indicated. **B** Restriction endonuclease double digestion (+) of pcFT and pcFTN plasmids with HindIII and EcoRV enzymes alongside undigested (–) controls (Section 2.2.4). Samples were subjected to electrophoresis in a 1% agarose gel containing ethidium bromide and immersed in buffer (Section 2.2.3). Lane 1 contains 1 Kb Plus DNA Ladder with fragment lengths indicated in kb. **C** Chromatogram of Sanger sequencing results over the ligation sites of the pcFTN vector with restriction endonuclease recognition sites indicated. Region between NheI and KpnI recognition sites with *RYR1* cDNA sequence (not sequenced) is indicated with '...'.

3.3.3 *Creation of full-length ftRYR1 expression vectors*

The 3' half of *RYR1* cDNA (9.3 kb; corresponding to the C-terminal half of the gene product) was cloned into the pcFTN vector by use of directional cloning. The 9.3 kb *RYR1* insert sequence was ligated into the 12.1 kb vector after restriction endonuclease double digestion with the enzymes KpnI and AvrII (Figure 3.10A). This produced the full-length WT expression vector (21.4 kb; ftRYR1) comprising the pcFT vector backbone and the full-length *RYR1* cDNA (see schematic in Figure 3.10A; plasmid map in Appendix B.2).

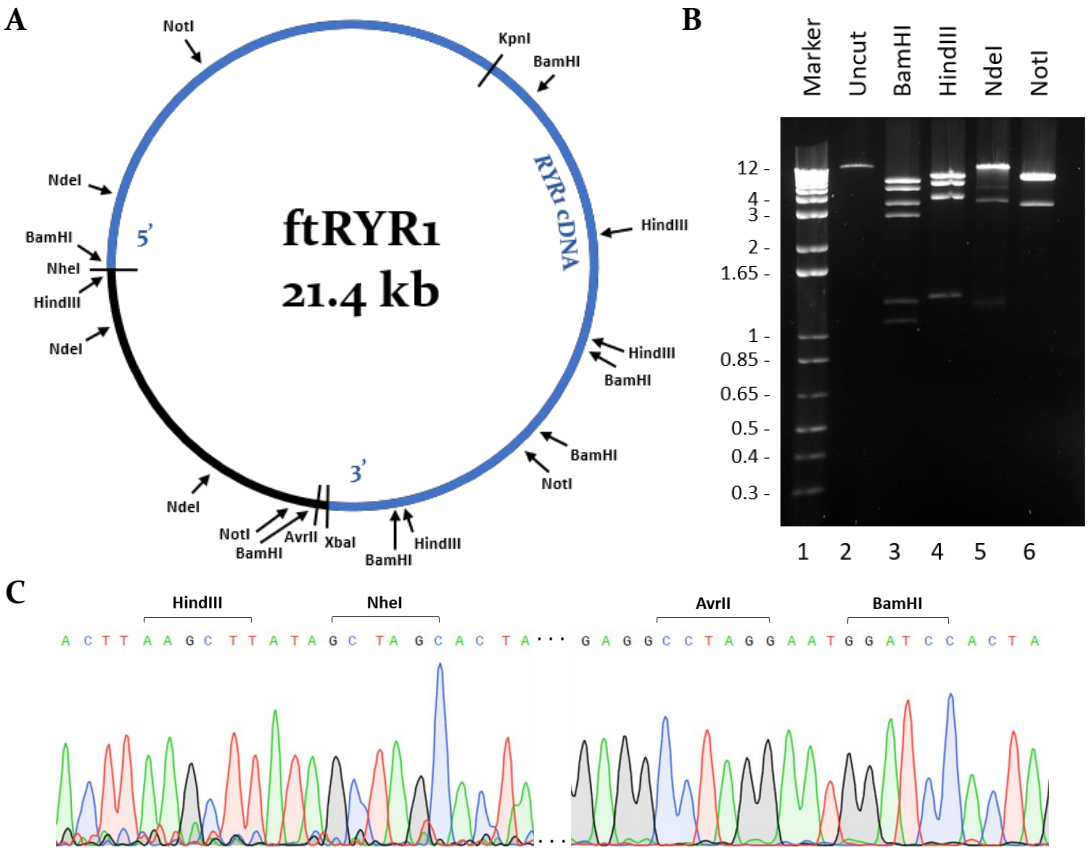

Figure 3.10 Creation of the ftRYR1 expression vector

A Map of ftRYR1 after cloning the 12.1 kb pcFTN vector and the 9.3 kb C-terminal *RYR1* insert. The relative locations of relevant recognition sites are indicated. **B** Wild type ftRYR1 was digested with BamHI, HindIII, NdeI, and NotI restriction endonucleases and subjected to electrophoresis in a 0.8% agarose gel containing ethidium bromide and immersed in buffer (Section 2.2.3). Lane 2 contains uncut DNA. Lane 1 contains 1 Kb Plus DNA Ladder with the fragment lengths indicated in kb. **C** Chromatogram of Sanger sequencing results over the flanking ligation sites of the ftRYR1 vector with restriction endonuclease recognition sites of interest indicated. Region between NheI and AvrII recognition sites with *RYR1* cDNA sequence (not sequenced) is indicated with '...'.

The identity of ftRYR1 was confirmed by restriction endonuclease digestion with BamHI, HindIII, NdeI, and NotI enzymes (Figure 3.10B; see Table 3.5 for predicted fragment lengths). This was followed by Sanger sequencing across the flanking ligation sites (Figure 3.10C). The creation of full-length expression plasmids with *RYR1* variants using this ftRYR1 vector was then conducted by Dr Anja Schiemann and Jeremy Stephens.

Table 3.5 Expected results of restriction endonuclease digestion of ftRYR1

Restriction endonuclease	Predicted fragment lengths (kb)
BamHI	1.1, 1.3, 2.9, 3.6, 5.1, 7.4
HindIII	1.3, 4.3, 6.2, 9.6
NdeI	1.2, 3.5, 16.7
NotI	3.4, 8.4, 9.6

Almost all full-length variants (*RYR1* c.38T>G, RyR1 p.Leu13Arg; *RYR1* c.1390C>A, RyR1 p.Gln464Lys; *RYR1* c.1615T>C, RyR1 p.Phe539Leu; *RYR1* c.5119C>T, RyR1 p.Arg1707Cys; *RYR1* c.14477C>T, RyR1 p.Thr4826Ile) were created by replacing either the 5' or 3' half of the WT *RYR1* cDNA with that containing a variant by use of the same restriction sites used previously, reconstructing the ftRYR1 plasmid. The full-length *RYR1* c.8378C>T (RyR1 p.Pro2793Leu) cDNA, however, was cloned by ligating together the same 12.1 kb pcFTN vector with an 8.3 kb *RYR1* insert sequence from a vector that was modified to have an AvrII recognition site. This method produced the full-length expression vector a-ftRYR1, also comprising the pcFT vector backbone and the full-length *RYR1* cDNA (plasmid map in Appendix B.7). The identities of the WT and variant constructs were confirmed by restriction endonuclease digestion with BamHI, HindIII, NdeI, and NotI enzymes and Sanger sequencing (see digests in Appendix C.1; sequencing results in Figure 3.11).

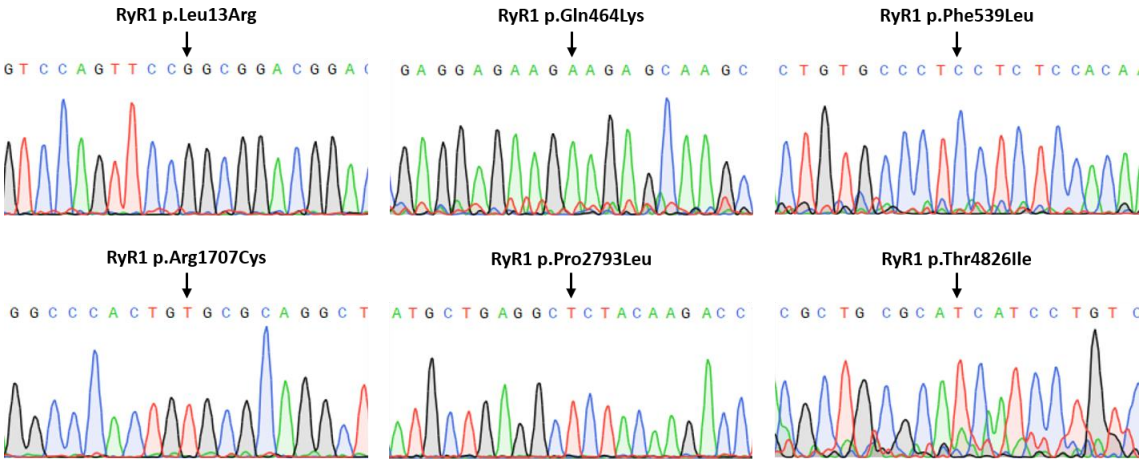

Figure 3.11 Sanger sequencing of variants in expression vectors

Chromatograms of Sanger sequencing results from each region of the expression vector with the variants (arrow) introduced: RyR1 p.Leu13Arg (c.38T>G ftRYR1), RyR1 p.Gln464Lys (c.1390C>A ftRYR1), RyR1 p.Phe539Leu (c.1615T>C ftRYR1), RyR1 p.Arg1707Cys (c.5119C>T ftRYR1), RyR1 p.Pro2793Leu (c.8378C>T a-ftRYR1), and RyR1 p.Thr4826Ile (c.14477C>T ftRYR1).

3.4 *Creation of stable expression lines*

In total, eight stable FT-293 expression lines were created: the empty vector (pcFT) as a negative RyR1 control; WT ftRYR1 as an negative MH control; c.14477C>T (RyR1 p.Thr4826Ile) ftRYR1 as a positive MH control; and the full-length *RYR1* variants of interest: c.38T>G (RyR1 p.Leu13Arg), c.1390C>A (RyR1 p.Gln464Lys), c.1615T>C (RyR1 p.Phe539Leu), c.5119C>T (RyR1 p.Arg1707Cys), and c.8378C>T (RyR1 p.Pro2793Leu). These plasmids were introduced into the host cell line by transfection, after which the integration of those plasmids into the genome was selected for by hygromycin resistance. Monoclonal cells were subsequently isolated and expanded.

To confirm successful integration of each construct into the genome of the host cell line, first the cells were analysed for zeocin sensitivity and then a segment of the plasmid was amplified from the genome by polymerase chain reaction (PCR) with two different primer pairs (listed in Appendix A.1). Primers located within the pcFT vector sequence were used to confirm successful integration of the plasmid into the genome of the empty vector FT-293 stable expression line, represented by black and orange arrows in Figure 3.12A

('vector' primers). PCR-amplification with the 'vector' primer pair of the genomic DNA (gDNA) from the pcFT stable expression line amplified a fragment consistent with the predicted size of 365 bp, confirming the presence of the transgene (Figure 3.12B). No PCR product could be observed when the same gDNA underwent PCR-amplification with the '*RYR1*' primer pair as a negative control (see Appendix C.3).

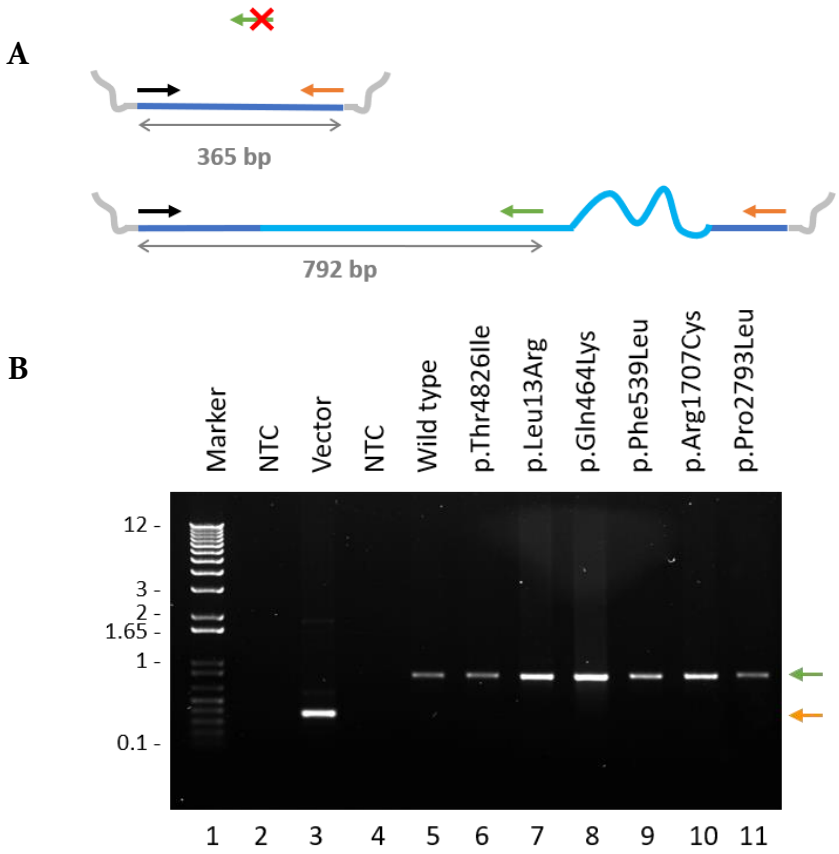

Figure 3.12 Confirmation of transgene integration

A Schematic of the PCR reactions that confirmed the presence of the transgene in the genomic DNA (grey) of stable expression lines. The vector (dark blue), ryanodine receptor 1 *(RYR1)* complementary DNA (cDNA; light blue), forward primer (black arrow), vector reverse primer (orange arrow) and *RYR1* cDNA reverse primer (green arrow) are shown. **B** Transgene integration confirmed by PCR amplification from the genomic DNA and subjected to electrophoresis in a 2% agarose gel containing ethidium bromide and immersed in buffer (Section 2.2.3). Migration of PCR products are indicated for the vector (orange arrow) and *RYR1* cDNA (green arrow). Samples are labelled: NTC (no template control), vector (pcFT), wild type, and *RYR1* variant nomenclature. Lane 1 contains 1 Kb Plus DNA Ladder as a size control with the length of each fragment indicated in kb.

3.4.1 Confirmation of RyR1 expression

RyR1 expression was established in the stable FT-293 cell lines by western blotting. Total protein samples were extracted from the cells, resolved by sodium dodecyl sulfate polyacrylamide gel electrophoresis (SDS-PAGE), transferred to a membrane and then analysed by use of specific antibodies. This was performed with the RyR-specific antibody 34C and an antibody for α-tubulin, included as a protein loading control. Approximately equal amounts of protein were loaded from each sample because equivalent levels of the α-tubulin signal can be observed migrating at approximately 50 kDa. A protein sample from HEK-293T cells (RRID: CVCL_0063) transfected with the WT ftRYR1 plasmid to transiently express WT RyR1 protein was included as a positive control (Figure 3.13). RyR1 expression was confirmed by the presence of a signal corresponding to RyR1 antibody binding; this signal was absent in the corresponding sample from cells transfected with empty vector.

The stable pcFT vector cell line does not express RyR1 at a level detectable by western blotting, confirming the lack of endogenous RyR1 in the host cell line (Figures 3.13A–B). A minimum of three distinct monoclonal lines were isolated and screened for RyR1 expression for WT RyR1, RyR1 p.Leu13Arg, RyR1 p.Gln464Lys, and RyR1 p.Thr4826Ile stable expression lines. Most cell lines were observed to express equally high levels of RyR1 protein by western blotting after induction by tetracycline (Figures 3.13A–D). The presence of additional bands with lower molecular weights was likely the result of over-exposure of the membrane and non-specific binding of the RyR1 antibody, although the presence of degradation products of RyR1 is a possibility.

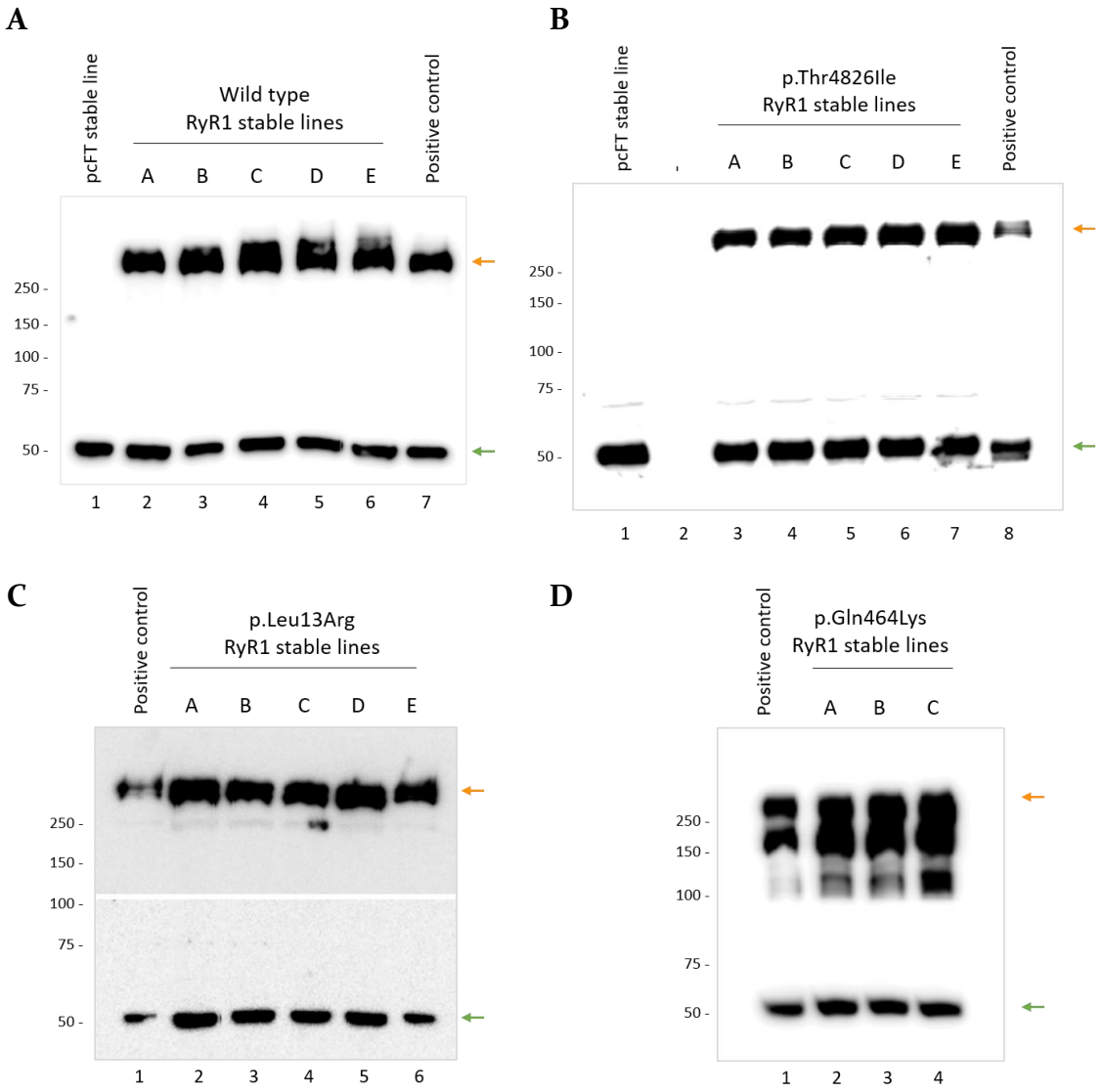

Figure 3.13 Immunoblots for expression of RyR1

Western blots of total protein extracted from FT-293 cell lines stably expressing ryanodine receptor 1 (*RYR1*) cDNAs alongside a sample from HEK-293T cells transiently expressing ryanodine receptor 1 (RyR1) protein as a positive control (Section 2.3.9, 2.3.10). Blots A and B also contain the stable vector FT-293 cell line as a negative control. Locations of RyR1 monomers (565 kDa) and α-tubulin (50 kDa) are indicated by orange and green arrows, respectively. **A** Stable wild-type FT-293 cell lines A–E. **B** Stable RyR1 p.Thr4826Ile FT-293 cell lines A–E. **C** Stable RyR1 p.Leu13Arg FT-293 cell lines A–E. **D** Stable RyR1 p.Gln464Lys FT-293 cell lines A–C.

Only one monoclonal cell line was isolated for the RYR1 c.8378C>T (RyR1 p.Pro2793Leu) construct, and thus a comparison of RyR1 expression from stable expression lines with the RyR1 p.Pro2793Leu was not required. There was also only one monoclonal cell line

originally isolated for the RYR1 c.1615T>C (RyR1 p.Phe539Leu) construct; however, when the RYR1 c.1615T>C (RyR1 p.Phe539Leu) stable expression line was found to express very low levels of RyR1 protein after induction with tetracycline, an additional five monoclonal lines (B–F) were isolated from a subsequent transfection. When examined by western blotting, all five stable *RYR1* c.1615T>C (RyR1 p.Phe539Leu) lines were found to have no detectable level of RyR1 protein similar to that of the original line (Figure 3.14A). RyR1 protein could also not be detected in any of the five *RYR1* c.5119C>T (RyR1 p.Arg1707Cys) cell lines (Figure 3.14B). The reason for this was unclear because the cDNA was confirmed to have been integrated into the genome (results of PCR in Figure 3.12B).

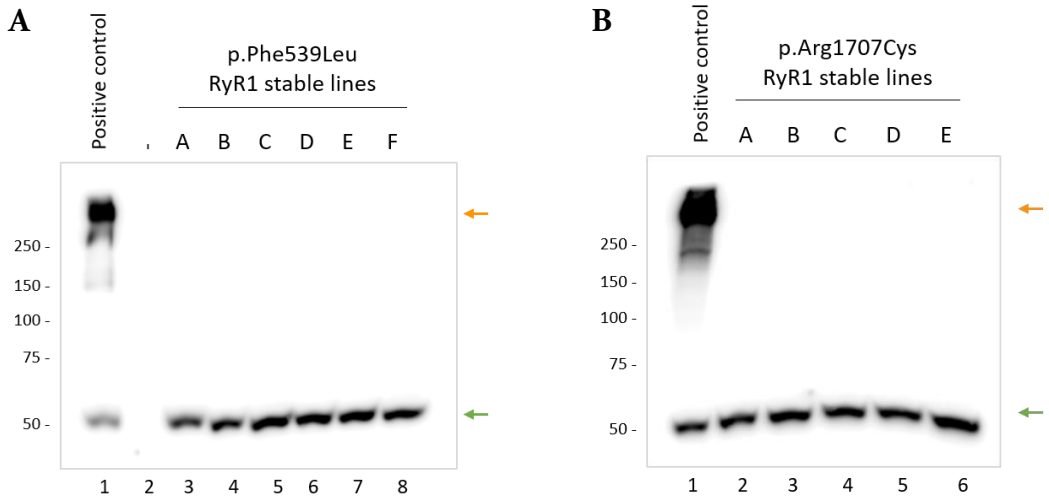

Figure 3.14 Immunoblots for expression of RyR1

Western blots of total protein extracted from FT-293 cell lines stably expressing ryanodine receptor 1 (*RYR1*) cDNAs alongside a sample from HEK-293T cells transiently expressing ryanodine receptor 1 (RyR1) protein as a positive control (Section 2.3.9, 2.3.10). Locations of RyR1 monomers (565 kDa) and α-tubulin (50 kDa) are indicated by orange and green arrows, respectively. **A** Stable RyR1 p.Phe539Leu FT-293 cell lines A and B–F. **B** Stable RyR1 p.Arg1707Cys FT-293 cell lines A–E.

A single, representative stable FT-293 cell line was then chosen for each variant for subsequent testing stages. For each construct, cell line 'A' was chosen and shall simply be referred to as the stable expression line for each construct. To correctly compare the expression levels of RyR1 protein between stable expression lines for each variant, total protein samples were simultaneously extracted from all FT-293 lines, both with and without tetracycline induction. All samples were then analysed by western blotting to

detect RyR1 protein and antibodies for α-tubulin was included as a protein loading control (Figures 3.15, 3.16). As expected, there was no RyR1 expression observed in the pcFT vector control. All stable expression lines—apart from the RyR1 p.Phe539Leu and RyR1 p.Arg1707Cys stable expression lines—showed a substantial increase in RyR1 protein when tetracycline was used to induce expression.

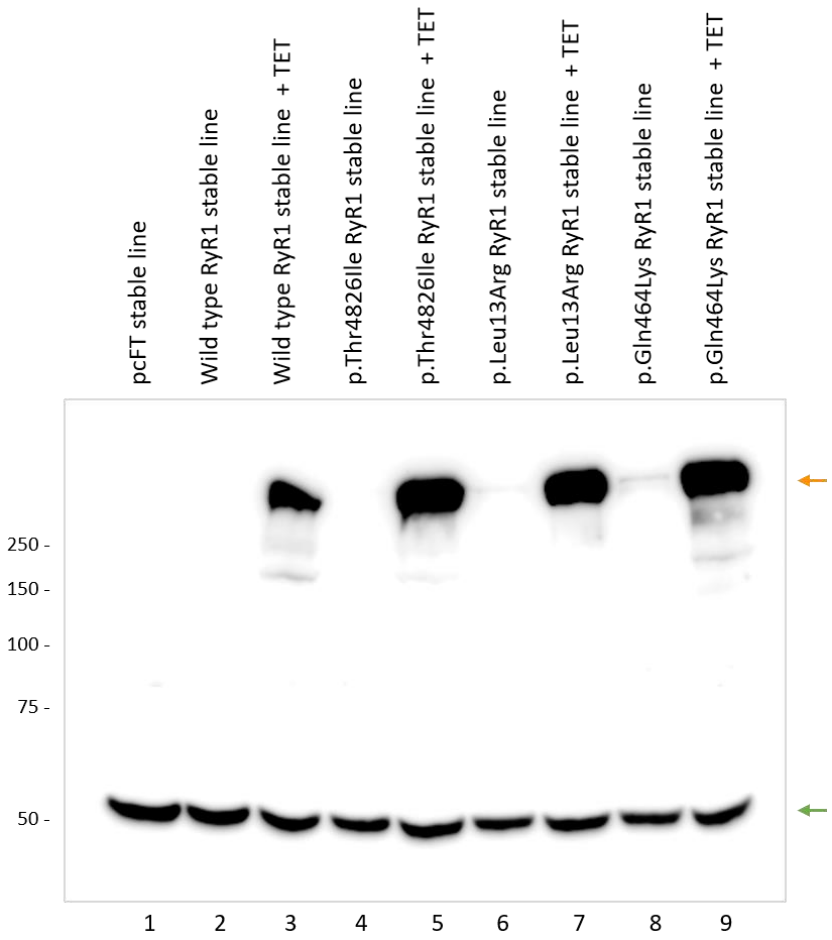

Figure 3.15 RyR1 protein expressed in representative stable cell lines

Western blot of total protein extracted from stable expression cell lines with primary antibodies specific for the ryanodine receptor (RyR1) and α-tubulin and secondary antibodies conjugated to horseradish peroxidase (Section 2.3.9–10). Identities of protein samples and the locations of RyR1 monomers (565 kDa; orange arrow) and α-tubulin (50 kDa; green arrow) are indicated.

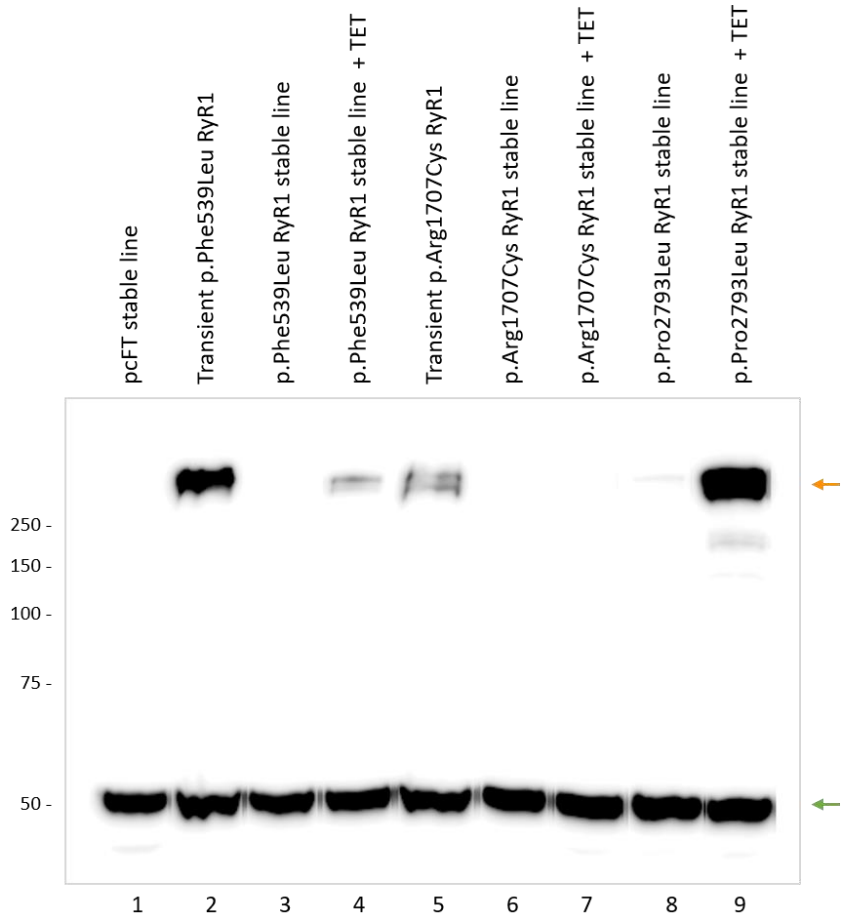

Figure 3.16 RyR1 protein expressed both stably and transiently

Western blot of total protein from stable cell lines and transfected HEK-293T cells. Primary antibodies for ryanodine receptor 1 (RyR1) and α-tubulin were used with secondary antibodies conjugated to horseradish peroxidase (Section 2.3.9–10). Identities of samples and locations of RyR1 monomers (565 kDa; orange arrow) and α-tubulin (50 kDa; green arrow) are labelled.

In addition, total protein was extracted from HEK-293T cells transiently expressing *RYR1* cDNAs with the c.1615T>C (RyR1 p.Phe539Leu) and c.5119C>T (RyR1 p.Arg1707Cys) variants after transfection with the corresponding ftRYR1 plasmid. These samples were included to verify that the low expression observed in the stable expression lines was not because of an issue with the expression vector. The RyR1 p.Phe539Leu stable expression line showed a modest increase in RyR1 expression when induced with tetracycline whereas that same construct produced a high level of RyR1 protein when expressed transiently in HEK-293T cells. The RyR1 p.Arg1707Cys stable expression line showed no expression in either of the stable expression line samples, whereas the same construct produced a low level of RyR1

protein when expressed transiently in HEK-293T cells. An omission from the western blotting results was the transient expression of WT *RYR1* and *RYR1* c.14477C>T (RyR1 p.Thr4826Ile) cDNAs in HEK-293T cells as negative and positive controls, to compare against the expression of the variants. Expression of these control cDNAs was, however, confirmed by microscopy (Section 3.4.2).

3.4.2 Confirmation of cellular localisation

The intracellular localisation of RyR1 in stable FT-293 cells was then confirmed by immunofluorescence after induction of RyR1 expression by addition of tetracycline (Figures 3.17, 3.18). This was carried out with antibodies specific for RyR1 and the ER and, with the exception of the pcFT vector negative control and the RyR1 p.Arg1707Cys stable line, RyR1 fluoresced in the same cellular location as the ER marker PDI. This was observed in the overlay image of Figure 3.19 in which the overlap of the red signal from the ER and the green signal from the RyR1 protein produced a yellow signal, confirming localisation of RyR1 channels to the Ca^{2+} store of the cell. The lack of RyR1 signal seen in the RyR1 p.Arg1707Cys stable line reflects the result from the western blot in which no protein expression could be seen, indicating that this stable line does not express observable levels of RyR1 (Figure 3.16).

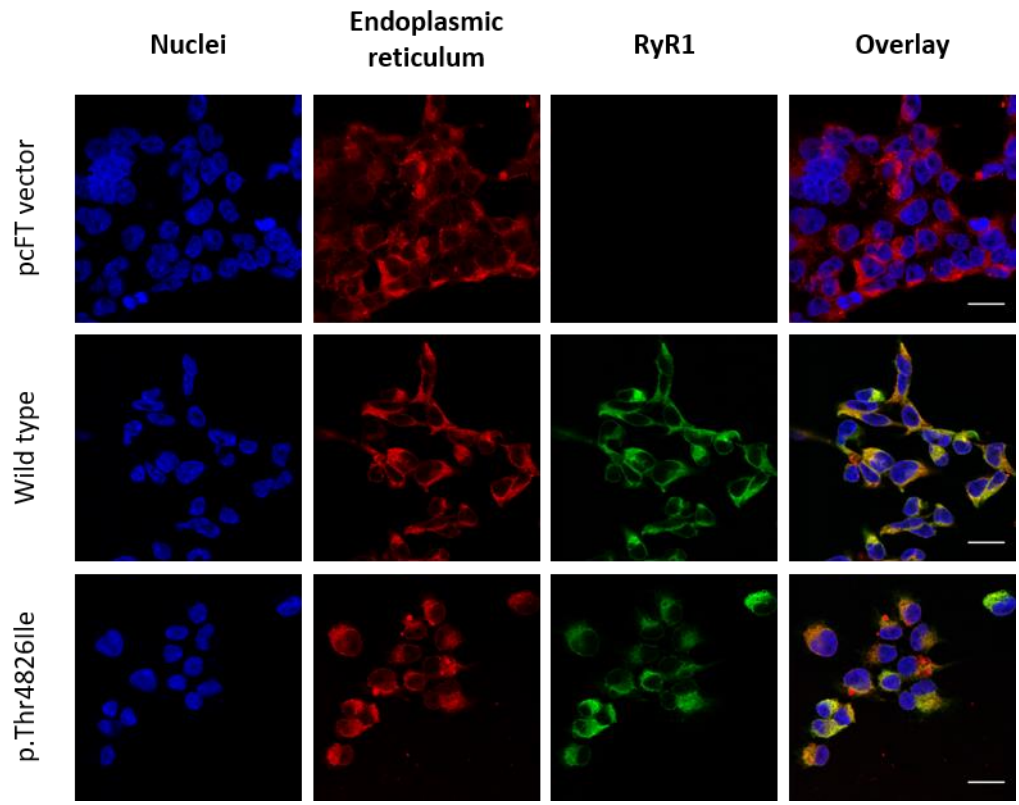

Figure 3.17 Localisation of ryanodine receptor 1 in control cell lines

Stable FT-293 cells were grown on a microscope slide and prepared for immunofluorescence (Section 2.3.11). Primary antibodies that recognise ryanodine receptor 1 (RyR1) and protein disulfide isomerase were used with fluorescently labelled secondary antibodies fluorescein isothiocyanate (FITC) and tetramethylrhodamine isothiocyanate (TRITC), respectively, to visualise the cellular localisation of RyR1 (green), and the endoplasmic reticulum (red). Nuclei (blue) were visualised with 4',6-diamidino-2-phenylindole (DAPI). Cells were examined by confocal fluorescence microscopy (1260× magnification). Scale bar in each merged image represents 20 microns.

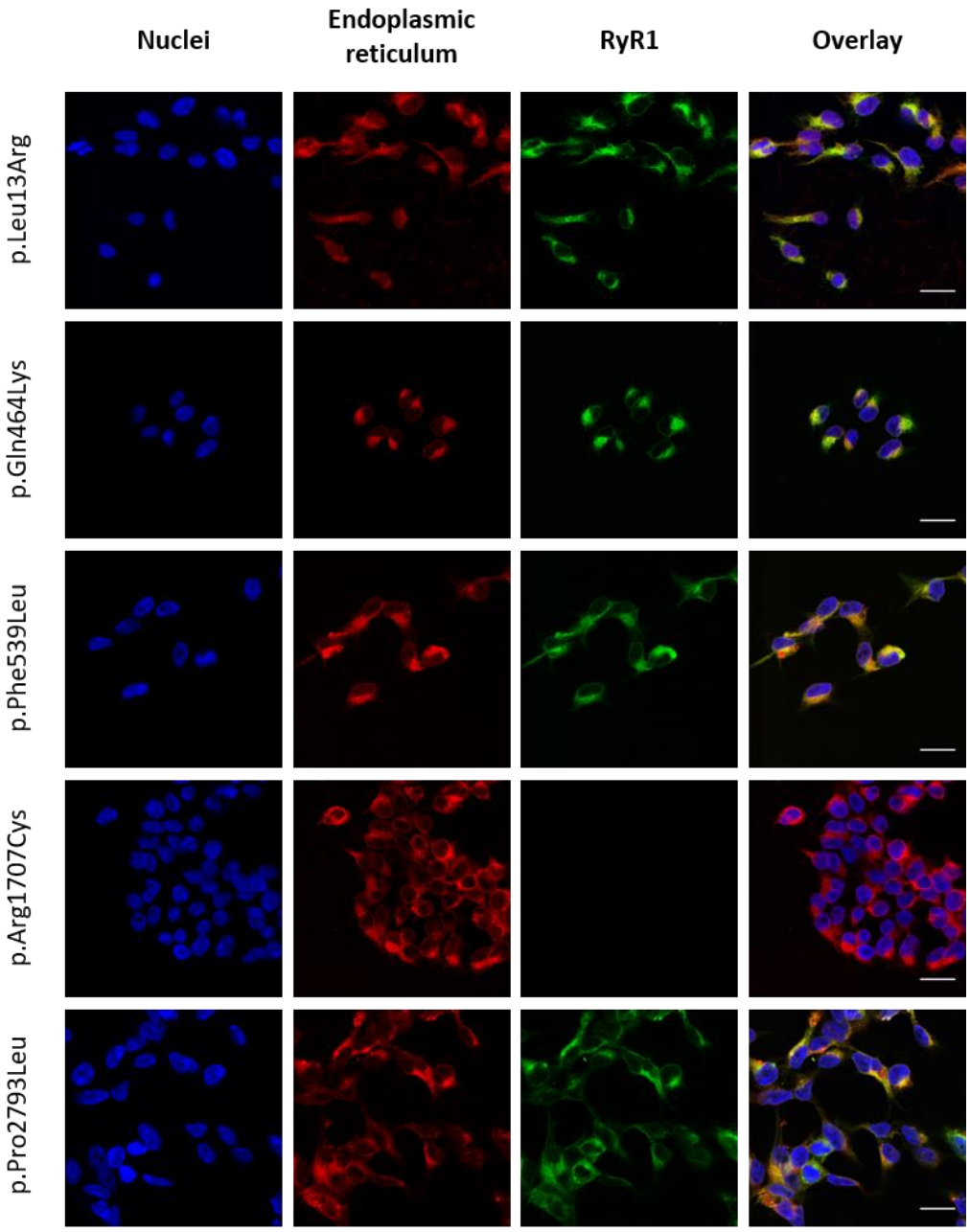

Figure 3.18 Cellular localisation of ryanodine receptor 1 in stable cells

Stable FT-293 cells were grown on a microscope slide and prepared for immunofluorescence (Section 2.3.11). Primary antibodies that recognise ryanodine receptor 1 (RyR1) and protein disulfide isomerase were used with fluorescently labelled secondary antibodies fluorescein isothiocyanate (FITC) and tetramethylrhodamine isothiocyanate (TRITC), respectively, to visualise the cellular localisation of RyR1, and the endoplasmic reticulum. Nuclei were visualised by staining the cells with 4',6-diamidino-2-phenylindole (DAPI). Cells were examined by confocal fluorescence microscopy at a magnification of 1260×. The scale bar in each merged image represents 20 microns.

The cellular localisation of RyR1 was also examined by immunofluorescence in HEK-293T cells transiently expressing c.1615T>C (RyR1 p.Phe539Leu) and c.5119C>T (RyR1 p.Arg1707Cys) *RYR1* cDNAs (Figure 3.19). This was performed to confirm that the expression vectors used to create the stable expression lines were not the cause of the low RyR1 expression indicated by western blotting. In addition, HEK-293T cells transiently expressing the pcFT vector as an RyR1-negative control, the WT ftRYR1 vector as an MH-negative control, and the c.14477C>T (RyR1 p.Thr4826Ile) ftRYR1 vector as an MH-positive control, were examined by immunofluorescence (Figure 3.19). With the exception of the pcFT vector, RyR1 fluoresced in the same cellular location as the ER marker PDI. This was observed in the overlay image of Figure 3.19 in which the overlap of the red signal from the ER and the green signal from the RyR1 protein produced a yellow signal, confirming localisation of RyR1 channels to the Ca^{2+} store of the cell.

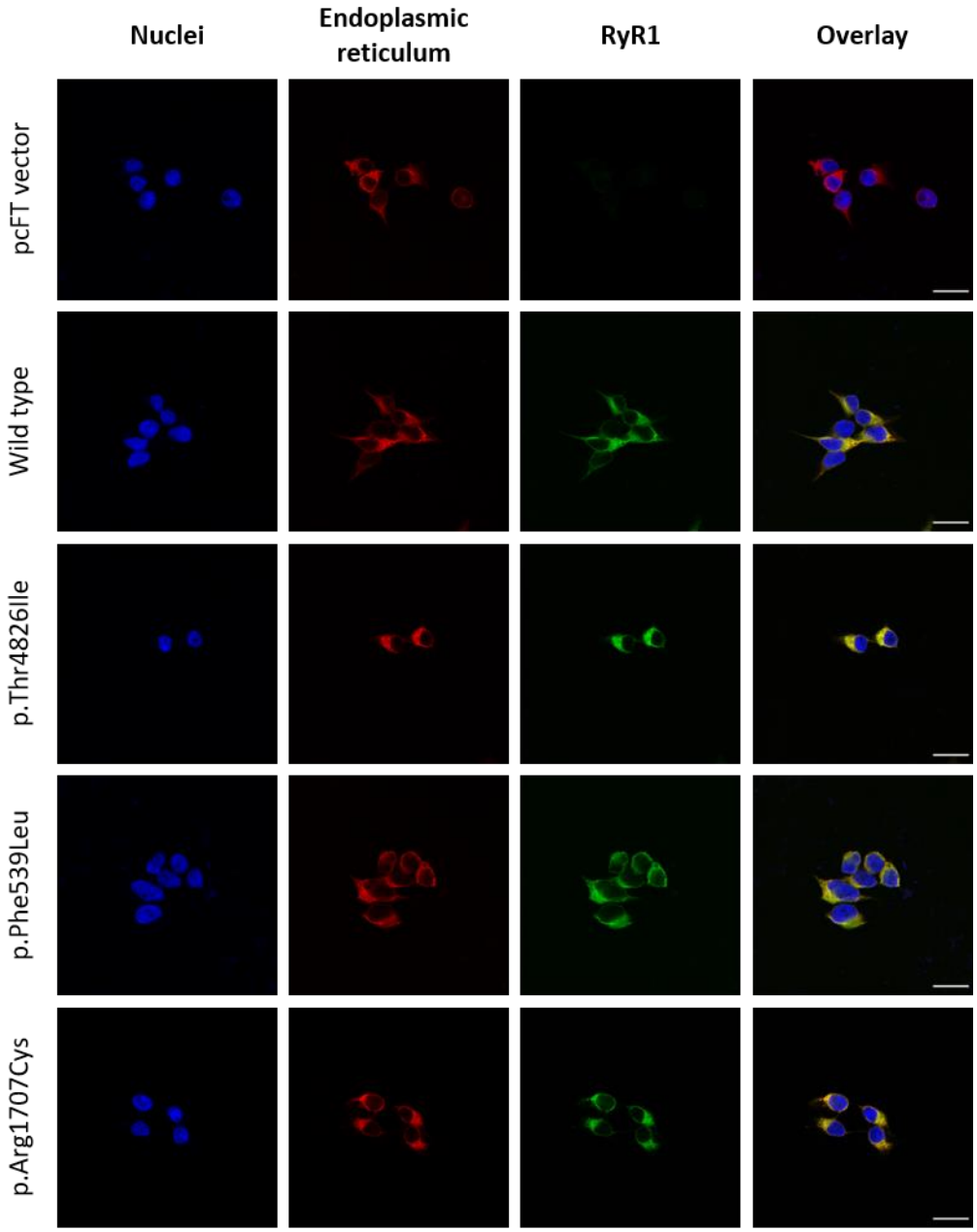

Figure 3.19 Localisation of transiently expressed ryanodine receptor

HEK-293T cells were grown on a microscope slide, transfected with an expression, and prepared for immunofluorescence (Section 2.3.3, 2.3.11). Primary antibodies that specifically recognise ryanodine receptor 1 (RyR1) and protein disulfide isomerase were used with fluorescently labelled secondary antibodies fluorescein isothiocyanate (FITC) and tetramethylrhodamine isothiocyanate (TRITC), respectively, to visualise the cellular localisation of RyR1 (green) and the endoplasmic reticulum (red). Nuclei (blue) were visualised by staining the cells with 4',6-diamidino-2-phenylindole (DAPI). Cells were examined by confocal fluorescence microscopy at a magnification of 1260×. The scale bar in each merged image represents a length of 20 microns.

3.5 *Analysis of RyR1 activity*

Next, the activities of the RyR1 channels in the stable expression lines were analysed by testing the response of the cells to the RyR-agonist 4-chloro-*m*-cresol (4-c*m*c). This was performed by use of the acetoxymethyl ester form of the ratiometric fluorescent Ca^{2+} indicator Fura-2, which enters the cells non-invasively and binds to free Ca^{2+}.[275] An acetoxymethyl ester group fused to Fura-2 allows the dye to permeate the cell membrane and is cleaved off by cellular esterases, preventing the dye from further transport.

Although the emission spectrum remains the same, the excitation spectrum of Fura-2 changes upon Ca^{2+} binding, enabling the relative amount of cytoplasmic Ca^{2+} to be measured ratiometrically. Unbound Fura-2 is excited at 340 nm whereas the Ca^{2+}-bound form is excited at 380 nm and both forms emit fluorescence at 510 nm. An increase in cytoplasmic Ca^{2+} levels causes the fluorescent signal excited at 380 nm to increase and the signal excited at 340 nm to decrease equivalently (see example in Appendix D.1). The data from these two signals are then combined to produce a ratio (the 380 nm signal divided by the 340 nm signal) that corresponds to relative cytoplasmic Ca^{2+} levels (see example in Appendix D.2).

3.5.1 *Optimisation of calcium release assays*

Preliminary testing revealed a small, delayed response to the agonist 4-c*m*c in the FT-293 host cell line (Figure 3.20). After addition of the agonist, the level of cytoplasmic Ca^{2+} increased slowly but steadily and this response was dose-dependent, with higher concentrations of agonist eliciting a stronger response. This result indicated the presence of an endogenous Ca^{2+} channel that is sensitive to the action of 4-c*m*c.

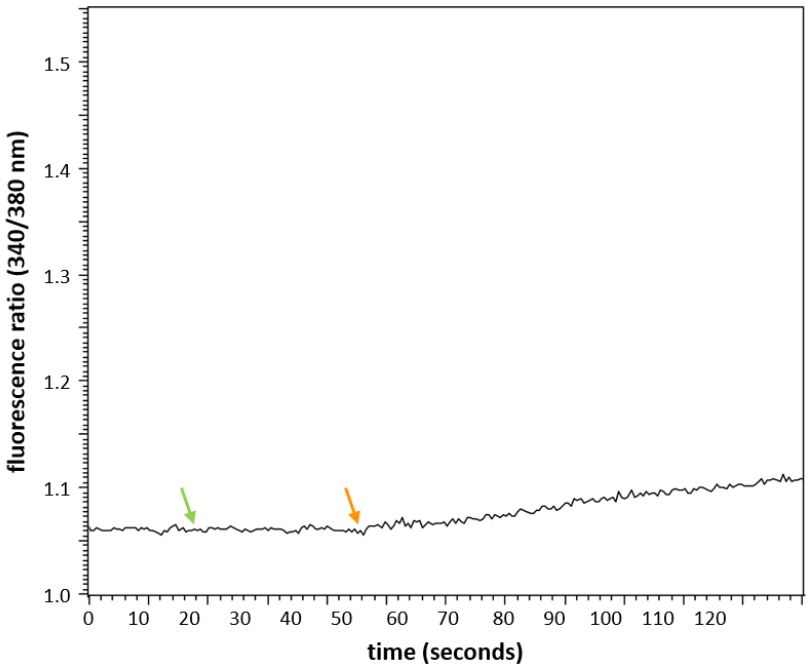

Figure 3.20 Non-specific calcium release from FT-293 cell stores

Increase in cytoplasmic [Ca^{2+}] in the FT-293 host cell line after addition of 1000 µM 4-chloro-*m*-cresol, measured as a ratio of fluorescence emission after excitation at 340 nm and 380 nm. Ca^{2+} release begins 28 seconds (orange arrow) after agonist addition (green arrow).

The non-specific response to 4-c*m*c was not the result of extracellular Ca^{2+} entry as the cells were washed with and assayed in Ca^{2+}-free buffer. The possible presence of endogenous RyR1 channels was also rejected as the source of the non-specific Ca^{2+} release because the response persisted after treatment of the cells with a high concentration of ruthenium red (Table 3.6). Ruthenium red is a broad-spectrum inhibitor of mammalian Ca^{2+} channels. Its effect is especially potent with ryanodine receptors for which treatment with 2 µM ruthenium red completely abolishes RyR activity.[276] In fact, after treatment of the FT-293 cells with 10 µM ruthenium red, the non-specific Ca^{2+} release was slightly increased in comparison with untreated cells (Table 3.6). This result is consistent with its inhibition of SERCA preventing reuptake of Ca^{2+} into stores, confirming that the ruthenium red treatment was successful.

Table 3.6 Calcium release in FT-293 cells after RyR1 inhibition

Treatment	Calcium release† (mean ± standard error)‡
None	0.11 ± 0.01
10 µM ruthenium red	0.16 ± 0.01

† Measured 100 seconds after addition of 1000 µM 4-cmc (n = 3).

‡ Measured in relative fluorescence units.

Although the exact cause of the non-specific response could not be determined, it is probable inositol 1,4,5-triphosphate receptor was involved because it was not inhibited by ruthenium red.[277] Inositol 1,4,5-triphosphate receptors are Ca^{2+} channels located across the ER membrane of most cell types. Their activities are not fully understood but they are one of the primary intracellular Ca^{2+} channels in many mammalian cells and are believed to be involved in a variety of Ca^{2+}-dependent cellular functions including store operated Ca^{2+} entry (SOCE).[278] The amount of Ca^{2+} released through this non-specific pathway was small and occurred following a substantial delay compared to cells expressing RyR1 channels. As shown in Figure 3.21A, the cytoplasmic Ca^{2+} increases observed in the pcFT vector stable expression line (and the host cell line in Figure 3.20) occurred over 20 seconds after agonist addition. The cell line expressing RyR1, however, had an almost immediate response—the signal peaked less than ten seconds after exposure to 4-cmc (Figure 3.21B). In addition, the magnitude of the non-specific response was much smaller than that of the cell line expressing RyR1, with a fluorescence ratio of less than 0.1 (Figure 3.21). These factors allowed the Ca^{2+} release data to be recorded from the stable cell lines expressing RyR1 channels with little or no background from the non-specific agonist response.

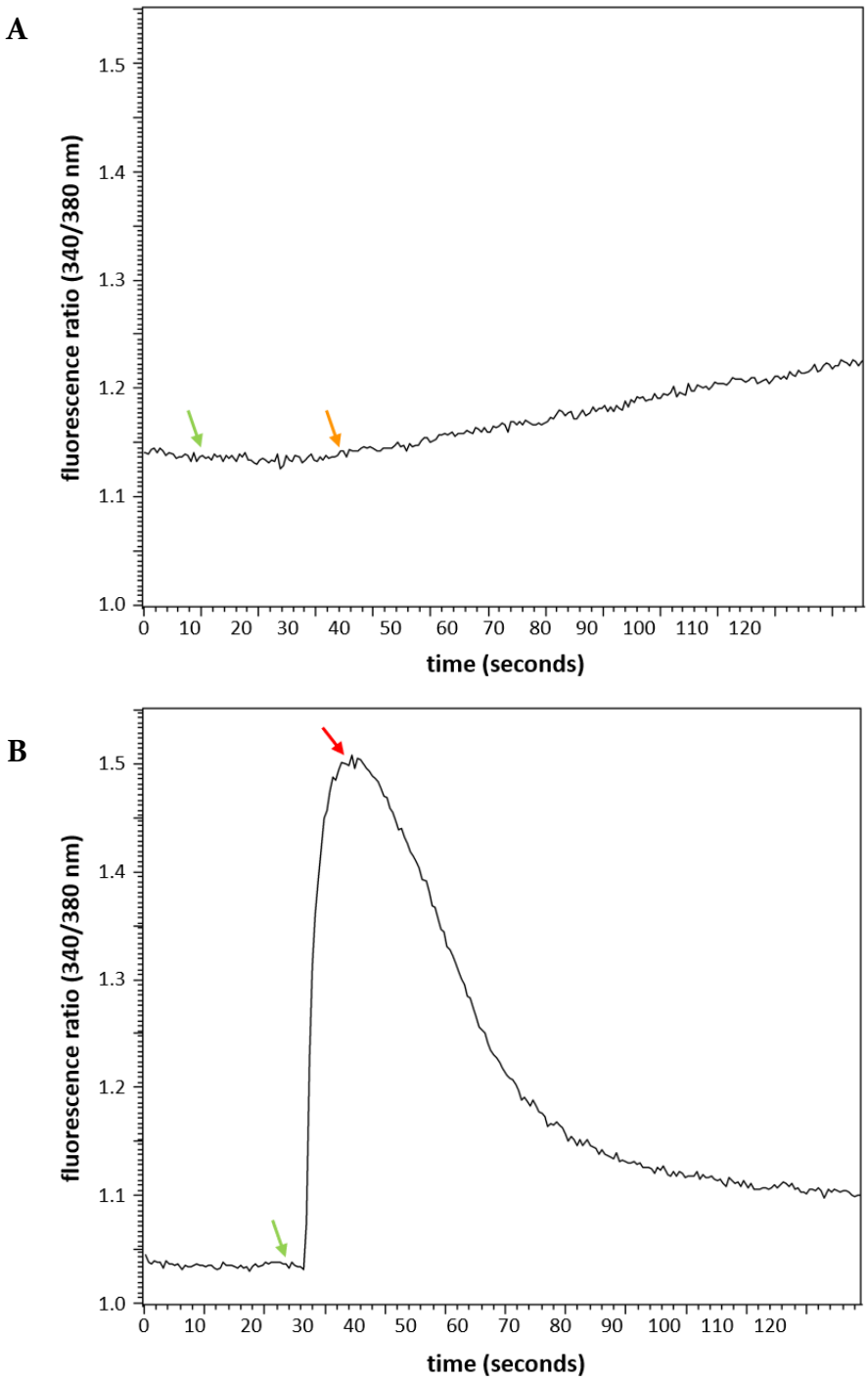

Figure 3.21 Timing of calcium released from stores after agonist addition

Increase in cytoplasmic [Ca^{2+}] in stable cell lines after addition of 1000 µM 4-chloro-*m*-cresol, measured as a ratio of fluorescence emission after excitation at 340 nm and 380 nm. **A** Ca^{2+} release in the stable vector line begins 24 seconds (orange arrow) after agonist addition (green arrow). **B** Ca2+ release in ftRYR1 stable expression line peaks 10 seconds (red arrow) after agonist addition (green arrow).

To determine the optimal time to add tetracycline to the stable cells before functional testing, the WT RyR1 stable expression line was assayed after treatment with tetracycline over different time periods (Table 3.7). Addition of 1 µg mL^{-1} tetracycline to the cell media up to 72 hours in advance of testing did not alter the release of Ca^{2+} from cell stores, even when steps were taken to ensure no tetracycline was present in the growth media. Invitrogen certified the foetal bovine serum added to the media as tetracycline free, charcoal-stripped foetal bovine serum was trialled with no change, and even the use of phenol red-free DMEM did not improve the results. This inability to control expression with tetracycline was unfortunate as one of the key features of the Flp-In™ T-REx™ 293 stable expression lines was the ability to 'turn off' expression of *RYR1* and reduce the risk of cellular stress.

Table 3.7 Calcium release in stable cells after induction by tetracycline

Hours exposed to 1 µg mL^{-1} tetracycline before assay	Calcium release †
0	0.19 ± 0.01
24	0.18 ± 0.02
48	0.20 ± 0.01
72	0.18 ± 0.02

† Average ± SEM fluorescence ratio (340/380 nm) increase after addition of 1000 µM 4-cmc.

These findings indicate that the induction of *RYR1* expression by tetracycline treatment is not required for functional assays. In light of those results, it can be theorised that a small number of RyR1 channels are necessary for maximal Ca^{2+} release in recombinant cells and that the huge amount of RyR1 protein observed by immunoblotting in the stable expression lines after tetracycline induction (or HEK-293T cells after transient transfection) is superfluous to requirements.

To verify that the tetracycline repressor responsible for the repression of *RYR1* transcription was present, cDNA was produced with total RNA extracted from the WT and

RyR1 p.Thr4826Ile stable expression lines. The tetracycline repressor cDNA was successfully PCR-amplified from these samples, indicating that the issue with leaky *RYR1* expression is not a lack of repression, but likely related to weak repression (Figure 3.22). Additional validation to confirm the identity of the tetracycline repressor from the PCR product in the form of Sanger sequencing was not performed.

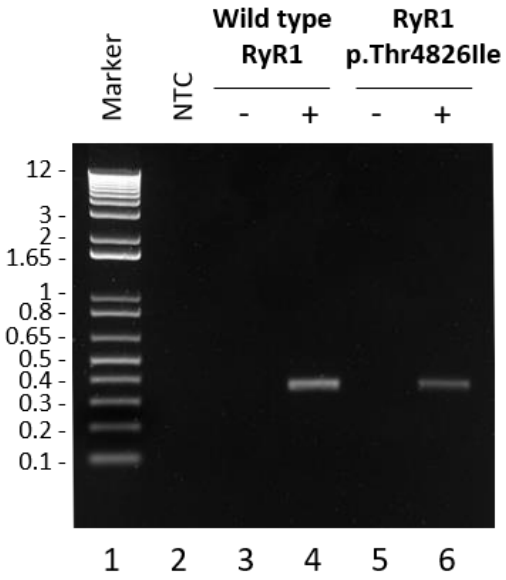

Figure 3.22 Expression of the tetracycline repressor

A segment of the tetracycline repressor gene was PCR-amplified with complementary DNA as a template. Complementary DNA was made from total RNA extracted from wild-type ryanodine receptor 1 (RyR1) and RyR1 p.Thr4826Ile stable FT-293 expression lines (+) together with negative controls (–) created without reverse transcriptase enzyme. Lane 1 contains 1 Kb Plus DNA ladder with fragment lengths labelled in kb and lane 2 contains a no template PCR control (NTC).

Finally, the activities of mutant RyR1 channels were analysed in functional assays by testing the responses of stable cell lines expressing RyR1 proteins to the RyR-agonist 4-c*m*c. As the cells were exposed to increasing doses of 4-c*m*c, the relative amount of Ca^{2+} released from stores was measured ratiometrically as described in Section 2.3.12. To establish the experimental system, the data from the WT RyR1 and RyR1 p.Thr4826Ile (MH positive control) stable expression lines were compared in this way (Figure 3.23). The RyR1 p.Thr4826Ile stable expression line was confirmed as being hypersensitive to the agonist because its Ca^{2+} release profile was shifted to the left by a sizeable amount when compared

with that of the WT channel. For the stable expression lines, statistical significance with 99% confidence was achieved when the calculated *p*-value of each data set by Student's *t*-test was lower than the Bonferroni-adjusted α-value of 2×10^{-3}. The purpose of this adjustment was to counteract the potential for false positives that can occur when multiple statistical comparisons are made. The difference between the data from the RyR1 p.Thr4826Ile and WT RyR1 stable expression lines was confirmed as being statistically significant, with a *p*-value of 2.7×10^{-4} (data in Table 3.8).

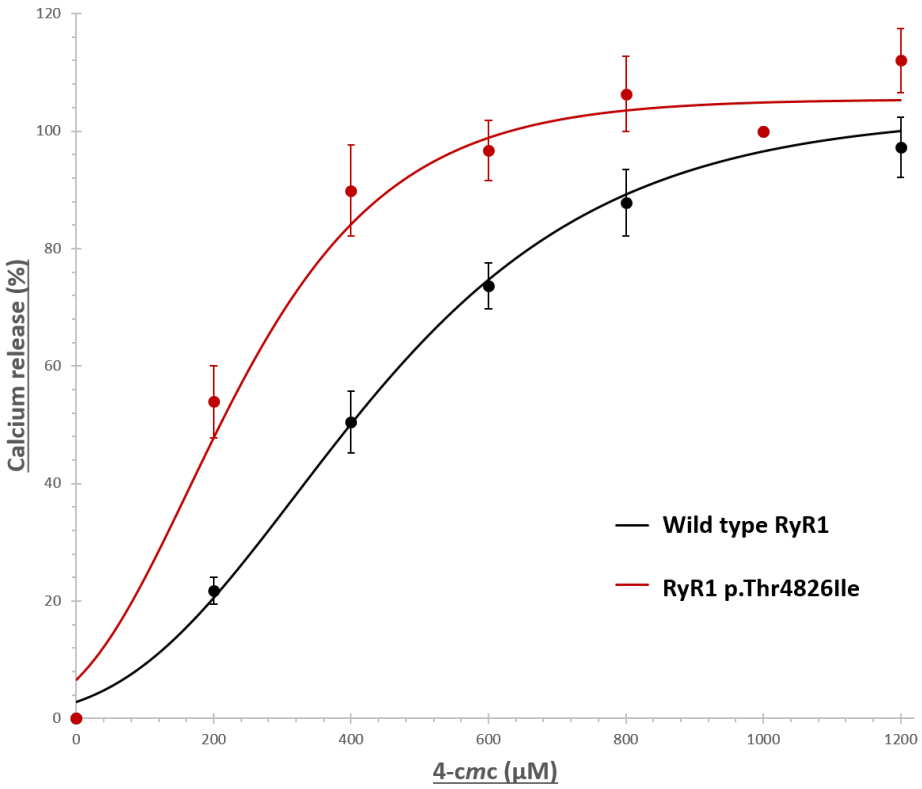

Figure 3.23 Calcium release data of control stable expression lines

After induction of ryanodine receptor 1 (RyR1) expression by tetracycline, stable FT-293 cells were exposed to incremental doses of the agonist 4-chloro-*m*-cresol (4-cmc) in the presence of the ratiometric Ca^{2+} indicator Fura-2 (Section 2.3.12). The increase of cytoplasmic [Ca^{2+}] upon introduction of the agonist was normalised to 100% Ca^{2+} release as defined by the response to 1000 µM 4-cmc. Error bars represent the standard error of the mean for each data point and are based on biological replicates (n ≥ 7). Sigmoidal curves were fitted to each data set (Section 2.4.3).

The Ca^{2+} release profile of the MH positive control RyR1 p.Thr4826Ile was also compared with that of the WT RyR1 after transient expression of cDNAs in HEK-293T cells (Figure

3.24). The Ca^{2+} release curve of the MH positive control was also found to be considerably shifted to the left compared with the WT channel in the transient expression system. For the Ca^{2+} release data collected after transient expression of *RYR1* cDNAs in HEK-293T cells, the Bonferroni-adjusted α-value for statistical significance with 99% confidence was 3.3×10^{-3}. Statistical significance was again confirmed for the data from the MH positive control RyR1 p.Thr4826Ile variant compared with that of WT RyR1 with a *p*-value of 1.2×10^{-3} (data in Table 3.9). These results indicated the stable expression system could produce data consistent with that of the transient expression. Once the system for data collection was established, the Ca^{2+} release data from each stable expression line was collected.

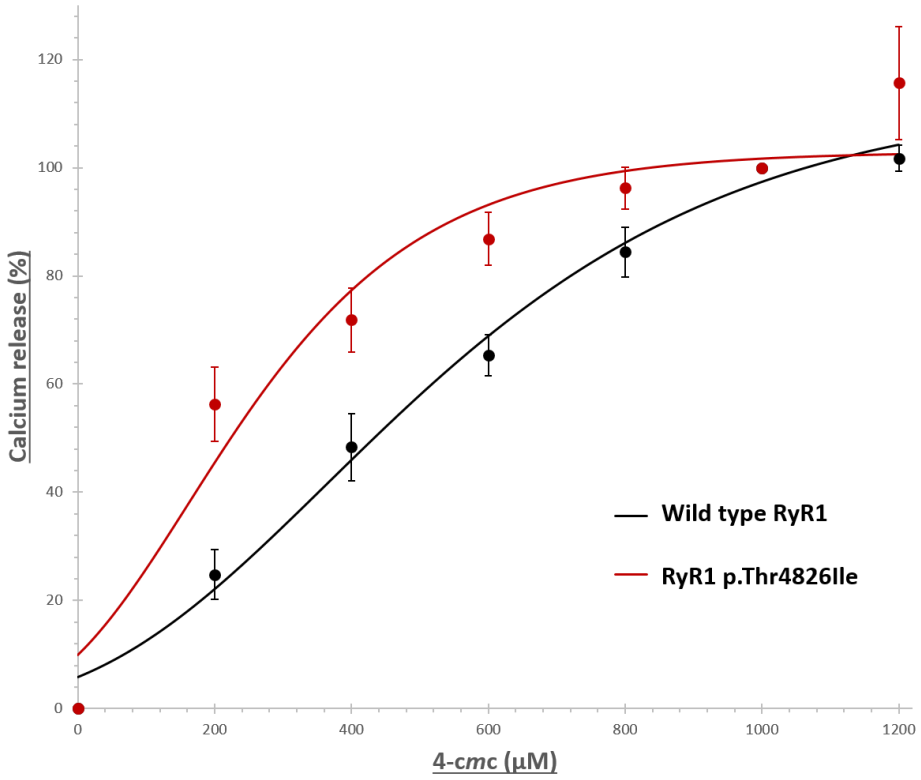

Figure 3.24 Calcium data from transient expression of RyR1

Following transient expression of ryanodine receptor 1 (RyR1) in HEK-293T cells (Section 2.3.3), fluorescence was measured after addition of incremental doses of 4-chloro-*m*-cresol (4-cmc) in the presence of the ratiometric Ca^{2+} indicator Fura-2 (Section 2.3.12). The increase of cytoplasmic $[Ca^{2+}]$ upon introduction of the agonist was normalised to 100% Ca^{2+} release as defined by the response to 1000 µM 4-cmc. Error bars represent the standard error of the mean for each data point and are based on biological replicates ($n \geq 5$). Sigmoidal curves were fitted to each data set.

3.5.2 *The RyR1 p.Leu13Arg variant*

Analysis of the stably expressed RyR1 p.Leu13Arg variant by use of the recombinant system showed that it was likely hypersensitive to the agonist. This can be observed in Figure 3.25 in which its Ca^{2+} release profile was clearly shifted to the left when compared with that of the WT channel, even more than that of the MH positive control RyR1 p.Thr4826Ile. This difference was confirmed as statistically significant with a *p*-value of less than 1×10^{-5} when compared with the WT Ca^{2+} release profile by Student's *t*-test (data in Table 3.8).

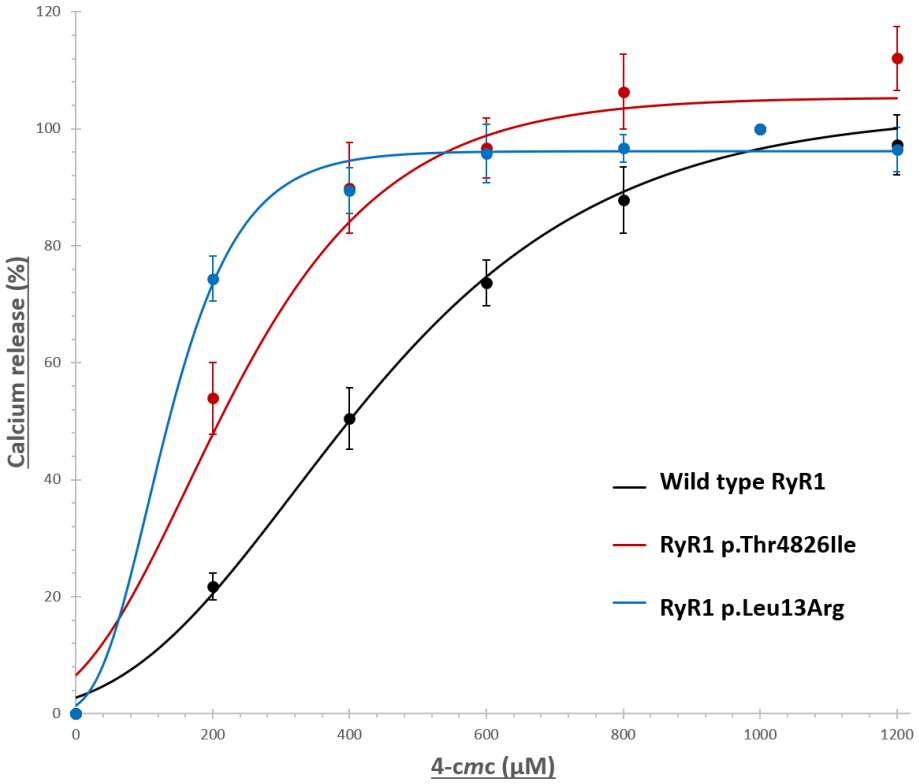

Figure 3.25 Calcium release data of RyR1 p.Leu13Arg stable line

After induction of ryanodine receptor 1 (RyR1) expression by tetracycline, stable FT-293 cells were exposed to incremental doses of the agonist 4-chloro-*m*-cresol (4-c*m*c) in the presence of the ratiometric Ca^{2+} indicator Fura-2 (Section 2.3.12). The increase of cytoplasmic [Ca^{2+}] upon introduction of the agonist was normalised to 100% Ca^{2+} release as defined by the response to 1000 µM 4-c*m*c. Error bars represent the standard error of the mean for each data point and are based on biological replicates ($n \geq 7$). Sigmoidal curves were fitted to each data set (Section 2.4.3).

The RyR1 p.Leu13Arg variant was identified as a potential cause of MH-susceptibility that was diagnosed in a small family (see Section 3.2.1). This variant was previously linked to MH-susceptibility in three pedigrees worldwide—Swiss, American, and Japanese.[231,279-281] Histological examination of muscle fibres from members of the Japanese family also revealed cores lacking oxidative enzymes. Subsequent *in silico* analysis indicated a likelihood for pathogenicity, and thus it was determined there was a high probability this variant affected RyR1 function. It was predicted that this variant may result in an RyR1 channel that is more prone to activation than a WT channel and therefore is susceptible to opening uncontrollably in the presence of triggering agents.

Located in the N-terminal region of RyR1, leucine 13 is positioned in a hydrophobic core. This region is predicted to be involved in the conformational changes that accompany channel opening, as predicted by the crystal structure of the domain and confirmed by cryogenic electron microscopy studies.[88,282,283] The substitution of leucine to the larger, basic arginine in this hydrophobic core may alter interactions with adjacent side-chains and disrupt the robust structure of the closed state because of steric hindrance.[284] The interactions that are likely disrupted from the presence of this variant are those predicted to change upon channel opening. It is therefore likely that the RyR1 p.Leu13Arg variant predisposes the channel to a more open state.[88] These data represented in Figure 3.25 were interpreted such that this variant creates RyR1 channels with much greater sensitivity to activation by agonists and therefore is likely to contribute to MH-susceptibility.

3.5.3 *The RyR1 p.Gln464Lys variant*

Comparison of the Ca^{2+} release profiles of the WT and RyR1 p.Gln464Lys stable expression lines after activation with the RyR-specific agonist 4-c*m*c revealed a substantial difference similar to that of the MH positive control (Figure 3.26). The left-shift of the curve for RyR1 p.Gln464Lys compared with the WT Ca^{2+} release profile is indicative of an increased sensitivity of the RyR1 channels to agonist in a similar fashion to that of the MH positive control RyR1 p.Thr4826Ile. Statistical significance with 99% confidence was calculated by Student's *t*-test in the form of a *p*-value of 2.2×10^{-4} (data in Table 3.8).

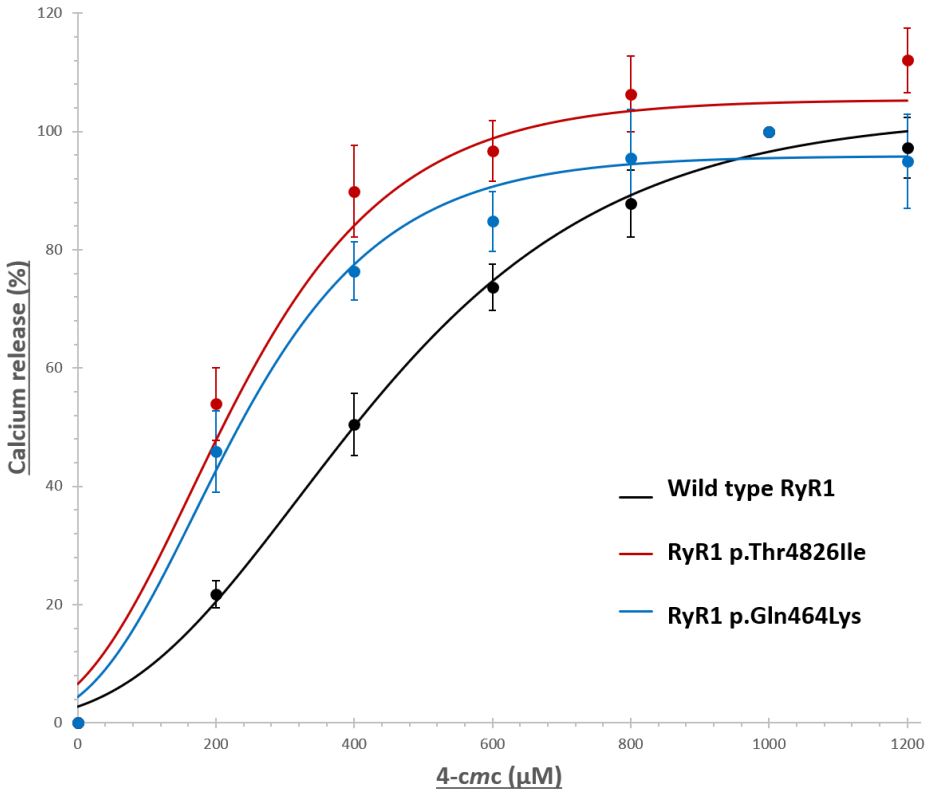

Figure 3.26 Calcium release data of RyR1 p.Gln464Lys stable line

Following induction of ryanodine receptor 1 (RyR1) expression by tetracycline, stable FT-293 cells were exposed to incremental doses of the agonist 4-chloro-*m*-cresol (4-c*m*c) in the presence of the ratiometric Ca^{2+} indicator Fura-2 (Section 2.3.12). The increase of cytoplasmic [Ca^{2+}] upon introduction of the agonist was normalised to 100% Ca^{2+} release as defined by the response to 1000 µM 4-c*m*c. Error bars represent the standard error of the mean for each data point and are based on biological replicates (n ≥ 7). Sigmoidal curves were fitted to each data set (Section 2.4.3).

Glutamine 464 is predicted to be located between mobile regions of the N-terminal domain that undergo substantial conformational changes upon channel opening, based on crystal structures and confirmed by cryogenic electron microscopy.[88,282,283] The introduction of a positive amino acid such as lysine may result in the weakening of those interactions and therefore a loosening of the channel in its closed state. Bolstering this hypothesis, a variant located in the same domain interface as RyR1 p.Gln464Lys, RyR1 p.Gln474His, also causes an amino acid change from a neutral residue to that of a positively charged one and has been found in a patient with central core disease (CCD).[199]

There are many examples of families with both MH-susceptibility and CCD attributed to a common RyR1 variant; this is why individuals that are diagnosed with CCD—or those suspected to have CCD—are treated as though they are also susceptible to MH.[202] Four of the five members of Family B that have both the RyR1 Gln464Lys variant and MH-susceptibility also present with a non-specific myopathy. Because of this link, there was robust evidence for a link between this variant and the MH-susceptibility in Family B. After testing the response of stably expressed RyR1 p.Gln474His in a recombinant system, it seems likely that interruption of the domain interface in which glutamine 464 resides contributes to MH-susceptibility. It is possible that this variant also causes myopathy that may be undiagnosed CCD.

3.5.4 The RyR1 p.Phe539Leu variant

The Ca^{2+} release data for the RyR1 p.Phe539Leu stable expression line was compared with that of the WT stable expression line and found to be strongly shifted to the left much like that of the MH positive control RyR1 p.Thr4826Ile stable expression line (Figure 3.27). Statistical significance with 99% confidence as a *p*-value of 2×10^{-5} was calculated by Student's *t*-test, confirming that this RyR1 variant confers a heightened sensitivity to agonists to the channel (data in Table 3.8).

The result from the stable line was convincing, but it was not known whether the low level of RyR1 p.Phe539Leu protein in the stable line had any bearing on the results of the Ca^{2+} release profile (western blot in Figure 3.16). It was possible that either the low RyR1 level was a consequence of the creation of the stable expression line or perhaps the RyR1 p.Phe539Leu variant conferred a loss of stability to the resulting mRNA or protein. This uncertainty made interpretation of the results difficult. In the medical field, ambiguous results may lead to the misdiagnosis of patients; thus, confidence in the data presented is essential. For this reason, Ca^{2+} release data were also collected from HEK-293T cells that transiently expressed *RYR1* cDNA with the *RYR1* c.1615T>C (RyR1 p.Phe539Leu) variant (Figure 3.28).

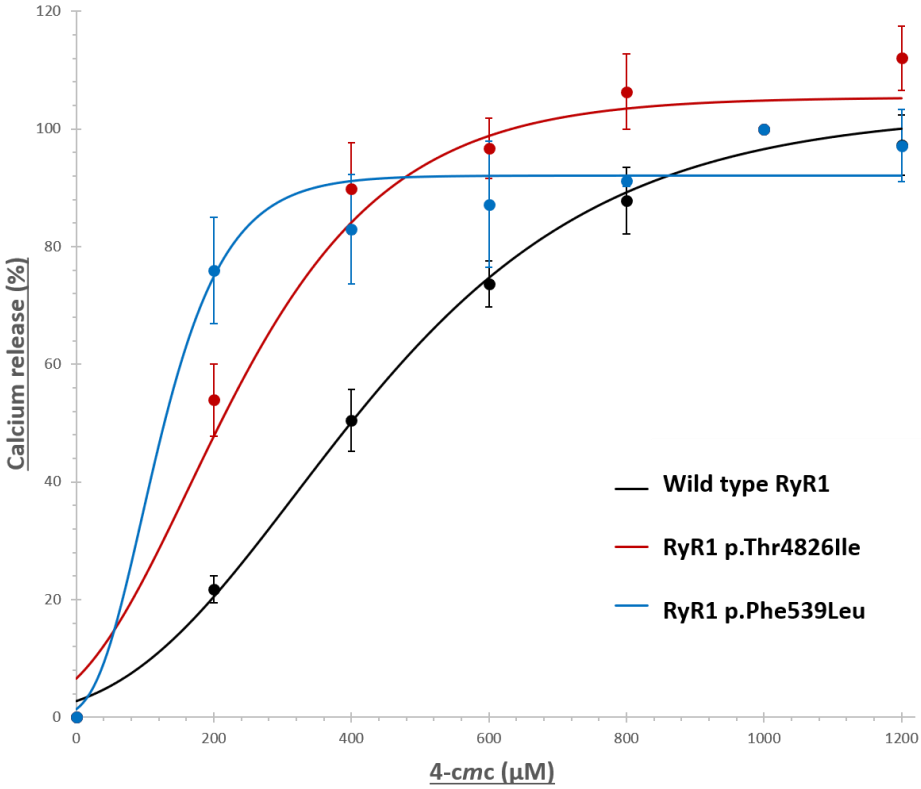

Figure 3.27 Calcium release curve of RyR1 p.Phe539Leu stable line

After induction of ryanodine receptor 1 (RyR1) expression by tetracycline, stable FT-293 cells were exposed to incremental doses of the agonist 4-chloro-*m*-cresol (4-cmc) in the presence of the ratiometric Ca^{2+} indicator Fura-2 (Section 2.3.12). The increase of cytoplasmic [Ca^{2+}] upon introduction of the agonist was normalised to 100% Ca^{2+} release as defined by the response to 1000 µM 4-cmc. Error bars represent the standard error of the mean for each data point and are based on biological replicates (n ≥ 6). Sigmoidal curves were fitted to each data set (Section 2.4.3).

The transient expression of the RyR1 p.Phe539Leu variant in HEK-293T cells produced a similar Ca^{2+} release curve to that of the MH positive control (Figure 3.28). The *p*-value of 1.8×10^{-4} calculated by Student's *t*-test easily passed the threshold for statistical significance with 99% confidence (data in Table 3.9). This substantiates the result in Figure 3.27 for which the RyR1 p.Phe539Leu stable expression line had greater sensitivity to the agonist.

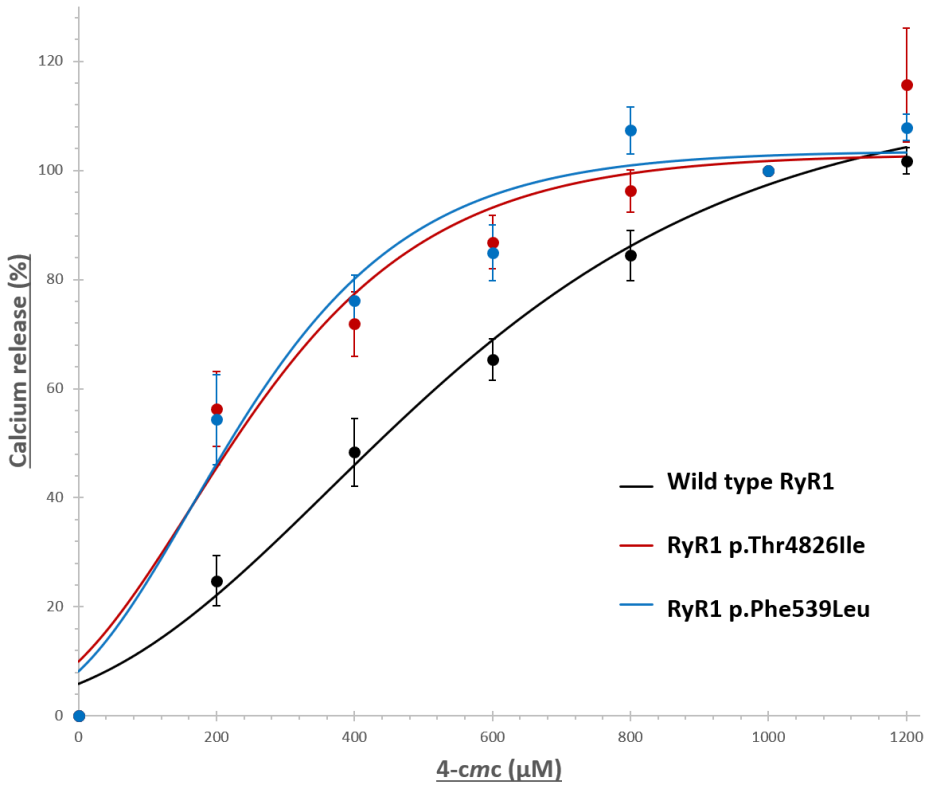

Figure 3.28 Calcium data from transient expression of RyR1 p.Phe539Leu

Following transient expression of ryanodine receptor 1 (RyR1) in HEK-293T cells (Section 2.3.3), fluorescence was measured after addition of incremental doses of 4-chloro-*m*-cresol (4-c*m*c) in the presence of the ratiometric Ca^{2+} indicator Fura-2 (Section 2.3.12). The increase of cytoplasmic [Ca^{2+}] upon introduction of the agonist was normalised to 100% Ca^{2+} release as defined by the response to 1000 µM 4-c*m*c. Error bars represent the standard error of the mean for each data point and are based on biological replicates ($n \geq 5$). Sigmoidal curves were fitted to each data set.

As the amount of RyR1 protein was normal for the HEK-293T cells transiently expressing RyR1 p.Phe539Leu as visualised by western blotting, it would indicate that the low levels of RyR1 protein observed in the stable expression lines was not the result of unstable mRNA or protein (see western blot in Figure 3.16). An argument against the creation of the stable expression lines being a factor, however, is that the same low expression was observed in monoclonal lines from two distinct transfection events. Therefore, it seems unlikely that similar deviations in integration would have occurred twice, resulting in low protein expression. Although the cause of the low RyR1 expression could not be

ascertained, the results from the transient expression of this variant in a recombinant system corroborated the results from the stable expression line.

The RyR1 p.Phe539Leu variant was found to segregate with an MH-susceptibility diagnosis in a large family after the proband suffered a fatal MH crisis during surgery. This variant was previously discovered in two small Australian pedigrees in which it segregated with MHS in four individuals as diagnosed by IVCT.[285] These pedigrees were believed to be related because they shared a common allele, although this is yet unconfirmed.[285] The RyR1 p.Phe539Leu variant is located in a dynamic region of RyR1 believed to be involved in multiple interactions during channel gating and therefore essential for normal functioning of the channel.[285] Phenylalanine 539 is located in the same helix as the well-characterised RyR1 p.Arg533Cys and p.Arg533His variants that are known to contribute to MH, providing further evidence that this dynamic region is essential for normal channel function.[243] A disruption to this part of the N-terminal domain may result in a lowered threshold for activation and channel opening.[243] The data presented in Figures 3.27 and 3.28 indicate that RyR1 channels with the p.Phe539Leu variant may be predisposed to open at a lower threshold of activation and therefore contribute to MH-susceptibility.

3.5.5 The RyR1 p.Arg1707Cys variant

When examined for RyR1 channel activity, the RyR1 p.Arg1707Cys stable expression line released no measurable Ca^{2+} upon addition of agonist. This was not unexpected because of the complete lack of RyR1 expression observed by western blotting and immunofluorescence methods. It is possible that this was related to an issue with the creation of the stable expression line; however, analysis of the variant in a transient expression system indicated the variant was expressed and co-localised to the ER in HEK-293T cells. Experimental work with the RyR1 p.Arg1707Cys stable expression lines was then abandoned.

The transient expression of this protein in HEK-293T cells produced a Ca^{2+} release curve similar to that of the stable WT RyR1 cell line, indicating that this channel is not hypersensitive to agonist (Figure 3.29). This result was confirmed when the Ca^{2+} release

profile of RyR1 p.Arg1707Cys was calculated to have a *p*-value of 0.62 by Student's *t*-test after transient expression in HEK-293T cells (data in Table 3.9).

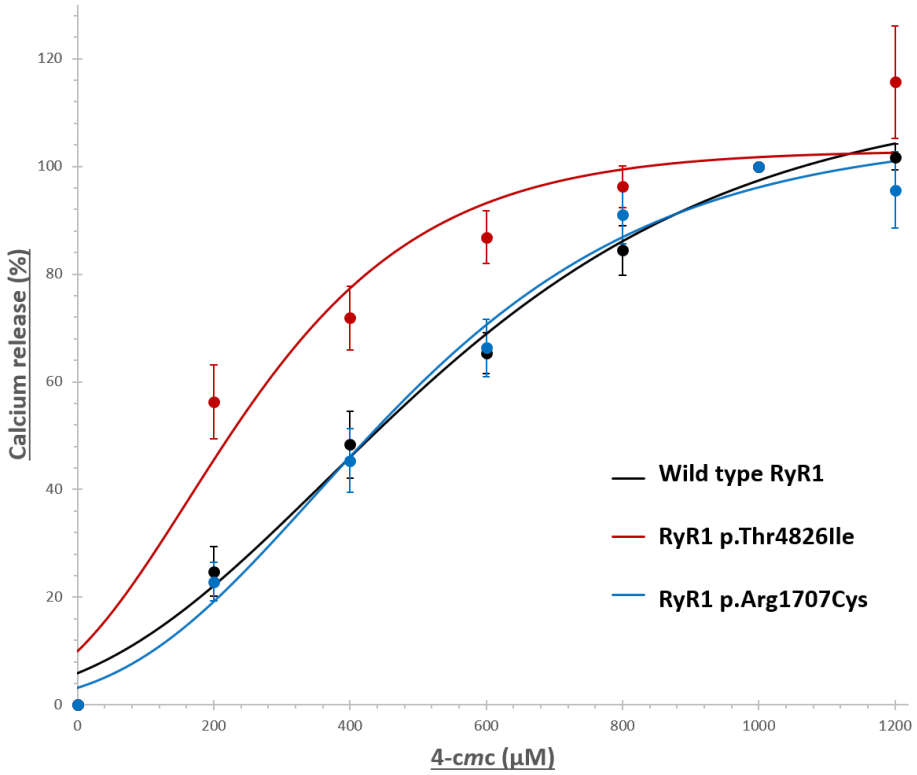

Figure 3.29 Calcium data from transient expression of RyR1 p.Arg1707Cys

After transient expression of ryanodine receptor 1 (RyR1) in HEK-293T cells (Section 2.3.3), fluorescence was measured after addition of incremental doses of the agonist 4-chloro-*m*-cresol (4-c*m*c) in the presence of the ratiometric Ca^{2+} indicator Fura-2 (Section 2.3.12). The increase of cytoplasmic [Ca^{2+}] upon introduction of the agonist was normalised to 100% Ca^{2+} release as defined by the response to 1000 µM 4-c*m*c. Error bars represent the standard error of the mean for each data point and are based on biological replicates (n ≥ 5). Sigmoidal curves were fitted to the data.

Little is known about the arginine 1707 residue that is located in the corona of RyR1, specifically the handle domain. The corona is a flexible structure and this flexibility reflects its role in long-range allosteric communication.[93] Its main role is thought to be relaying signals from the peripheral domains through extensive interactions with the central tower; however, it also participates in the mechanical association with the DHPR.[94] In addition, the handle domain is believed to be mechanically linked to the peripheral regions of

adjacent tetramers where these lateral interactions facilitate the coordinated gating of uncoupled RyR1 channels.[95] It is possible that mutations in the handle domain restrict the ability of RyR1 channels to assemble in the sarcoplasmic reticulum (SR) membrane by destabilising interactions with neighbouring channels. The low level of RyR1 p.Arg1707Cys protein observed by western blotting after transient expression in HEK-293T cells may be explained by this weakening of protein-protein interactions (western blot in Figure 3.16). It is also possible that the introduction of the smaller, uncharged cysteine residue at this location could introduce complications in protein folding or create instability in the protein product, resulting in lower levels of RyR1.

The novel RyR1 p.Arg1707Cys variant was identified in Family D in combination with the previously characterised RyR1 p.Val4849Ile variant in an individual with a non-specific myopathy. Genetic testing of both asymptomatic parents of the proband revealed that each variant allele was inherited from a different parent. This would indicate that either variant RyR1 allele is not independently capable of producing a disease phenotype. A similar instance to that of Family D was reported in 2005 in which a child of asymptomatic parents presented with CCD and was subsequently found to have inherited the RyR1 p.Val4849Ile allele from one parent and a truncated RyR1 allele from the other.[266] The lack of visible symptoms in the parents of the proband is not conclusive, however, because myopathies are prone to incomplete penetrance, even within families.[286]

The RyR1 p.Val4849Ile variant was initially disregarded as a pathogenic variant when it was identified in a control individual from a large cohort.[270] However, it has since been linked to numerous instances of CCD and MH-susceptibility as a homozygous allele.[201,266-269] When analysed for RyR1 sensitivity in a recombinant expression system, the variant had a moderate increase in sensitivity to agonists that was intermediate between that of the WT and an MH positive control.[264] A different study, however, reported a significant difference in Ca^{2+} release between RyR1 channels with and without the p.Val4849Ile variant in a similar recombinant expression system.[265] This variant has now been accepted as diagnostic for MH-susceptibility by the European malignant hyperthermia group.

Existing evidence indicates that the RyR1 p.Val4849Ile variant may not be individually sufficient to produce a disease phenotype and that its combination with another RyR1 variant is required for disease progression. In the instance of Family D, it is possible that low expression of the RyR1 p.Arg1707Cys protein may have enabled the RyR1 p.Val4849Ile protein to dominate the formation of tetramer channels. Although unable to be analysed in this recombinant system, it is possible that each allele was suppressed by the expression of WT RyR1 in the asymptomatic parents. This could be the reason that symptoms of myopathy presented only in the individual with both variants. Although they only have one copy of the RyR1 p.Val4849Ile variant, the proband from Family D may have a disease phenotype similar to that of an individual with two copies of the RyR1 p.Val4849Ile variant.[264,266,270] However, muscle tissue was not available to test this suggestion.

3.5.6 The RyR1 p.Pro2793Leu variant

Examination of channel sensitivity of the RyR1 p.Pro2793Leu variant to the agonist 4-c*m*c revealed the Ca^{2+} release profile to be substantially shifted to the left when compared with the WT response, much like the MH positive control (Figure 3.30). The statistical significance of the difference between the Ca2+ release profiles of the RyR1 p.Pro2793Leu stable expression line and that of the WT RyR1 channel was calculated with 99% confidence. This was performed by a Student's *t*-test and the *p*-value of 1.4×10^{-4} was well below the Bonferroni-adjusted α-value of 2×10^{-3} (data in Table 3.8). This result confirms the hypothesis that the RyR1 p.Pro2793Leu variant creates a RyR1 channel that has a lowered activation threshold and is therefore prone to inappropriate Ca^{2+} release.

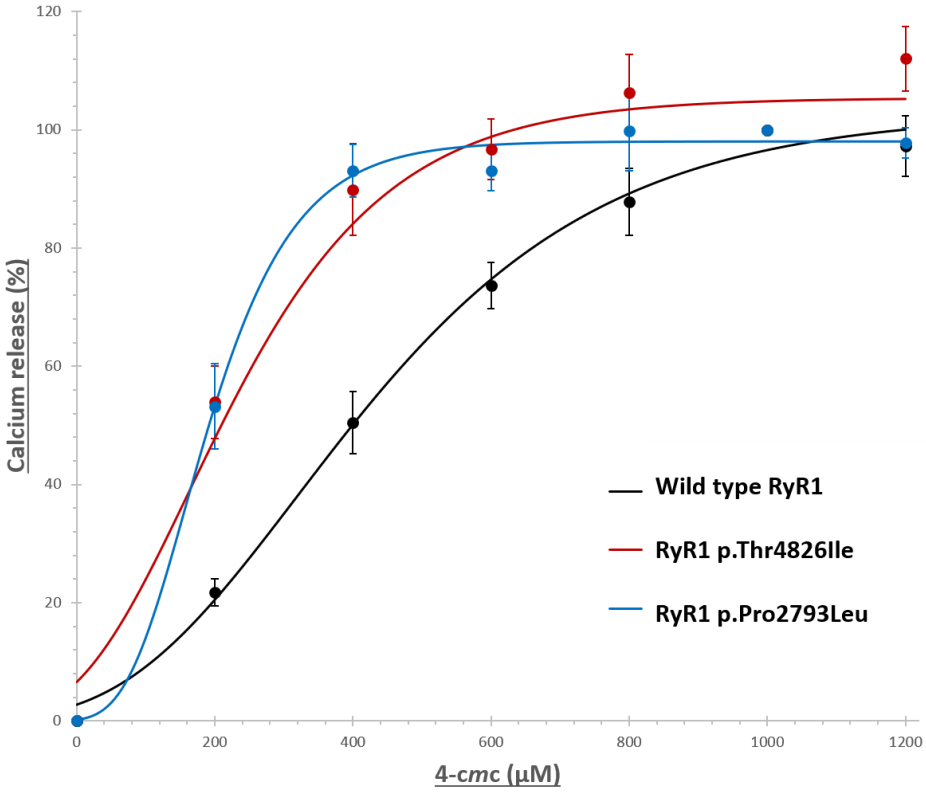

Figure 3.30 Calcium release data of RyR1 p.Pro2793Leu stable line

Following the induction of ryanodine receptor 1 (RyR1) expression by tetracycline, stable FT-293 cells were exposed to incremental doses of the agonist 4-chloro-*m*-cresol (4-c*m*c) in the presence of the ratiometric Ca^{2+} indicator Fura-2 (Section 2.3.12). The increase of cytoplasmic [Ca^{2+}] upon introduction of the agonist was normalised to 100% Ca^{2+} release as defined by the response to 1000 µM 4-c*m*c. Error bars represent the standard error of the mean for each data point and are based on biological replicates (n ≥ 6). Sigmoidal curves were fitted to each data set (Section 2.4.3).

The novel RyR1 p.Pro2793Leu variant was first discovered during genetic testing of an individual who had suffered an MH crisis after undergoing surgery. Proline 2793 has been mapped to the peripheral regions of RyR1 which experience the most substantial physical changes during channel gating.[96] As the most exposed elements of the channel in the cytoplasm, the peripheral domains have strong roles in several protein-protein interactions that facilitate opening of the channel. The peripheral domains contain the location of the FKBP12 binding site, they participate in interdomain interactions within RyR1, and they are the major location for the mechanical association with DHPR subunits.[100,101] Moreover, this region contains the site of phosphorylation of which kinases

are predicted to bind and strongly activate opening of the channel.[98,287] Accordingly, mutations in this part of the channel may lead to greater accessibility of the phosphorylation sites to kinases and therefore a channel more prone to opening. This feature is likely why many instances of MH-susceptibility have been linked to genetic variants in this location.[266,287]

3.5.7 Summary of results

A stable expression system that was employed to characterise five RyR1 variants linked to MH-susceptibility or myopathy—individually or in combination—produced variable results. Stable expression lines for all five variants, the WT channel, and an MH-positive control RyR1 p.Thr4826Ile were created by use of the Flp-In™ T-REx™ System from Invitrogen.[288] Four of the five RyR1 variants (p.Leu13Arg, p.Gln464Lys, p.Phe539Leu, and p.Pro2793Leu) were stably expressed in a recombinant system and subsequently analysed for their response to the RyR-agonist 4-c*m*c. All stable expression lines were found to be significantly sensitive to the agonist when compared against the WT RyR1 channel (Table 3.8).

The fifth variant (RyR1 Arg1707Cys) was assessed in a transient expression system and found to be expressed at low levels, although it had a similar Ca^{2+} release profile to that of the WT channel (Table 3.9). This indicates that, if this variant does indeed contribute to the myopathy phenotype observed in the proband of Family D, then it is likely through an alternative mechanism than a hyperactive RyR1 channel. Although the potential effect of the RyR1 Arg1707Cys variant on channel function requires further examination, the analysis of the remaining four RyR1 variants was convincing. Indeed, these findings indicate the RyR1 variants p.Leu13Arg, p.Gln464Lys, p.Phe539Leu, and p.Pro2793Leu meet the criteria for pathogenicity and should be added to the list of diagnostic variants for MH-susceptibility as set out in the guidelines by the European malignant hyperthermia group.[230]

Table 3.8 Statistical analysis of data from stable expression lines

Ryanodine receptor 1 variant	Goodness of fit (R^2 value)	EC50 ± SEM†	Statistical significance (p-value)
Wild type	0.93	399.0 ± 25.4	–
p.Thr4826Ile	0.80	209.4 ± 29.5	2.7×10^{-4}
p.Leu13Arg	0.93	135.5 ± 16.5	$< 1 \times 10^{-5}$
p.Gln464Lys	0.82	232.6 ± 27.0	2.2×10^{-4}
p.Phe539Leu	0.80	128.0 ± 24.9	2×10^{-5}
p.Pro2793Leu	0.92	191.5 ± 26.0	1.4×10^{-4}

† Half maximal concentration of 4-chloro-*m*-cresol ± standard error of the mean.

Table 3.9 Statistical analysis of data from transient *RYR1* expression

Ryanodine receptor 1 variant	Goodness of fit (R^2 value)	EC50 ± SEM†	Statistical significance (p-value)
Wild type	0.88	432.6 ± 30.9	–
p.Thr4826Ile	0.78	242.4 ± 36.4	1.2×10^{-3}
p.Phe539Leu	0.90	218.0 ± 26.9	1.8×10^{-4}
p.Arg1707Cys	0.90	428.8 ± 29.0	0.62

† Half maximal concentration of 4-chloro-*m*-cresol ± standard error of the mean.

3.6 Concluding remarks

3.6.1 Discussion of results

3.6.1.1 Functional analysis of variants

The dysregulation of Ca^{2+} homeostasis in the skeletal muscle of those susceptible to MH is believed to be caused by the inappropriate gating of RyR1. In normal muscle, the channel remains closed in the absence of a signal from the DHPR—even in the presence of volatile anaesthetics. The threshold for channel opening in MH-susceptible people, however, is substantially reduced and therefore more easily overcome by the action of volatile anaesthetics.[289] These suggestions have been supported in a study in which halothane exposure to MH-susceptible muscle fibres induced strong Ca^{2+} release in the presence of physiological [Mg^{2+}].[290] In this same study, normal muscle fibres released Ca^{2+} from stores in response to halothane only when the inhibitory effect of Mg^{2+} was removed.

The primary goal of this research was to examine the hypothesis that MH-associated RyR1 variants result in altered Ca^{2+} release from intracellular stores; that is, to understand the link between a genetic variant and the phenotype observed during an MH episode. This investigation involved the creation and analysis of stable expression lines based on the model cell line HEK-293 in which five RyR1 variants that were associated with MH-susceptibility, non-specific myopathy, or both, were examined for RyR1 activity. Four of those RyR1 variants (p.Leu13Arg, p.Gln464Lys, p.Phe539Leu, and p.Pro2793Leu) meet the requirements for diagnostic testing for MH-susceptibility based on their increased sensitivities to the agonist that were described experimentally in this study.[230]

The fifth RyR1 variant examined in this research, p.Arg1707Cys, did not show any hypersensitivity to 4-c*m*c. The low expression of the protein product observed by western blotting may have been a confounding factor and limited the collection of meaningful data. It is also possible that a phenotype for this variant cannot be measured by use of this non-muscle cell system. For instance, the model cell line used for analysis of the variants does not express many of the components of the complex network that normally regulate

Ca^{2+} handling in skeletal muscle. Additionally, the RyR1 p.Arg1707Cys variant identified in Family D was only associated with a non-specific myopathy in combination with the previously studied RyR1 p.Val4849Ile variant. The proband of Family D inherited a variant from each parent, both of whom were asymptomatic. This discrepancy may be the result of incomplete penetrance, which is not uncommon, or it may indicate a requirement for the co-expression of both RyR1 p.Arg1707Cys and RyR1 p.Val4849Ile variants for altered Ca^{2+} handling. Further analysis of RyR1 p.Arg1707Cys— and especially examination of the two variants in conjunction—is required before definitive conclusions may be drawn.

3.6.1.2 Functional basis for MH

Previously, it was believed that there were two categories of *RYR1* variants with divergent causal mechanisms—gain-of-function and loss-of-function.[291] Gain-of-function variants were thought to cause MH-susceptibility by producing a hyperactive channel that was highly responsive to pharmacological agents.[292,293] Loss-of-function variants and mechanically uncoupled channels were thought to cause a myopathy by the action of a leaky channel that depleted SR stores and reduced contractibility.[294,295] The apparent paradox of the MH phenotype observed in patients with diminished muscle function such as that of CCD or Native American myopathy cannot be explained by this loss-of-function hypothesis. Certainly, this would not explain the phenotypes observed in Family B in which both MH-susceptibility (a gain-of-function disorder) and non-specific myopathy (a loss-of-function disorder) were observed in combination in several family members.

More recently, evidence points towards the altered luminal Ca^{2+} modulation of RyR1 in a phenomenon known as store overload-induced Ca^{2+} release (SOICR) as a common feature in the distinct phenotypes observed with MH-susceptibility and RyR1 myopathies. The key element in the SR leak hypothesis is that, in the presence of a volatile anaesthetic, repetitive cycles of SOICR are triggered before Ca^{2+} can be returned to the SR, increasing cytosolic Ca^{2+} levels across the length of the fibre. This signals the influx of extracellular Ca^{2+} and therefore depolarisation of the sarcolemma, resulting in spontaneous EC coupling and muscle contracture.[67,296]

This hypothesis may explain the dominant inheritance pattern of MH-susceptibility, because SOICR may be induced by a small number of mutant channels, resulting in the opening of all channels by EC coupling and inappropriate muscle contraction.[75] So-called 'awake' episodes could also be explained by this hypothesis because environmental stress such as that observed during prolonged exercise or heat exposure can increase the Ca^{2+} stores substantially. This hypothesis is supported by experimental studies on the cardiac disease CPVT (catecholaminergic polymorphic ventricular tachycardia) for which both pharmacological stimuli and environmental stress lower the SOICR threshold substantially.[296] If a similar situation existed in skeletal muscle, then heat stress may result in an MH or MH-like episode. Not all instances of MH can be attributed to dysregulated Ca^{2+} leak, however, because *RYR1* variants *in vitro* and *in vivo* have produced the MH phenotype without affecting Ca^{2+} stores or resting myoplasmic Ca^{2+} levels.[249,291] Whether this is because of differences in experimental design or genuine divergence is yet undetermined.

3.6.2 Limitations of research

This study represents an attempt to produce monoclonal cell lines that allow the functional analysis of stably expressed genetic variants in a recombinant system. The advantages of recombinant systems in scientific research are many; namely, simplicity, convenience, and low cost.[242,243] In light of this, consistency is desirable for the purpose of comparison when variants associated with a complex disorder such as MH-susceptibility are placed in the context of a simple recombinant system.

The main concern when interpreting results in this part of the research was the variability of *RYR1* cDNA expression in the Flp-In™ T-REx™ System. The low RyR1 expression observed by western blotting in the RyR1 p.Phe539Leu stable expression line was unusual in that it had no effect on the Ca^{2+} release profile of the channel when exposed to 4-c*m*c. Even more unusual was the complete lack of RyR1 protein observed in the RyR1 p.Arg1707Cys stable expression line in which the presence of the corresponding cDNA in the genome was confirmed. The expression of both RyR1 variants was confirmed by transient expression in HEK-293T cells—an observation that did not reflect the minimal

level (or absence) of RyR1 protein observed in the stably expressing cell lines. The differences in phenotype between RyR1 variants *in vitro* may therefore be indicative of their phenotypes *in vivo* or a function of the expression system used.

There were two minor issues with the use of the Flp-In™ T-REx™ System; these were that that non-specific Ca^{2+} release was observed in the absence of introduced RyR1 channels and the tetracycline repression was not complete. These were not problematic for the simple data collection required for this study; however, they may compromise future experiments if the scope of the research expands beyond that described in this thesis. For example, the inability to completely regulate gene expression by use of the tetracycline repressor may be a concern if comparisons are required of cells with and without target gene expression in more complex experiments (described in Section 3.6.3). Additionally, the source of the RyR1-independent Ca^{2+} release remains unknown and requires further study to determine the cause and investigate potential antagonists that may be used to inhibit the pathway.

3.6.3 Future directions

3.6.3.1 Advancing the stable expression system

As the Flp-In™ T-REx™ experimental system developed in this research appears to produce useable results, the obvious next step would involve the creation of additional stable expression lines. The analysis of currently uncharacterised variants could be achieved in a short time-frame and the results may be used to identify diagnostic variants for MH-susceptibility. However, the greatest potential of the stable expression lines for a more complete explanation of the function of RyR1 channels lies in the ability to transiently express additional cDNAs.

The foremost initiative would be the transient expression of additional *RYR1* transcripts for the promotion of RyR1 heterotetramers. The majority of RyR1 variants are inherited in a dominant manner, and thus are co-expressed with the WT protein *in vivo*. There is *in vitro* experimental evidence for the existence of heterotetrametric channels with altered stabilities and conduction properties compared to their homotetramer counterparts.[297,298]

Another direction that may be explored in this way is the investigation of variant combinations such as that of Family D described in this thesis, concerning RyR1 variants p.Val4849Ile and p.Arg1707Cys. Analysis of these variants individually is essential for the understanding of their contribution to the phenotype; however, the findings are constrained without analysis of how they may combine to produce the myopathy phenotype observed in the proband of Family D.

3.6.3.2 Experimental approaches for functional analysis

Despite the vast body of knowledge relating to the protein complement of the EC coupling machinery in skeletal muscle, the current understanding of the various players and their roles in finely adjusting Ca^{2+} homeostasis remains limited. There are conflicting explanations of the molecular aetiology of MH; however, there is experimental evidence for the hypothesis that the inappropriate channel gating related to SOICR could be the foundation of most instances of MH. Furthermore, the altered activities of EC coupling accessory proteins *in vitro* have been experimentally linked to a lowered threshold for SOICR and Ca^{2+} dysregulation.

For example, MH-linked variants in *CACNA1S* can confer increased caffeine sensitivity to myotubes that is coupled with decreased SR stores and elevated cytoplasmic [Ca^{2+}], indicating a Ca^{2+} leak.[124-126] Moreover, the presence of a mutant form of HRC in the Ca^{2+} store with reduced Ca^{2+} buffering capacity lowers the SOICR threshold substantially.[299] The interaction between the DHPR and RyR1 may also regulate SOICR because a loss of the DHPR α1 subunit results in an increased sensitivity for SOICR and DHPR-uncoupled RyR1 channels are more likely to leak Ca^{2+}.[126,300] Stable expression lines represent an experimental system that will allow the *in vitro* examination of two or more components of the EC coupling pathway by the transient expression of accessory proteins in stable expression lines.

In addition to transfection of additional proteins, the stable expression lines represent an opportunity to explore new methods to investigate the consequences of genetic variants linked to MH. Addition of markers to recombinant proteins may be used to monitor

protein-protein interactions within the cell. An experimental example of this is a study in which the expression of fluorescently labelled Stac3 enabled the trafficking of the fluorescently labelled DHPR α1 subunit to the plasma membrane of a mammalian cell line through direct interaction of these proteins.[143] The use of protein markers to investigate specific interactions may be enhanced by techniques that require proximity to produce a signal such as fluorescence resonance energy transfer (FRET), bioluminescence resonance energy transfer (BRET), or the proximity ligation assay.[123,301,302]

Protein-protein interactions may also be investigated by use of affinity markers fused to introduced cDNAs that enable the isolation of protein extracts and subsequent *in vitro* analysis of interacting partners.[144,303] This category of experiments has been used extensively to describe interactions within the EC coupling machinery and how they may be modified under changing conditions. For example, FKBP12 proteins fused to a glutathione S-transferase tag were analysed by sandwich enzyme-linked immunosorbent assay and were found to bind RyR1 channels in a manner that was dependent on RyR1 open probability.[303]

Co-immunoprecipitation has been used *in vitro* to determine the interaction of the DHPR β subunit with a specific region of RyR1 by use of a polyhistidine tag on the DHPR subunit.[304] Co-immunoprecipitation was also used for a study in which a small region of RyR1 was discovered to be essential for triadin-binding.[159] Using co-immunoprecipitation, the authors found that a triple mutation in this region specifically reduced triadin binding in a manner that was comparable to the reduction in RyR1 channel conductance—the interaction between RyR1 and junctin was unaffected. This is an example of how biochemical techniques such as affinity markers may be combined with *in vitro* functional assays to provide perspective of how an altered interaction may result in an altered phenotype.

3.6.3.3 Investigating the role of SOICR

A key feature of the SR leak hypothesis is that the presence of one or more genetic variants that contribute to MH-susceptibility result in a lowered SOICR threshold; this, in turn,

causes a reduction of SR Ca^{2+} levels to partially compensate for the changed threshold. The role of SOICR in the aetiology of MH-susceptibility may be explored further by the use of genetically encoded fluorescent markers. Several fluorescent markers that bind Ca^{2+} with low affinity have been developed specifically for measuring Ca^{2+} levels in internal organelles. For example, GCaMPer has been used to examine Ca^{2+} changes in the ER of human induced pluripotent stem cell-derived cardiomyocytes.[305] Another example is Fluo-5N, a single-wavelength dye that has been used to estimate the Ca^{2+} content of skeletal muscle fibres from mice.[306] D1ER is another fluorescent marker that functions through fluorescence resonance energy transfer, and has been used in conjunction with Fura-2 (the fluorescent cytoplasmic Ca^{2+} indicator used in this research) in HeLa and MCF-7 cells.[307] Because transfection is required for these molecular techniques, the stable expression lines have great potential for the investigation of the SR leak hypothesis.

To conclude, the use of the Flp-In™ T-REx™ System to create stable expression lines represents a valuable resource for analysing variants by way of a simple phenotypic change such as RyR1 hyperactivity. Accordingly, this system will be the starting point of future work. Questions regarding the molecular aetiology of MH may be addressed with stable expression lines such as those described in this thesis together with a range of different biochemical and physiological assays.

4 Gene editing in human myoblasts

4.1 Considerations for gene editing methodology

The aim of this research was to develop and optimise a gene editing system for the introduction of single nucleotide changes into human skeletal myoblasts isolated from patients susceptible to malignant hyperthermia (MH). Initially, the system was designed for the introduction of ryanodine receptor 1 (RyR1) variants into the genome of an immortalised human myoblast cell line. This would theoretically enable the direct comparison of variants in a physiologically relevant system, without the complication of different genetic backgrounds. The expectation of this project was that, after the methodology was optimised, gene editing would then be employed for use in patient-derived myoblasts. The myoblasts of MH-susceptible individuals would undergo gene editing to 'correct' the variant suspected to cause the disease phenotype; these myoblasts would be analysed for RyR1 hyperactivity, both before and after this gene editing. Additionally, the myoblasts from 'normal' relatives of MH-susceptible individuals would be analysed for RyR1 hyperactivity, both before and after gene editing to introduce the same variant of interest. In this way, gene editing would provide a tractable system for functional characterisation of genetic variants associated with MH-susceptibility.

The gene editing method was new to the laboratory and required development from first principles. Although successful gene editing in myoblasts had been reported, the use of the gene editing system in this way was predicted to be challenging, because the primary repair pathway favoured by the cell is error-prone and many of these repair events will likely result in gene disruption.[308-310] It was thus decided that the novel molecular editing technique would be optimised by use of a well-characterised genetic variant as a model of MH, because the phenotype of any successfully edited cells could be predicted. The initial testing of this novel system was, therefore, designed for the heterozygous introduction of the *RYR1* c.14477C>T variant into the *RYR1* gene. This corresponds to the known diagnostic RyR1 variant p.Thr4826Ile, a variant that has a phenotype which is consistent with that of MH-susceptibility by conferring hypersensitivity to agonists on RyR1 function.[240,246,288]

4.1.1 System used to characterise variants

Several *in vitro, in vivo*, and *ex vivo* systems have been used to functionally characterise variants associated with MH-susceptibility, each with advantages and disadvantages. One of the most commonly used systems is the recombinant approach, such as that described in Chapter 3, which is used for the study of MH-susceptibility because of its simplicity. In this way, the properties of introduced mutated and normal proteins may be directly analysed *in vitro*; the simplicity, however, limits the scope of recombinant systems. The complexity of a disorder such as MH-susceptibility cannot be fully investigated without the presence of essential components of the EC coupling apparatus that are lacking in a non-muscle model cell. Variants associated with MH-susceptibility could ideally be analysed in a near physiologically relevant system to human muscle, such as human skeletal myotubes. These are the precursors to the mature muscle cell that express most of the EC coupling machinery endogenously. *Ex vivo* experiments with patient-derived cells have been used extensively, because they are valuable for the study of how a variant may produce a particular phenotype.[311–314]

The use of primary myotubes is limited, however, because the genetic background of an individual may confound the results when studying the role of a single genetic variant for MH-susceptibility. Moreover, it is estimated that the proliferative capacity of primary myoblasts derived from patients is limited to between 25 and 50 cell doublings. Therefore, after a period of time in culture, cellular senescence would begin to alter the characteristics of the myoblasts, halt cell cycle progression, and affect the ability of the myoblasts to differentiate into myotubes suitable for functional studies.[315] For these reasons, the acquisition of immortalised human myoblasts was essential before any meaningful research with human myotubes could be conducted.

Indeed, the ability to directly compare genetic variants from potentially any gene in the same genetic background would have wider implications than simply in the development of a new functional system. Accordingly, an immortalised cell line derived from immature skeletal myoblasts, HMCL-7304 (RRID: CVCL_T053), was acquired for this research from the UK Biobank.[316] This cell line had been previously differentiated into myotubes after

withdrawal of serum, after which the expression of EC coupling components were confirmed, and the response to Ca^{2+} release agonists was comparable to that of primary myotubes.[315,316] The HMCL-7304 cell line, therefore, represented a useful experimental model to develop an innovative technique for the functional characterisation of genetic variants in patient-derived myoblasts. It would also allow the definitive analysis of genetic variants without the complicating factors of an unknown genetic background.

4.1.2 Delivery of DNA into myoblasts

The approach taken to introduce the gene editing components into the cells was vital to the success of the research, because human myoblasts are difficult to manipulate. Most common methods of transfection have a reported transfection efficiency of between 20% and 40% in myoblasts, which is negatively correlated to plasmid size.[317-319] Both Nucleofection and lentiviral transduction were considered as options for the introduction of gene editing components into the immortalised myoblast cell line. Nucleofection has been reported to be effective in introducing DNA to sensitive or difficult-to-transfect cells without compromising cell survival.[320,321] This technique is a modified form of electroporation and uses a specific combination of proprietary reagents and voltage settings that are optimised for each cell type. It requires an electroporation apparatus known as a Nucleofector™ that was purchased from Lonza specifically for this project.

Lentiviral transduction was also considered as a method of introducing DNA into human myoblasts because it was thought to be the most reliable vehicle for skeletal myoblasts in common use.[322] Other viral transduction methods and chemical and physical transfection methods were either inefficient or too harsh on many cell types to be a viable option. The lentivirus represents an efficient vehicle for the introduction of genetic material to a wide range of cell types, but it has several disadvantages. First, it is time-consuming and labour-intensive because it requires three steps be performed before transduction can occur: 1) the transfection of a host cell line, 2) viral harvest, and 3) subsequent titration. There is also a safety risk in the potential to generate replication-competent lentiviral particles; however, this risk is mitigated with second and third-generation viral systems. Second-

generation systems require the use of three plasmids for competent virus whereas third-generation systems require four plasmids—these improve safety at the cost of viral titre.

In addition to a potential safety-risk, a major issue with the use of lentivirus is that it can produce several unwanted effects by means of stable integration of its genetic material into the genome of the host cell. This would be particularly undesirable because this may enable the constitutive expression of the gene editing components, increasing the chances of off-target effects. The replacement of an aspartate residue with a valine residue in the integrase enzyme encoded by the viral packaging plasmid, psPAX2-D64V (Addgene; plasmid map in Appendix B.8) would enable its use in transient transfection without integration.[323-325] This 'non-integrating' virus may still integrate into the genome at a low rate, however, with the potential for off-target effects.[325] Both approaches—Nucleofection and lentiviral transduction—were trialled as described in Sections 4.2.4 and 4.2.5.

4.1.3 Overview of CRISPR gene editing

One of the greatest advancements in molecular biology over the past decade has been the development of the clustered regularly interspaced short palindromic repeats (CRISPR) and CRISPR-associated protein 9 (Cas9) system into a gene editing technique by two research groups in 2013.[326,327] This innovative technology was developed from an adaptive bacterial immune defence system that operates by means of the RNA-guided recognition and elimination of invading genetic material via DNA cleavage.[328] Precise gene editing was developed by harnessing the capabilities of the CRISPR/Cas9 system to recognise a specific target DNA sequence and subsequently introduce a double-strand break (DSB) into that exact location.

Methods utilising the creation of DSBs in DNA have been used for targeted gene modification in the genomes of eukaryotic cells since the early 1990s. The most widely used of these were zinc finger nucleases (ZFNs) and transcription activator-like effector nucleases (TALENs). ZFNs and TALENs combined the endonuclease activity of the Fok1 enzyme with the DNA-recognition properties of zinc finger and transcription activator-like effector proteins, respectively. The DNA-binding portions of ZFNs comprised zinc

finger proteins (ZFPs) that recognise specific nucleotide triplets, whereas the DNA-binding portions of TALENs recognise individual nucleotides (Figure 4.1).

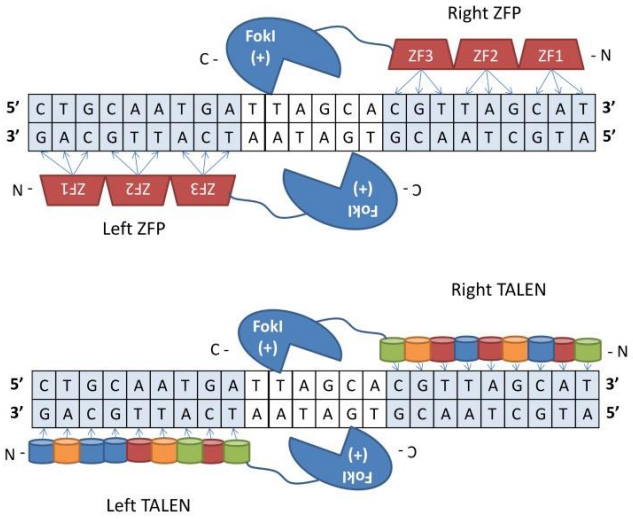

Figure 4.1 Method of earlier gene editing technologies

Zinc finger nucleases and transcription activator-like effector nucleases (TALENs) recognise two short, adjacent DNA sequences (shaded blue) and create double-strand breaks. Zinc finger proteins (ZFP; red blocks) recognise nucleotide triplets and TALEN domains (coloured blocks) each recognise a nucleotide. FokI restriction endonuclease subunits are shown (dark blue). *Image reproduced from 'Nuclease-Mediated Gene Therapies for Inherited Metabolic Diseases of the Liver' by Bryson, Anglin, Bridges, and Cottle under the Creative Commons licence 4.0.*[329]

The requirement of two FokI endonuclease subunits that work in concert to create a DSB increases the specificity of the targeting because it requires the recognition of two unique, neighbouring DNA sequences by the nucleases (Figure 4.1). These technologies, although still effective and widely used, require complex and time-consuming protein engineering strategies. In contrast, the development of the CRISPR/Cas9 system made gene editing readily accessible because it requires relatively simple molecular biology manipulations.[330]

Basic CRISPR/Cas9 technology requires just two components, a short guide RNA sequence (gRNA) and Cas9 endonuclease. These together form a ribonucleoprotein complex through the interaction of Cas9 with the 3' end of the gRNA, known as the scaffold (Figure 4.2). The target site of this gRNA/Cas9 complex comprises a unique protospacer sequence

that is 20 base pairs in length. This protospacer resides directly upstream of a defined sequence that is specific to the Cas9 endonuclease, known as the protospacer-adjacent motif (PAM). The ribonucleoprotein complex recognises its target site by means of two highly specific interactions. Cas9 tightly binds the PAM, and a short sequence at the 5' end of the gRNA (the spacer) binds its complementary protospacer sequence in the genome (Figure 4.2).[331,332] Upon recognition of its target site, the ribonucleoprotein complex binds tightly to—and subsequently cleaves—both strands of the DNA within the protospacer sequence (Figure 4.2).

Targeted gene knockouts by means of inserts and deletions (indels) can be produced through the error-prone non-homologous end-joining (NHEJ) DNA repair pathway. Knockouts generated in this way have been used in several mammalian cell systems to interrogate gene function and regulatory networks.[333-336] Although most DSBs are preferentially repaired in the NHEJ pathway, homology-directed repair (HDR) at the break site can be induced by providing the cell with a DNA repair template. The repair template, introduced with the CRISPR/Cas9 machinery, comprises the sequence to be introduced flanked by homology arms (Figure 4.2). These are sequences of varying length that are homologous to the surrounding residues where the change will be made.

There will often be a copy of the target site in the repair template because of the proximity between the DSB and the introduced sequence. In these instances, silent changes must be integrated into the corresponding repair template sequence. This is to prevent recognition and subsequent degradation of the donor DNA by Cas9 before incorporation and further editing by Cas9 after successful repair of the DSB. Silent changes are usually introduced to alter the PAM sequence because PAM recognition is essential for Cas9 endonuclease binding (Figure 4.2).[326]

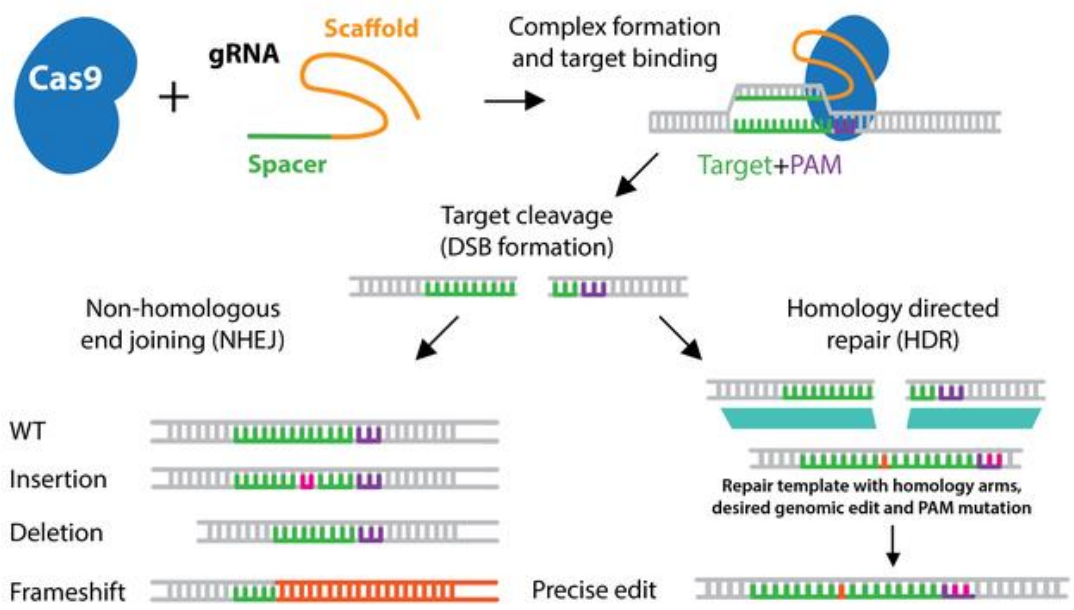

Figure 4.2 Schematic of CRISPR/Cas9 editing

The mechanism by which gene editing repair occurs after the introduction of a double stand break (DSB) in the genome (grey) by clustered regularly interspaced short palindromic repeats (CRISPR) and CRISPR-associated protein 9 (Cas9) endonuclease activity. The components required for gene editing are shown with the scaffold and spacer segments of guide RNA (orange and green), Cas9 endonuclease (blue), the protospacer (green), and the protospacer-adjacent motif (PAM; purple). DSBs are resolved by either non-homologous end joining (NHEJ) repair or homology directed repair (HDR). NHEJ may either result in wild-type (WT) sequence from correct repair, or introduce mutations whereas the presence of an appropriate repair template with a variant (red) induces HDR. Thick lines coloured cyan between the target sequence and the repair template indicate sequence homology. *Image reproduced with permission from the rightsholder, Addgene.*[337]

Homology-directed repair is a valuable CRISPR/Cas9 application because it has been used successfully to both model and correct certain disease phenotypes including the study of human disease by use of animal models.[338-340] This is because a range of changes can be made by designing an appropriate repair template. These may be precise changes such as single nucleotide substitutions or large changes such as whole gene inserts or deletions.[341] A notable example of the robust editing ability of CRISPR/Cas9 technology was the partial restoration of dystrophin in beagles that suffered from the canine equivalent of Duchenne muscular dystrophy, after successful deletion of an exon by means of CRISPR/Cas9.[342]

4.1.4 Selecting a Cas9 endonuclease system

The CRISPR/Cas9 systems of several bacterial species have been characterised that recognise distinct PAM sequences, but all function in much the same way. The majority of CRISPR/Cas9-related research to date has been conducted with the Cas9 endonuclease that was isolated from *Streptococcus pyogenes* (SpCas9); this strain of Cas9 has a PAM sequence of 5'–NGG–3'.[331,332] The SpCas9 endonuclease system is currently the most well-established CRISPR/Cas9 system. It was optimised for use in this research because it had the largest number of resources available for its use.[343] The SpCas9 endonuclease will be referred to as Cas9 for simplicity.

Although CRISPR/Cas9 has far greater specificity for target recognition than other genome engineering technologies, Cas9 can tolerate mismatches between the protospacer and the target sequence and potentially induce off-target mutagenesis.[344-346] This flaw is likely related to the binding procedure of the ribonucleoprotein complex to its genomic target. It is predicted that Cas9 initially scans the genome for PAM sequences and, upon detection, gRNA then binds the protospacer in a 3' to 5' direction. This is based on evidence that mismatches are more likely to be tolerated in the sequence distal to the PAM, whereas mismatches proximal to the PAM are rarely tolerated and mismatches within the PAM completely abolish binding.[347,348] In an attempt to negate this risk, Cas9 endonucleases have been developed with altered function that reduce off-target binding at the expense of available target sites and editing efficiency.

Most schemes that increase the fidelity of Cas9 activity require the binding of a pair of guides to the same genomic location; this involves the recognition of two distinct target sequences for the creation of a single DSB. The Cas9 nickase system takes advantage of a mutant form of Cas9 that can only cleave one DNA strand, creating a nick; accordingly, two adjacent nicks on opposing DNA strands are required for full cleavage (Figure 4.3).[349]

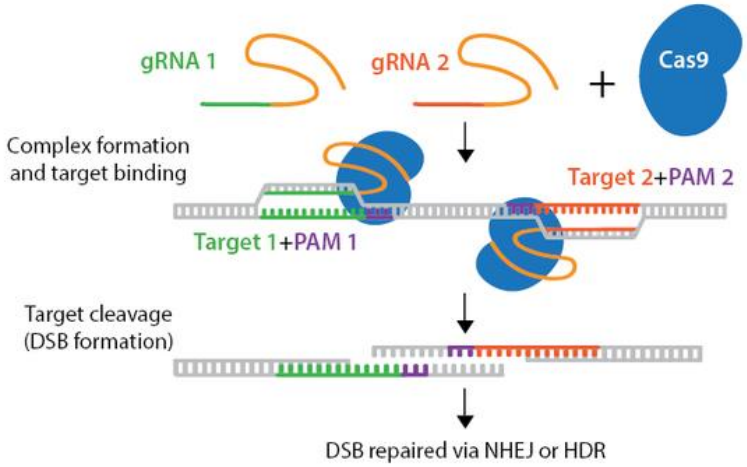

Figure 4.3 Action of Cas9 nickase

The mechanism by which two ribonucleoprotein complexes introduce adjacent nicks on opposite strands of the genome (grey) to create a double-strand break (DSB). The components required for gene editing are shown with the spacer segments of each guide RNA (gRNA) and their respective protospacer sequences in the genome shown in either green or red. The scaffold segments of both gRNA sequences (orange), Cas9 endonuclease (blue), and PAMs (purple) are shown. *Image reproduced with permission from the rightsholder, Addgene.*[337]

In a comparable manner, the fCas9 system combines the DNA-recognition capabilities of a catalytically inactive Cas9 with the endonuclease capability of Fok1. This mechanism requires the dimerisation and therefore proximity of two Fok1 subunits before cleavage may occur.[350] Unfortunately, the use of these paired Cas9 endonucleases is limited by the availability of useable target sequences. There were no appropriate pairs of target sequences in the human genome in close proximity to the *RYR1* c.14477C>T (RyR1 p.Thr4826Ile) variant that could be used in this research.

Several attempts have been made to engineer a high-fidelity Cas9 endonuclease that requires a single target sequence. These attempts involve weakening the interactions between the positively charged amino acids in the DNA-binding groove of Cas9 and the negatively charged DNA backbone. Cas9 variants created in this way have a reduced affinity for DNA binding and therefore substantially reduced off-target effects; however, this increase in fidelity is coupled with a decrease in editing efficiency.[351,352] Consequently, the standard Cas9 endonuclease system was chosen for the purpose of beginning this

research, whereas an alternative, less-efficient method could be used in future if fidelity is found to be an issue.

4.1.5 Design of guide RNAs

The targeting of the Cas9 endonuclease to a specific sequence within the genome relies almost solely on the performance of the gRNA with which it is complexed. The accepted design of a gRNA sequence for use with Cas9 endonuclease is a unique, 20-nucleotide sequence at the 5' end of the 5'–NGG–3' PAM. A study in 2014 found that use of a truncated guide sequence that was 17 nucleotides in length increased the fidelity of CRISPR/Cas9 recognition in HEK-293T cells many-fold without compromising editing efficiency.[353] At the time of guide design for this study, there was no software available that enabled the design of truncated guides, therefore the standard 20-nucleotide gRNA format was used. Research has since shown, however, that in more complex cell types such as stem cells, the reduction in off-target effects with truncated guides comes at a cost of up to 20% of the editing efficiency; thus, the decision to use the 20-nucleotide gRNA design may have been fortuitous.[354]

Theoretically, any sequence upstream of two adjacent guanine nucleotides (on either DNA strand) can function as a gRNA sequence for SpCas9. Because of this, the ability to use specially created software to design guide sequences is invaluable because hundreds of potential guide sequences surrounding the target site can be evaluated *in silico*. The design of the guide sequences for this study was performed with the CRISPR Design Tool created at Massachusetts Institute of Technology.[355] The four main parameters for selection of candidate guide sequences was: 1) the number of off-target sites, with particular emphasis put on those within coding sequences; 2) sequence similarity to off-target sites, with mismatches closer to the PAM and neighbouring mismatches more likely to be tolerated; 3) proximity to the desired genetic change; and 4) the ability to introduce silent mutations into the guide sequence within the repair template to prevent unwanted Cas9 recognition—mutations within the PAM being the preferred option.[345]

4.1.6 Design of the repair templates

A unique repair template was required for each gRNA sequence because, in addition to the *RYR1* c.14477C>T (RyR1 p.Thr4826Ile) variant, silent mutations were incorporated into the gRNA binding site contained within each repair template. Although short single-strand and double-strand repair templates (between 100–150 base pairs) are believed to be more efficient in most instances, for the purposes of this research a plasmid-based repair template was used to allow greater flexibility in the introduction of the donor DNA, for example with lentivirus.[356] This also allowed for a larger pool of potential guide sequences to select from because the homology arms would be much larger with this approach and coverage of both the DSB and the desired genetic change would be possible.

To ensure homology between the donor DNA and the target sequence in the genome, each unique repair sequence was created by use of PCR-amplification with genomic DNA (gDNA) extracted from the human myoblast cell line as a template. Mutagenesis was achieved with the three-step, overlap-extension PCR method described by Heckman and Pease.[357] This involved PCR with internal mutagenic and flanking non-mutagenic primers to amplify three overlapping fragments of DNA with the introduced changes. Pairs of primers named A, B, and C produced the fragments represented by the colours blue, orange, and green, respectively in Figure 4.4A (primers listed in Appendix A.1). Subsequent PCR steps extended these three fragments until full-length products were able to be amplified with the non-mutagenic flanking primers from primer pairs A and C, as shown in Figures 4.4B–C. These full-length PCR products contained both the *RYR1* c.14477C>T (RyR1 p.Thr4826Ile) variant of interest and the silent PAM mutations to prevent premature Cas9 endonuclease binding (Figure 4.4C).

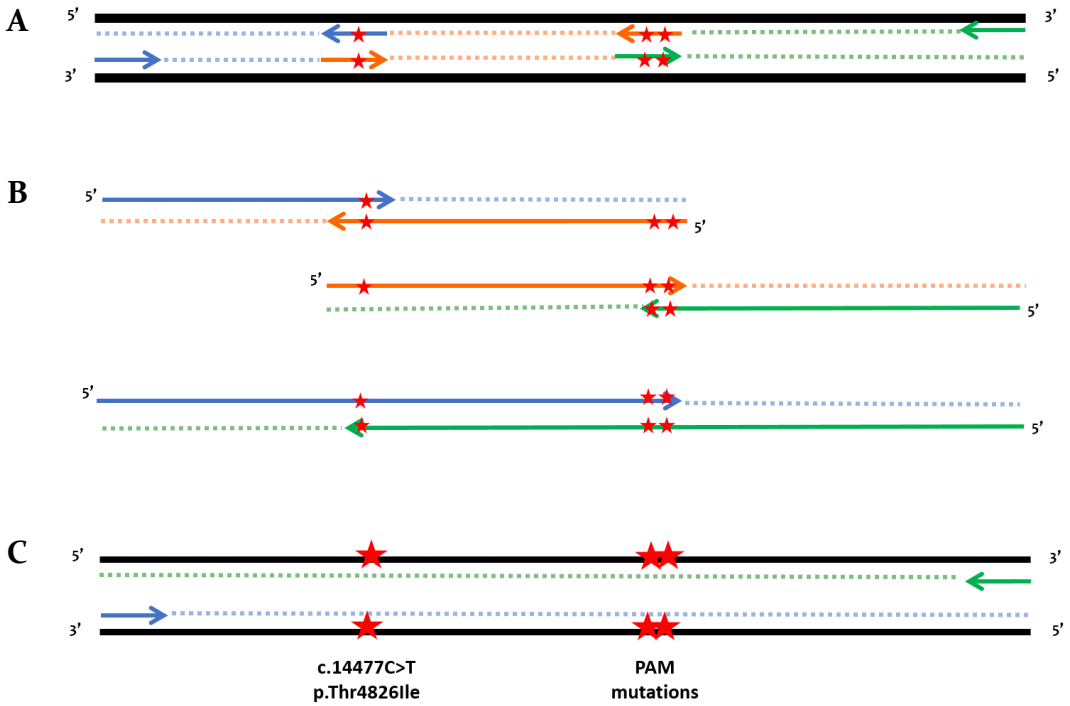

Figure 4.4 Schematic of repair template creation

A Stage one uses mutagenic and non-mutagenic primers (arrows) to amplify three overlapping fragments (blue, orange, and green) from the HMCL-7304 genome (black). Introduced variants are shown by red stars. **B** Stage two involves the extension of the overlapping fragments (arrows) by further PCR amplification after all three fragments are combined. **C** Stage three uses flanking PCR primers (arrows) to amplify the full-length product. Variants are labelled and indicated by red stars. *Figure created by the Author.*

4.1.7 Monoclonal selection of edited cells

One of the most difficult elements of the strategy to be considered was the method of selection for successfully edited myoblasts. At the time of project design, the frequency of HDR-editing events was predicted to be low, with reported frequencies of less than 1%.[358,359] Enrichment of cells that express Cas9 through biochemical selection was unfavourable because selection for a transiently expressed marker is difficult and may result in enrichment of cells with a stably integrated Cas9 gene into the genome. Biochemical selection for edited cells was also not possible because it would have required the stable introduction of a selection marker such as antibiotic resistance or fluorescent tag into the repair template and therefore within the *RYR1* gene. For these reasons, there

was no enrichment for edited cells and the method for identification of edited cells was the post-PCR method of high resolution amplicon melting (HRM) analysis.[360]

Because of the low frequency expected from HDR, considerable numbers of cells needed to be isolated and then gDNA was extracted from each of the resulting monoclonal cell lines. The limiting dilution method was chosen to isolate single cells. This involved seeding multi-well plates with a suspension of cells at a density such that the wells outnumbered the myoblasts by a factor of 3. The growth of these cells was then monitored to identify and subsequently exclude any wells that were likely to have been seeded with two or more myoblasts. Because the frequency of correctly edited cells was predicted to be low, monoclonal cell cultures were grown and then analysed on a large scale. Growing the cells in a 96-well plate format was a compromise between the practical consideration of growing hundreds of cell lines in a reasonable number of tissue culture plates and growing enough cells in each well to extract a useable amount of gDNA from each sample.

4.1.8 Detecting Cas9 endonuclease activity

As no selectable markers were introduced during the editing process, it was not possible to monitor the efficiency of the Cas9-directed cleavage of the HMCL-7304 genome. Accordingly, the ability of each gRNA to direct Cas9 to a specific genomic region was determined independently of the actual editing procedure. The T7 Endonuclease I (T7E1) assay, a post-PCR method used to detect DNA mismatches, was chosen for this process. This method takes advantage of the NHEJ editing pathway that results in small, non-specific genomic alterations such as indels in the absence of an appropriate repair template. These changes were introduced into the genome after gRNA-directed Cas9 cleavage and subsequently detected by the T7E1 assay shown in Figure 4.5.

This detection involves the PCR-amplification of the genomic region surrounding the DSB, after which the PCR product is denatured and then allowed to re-anneal. If the gDNA contains any indels at that genomic location, then some of the PCR products will anneal as a heteroduplex, although PCR products may anneal to an exact match (Figure 4.5). Because T7 Endonuclease I recognise and cleave DNA mismatches, the PCR product will

be cleaved at the site of the mismatch in the heteroduplex, producing fragments of predicted lengths that can be visualised by gel electrophoresis.

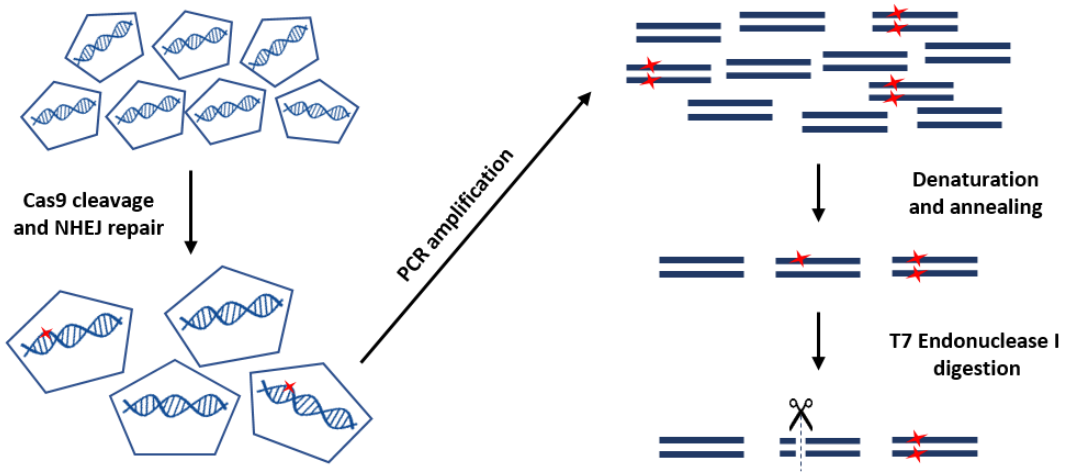

Figure 4.5 T7 Endonuclease assay for editing detection

Schematic of the T7 Endonuclease I assay. The Cas9-mediated cleavage of a genomic locus specified by the guide RNA is followed by the endogenous non-homologous end joining (NHEJ) repair mechanism, introducing a proportion of insertions and deletions (red stars). This locus is then PCR-amplified, denatured, and re-annealed, producing a mixture of homoduplexes and heteroduplexes. These are subjected to digestion with the T7 Endonuclease I enzyme (scissors) in which the heteroduplexes are selectively cleaved at the site of the mutation. *Figure created by the Author.*

4.2 *Preparation of gene editing components*

The primary goal of this research was to optimise the innovative molecular technique of CRISPR/Cas9 gene editing for eventual use with primary human myoblasts, and consequently the phases of planning and development were extensive.

4.2.1 *Working with immortalised human myoblasts*

Before commencing gene editing with the skeletal myoblast cell line, the ability of these precursor muscle cells to differentiate into mature myotubes was confirmed by immunofluorescence. Immature skeletal muscle cells have a single nucleus and do not express any of the EC coupling machinery, including RyR1 (Figure 4.6). Upon withdrawal

of serum, several of these cells fuse to form multinucleated muscle cells known as myotubes that possess most EC coupling components.[316] The progression of differentiation is shown in Figure 4.6 in which the fusion of just two myoblasts is sufficient to promote strong expression of RyR1, and thus gene expression changes occur early in the differentiation process. Mature myotubes can be visualised by the large tubular morphology in addition to the presence of multiple nuclei within the myotube (Figure 4.6).

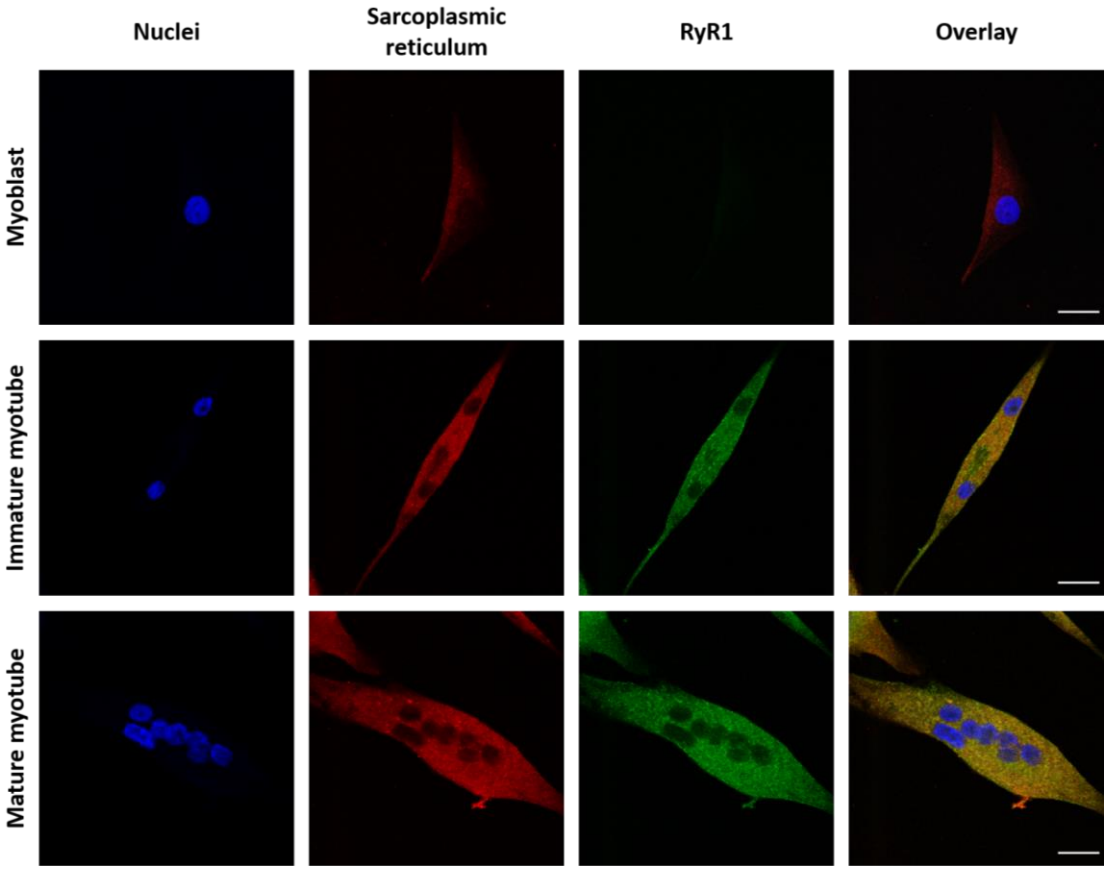

Figure 4.6 Differentiation of myoblasts into myotubes

HMCL-7304 cells were cells were grown on a microscope slide and then visualised during the progression of immature skeletal myoblasts to multinucleated myotubes after withdrawal of serum (Section 2.3.11). Primary antibodies for ryanodine receptor 1 (RyR1) and protein disulfide isomerase (sarcoplasmic reticulum marker) were used with fluorescently labelled secondary antibodies fluorescein isothiocyanate (FITC; green) and tetramethylrhodamine isothiocyanate (TRITC; red), respectively. Nuclei (blue) were visualised by staining the cells with 4',6-diamidino-2-phenylindole (DAPI). Cells were examined by confocal fluorescence microscopy at a magnification of 1260×. The scale bar in each merged image represents a length of 20 microns.

The goal of this research was to create a system that could be used to produce myoblast cell lines that express variant RyR1 channels for the purpose of assessing those cell lines for altered sensitivity to agonists. For this reason, RyR1 channel activity was analysed in HMCL-7304 myotubes to determine whether consistent results could be achieved. This analysis was performed by measuring the release of intracellular Ca^{2+} after the addition of the RyR-agonist 4-chloro-*m*-cresol (4-c*m*c; Figure 4.7). This was conducted by means of the acetoxymethyl ester form of the fluorescent Ca^{2+} indicator Fura-2 which specifically binds to Ca^{2+}. This dye can be detected by a ratiometric method (described at the beginning of Section 3.5); this method of detection reduces potential differences between biological replicates from dye leakage, photobleaching, or variable cell thickness. The rise in cytoplasmic Ca^{2+} levels was measured after addition of increasing amounts of 4-c*m*c and normalised to 100% Ca^{2+} release at 1000 µM 4-c*m*c, a method based on published results with human myotubes (Figure 4.7).[246,316,361]

This assay was found to produce consistent results because the Ca^{2+} release values were similar for each concentration of 4-c*m*c from ten individual myotubes. The resulting data were fitted to a sigmoidal curve to represent the Ca^{2+} release profile of RyR1 upon pharmacological activation (Figure 4.7).[316] Based on the dose-response curve, the half maximal concentration (EC50) of 4-c*m*c was calculated to be 428.7 µM (Figure 4.7). This was consistent with results from similar Ca^{2+} release assays of HMCL-7304 and primary myotubes in which reported EC50 values range from 200 µM up to 580 µM 4-c*m*c.[316,361,362]

After the data were analysed, it was not clear if the Ca^{2+} release observed after treatment with 1000 µM 4-c*m*c was the maximal level for the cells because the graph did not plateau. In future, higher concentrations of 4-c*m*c should be used to ensure that maximal Ca^{2+} release has been reached and therefore the correct half maximal concentration of 4-c*m*c has been determined. Further analysis of the myotubes, for example with alternative agonists, may reveal greater phenotypic data. At present, however, this result shows the myoblasts can differentiate into myotubes and respond to agonists appropriately.

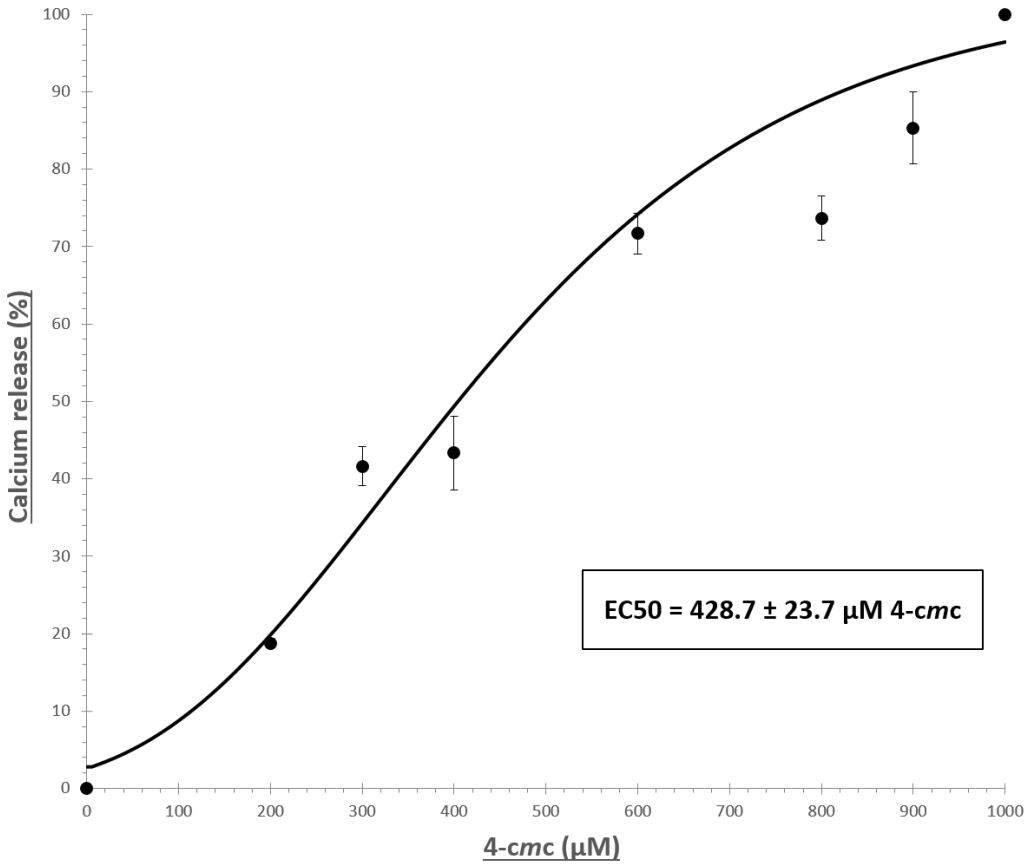

Figure 4.7 Pharmacological activation of RyR1 in HMCL-7304

HMCL-7304 myotubes were exposed to incremental doses of the ryanodine receptor agonist 4-chloro-*m*-cresol in the presence of the ratiometric Ca^{2+} indicator Fura-2 (Section 2.3.12). The increase of cytoplasmic [Ca^{2+}] upon introduction of the agonist was measured with a fluorescence microscope and normalised to 100% Ca^{2+} release. Error bars represent the SEM for each data point and are based on biological replicates (n = 10). Sigmoidal curves were fitted to each data set (n = 10) with CurveExpert software.

4.2.2 Production of guide RNAs

Each ribonucleoprotein complex comprising Cas9 endonuclease and gRNA contains a unique guide sequence that targets a specific location in the genome. Three unique guide sequences were designed that would be an integral part of each unique gRNA. Two guides were designed to introduce a DSB in an exon approximately 300 base pairs from the variant and the third was located in an intron within 200 base pairs of the variant—all were upstream of the *RYR1* c.14477C>T (RyR1 p.Thr4826Ile) variant. All three guides had high

guide scores, indicating a relatively low likelihood of off-target editing because a score of 50% or higher may be considered acceptable for use (Table 4.1).[345] The guide scores are based on a predicted targeting fidelity, for which each guide sequence has an initial score of 100% and the amount of percentage points subtracted is determined by a weighted score of predicted off-target binding.

Table 4.1 Output of CRISPR/Cas9 guide design

Guide	Guide score	Location	DNA strand	Number of off-targets	Highest off-target score
1	94%	exon	coding	23	0.9%
2	90%	exon	template	48	1.4%
3	80%	intron	coding	184	1.5%

There were many predicted off-target sites for guide sequence 3; however, these were all located in non-coding regions of the genome (as was the case for all three guide sequences). Furthermore, the guide scores for predicted off-target gRNA binding sites were lower than 2% (Table 4.1). Off-target scores are based on the likelihood of gRNA binding for each off-target site. Off-target binding for all three guides would require a minimum of three base pair mismatches between the gRNA and the off-target sequence, and as such, the off-target scores were small.

Three 20-nucleotide guide sequences in relative proximity to the *RYR1* c.14477C>T (RyR1 p.Thr4826Ile) variant were designed for use in this study with unique features as described in Table 4.1. Sanger sequencing confirmed the presence of these guide sequences in this genomic region of the HMCL-7304 cell line (sequencing data in Appendix E.1; primers listed in Appendix A.2). It is preferable for the introduced DSB to be as close as possible to the genetic change; however, the genomic sequence directly surrounding the site of the *RYR1* c.14477C>T (RyR1 p.Thr4826Ile) variant was not useable for guide design, and thus sequences distal to the substitution were used.[363,364] An advantage of this was the low likelihood of cells that would have the genetic change incorporated into both alleles as

one study found, in which zygosity was manipulated by changing the distance between the DSB and the genetic change.[365] The authors reported that homozygous genotypes were favoured by a DSB in close proximity to the variant and that the proportion of mono-allelic changes increased with the distance of the DSB from the allele change.

For each guide sequence, a single expression vector with the sequences for both the gRNA and Cas9 endonuclease was created to ensure Cas9 endonuclease and the gRNA were introduced into the cells simultaneously. This expression vector was the lentiviral transfer plasmid, lentiCRISPR v2, which was chosen because it was compatible for use with either lentivirus or Nucleofection for DNA delivery (plasmid map in Appendix B.9).[366] This expression vector produced a relatively high titre of virus, contained both Cas9 cDNA and the gRNA scaffold, and required only the insertion of each unique guide with simple cloning methods. Introduction of the guide sequences to lentiCRISPR v2 was theoretically straightforward. First, each guide sequence was created from specially designed oligonucleotides that were annealed together to produce complementary DNA overhangs with digested lentiCRISPR v2 (oligonucleotides listed in Appendix A.4). Next, a 1.9 kb filler flanked by restriction sites was removed from lentiCRISPR v2 by restriction endonuclease digestion with BsmBI enzyme. Finally, each guide was introduced to the lentiCRISPR v2 vector by the ligation of complementary overhangs.

Unfortunately, the cloning of the guides into the lentiCRISPR v2 vector was not simple. Although the vector seemed to be intact when visualised by gel electrophoresis, restriction endonuclease digestion of lentiCRISPR v2 with BsmBI repeatedly resulted in partial degradation—or sometimes complete degradation—of the vector when examined by gel electrophoresis. After adjustments to the restriction endonuclease digestion method did not improve the result, plasmid instability was hypothesised as the cause of the cloning difficulties; lentiviral vectors are known to have high rates of recombination when grown in *E. coli*.[367] Several alterations to the original method were investigated, including changing the amount of restriction endonuclease and the length of time for digestion; these changes reduced visible vector degradation but did not improve cloning efforts. Successful insertion of the guides into lentiCRISPR v2 was eventually achieved through

reduction of the incubation temperature for growth of *E. coli* to 30 °C, effectively slowing the rate of growth and reducing the probability of recombination as well.

The creation of the double-strand guides was confirmed by visualisation of the annealed oligonucleotides alongside their unannealed controls by gel electrophoresis (Figure 4.8). The mobilities of the 20 base oligonucleotides were high as was expected because they were single-stranded, whereas the 29 base pair annealed guides had a lower mobility consistent with 25 and 35 base pairs when compared with the DNA Ladder.

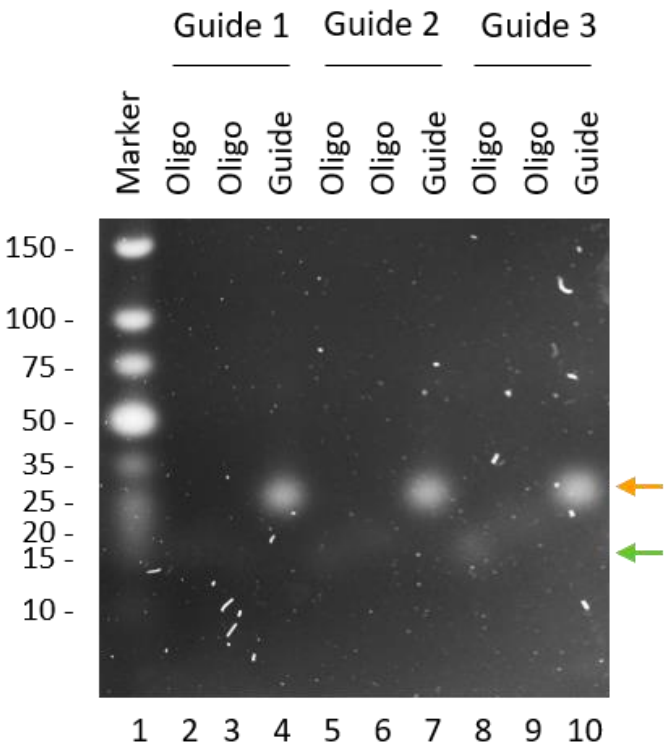

Figure 4.8 Creation of guide sequences for cloning

Complementary oligonucleotides (green arrow) were annealed together to create 'guides' (orange arrow) that were resolved by gel electrophoresis in a 5% agarose gel containing ethidium bromide and immersed in buffer (Section 2.2.3). Lane 1 contains GeneRuler Ultra Low Range DNA Ladder as a size marker with the length of each fragment indicated in base pairs.

Replacement of the 1.9 kb DNA filler with guides 1, 2, and 3 in the lentiCRISPR v2 vector produced the expression vectors LentiGuides 1, 2, and 3, respectively (schematic in Figure 4.9A; plasmid map in Appendix B.10). The identities of these constructs were established

by double digestion with EcoRV and NotI restriction endonucleases. This digestion was predicted to clearly distinguish between the original lentiCRISPR v2 vector and the newly created LentiGuide vectors. Two DNA bands were observed in each sample after gel electrophoresis: a 9.4 kb band and a smaller distinguishing band of either 5.4 kb or 3.6 kb for lentiCRISPR v2 or LentiGuide, respectively (Figure 4.9B). Correct cloning of the LentiGuides was further confirmed with Sanger sequencing in which the specific sequence of guides 1–3 were observed to reside in LentiGuides 1–3, respectively (Figure 4.10).

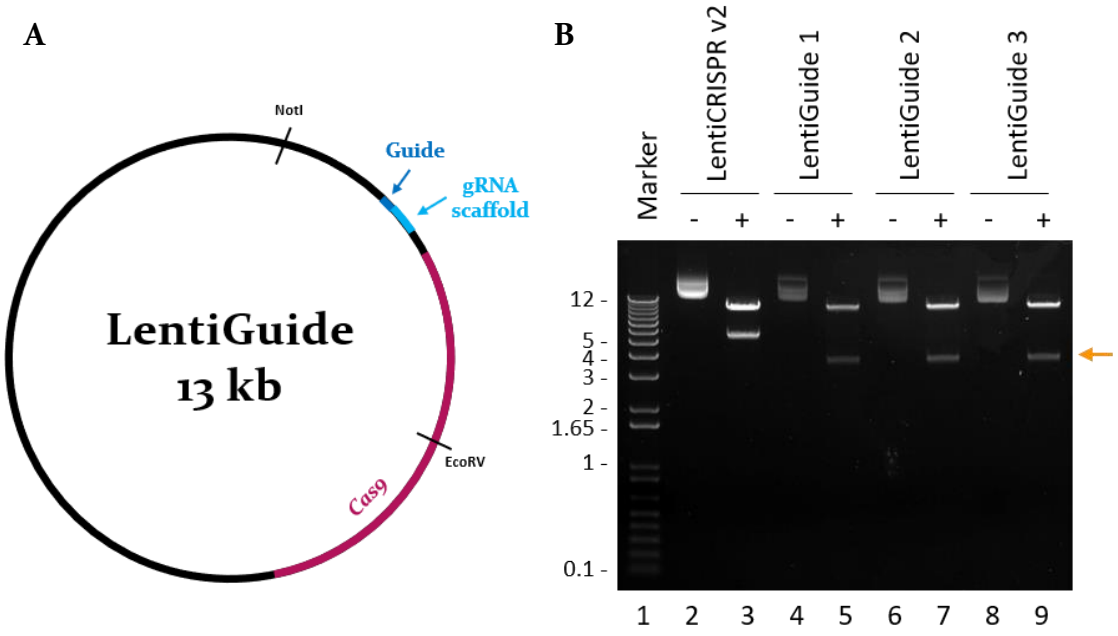

Figure 4.9 Creation of the LentiGuide expression vectors

A Plasmid map of a LentiGuide plasmid with the guide sequence (dark blue) adjacent to the guide RNA (gRNA) scaffold (light blue) and the Cas9 coding sequence (purple). Relative locations of relevant restriction endonuclease recognition sites are indicated. **B** After digestion with restriction endonucleases EcoRV and NotI (Section 2.2.4), lentiCRISPR v2 and LentiGuides 1–3 were resolved by gel electrophoresis (Section 2.2.3) alongside their uncut controls in a 1% agarose gel containing ethidium bromide and immersed in buffer. Successful cloning of the guide sequences was represented by a band migrating to approximately 3.6 kb (arrow). Lane 1 contains 1 Kb Plus DNA Ladder with the length of each fragment indicated in kb.

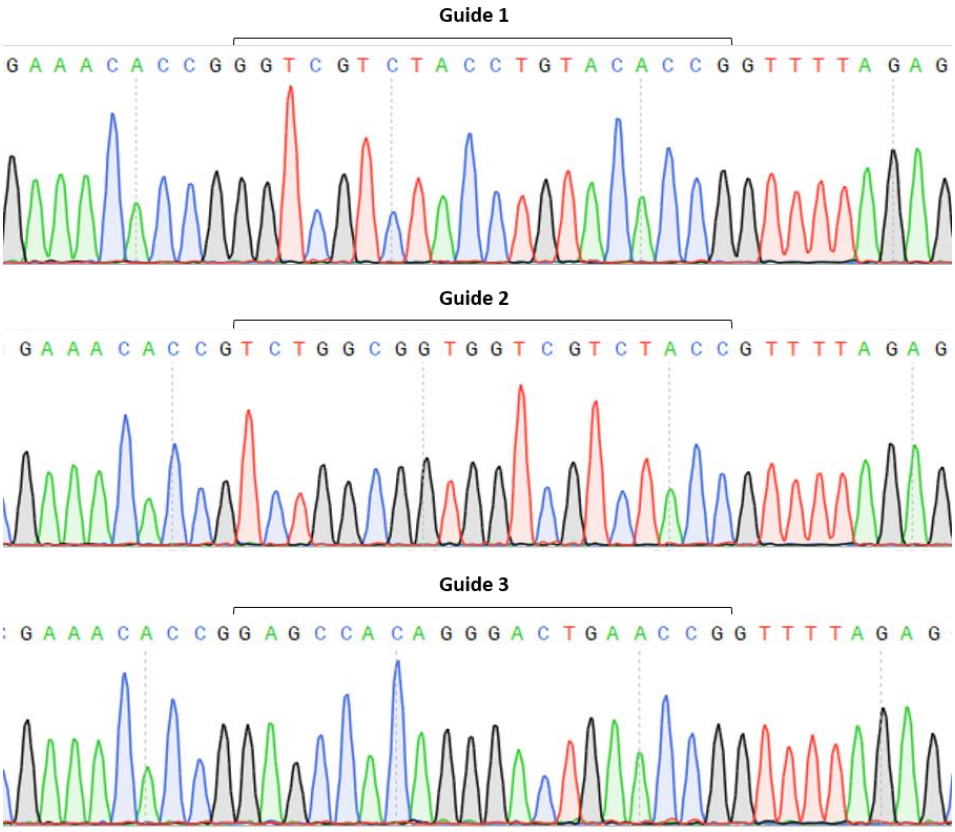

Figure 4.10 Validation of LentiGuide expression vectors

A representative chromatogram of Sanger sequencing in the 'forward' orientation is shown for each LentiGuide plasmid, with the sequences of guides 1–3 indicated.

4.2.3 Creation of the repair templates

The three unique repair templates designed for each guide sequence ranged in size from 500 base pairs to 800 base pairs; a factor that was dependent on the distance between the predicted DSB and the variant. These were created by the three-step, overlap-extension PCR method as outlined in Figure 4.4, with HMCL-7304 gDNA as the PCR template. For each repair template, three short overlapping DNA fragments were amplified in the first phase of PCR (Figure 4.11). These were subjected to electrophoresis so they could be analysed visually and were observed to be consistent with their predicted lengths as listed in Table 4.2.

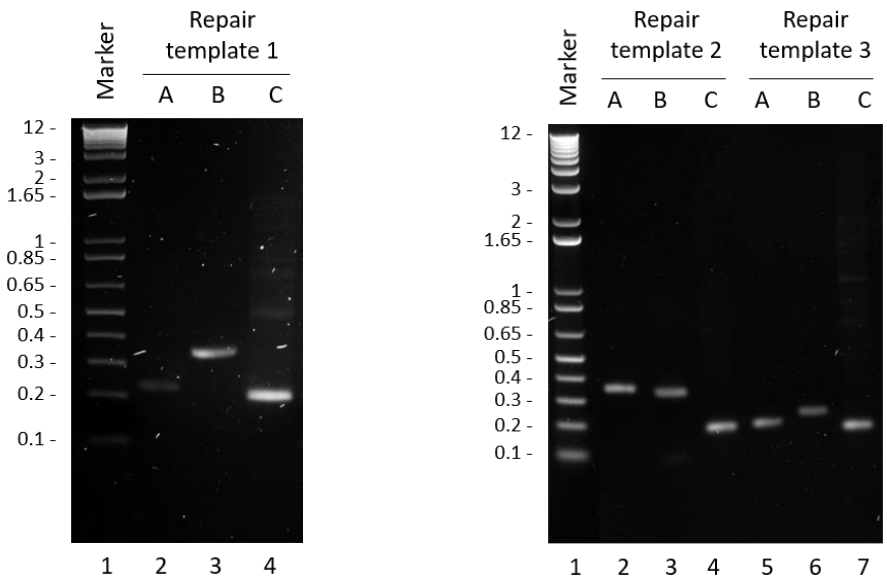

Figure 4.11 First stage of repair template creation

Stage one of overlap-extension PCR produced three fragments each (A, B, C) for repair templates 1–3. These were resolved by gel electrophoresis in 2% agarose gels containing ethidium bromide and immersed in buffer (Section 2.2.3). Lane 1 contains 1 Kb Plus DNA Ladder with the fragment lengths indicated in kb.

Table 4.2 Sizes of DNA fragments in repair template creation

Target	DNA fragment	Fragment length (bp)	Final product length (bp)
Repair template 1	A	247	749
	B	353	
	C	209	
Repair template 2	A	343	800
	B	326	
	C	194	
Repair template 3	A	196	537
	B	230	
	C	175	

For the next phase of PCR (outlined in Figure 4.4), the combination of the three fragments (A, B, and C) for each repair template enabled the extension of these fragments into full-length products. These PCR products were further amplified by PCR in the final stage by use of flanking primers. Because of the difficult nature of the PCR, non-specific PCR products were unavoidable for repair templates 1 and 2. For this reason, PCR products were excised from the gel and purified with the Wizard SV Gel and PCR Clean-Up System (Promega). Effective purification of the repair templates was confirmed visually by gel electrophoresis to establish that they were of the predicted lengths as listed in Table 4.2 (Figure 4.12).

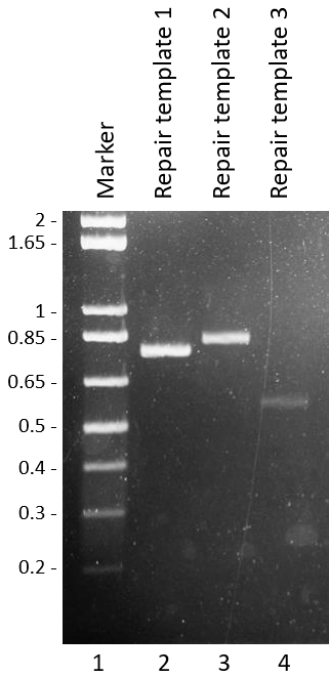

Figure 4.12 PCR-amplification of full-length repair templates

The final products for repair template 1 (749 bp), repair template 2 (800 bp), and repair template 3 (537 bp) were resolved by gel electrophoresis in a 2% agarose gel containing ethidium bromide and immersed in buffer (Section 2.2.3). Lane 1 contains 1 Kb Plus DNA Ladder with the fragment lengths indicated in kb.

All three repair templates were initially cloned into the pGEM-T Easy vector (Promega), creating the new repair template constructs, pGEM-RT 1, 2, and 3 (schematic in Figure 4.13A; plasmid map in Appendix B.11). The accuracy of this cloning step was confirmed by

restriction endonuclease digestion with EcoRI enzyme because EcoRI recognition sites directly flanked the insert in the original pGEM-T Easy vector. After the restriction endonuclease digestion and subsequent visualisation by gel electrophoresis, the 3 kb vector fragment can be observed in all digests (Figure 4.13B). The identifying fragments of repair templates 1, 2, and 3 were observed—749 bp, 800 bp, and 539 bp in length, respectively—confirming successful creation of the three pGEM-RT constructs.

Both the faithful amplification of each template and the presence of the intended changes were confirmed by Sanger sequencing (Figure 4.14; sequencing data in Appendices E.2–4). Each repair templates was then subcloned into the lentiviral transfer plasmid, pLJM1-EGFP (Addgene), by use of the EcoRI restriction endonuclease.[368] The single restriction site for EcoRI enzyme in pLJM1-EGFP was located in a region of the plasmid that was predicted to tolerate an insert without disruption to vector function (plasmid map in Appendix B.12). This cloning created the new lentiviral repair template plasmids, Lenti-RT 1, 2, and 3 (schematic in Figure 4.13A; plasmid map in Appendix B.13). This result was confirmed visually by restriction endonuclease digestion with EcoRI enzyme followed by gel electrophoresis (Figure 4.13B). Digestion of Lenti-RT plasmids 1, 2, and 3 with EcoRI enzyme produced two DNA bands for each construct as predicted. The 8.1 kb vector band could be seen in all samples and the same distinguishing band for repair templates 1, 2, and 3 could be observed.

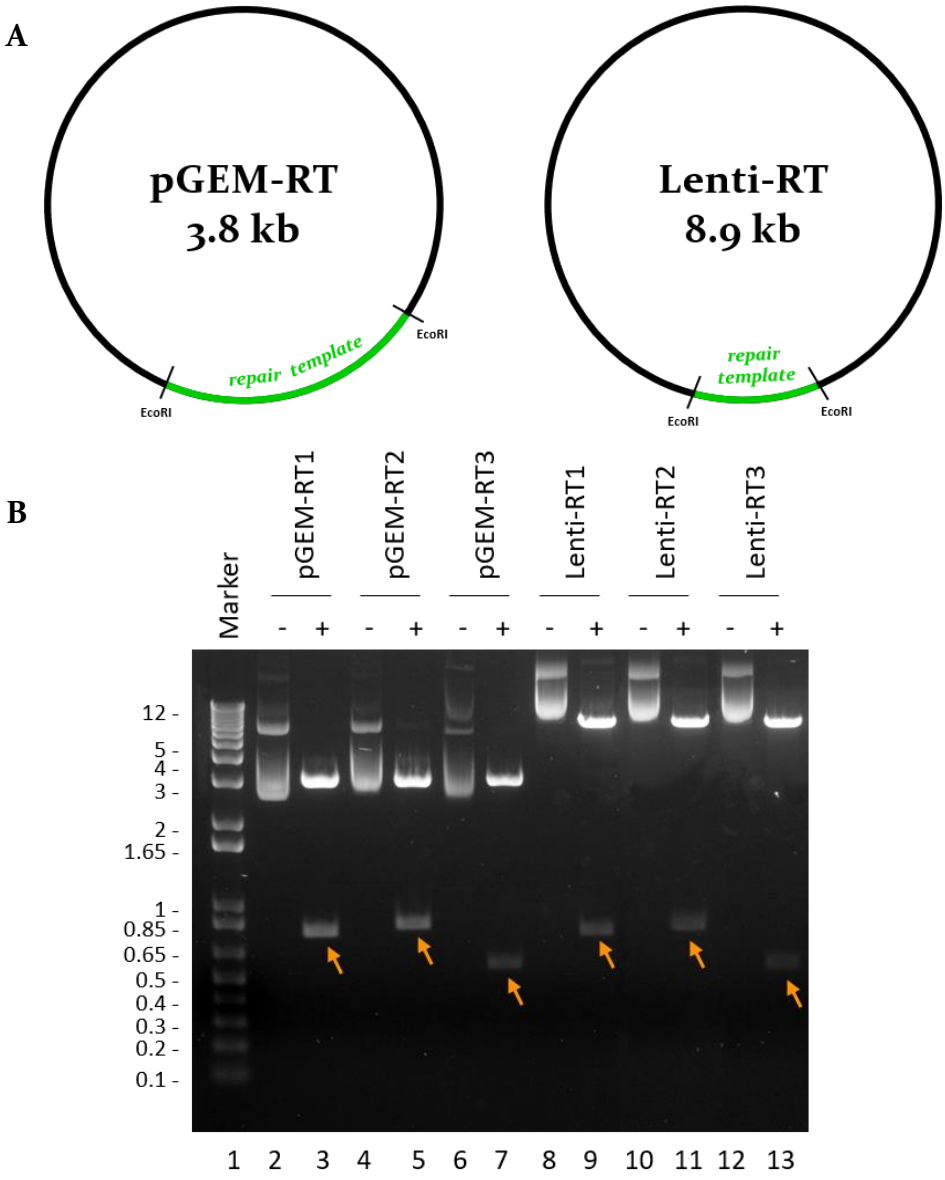

Figure 4.13 Creation of the repair template integration vectors

Repair templates 1–3 were cloned into the pGEM-T Easy vector and subsequently cloned into a lentiviral vector pLJM1-EGFP creating the pGEM-RT and Lenti-RT integration vectors, respectively. **A** Representative vector maps of the pGEM-RT1 and Lenti-RT1 plasmids containing the 749 bp repair template 1. Relative location of the repair template (green) and relative locations of EcoRI recognition sites are shown. **B** Plasmids were digested with EcoRI restriction endonuclease (+) and then resolved by gel electrophoresis (Section 2.2.3) alongside uncut controls (–) in a 1% agarose gel containing ethidium bromide and immersed in buffer. Lanes 2–7 contain pGEM-RT vectors and lanes 8–13 contain Lenti-RT vectors. Lane 1 contains 1 Kb Plus DNA Ladder with the length of each fragment indicated in kb. Identifying fragments of 749 bp, 800 bp, and 539 bp for repair templates 1, 2, and 3, respectively, are shown with orange arrows.

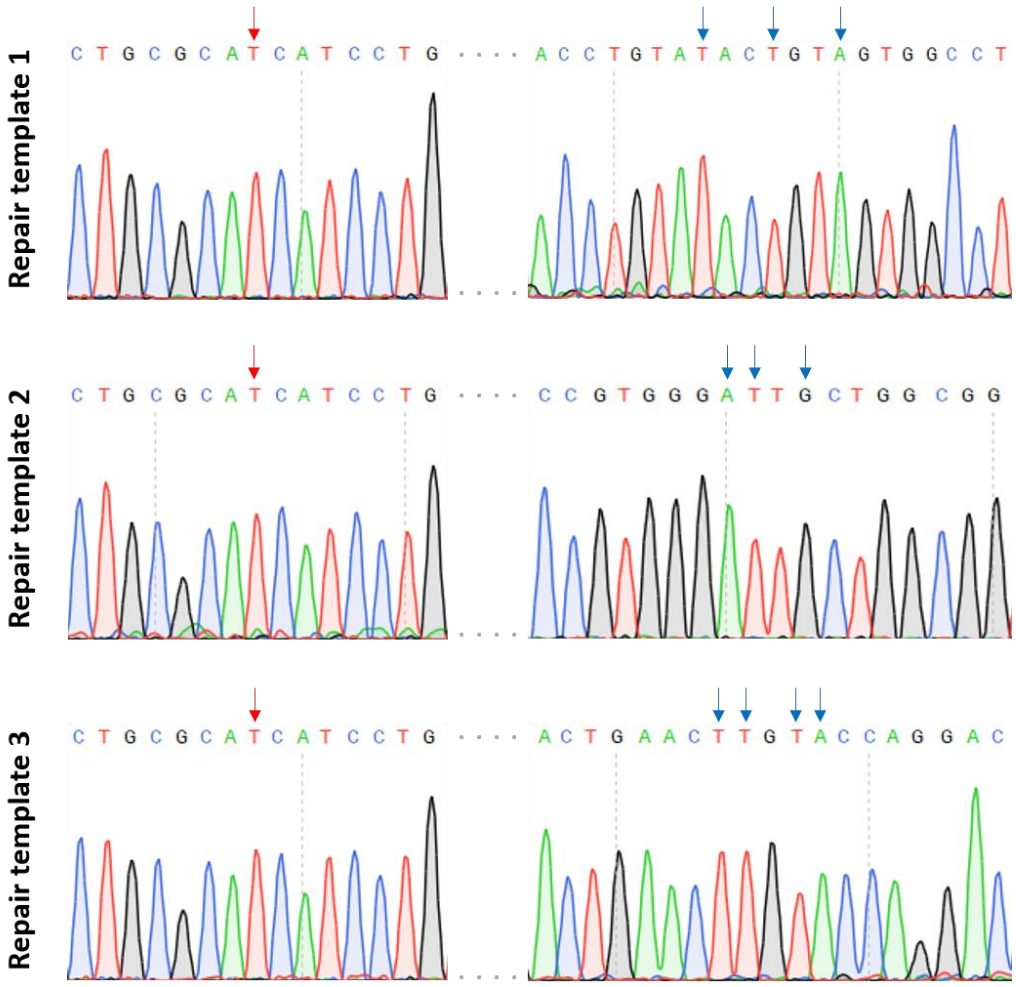

Figure 4.14 Validation of repair template creation

Representative chromatograms of Sanger sequencing for each repair template. The variant corresponding to the RyR1 p.Thr4826Ile change (red arrow) and changes to the guide sequence (blue arrows) are shown. Sequence between two locations are indicated with '...'

4.2.4 Optimisation of Nucleofection

A series of different Nucleofection programmes were trialled and optimised with a GFP expression plasmid for their transfection efficiency and cell viability (listed in Table 2.5). The P5 Nucleofection kit was selected for Nucleofection of the human myoblast cell line based on a recommendation from Lonza for use with human skeletal myoblasts.[369] The initial optimisation involved a comparison of five Nucleofection programmes (Programmes A–E) that were selected on the basis of recommendations from Lonza.

Optimisation was performed with GFP expression as an indication of transfection efficiency and a total cell count based on staining of nuclei was used to calculate cell viability (Figure 4.11). Each Nucleofection trial produced slightly different results as the methodology favours the health of the cells over accuracy while still maintaining integrity. For example, after Nucleofection of the cells it is recommended to immediately add growth media to allow the cells to recover and a slight difference in time may alter the results. For this reason, comparisons between Nucleofection programmes were performed within each Nucleofection trial because they were considered equivalent.

With the exception of Programme A, all Nucleofection programmes initially analysed produced similar cell viabilities and of these Programme D was found to have the highest rate of transfection efficiency at approximately 11% (Table 4.3). Programme D was then established as a baseline from which the method could be optimised further by use of the Lonza fine tuning matrix.[370] Because successful transfection was not possible for selection during CRISPR/Cas9 gene editing, the output required from this transfection technique was weighted toward maximum transfection efficiency instead of cell viability. Accordingly, the programmes that were predicted to further increase transfection efficiency at the potential detriment of cell viability—Programmes F and G—were then analysed.

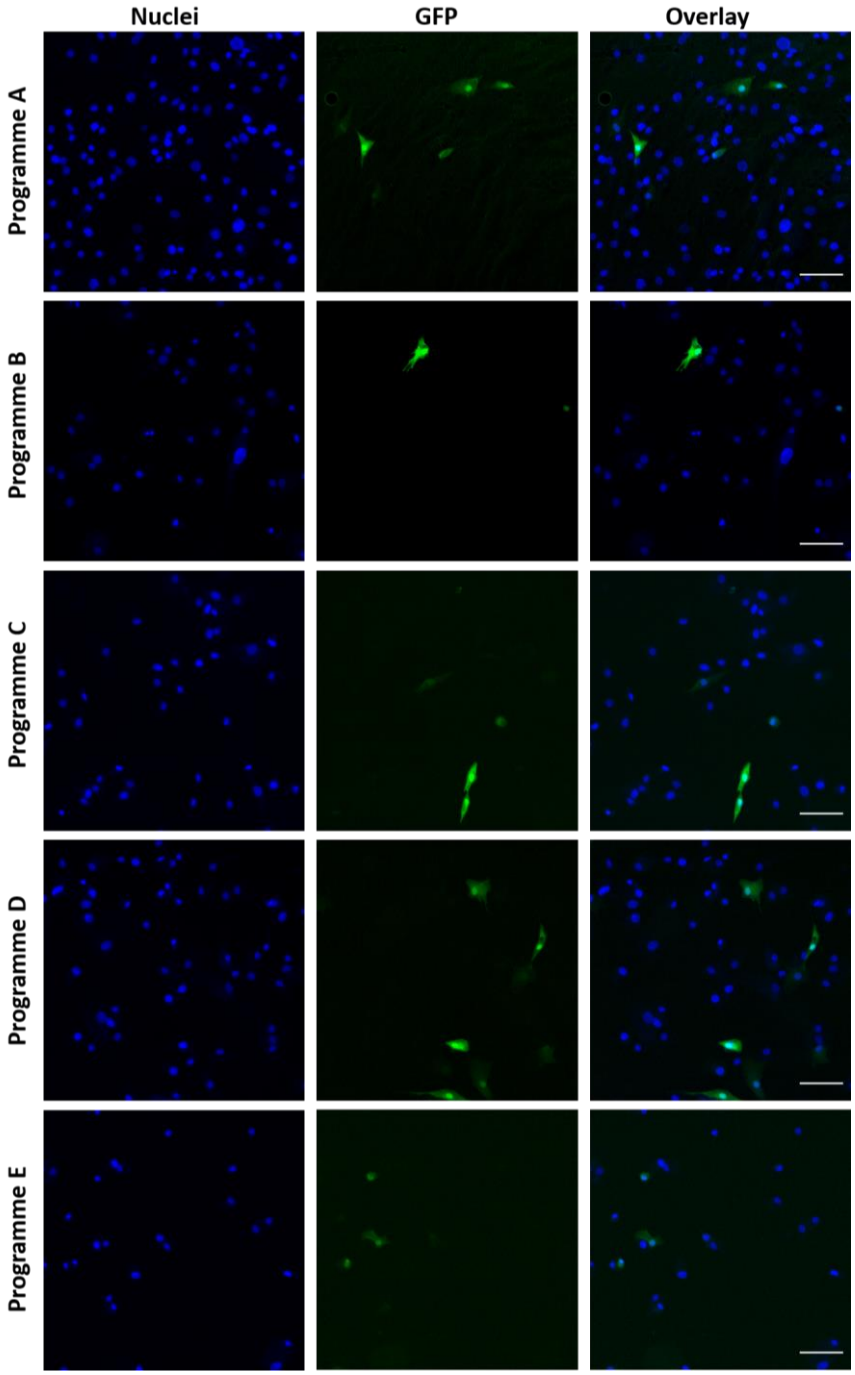

Figure 4.15 Initial Nucleofection optimisation

HMCL-7304 cells were transfected with a plasmid expressing green fluorescent protein (GFP) in a UV-transparent 96-well plate using five Nucleofection programmes and prepared for immunofluorescence (Section 2.3.5; 2.3.11). Successfully transfected cells were visualised by expression of GFP and all cells were visualised by the nuclei stain 4',6-diamidino-2-phenylindole (DAPI). Cells were examined by inverted fluorescence microscopy at a magnification of 100×; the scale bar in each merged image represents a length of 100 microns.

Table 4.3 Initial optimisation of Nucleofection methods

Nucleofection programme	Transfection efficiency	Cell viability
A	3.3%	98%
B	2.4%	33%
C	9.8%	33%
D	11.1%	43%
E	7.9%	31%

Analysis of Programmes F and G was also performed with GFP expression as an indicator of transfection efficiency and a total cell count based on staining of nuclei was used to calculate cell viability, like with the previous assay (Figure 4.16). When evaluated against Programme D, both Programmes F and G produced much higher transfection rates with similar cell survival with the highest efficiency observed from Programme G at approximately 32% (Table 4.4).

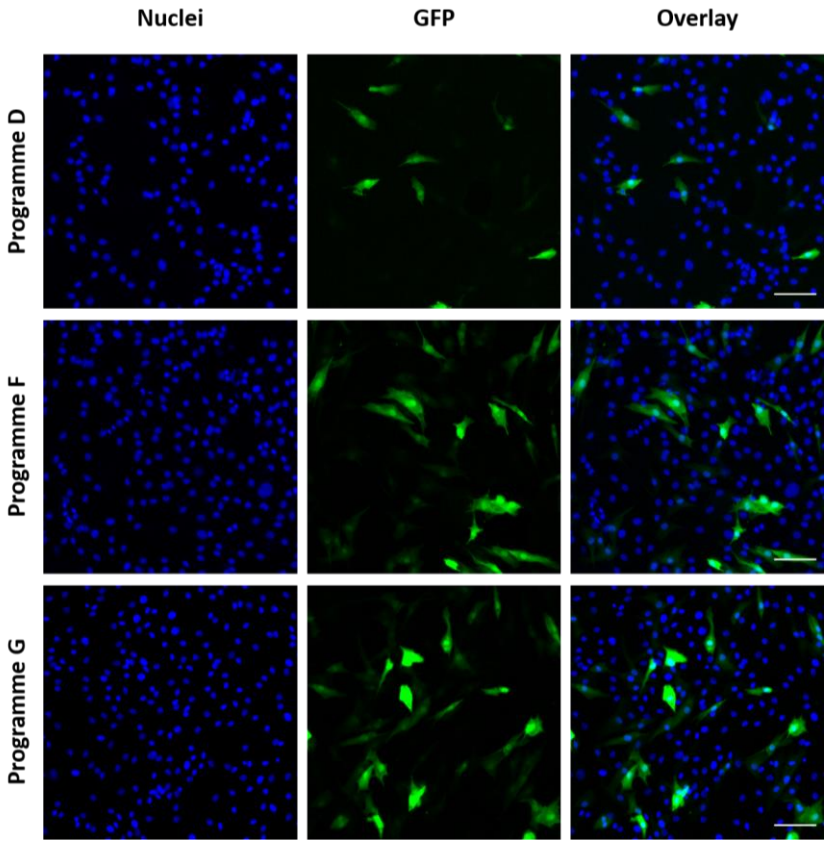

Figure 4.16 Fine-tuning Nucleofection

Three Nucleofection programmes were directly compared in their ability to transfect HMCL-7304 cells with a plasmid expressing green fluorescent protein (GFP) in a UV-transparent 96-well plate (Section 2.3.5, 2.3.11). Successfully transfected cells were visualised by expression of GFP (green) and all cells were visualised by the nuclei stain 4',6-diamidino-2-phenylindole (DAPI; blue). Cells were examined by inverted fluorescence microscopy at a magnification of 100×; the scale bar in each merged image represents a length of 100 microns.

Table 4.4 Further optimisation of Nucleofection

Nucleofection programme	Transfection efficiency	Cell viability
D	5.1%	40%
F	20.3%	54%
G	32.3%	51%

To establish the programme that would give the maximum transfection efficiency in the HMCL-7304 cell line, Nucleofection was further optimised as described previously by use of a GFP plasmid (Figure 4.17). Both new programmes—Programmes H and I—resulted in higher survival rates when compared with Programme G (Table 4.5) They also, however, both produced much lower transfection efficiencies whereas Programme G gave a transfection efficiency of approximately 41% (Table 4.5). This validated the use of Nucleofection Programme G for DNA delivery of the CRISPR/Cas9 components in this research because it was found to be both efficient and reliable.

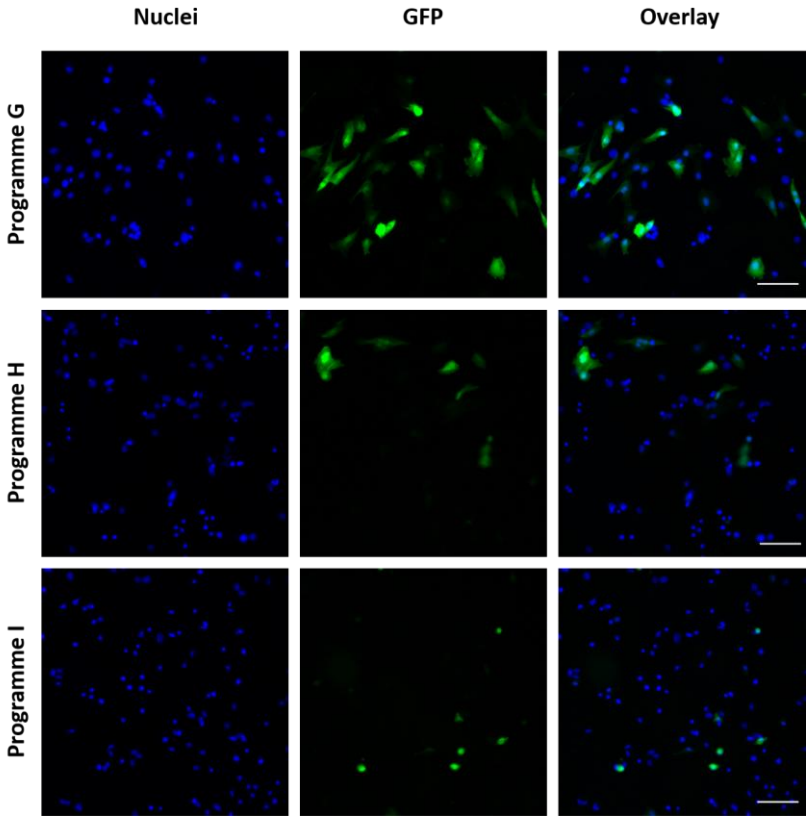

Figure 4.17 Further Nucleofection validation

HMCL-7304 cells were transfected with a plasmid expressing green fluorescent protein (GFP) through two more Nucleofection programmes and examined by inverted fluorescence microscopy at a magnification of 100× (Section 2.3.5; 2.3.11). Successfully transfected cells were visualised by expression of GFP and all cells were visualised by the nuclei stain 4',6-diamidino-2-phenylindole (DAPI). The scale bar in each merged image represents a length of 100 microns.

Table 4.5 Final optimisation of Nucleofection

Nucleofection programme	Transfection efficiency	Cell viability
G	41.4%	55%
H	12.1%	67%
I	4.8%	72%

4.2.5 Production of lentivirus

Although Nucleofection was found to be both effective and reliable, lentiviral transduction was also optimised for use with human myoblasts to determine the optimal vehicle for introduction of DNA into the HMCL-7304 cell line. In this research, a second-generation lentiviral system was used, which involved the production of viral particles in HEK-293T cells transfected with the psPAX2-D64V packaging plasmid, the pCMV-VSV-G envelope plasmid (Addgene; plasmid map in Appendix B.14), and the specific transfer plasmid with the genetic material to be introduced upon cell transduction.[371]

Similar to the testing of Nucleofection methods, this system was optimised with a GFP expression vector so that transduction efficiency could be observed visually. Viral titre was calculated to be 8.35×10^6 viral particles per millilitre by quantitative reverse transcription PCR (RT-qPCR; Figure 4.18). This result was within the acceptable range for integrase-deficient lentivirus, and thus was used to estimate multiplicity of infection for the purpose of transducing HMCL-7304. The lentiviral system sometimes produced satisfactory results, with the highest transduction efficiency measured at 35% (Figure 4.19). The results of this were not consistent, however, and many of the transduction attempts made during optimisation of the protocol were unsuccessful, indicating this method may be unreliable. Lentiviral stocks were nonetheless produced with the LentiGuide and Lenti-RT transfer plasmids to maintain the option for use of lentivirus-based DNA delivery. The viral titres of these samples were acceptable for use, ranging between 2.4×10^7 and 1.3×10^8, as

determined by RT-qPCR (RT-qPCR results in Appendix F.1; viral titres in Appendix F.2). The stocks were kept as a contingency against potential issues with Nucleofection

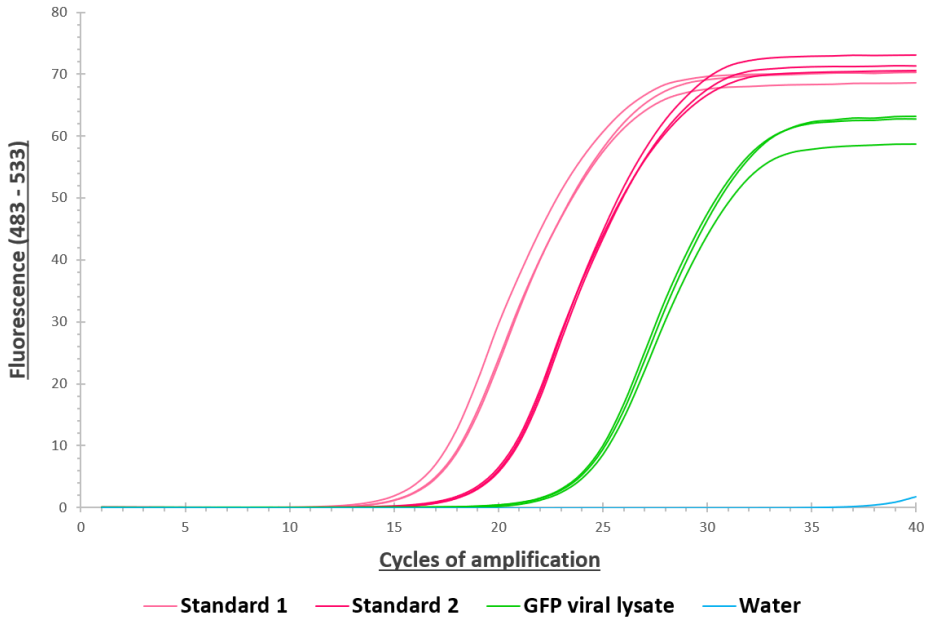

Figure 4.18 Determination of viral titre

The preparation of green fluorescent protein (GFP) control lentivirus (green) was titrated in triplicate with reverse transcription quantitative PCR and compared with two internal RNA standards (thin pink and thick pink lines) provided with the titration kit (Section 2.3.6). Kinetics of amplification were measured by the increase in fluorescence between 483–533 nm wavelengths (corresponding to the increase in double-stranded DNA bound to the fluorescent dye) over successive cycles of amplification.

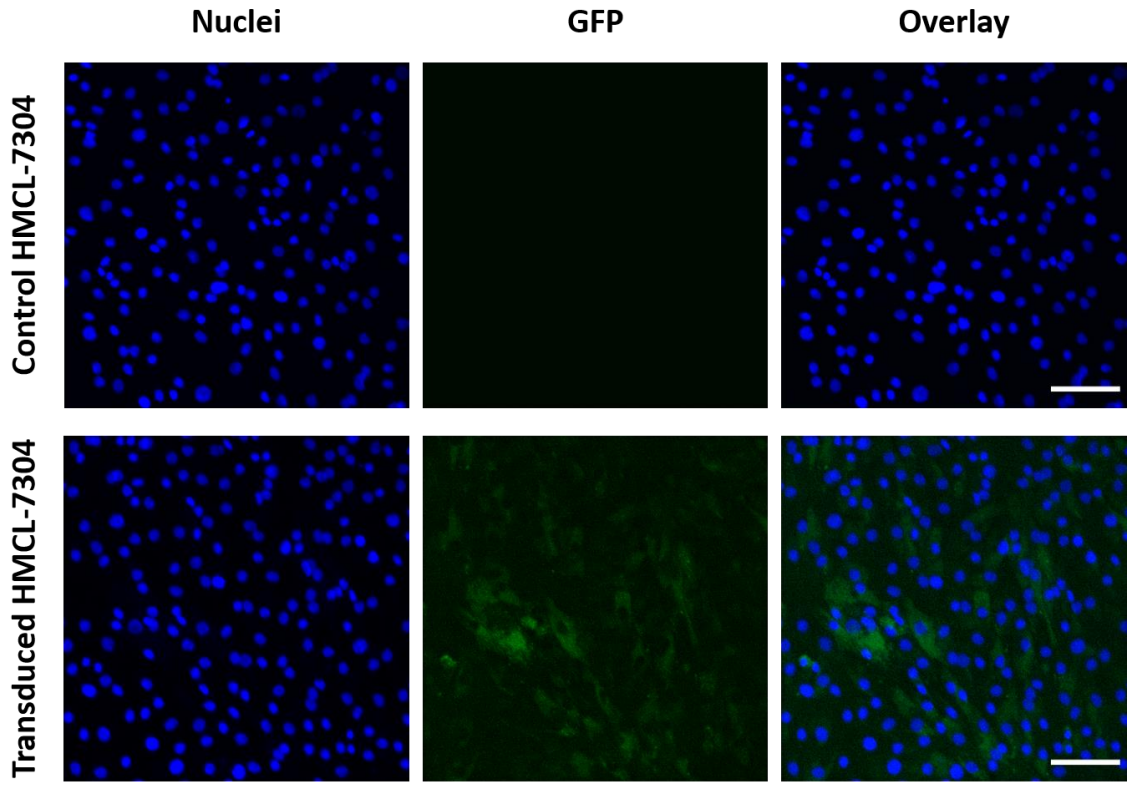

Figure 4.19 Lentiviral transduction with control plasmid

Lentiviral transduction of HMCL-7304 cells with the GFP control lentivirus preparation (Section 2.3.7). Cells were visualised with an inverted fluorescent microscope after staining with 4',6-diamidino-2-phenylindole (DAPI) at a magnification of 100×. Scale bar in merged image represents 100 µm.

4.2.6 Testing for editing efficiency

The T7E1 assay was used to assess the rate at which the gRNAs directed Cas9-mediated cleavage of the genome. This takes advantage of the error-prone NHEJ repair mechanism endogenous to the cell that is predicted to introduce a proportion of genetic changes during repair. Following Cas9 gene editing guided by a specific gRNA, editing efficiency can be determined with the T7E1 assay by producing fragments of expected lengths from a PCR product, as described in Section 4.1.8. In this way, the proportion of edited DNA can be determined visually after DNA electrophoresis. This method was initially trialled with gDNA samples from patients with a known heterozygous deletion of 14 nucleotides.

The region that contained the deletion was amplified by PCR in two wild-type (WT) control samples and two heterozygous deletion samples to produce differently sized fragments, depending on the alleles present. The size of the full-length product was predicted to be 337 bp whereas the predicted size of the fragment containing the deletion was 323 bp. The PCR products were melted, re-annealed, and then digested with T7 Endonuclease I (Figure 4.20).

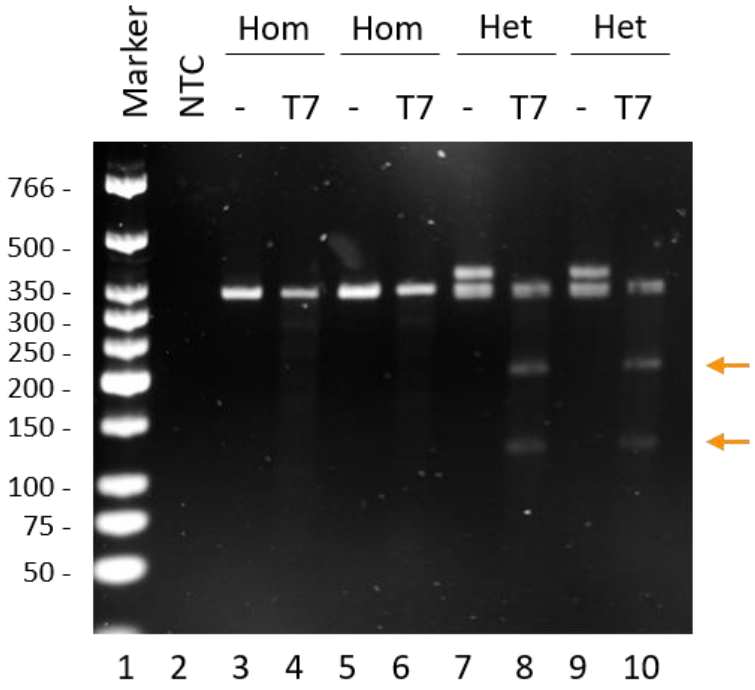

Figure 4.20 T7 Endonuclease assay

The T7 Endonuclease I assay was performed on two homozygous wild-type (lanes 3–6) and two heterozygous deletion (lanes 7–10) genomic DNA samples in which digested (T7) PCR products were subjected to electrophoresis in a 3% agarose gel containing ethidium bromide and immersed in buffer alongside undigested (–) controls (Section 2.2.3). Fragments arising from the digestion of heteroduplexes migrated to approximately 130 bp and 210 bp as expected (arrows) whereas the full-length PCR product was 337 bp. Lane 1 contains the Low Molecular Weight DNA Ladder with fragment lengths indicated in base pairs. Lane 2 contains a no template PCR control (NTC).

The control samples—homozygous WT—had no mismatches upon annealing and therefore were not digested with the enzyme (Figure 4.20). The heterozygous samples, however, would have had a substantial number of mismatches after annealing that presented as two additional fragments after restriction endonuclease digestion. The bands

corresponding to the 128 bp and 209 bp fragments could be clearly observed after gel electrophoresis, confirming cleavage within the deletion region and therefore within the DNA mismatch (Figure 4.20). Furthermore, the restricted movement of the heteroduplexes through the agarose could even be seen in the undigested heterozygous samples in which an additional fragment of lower mobility was present that was absent from the homozygous samples.

Screening considerable numbers of edited and isolated HMCL-7304 cell lines would require extraction of gDNA from cells grown in 96-well plates. Because HRM analysis would likely require a minimum of 200 ng high-quality gDNA to allow for repeated assays, a protocol was developed for maximum extraction of gDNA from human myoblasts grown in a 96-well plate format. The Wizard Genomic DNA Purification Kit (Promega) protocol that was previously used successfully to extract gDNA from myoblasts grown in a T25 flask was scaled down to produce four modified protocols (Table 4.5). These four modified protocols were each analysed in triplicate with HMCL-7304 myoblasts grown to 70% confluence in a 96-well plate as the source of gDNA, just as the edited cells would be used later. When these samples were analysed by gel electrophoresis, all four methods were found to have extracted high molecular weight DNA (Figure 4.21).

Table 4.6 Volumes of Wizard gDNA Purification Kit solutions used

Solution	T25 flask method	96-well plate method			
		A	B	C	D
Nuclei lysis buffer (µL)	600	30	60	120	200
Protein precipitation buffer (µL)	200	10	20	40	70
Isopropanol (µL)	600	30	60	120	200
70% ethanol (µL)	600	30	60	120	200
Resuspension buffer (µL)	50	5	5	5	5

Of the four methods investigated, protocol B was determined to be the most reliable because all three triplicates from this method yielded approximately 500 ng high

molecular weight DNA when compared against the 1.6 kilobase reference band in the 1 Kb Plus DNA Ladder. Protocol A and protocol C also were observed to be capable of that yield, albeit inconsistently, with at least one replicate producing less than 100 ng total gDNA (Figure 4.21). The yields from protocol D were consistent; however, this method produced lower gDNA yields of approximately 200 ng gDNA. This result indicated that the 96-well plate format would be feasible for monoclonal selection of edited cells, allowing a much higher throughput methodology after gene editing.

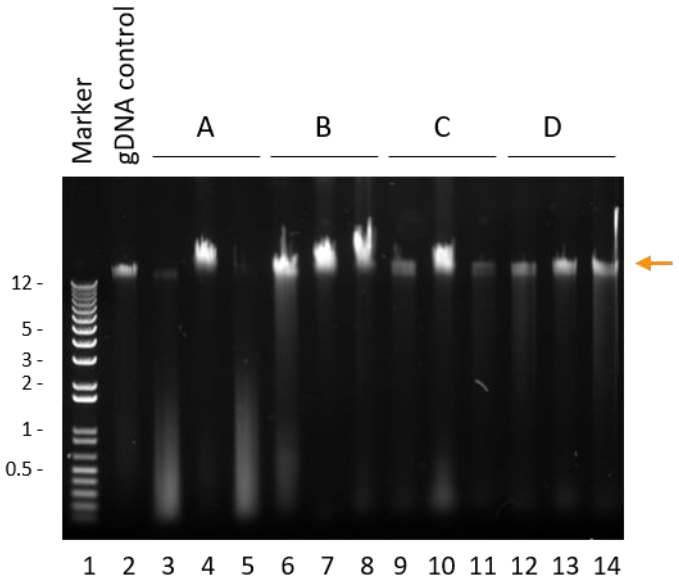

Figure 4.21 Optimisation of genomic DNA extraction method

Results of four different protocols (A–D) for extraction of genomic DNA from human myoblasts grown in a 96-well plate format. Samples were resolved by gel electrophoresis in an 0.8% agarose gel containing ethidium bromide and immersed in buffer (Section 2.2.3) alongside a control sample extracted in a larger format in lane 2. Lane 1 contains 1 Kb Plus DNA ladder with the length of each fragment indicated in kb. The location of gDNA is indicated (arrow).

The high-resolution amplicon melting assay that was to be used for screening for cells with the RyR1 p.Thr4826Ile variant was previously optimised for use with validated positive and negative control samples. For the purpose of identifying edited cell lines with the variant, gDNA from the unedited HMCL-7304 line was used as a negative control. Before this screening could take place, the use of this sample as a negative control was examined by HRM analysis. Simply put, the melt profile of the negative control needed to be distinct

from that of the *RYR1* c.14477C>T (RyR1 p.Thr4826Ile) positive control to allow for reliable identification of unknown samples. The melt profile of the HMCL-7304 gDNA produced a single melting peak that was comparable to that of the previously validated negative control and could be distinguished from the two melting peaks observed with the positive control (Figure 4.22). This result was confirmed by the clear differentiation between the data from the positive and negative samples when displayed as either melt curves or a difference plot (Figure 4.23). This result validates the use of the HRM assay in screening for edited HMCL-7304 monoclonal lines.

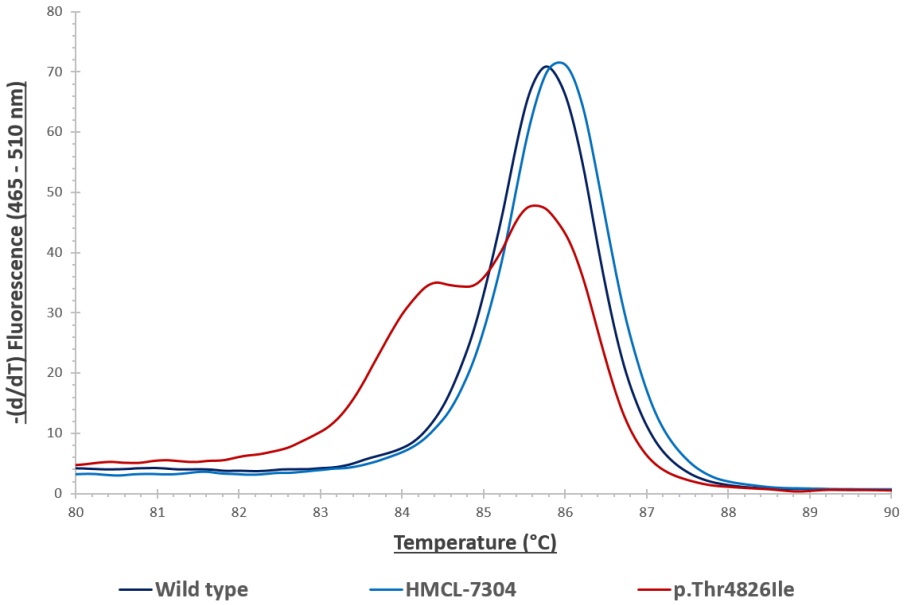

Figure 4.22 Control DNA melting peaks from HRM analysis

The site of the *RYR1* variant was amplified from genomic DNA and then melted in the presence of a fluorescent dye (Section 2.22.12). Melt profiles of the HMCL-7304 sample (light blue) and samples from patients either heterozygous (red) or wild-type (dark blue) are shown. Data is displayed as temperature versus the negative first derivative of the normalised fluorescence intensity.

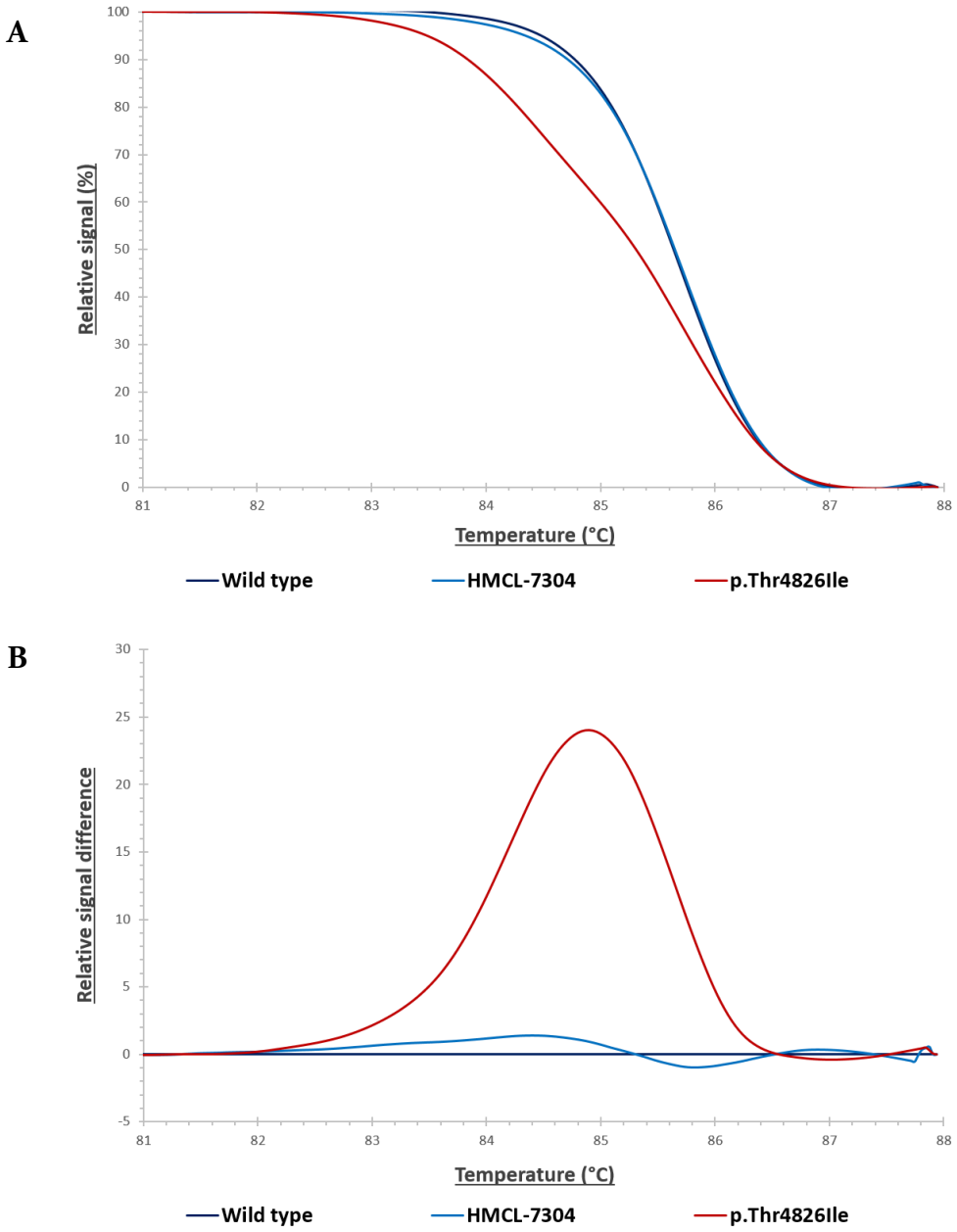

Figure 4.23 Melt profiles for HRM analysis controls

The site of the *RYR1* variant was amplified from genomic DNA and then melted in the presence of a fluorescent dye (Section 2.22.12). Melt profiles of the HMCL-7304 sample (light blue) and samples from patients either heterozygous for the variant (red) or wild-type (dark blue) are shown. **A** DNA melt curves: data is displayed as temperature versus the normalised fluorescence intensity. **B** Melt data difference plot: melt curves were subtracted from that of the wild-type negative control.

4.3 Editing the ryanodine receptor 1 gene

When the required components were prepared and the techniques optimised, CRISPR/Cas9 gene editing in the immortalised human myoblast cell line HMCL-7304 commenced. First, the ability of the designed gRNAs to direct Cas9 endonuclease activity to the specific genomic regions for which they were designed was analysed with the T7E1 assay. Then, myoblasts were transfected with the three gRNA and repair template combinations in an attempt to introduce the *RYR1* c.14477C>T variant corresponding to the RyR1 p.Thr4826Ile mutation into the genome of these cells. Finally, large-scale screening of these edited cells for the variant was performed by HRM analysis and any results indicating introduction of the variant were further examined by Sanger sequencing.

4.3.1 Analysing effectiveness of guides

To analyse the effectiveness of the guides in targeting Cas9 cleavage, the T7E1 assay was employed. This analysis was performed with both HMCL-7304 cells after Nucleofection and HEK-293T cells after chemical transfection of the three LentiGuide plasmids. At first, PCR primers were designed to produce a 900–nucleotide amplicon containing all three predicted target sites from guides 1, 2, and 3. After digestion with T7 endonuclease I, this PCR product was predicted to produce DNA fragments of predicted sizes for each guide. However, the digestion yielded ambiguous results because the endonuclease often completely digested the PCR products, and thus provided no useful information.

A smaller DNA fragment of approximately 400 bp was then trialled for use with the assay and subsequently produced a similar result. Alternative PCR reactions were then trialled that produced an even smaller PCR product (less than 200 bp) as this was predicted to provide results that were easier to interpret. Amplifying a small fragment containing the predicted DSB locations—and therefore the NHEJ edits—from all three guides was impractical because guide 3 was located approximately 100 bp away from guides 1 and 2. Unfortunately, a PCR reaction designed to amplify guide 3 alone was also not a viable option because it was located within an intronic region with high GC-content that was problematic for PCR amplification. Because the predicted cleavage sites of guides 1 and 2

were separated by only 23 nucleotides, PCR reactions were investigated that amplified a short region surrounding only guides 1 and 2. The amplification of a 124 bp fragment was found to be the most effective of those tested as it had a high yield of product without visible non-specific product; therefore, guide targeting efficiencies were examined with this PCR product (Figure 4.24).

LentiGuide plasmids with both the Cas9 endonuclease coding region and gRNA sequence were introduced transiently to either HMCL-7304 by Nucleofection or HEK-293T cells by chemical transfection. The cells were left for ten days following transfection, allowing maximum exposure of the cells to the CRISPR/Cas9 machinery, and therefore maximising the potential for indels as a consequence of NHEJ cellular repair. The gDNA was then extracted from each mixed cell population and the 124 bp region was PCR-amplified (Figure 4.24). Initially, the T7E1 assay was performed with DNA from cells edited with either the original lentiCRISPR v2 plasmid—containing Cas9 but no guide—or LentiGuide plasmids 1, 2, or 3 (Figure 4.25). Guide 3 was included because the assay often produced ambiguous results, and thus the use of a second negative control in the form of a guide sequence that was not complementary to the target region was appropriate.

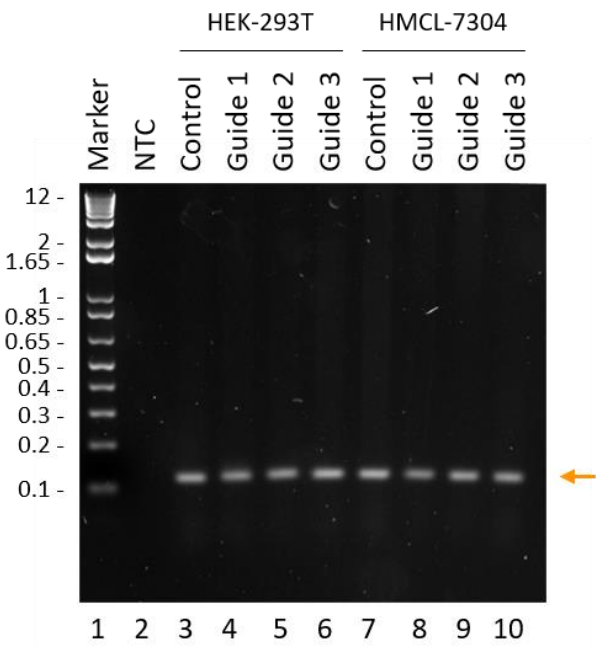

Figure 4.24 Guide efficiency PCR

The genomic region with the predicted locations of double-strand breaks were PCR-amplified from edited HEK-293T and HMCL-7304 genomic DNA (Section 2.2.6). Samples were resolved by gel electrophoresis in a 2% agarose gel containing ethidium bromide and immersed in buffer (Section 2.2.3) alongside a no template control (NTC) sample in lane 2. The 124 bp PCR product (arrow) can be seen in lanes 3–10. Lane 1 contains 1 Kb Plus DNA ladder with fragment lengths indicated in kb.

The results of NHEJ repair were not observed in the DNA samples extracted from HMCL-7304 cells after CRISPR/Cas9 editing. Conversely, NHEJ repair in the form of indels was evident in HEK-293T cells that were edited by use of guides 1 and 2 (Figure 4.25). The T7-cleaved PCR products were subjected to electrophoresis by use of a native polyacrylamide gel alongside the same samples without enzyme added that were included as a control for endonuclease digestion. The presence of two bands that migrated though the gel in agreement with the expected lengths of 53 bp and 71 bp (guide 1) and 48 bp and 76 bp (guide 2) confirmed that Cas9-mediated editing occurred (Figure 4.25). These bands were only evident in the T7-digested samples of guides 1 and 2 and were not observed in the samples from the no-guide control or of that edited with guide 3, corroborating the result.

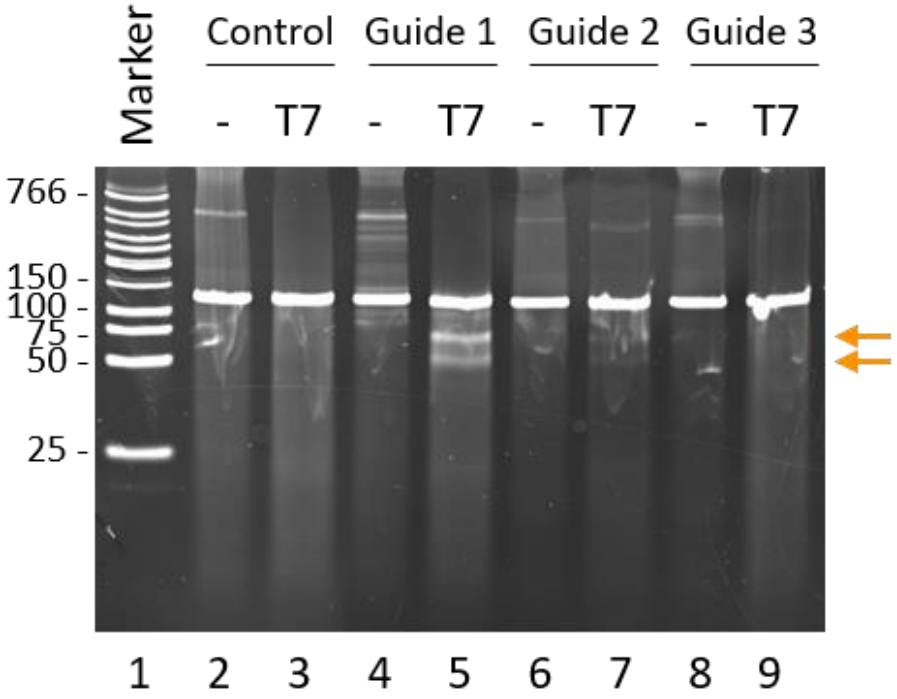

Figure 4.25 Initial analysis of guide-mediated Cas9 cleavage

Amplified regions of genomic DNA extracted from HEK-293T cells transfected with LentiGuides 1-3 or lentiCRISPR v2 were subjected to the T7 endonuclease I assay (Section 2.2.10). Products of digestion (T7) were resolved by electrophoresis alongside undigested controls (–) in a 15% native polyacrylamide gel immersed in buffer and stained with ethidium bromide (Section 2.2.10). Lane 1 contains Low Molecular Weight DNA Ladder as a size marker with the fragment lengths indicated in bp. Lanes 5 and 7 contain two higher-mobility bands (arrows) from digestion of heteroduplexes.

Although the results obtained by use of the T7E1 technique were previously inconsistent, this particular result was found to be robust because it was confirmed in two subsequent assays. To validate the results, the samples were visualised following all three stages of the assay—PCR, heteroduplex formation, and T7 endonuclease I digestion (Figure 4.26). The two bands corresponding to heteroduplex digestion were unambiguous for both guide 1- and guide 2-edited gDNA samples. In all three attempts of the assay, guide 1-edited gDNA was found to have a higher proportion of digested fragments—and therefore indels—than that of guide 2 (Figure 4.26). These results indicate that, although both guide 1 and 2 are directing Cas9 to create DSBs in the genome of these cells, guide 1 has the highest potential editing efficiency of the two.

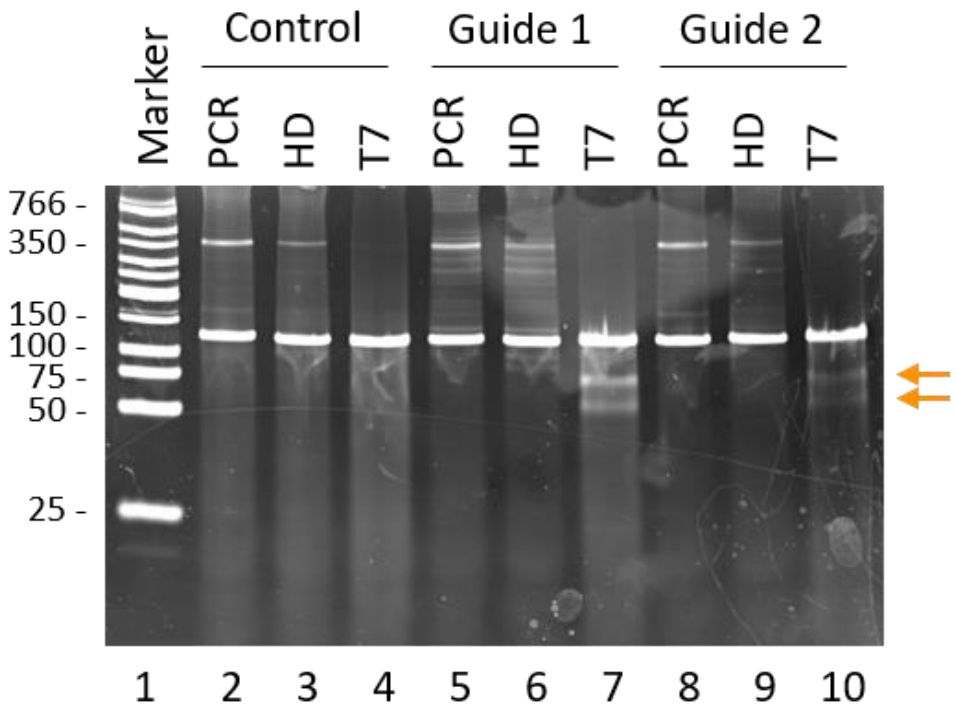

Figure 4.26 Validation of guide-mediated Cas9 cleavage

Amplified regions of genomic DNA extracted from HEK-293T cells transfected with LentiGuide plasmids 1 and 2 were melted, re-annealed, and then digested with T7 endonuclease I alongside a negative control transfected with lentiCRISPR v2 (Section 2.2.10). Samples were resolved by electrophoresis in a 15% native polyacrylamide gel immersed in buffer and stained with ethidium bromide (Section 2.2.10). Samples included those following PCR; melting and re-annealing (labelled HD for heteroduplex); and T7 digestion. Digestion of heteroduplexes formed from Cas9 cleavage are visualised in lanes 7 and 10 as two higher-mobility bands, labelled with arrows. Lane 1 contains Low Molecular Weight DNA Ladder as a size marker; fragment lengths indicated in bp.

4.3.2 First phase of gene editing

After confirmation that a minimum of two gRNAs designed for the *RYR1* c.14477C>T variant corresponding to the RyR1 p.Thr4826Ile mutation were successfully directing Cas9 to their respective genomic locations, gene editing commenced. LentiGuide plasmids 1–3 (containing gRNAs and the Cas9 coding sequence) were introduced into HMCL-7304 cells by Nucleofection and left to recover for 24 hours. Those cells were subsequently transfected with repair templates 1–3 (corresponding to LentiGuides 1–3) and allowed to recover for a further 24 hours before single cells were isolated by limiting dilution. Growth

of the colonies was monitored to identify any wells with more than one seeding cell because the cultures were required to be monoclonal.

The number of isolated cells were 106 (guide 1), 112 (guide 2), and 148 (guide 3), making a total of 366 monoclonal HMCL-7304 lines. When the colonies had expanded to approximately 50% confluence, the cells were removed to duplicate 96-well plates. After the duplicate colonies expanded to approximately 90% confluence, gDNA was extracted from one set of plates and the duplicate plates of cells were stored for later reanimation upon successful testing. This storage was performed by replacing the growth media on the cells with FBS containing 10% dimethyl sulfoxide and wrapping each plate in several layers of paper towels before placing in a –80 °C freezer.

The gDNA extracted from the 96-well plates was analysed for the presence of the *RYR1* c.14477C>T (RyR1 p.Thr4826Ile) variant by HRM analysis. Most samples tested negative for the variant in the initial analysis because their melt profiles aligned with the WT sequence. This was not unexpected because only the results of HDR editing would be observed with this assay; evidence of NHEJ repair such as indels would not be detected by HRM analysis because the small region amplified by PCR did not contain any of the guide sequences. Of the 366 gDNA samples examined by HRM analysis, three samples produced melt curves sufficiently similar to that of the positive control, signifying that they may contain the *RYR1* c.14477C>T (RyR1 p.Thr4826Ile) variant (Figure 4.27). One of these three samples (HMCL-7304 cell line A) was created by use of guide 2, whereas the other two (HMCL-7304 cell lines B and C) were both obtained with guide 3.

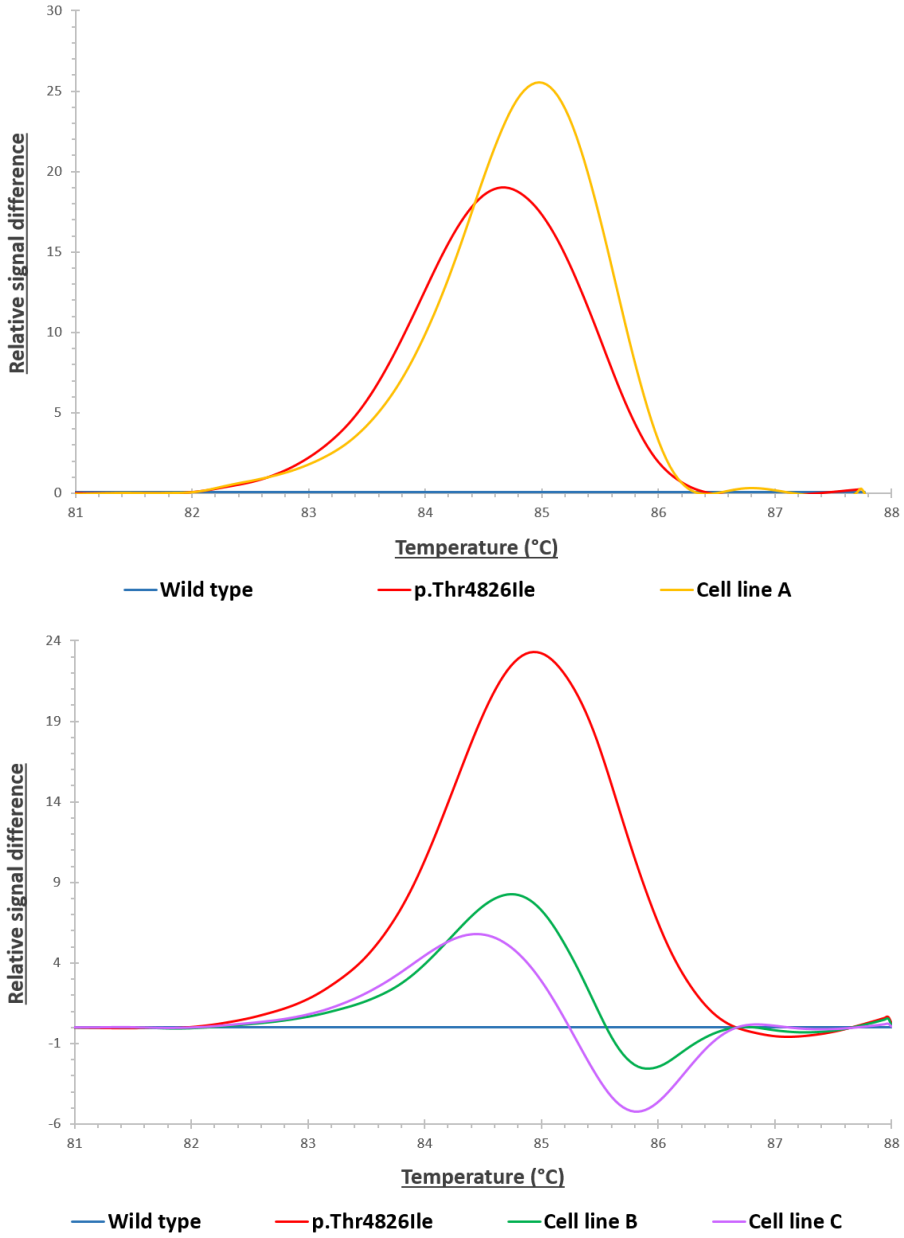

Figure 4.27 Initial difference plots for HMCL-7304 cell lines A, B and C

High resolution amplicon melt data difference plot for genomic DNA sample A is shown in the first graph whereas samples B and C are shown in the second graph. Genomic DNA extracted from monoclonal Cas9-edited HMCL-7304 cells were analysed for the *RYR1* c.14477C>T (RyR1 p.Thr4826Ile) variant by high resolution amplicon melt analysis (Section 2.2.11). Unedited HMCL-7304 genomic DNA was a negative control (blue) and a genomic DNA sample from a patient with the variant was a heterozygous positive control (red). Melt curves were subtracted from that of the negative control (unedited HMCL-7304 genomic DNA) and data is displayed as temperature versus the difference in fluorescence.

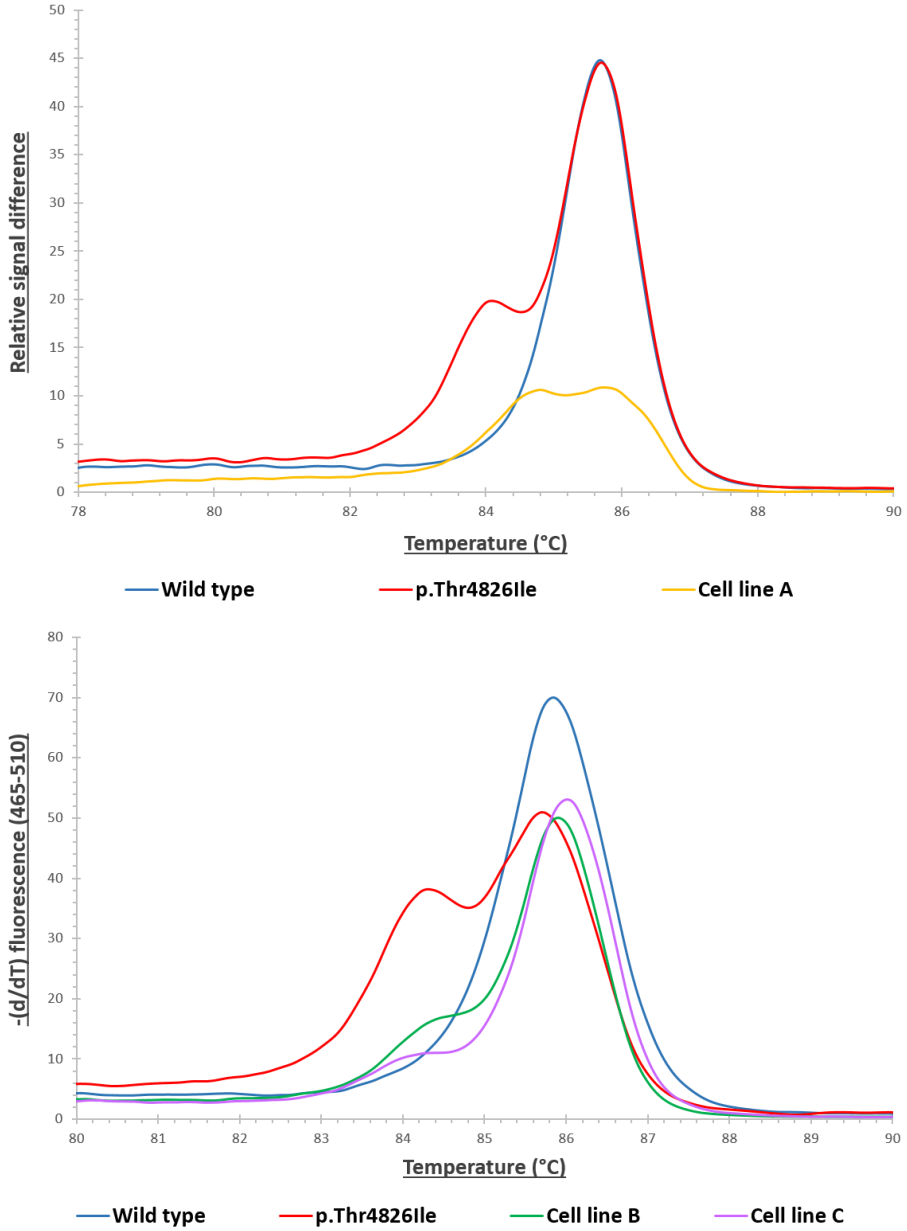

Figure 4.28 Initial melt curves for HMCL-7304 cell lines A, B and C

DNA melt profile for genomic DNA sample A is shown in the first graph whereas the results for samples B and C are shown in the second graph. Genomic DNA extracted from monoclonal Cas9-edited HMCL-7304 cells were analysed for the *RYR1* c.14477C>T (RyR1 p.Thr4826Ile) variant by high resolution amplicon melt analysis (Section 2.2.11). Unedited HMCL-7304 genomic DNA was a negative control (blue) and a genomic DNA sample from a patient with the variant was a heterozygous positive control (red). Data are displayed as temperature versus the negative first derivative of the normalised fluorescence intensity.

To substantiate this preliminary result and ensure the accuracy of the analysis, the HRM assay was repeated with the three samples in single assay; accordingly, all samples again tested positive for the variant (Figure 4.29). Because two distinct melting peaks were visible—corresponding to two different alleles—the results also indicated that the edited cell lines were heterozygous for the variant.

The presence of the RyR1 p.Thr4826Ile variant was then investigated in each of the three gDNA samples by Sanger sequencing of the PCR products from the assay (Figure 4.30). The variant was evident in the sequencing chromatogram for all three of the HMCL-7304 edited cell lines. The sequencing results also confirmed that the edited cell lines were heterozygous for the RyR1 p.Thr4826Ile variant because, in addition to the edited allele, the original WT residue can be observed in the chromatogram (Figure 4.30).

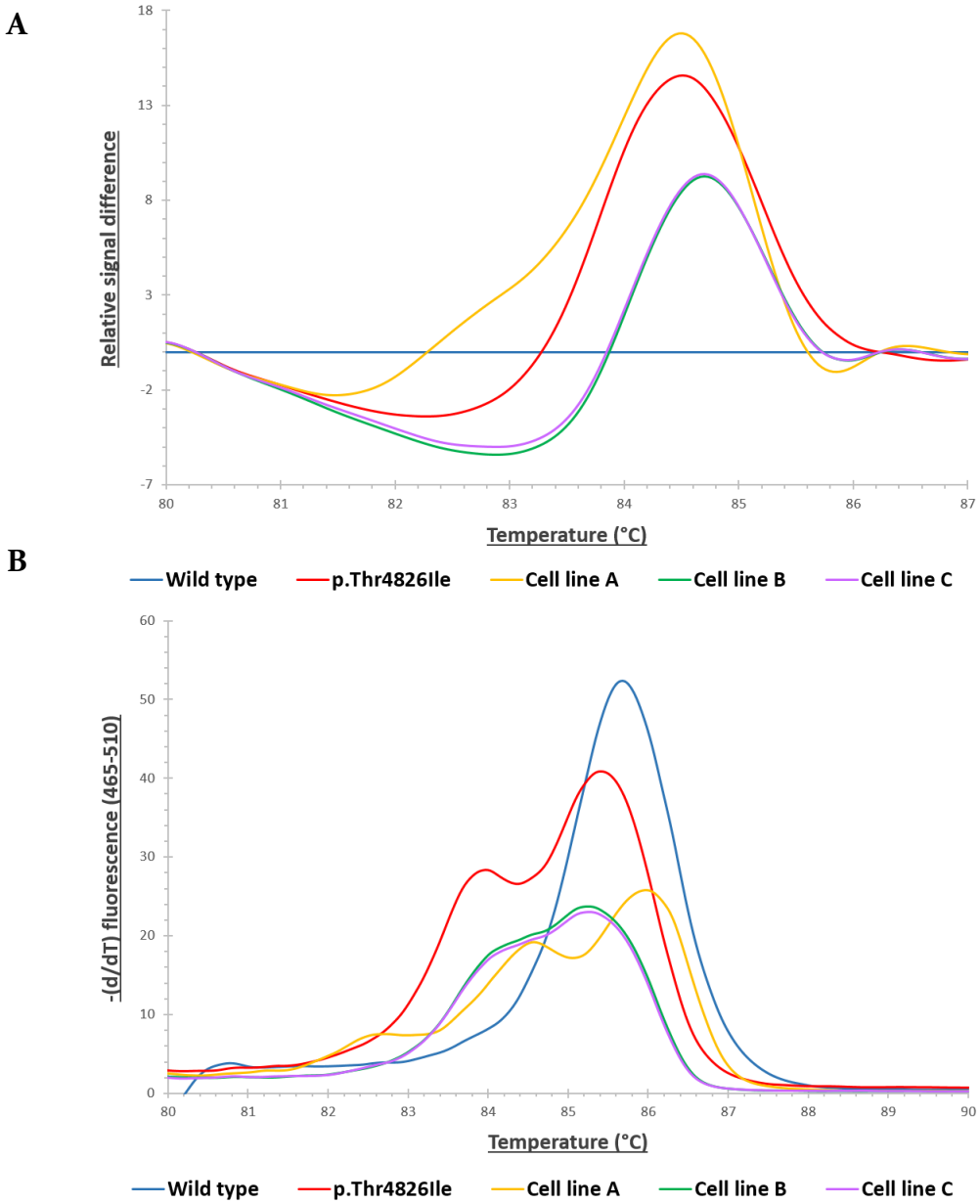

Figure 4.29 Validation of HRM results for edited HMCL-7304 lines

Genomic DNA extracted from Cas9-edited HMCL-7304 cells were analysed for the *RYR1* c.14477C>T (RyR1 p.Thr4826Ile) variant by high resolution amplicon melt analysis (Section 2.2.11). Unedited HMCL-7304 genomic DNA was a negative control (blue) and a sample with the variant was a heterozygous positive control (red). **A** Melt curves were subtracted from that of the negative control and data is displayed as temperature versus the difference in fluorescence. **B** Data is displayed as temperature versus the negative first derivative of the normalised fluorescence intensity.

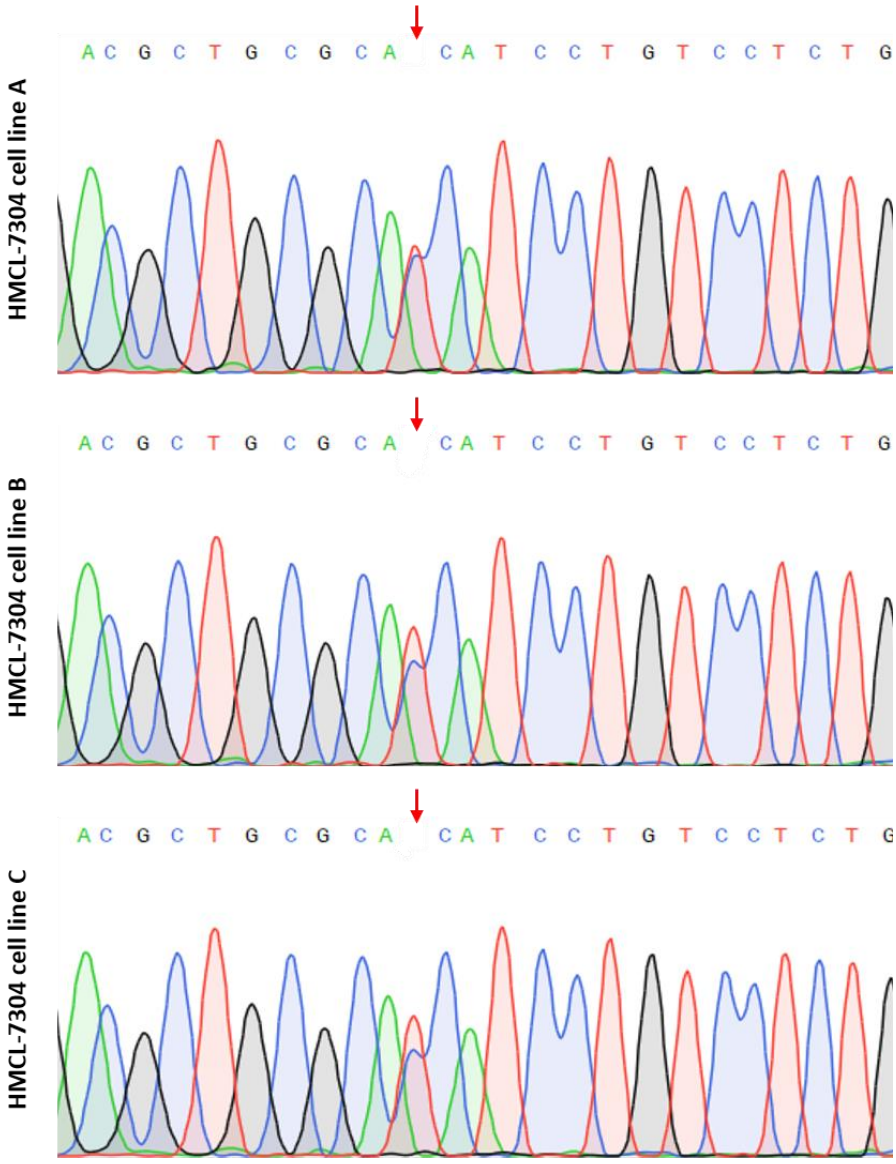

Figure 4.30 Sanger sequencing of edited cell lines A, B and C

Sanger sequencing results confirming the *RYR1* c.14477C>T (RyR1 p.Thr4826Ile) variant is present (arrow) in the genome of the HMCL-7304 edited cell lines A, B, and C.

At this point of the process, the small amount of gDNA extracted from the cell cultures was exhausted and more was required for further testing such as the examination of off-target editing. The reanimation of duplicate cell stocks for HMCL-7304 cell lines A, B, and C that were frozen in 96-well plates was attempted. Unfortunately, after many attempts to revive the cells, it was discovered that the cells did not survive the freezing

process and had to be discarded. This resulted in the complete loss of all edited HMCL-7304 cell stocks and therefore brought an end to the initial phase of gene editing.

4.3.3 Second phase of gene editing

Despite the regrettable loss of viable cells for further analysis, the preliminary results from the first round indicated that gene editing had been achieved. For this reason, the isolation of edited cells was attempted a second time. After the Nucleofection of HMCL-7304 cells with the CRISPR/Cas9 components in the first phase of gene editing, only a small proportion of cells were isolated by limiting dilution for subsequent testing. The remaining cells were reserved as a pooled cell population by cryopreservation and were therefore available for single cell isolation. These potentially edited cells were reanimated and subsequently isolated by limiting dilution in 96-well plates, after which their growth was again monitored for any wells seeded with more than one cell. It was observed during this early growth period that most—if not all—of the wells were unintentionally seeded with multiple cells, and therefore it was likely that all resulting cell populations would be polyclonal.

The isolation of monoclonal cell cultures was an essential step of the procedure; however, the stock of edited cells from the first phase of gene editing was exhausted in this second round, and thus the decision was made to continue to grow the cells as polyclonal cell populations. When the colonies had grown to approximately 70% confluence, 90% of the cells were removed for gDNA extraction and the remaining 10% of cells were supplemented with fresh growth media and expanded. These cells were allowed to continue growing as a measure to avoid issues encountered when freezing the cells. The gDNA samples from these polyclonal cultures were then tested for the *RYR1* c.14477C>T (RyR1 p.Thr4826Ile) variant by HRM analysis (Figure 4.31).

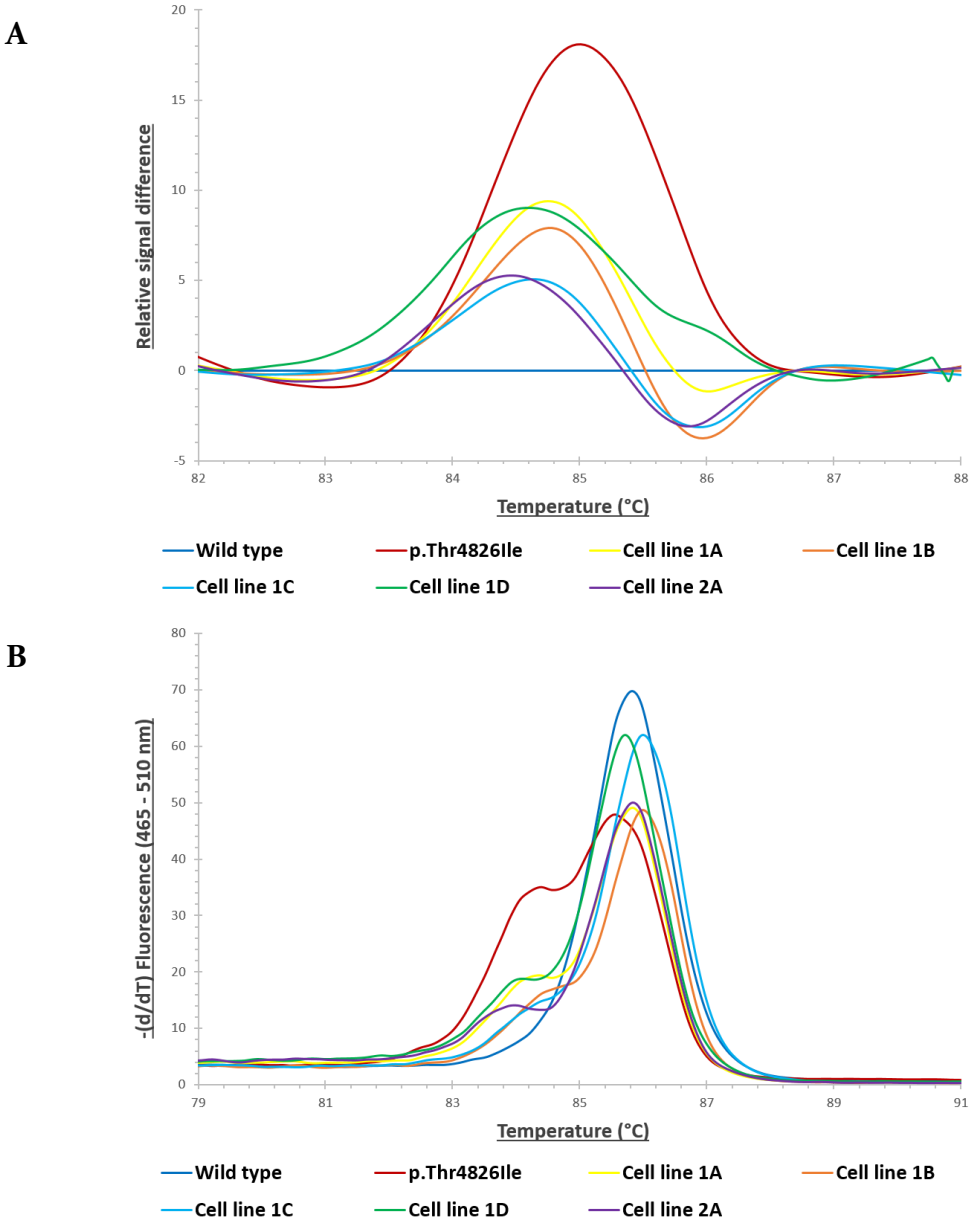

Figure 4.31 Identification of polyclonal edited HMCL-7304 lines

Genomic DNA extracted from polyclonal Cas9-edited HMCL-7304 cells were analysed for the *RYR1* c.14477C>T (RyR1 p.Thr4826Ile) variant by high resolution amplicon melt analysis (Section 2.2.11). Unedited HMCL-7304 was a negative control (blue) and a known heterozygous sample was a positive control (red). **A** Data is displayed as temperature versus the difference in fluorescence. Melt curves were subtracted from that of the negative control. **B** Melt curve profiles. Data is displayed as temperature versus the negative first derivative of the normalised fluorescence intensity.

The results of this assay revealed five cell populations that may have comprised both WT and edited cells (Figure 4.31). Four of those (cell lines 1A, 1B, 1C, and 1D) arose from editing with guide 1 and the fifth (cell line 2A) resulted from editing with guide 2. The most convincing results from the HRM analysis were those of cell lines 1A, 1D, and 2A because they produced melting peaks most closely resembling those of the RyR1 p.Thr4826Ile positive control (Figure 4.31).

To verify the presence of the RyR1 p.Thr4826Ile variant in these polyclonal cell populations, the PCR product from the HRM analysis was subjected to Sanger sequencing. The presence of the variant was indicated in all five cell lines, manifesting as a red signal in the sequencing chromatograms (Figure 4.32). Although the size of the signal corresponding to the variant differed between cell lines, it was substantially smaller than the WT signal for all five samples. This indicated that the cell populations were indeed polyclonal and comprised a large proportion of WT cells with a much smaller proportion of edited cells.

The sequencing data revealed that cell lines 1D and 2A had the strongest variant signal; however, cell line 1D also appeared to have a non-synonymous *RYR1* c.14483T>A (RyR1 p.Leu4828Gln) substitution (Figure 4.32). Cell lines containing *RYR1* variants other than the *RYR1* c.14477C>T (RyR1 p.Thr4826Ile) variant would not be useable. However, the signal representing the *RYR1* c.14483T>A variant was relatively large compared with the *RYR1* c.14477C>T (RyR1 p.Thr4826Ile) variant signal, and therefore the unwanted *RYR1* c.14483T>A variant could have been present in different cells of the same mixed culture. Confirmation of this theory would require the isolation of single cells from mixed cell line 1D and subsequent testing for these variants.

Regrettably, the isolation, growth, gDNA extraction, and HRM analysis of monoclonal HMCL-7304 cell cultures from a mixed batch requires weeks of work and therefore the further analysis of these cell lines was outside the time-frame of this research. Subsequent work conducted by Dr Anja Schiemann identified a monoclonal cell line with a heterozygous *RYR1* c.14477C>T (RyR1 p.Thr4826Ile) variant. Attempted regrowth of this cell line from the 96-well plate indicated that the potentially edited cells were no longer

viable. It will therefore be necessary to optimise the system further to obtain viable, edited monoclonal myoblasts.

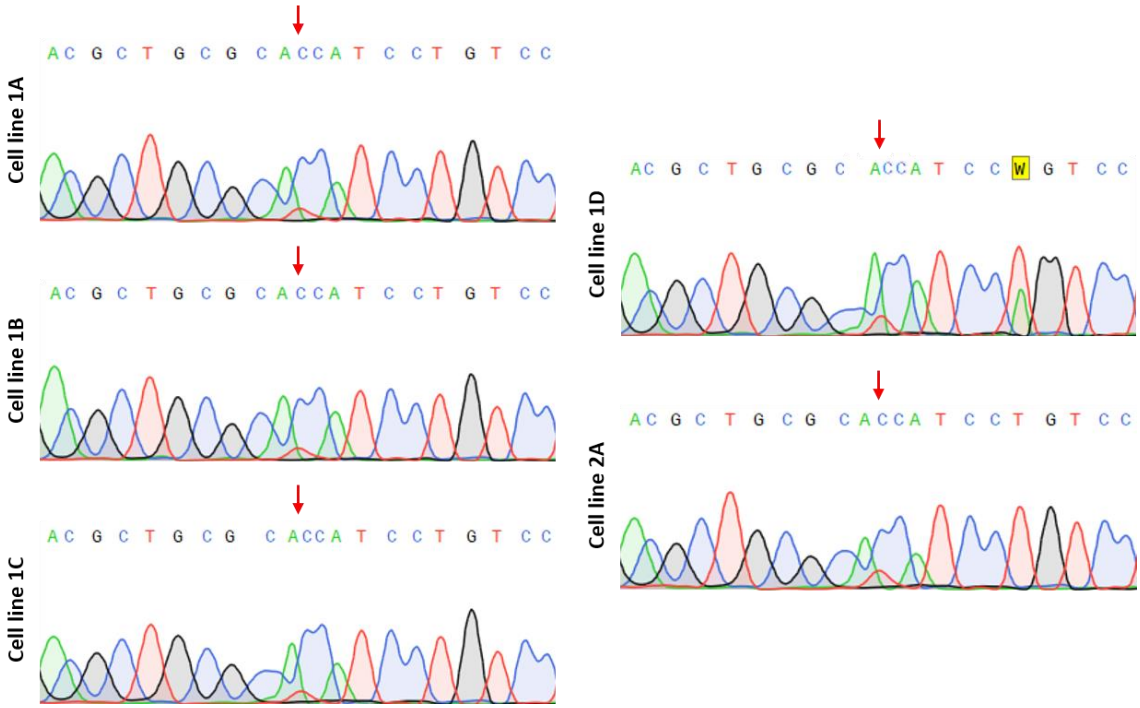

Figure 4.32 Sanger sequencing of polyclonal edited HMCL-7304 cell lines

Sanger sequencing chromatograms show the presence of the *RYR1* c.14477C>T (RyR1 p.Thr4826Ile) variant in the genome of polyclonal HMCL-7304 cell lines. Indicated by an arrow, the large blue peak corresponds to the original cytosine residue and the smaller red peak corresponds to the introduced tyrosine residue. Cell line 1D also has a *RYR1* c.14483T>A substitution that is indicated with a 'W' highlighted yellow.

4.4 *Concluding remarks*

4.4.1 *Discussion of results*

The key objective of this research was the investigation and development of new techniques to study the molecular basis of MH, with the aim of increasing the capability for DNA-based diagnosis of the disorder. These were to be used both within this study and in future endeavours to explore the hypothesis that RyR1 variants associated with MH-susceptibility cause dysregulation of Ca^{2+} release from intracellular stores. The specific

purpose of the second half of this research within the overarching theme was to develop the CRISPR/Cas9 gene editing system for use with human myoblasts; this technique would be used to directly introduce genetic variants linked to MH-susceptibility into the genome of those cells. The system was developed by use of an immortalised human myoblast cell line (HMCL-7304) with the intention that it may subsequently be adapted for use with patient-derived myoblasts. Because this methodology was new to the laboratory, this portion of the research involved a substantial proportion of literature searching and method development.

Despite the challenges in the progression of this objective, evidence was provided that the RyR1 p.Thr4826Ile variant had been successfully inserted into the genome of HMCL-7304. Unfortunately, the monoclonal cell lines into which the variant was initially introduced did not survive reanimation for further analysis and the subsequent cell lines in which the variant was observed were polyclonal. Because of this, the existence of any off-target effects caused by the gene editing could not be determined and the functional analysis of the cells with and without the variant for RyR1 hypersensitivity could not take place. The successful genome editing that did occur, however, indicates that the research described in this thesis has provided proof-of-principle.

Before this research may be expanded to examine currently uncharacterised genetic variants for Ca^{2+} dysregulation, the efficacy of the current work should be confirmed. This will first require that monoclonal cells are isolated following editing and subsequently confirmed as having the introduced variant by Sanger sequencing. Next, a lack of off-target editing will need to be confirmed in those cell lines—either by site-specific Sanger sequencing of predicted off-targets or, for a more comprehensive examination, by use of whole exome or genome sequencing. If these experiments are successful, then functional assays may be conducted to compare RyR1 function in the edited cell lines with that in the unedited HMCL-7304 cell line.

The analysis of genetic variants in myoblasts would contribute to the body of knowledge of MH. This is because the limitation in DNA-based diagnosis for MH-susceptibility remains not only in the lack of functionally characterised variants, but also in the inability

to make an MHN diagnosis with DNA. This is attributable to the 2.6% rate of discordance observed between genotype and phenotype in families tested for MH-susceptibility.[255] Discordance occurs when a family member who does not have the familial MH variant is diagnosed as MHS by IVCT.[255-257] This may be caused by modifier alleles that result in different phenotypes that cannot be properly examined in a simple recombinant expression system, or a false-positive IVCT result. Therefore, the ability to directly repair the genome of difficult-to-transfect cells such as human myoblasts is a worthwhile technique to develop.

4.4.2 Improvements to the method

The challenge posed by use of a molecular technique that was new to the scientific field—and to the laboratory in which this research occurred—was substantial. Because of this, there were several limitations on the research that may be addressed in future work by trialling simple adjustments to the experimental approach.

4.4.2.1 Alternatives for gene editing components

An observation with respect to improvement of the method is that the adoption of lentiviral expression vectors for all gene editing components is no longer required. An alternative DNA delivery mechanism was included to allow for the possibility that Nucleofection was unsuccessful. Because lentivirus is reported to be one of the most efficient methods for DNA delivery for difficult-to-transfect cells such as human myoblasts, lentiviral vectors were integrated in method development.[322] The unexpected difficulties experienced during cloning by use of these vectors caused a considerable delay in the gene editing project that could be attributed to the recombinant nature of these vectors, and thus their exclusion should eliminate that obstacle. Because success was achieved with the Nucleofection system, in future work, expression vectors that do not have lentiviral genes should be used.

It is noteworthy that removing the lentiviral component of the project would also allow greater flexibility in the format of the donor DNA. Short repair templates of approximately 100 to 150 base pairs—either double-strand or single-strand—may be trialled because a

plasmid-based repair template is not a requirement of Nucleofector™ technology. This could improve the efficiency of gene editing greatly because short strands of donor DNA have been established to produce higher proportions of HDR editing than large, plasmid-based templates.[356] The purchase of custom-made commercial expression vectors (as well as repair templates) would also eliminate the issues that may arise during difficult cloning procedures and may present a cost-effective means to increase the throughput of this research.

Another enhancement to the gene editing method would be to reduce the size of the area in which potential guide sequences are identified. The proximity of the guide recognition sequence to the site of the variant of interest is a critical factor in gene editing efficiency.[363,364] Reducing the distance between the locations of the DSB and the variant to be introduced should increase the likelihood of variant incorporation as well as remove the necessity of a repair template with long homology arms, thereby enabling the use of short repair templates. Identifying appropriate guide sequences proximal to the site of the variant will not be feasible for many variants, as was the case with the RyR1 p.Thr4826Ile variant investigated in this research. However, the inclusion of guide sequences with lower predicted targeting fidelities (as described in Section 4.2.2) that are proximal to the site of the variant is an avenue that could be investigated to increase editing efficiency and reduce screening time.[365]

4.4.2.2 Cell storage and isolation

The most obvious limitation of the method was the lack of surviving cells after storage in a frozen state for several weeks as discussed in Section 4.3.2. Although this technique was trialled with the HMCL-7304 cell line prior to gene editing on a small scale, one or more of the adjustments made to the method when the actual experiment occurred contributed to the loss of viability observed. First, the cells were kept frozen for several weeks while an issue with the HRM procedure was investigated, instead of the one week as in the trial run. Second, the cells were frozen at a higher confluence (90%) in the experiment compared with the 50% confluence used in the trial run. Finally, the experiment required that all cells in the 96-well plate be frozen at once and many cells were exposed to freezing media

containing dimethyl sulfoxide for a relatively long period compared to that of the trial run in which only two rows of cells were frozen.

The technique adopted in the second phase of gene editing (see Section 4.3.3) of maintaining the live cells after passaging them at low confluence (10%) while DNA testing was carried out appeared to be effective. However, there is one built–in constraint with this technique—it requires that testing be completed within approximately one week of passaging, before the cells require passaging again. The maintenance of several 96-well plates with growing myoblasts is laborious and potentially wasteful of resources, therefore a reliable method for freezing the cells for storage during testing would be preferable. This will likely involve the resuspension of each well of myoblasts in a freezing media which can also be laborious, although the use of multichannel pipettors would make this process somewhat more efficient. There has been some success reported for freezing human muscle cells in a multi-well plate format without the need for detachment from the plate; however, the loss of up to 90% of cells was observed.[372] The use of storage cases for the gradual decrease in temperature required for cryopreservation will also need to be investigated; an example of the type of container that may be used is a simple polystyrene box filled with tissue paper.[372,373]

A major limitation of the gene editing technique developed in this research was the laborious screening stage in which monoclonal cells were isolated in large numbers and subsequently tested for the variant of interest. Most strategies described in the literature that aim to simplify this step involve the enhancement of HDR editing by increasing either editing efficiency or selection for desirable cells. In contrast, two experimental techniques have been combined to successfully improve methods of single cell isolation and screening.[374] This novel combination enabled the selection of rare clones following HDR by several rounds of sib-selection followed by droplet digital PCR. Sib-selection is a method commonly used in yeast studies for isolation of single clones and involves the testing of polyclonal populations that are successively purified until a monoclonal culture of interest is isolated. This was used in combination with droplet digital PCR; a method for absolute quantification of a mixed DNA sample with a higher rate of precision reported than current real time PCR methods.[375] While this novel method requires specialty

equipment, it may be the key to limiting the laborious and time-consuming screening stage in creating edited clones.

4.4.2.3 Enrichment of edited cells

The efficiency of gene editing observed in this research was predicted to be approximately 0.8%—a figure that is comparable to the reported HDR frequencies of less than 1% with CRISPR/Cas9 technology.[358,359] Because of this, strategies for enrichment of transfected cells at the stage of editing should be trialled to reduce the number of cell lines that require screening later in the process. One possibility is the enrichment of cells successfully transfected with the Cas9/gRNA expression vector through biochemical selection. The most accessible method would be through selection of an antibiotic resistance marker included in the expression vector, although selection of cells for a fluorescent marker is also possible with fluorescence-activated cell sorting. Such a marker could be cloned into the Cas9 vector, or a commercial Cas9 vector could be sourced based on its selection properties. For example, the lentiCRISPR v2 vector used in this research contained the coding sequences for both puromycin and bleomycin antibiotic resistance (plasmid map in Appendix B.9). However, this selection method has several disadvantages. For example, it would not be comprehensive because any selection would have to be carried out in a short period—up to 72 hours after transfection—to prevent stable integration of the vector into the genome and to reduce the risk of selecting against cells that were transfected transiently. Additionally, the selection of cells transfected with the repair template is not feasible as it would involve the use of a different selection marker and would require the use of a plasmid-based repair template. Experimental techniques that increase editing efficiency without the need for biochemical selection are therefore preferable.

Enrichment for transfected cells through biochemical selection may also improve the efficacy of the T7 Endonuclease I assay that was used to analyse the gRNAs for editing efficiency. The assay was ineffectual in this research for the determination of guide efficiency in the HMCL-7304 cell line—likely due to the low rate of editing overall. Enrichment for transfected cells prior to this assay may increase the proportion of edited cells and therefore make visualisation of this editing possible. This would be beneficial

because, although guide targeting was observed in the HEK-293T cell line by use of the T7 Endonuclease I assay, the efficiency of the gRNAs should be analysed in the HMCL-7304 cell line in which the editing will take place.

Strategies that increase HDR efficiency may also be incorporated. For example, cell synchronisation prior to editing by use of cell cycle inhibitors have been effective in increasing editing rates in HEK-293T cells; although its success can be limited in more complex cell types such as human fibroblasts.[376] An observation from previous gene editing technologies was that transient hypothermia (incubating the cells at approximately 30 °C) following transfection of the zinc finger gene editing components increased both the efficiency and the fidelity of HDR editing.[377] The cold-shock treatment can also increase HDR efficiency from CRISPR/Cas9-mediated gene editing and therefore represents a straightforward means to potentially increase editing efficiency without loss in viability.[378]

4.4.3 Future directions

4.4.3.1 Alternative uses for myotubes

The increased access to rapid and reliable sequencing technology in recent years has substantially expanded the list of candidate variants associated with MH. The clinical implication of those variants is currently assessed on an individual basis and therefore the rate of variant identification far exceeds the rate at which the impact of those genetic variants can be resolved. Indeed, the evaluation of variants of unknown significance requires the advent of high-throughput strategies for functional screening.

A high level of success was reported recently for the characterisation of variants in a voltage-gated potassium channel associated with cardiac arrythmias.[379] The authors described an experimental approach that combined the high-efficiency transfection of cells with automated patch-clamp technology. With this method, the cells are first electroporated with a plasmid containing the variant, followed by seeding into a multiwell plate and automated analysis of channel activity by use of a planar patch-clamp. In this particular study, analysis was performed on a large scale with 78 variants functionally

characterised.[379] Cloning of variants into expression plasmids is still required with this method; however, the relatively high transfection rate from Nucleofection observed in this research with human myoblasts represents a suitable starting point if it were implemented for use in MH research.

4.4.3.2 Variations of gene editing

Genome editing may represent a means to overcome this hurdle of variant discovery outpacing variant classification as the technique is modifiable for differently intended experimental outcomes. One such modification may be allele-specific knockout by use of gene editing in patient-derived cells, taking advantage of the dominant inheritance pattern of MH. Allele-specific knockout is a technique that is similar to one that has been used successfully to study dominant-negative mutations by use of RNA interference technology, whereby the expression of a dominant mutant allele is knocked down, allowing the wild-type phenotype to be observed.[380] This differs from the original intention of this research to 'correct' a variant using a repair template containing the WT sequence in that it aims to remove the variant allele entirely.

Adaption of this technique for use with CRISPR/Cas9 gene editing may involve the design of gRNAs that contain the variant and the subsequent ablation of the mutant allele through the NHEJ pathway. Several guides would need to be trialled for each variant to determine their specificity to the mutant allele as this technique requires the remaining wild-type allele to remain intact. Although guide fidelity varies greatly, this method has been used successfully with CRISPR/Cas9 gene editing.[381,382] This process may even circumvent the need for monoclonal cell selection as, if gRNAs can be designed that target the mutant allele with high specificity, polyclonal populations may be analysed for functional characterisation. This method would advance the aim of establishing that a single genetic variant causes MH-susceptibility. This gap in the knowledge is a substantial obstruction in the DNA-based diagnosis of MH because the absence of the known familial variant in a pedigree is not currently sufficient for a 'normal' diagnosis and therefore the invasive muscle testing is still required for those family members.

4.4.3.3 Alternative assays for functional studies

One of the key advantages in working with human myoblasts when functionally characterising variants is the ability to monitor phenotypic changes in a more physiological context. This is because genetic variants that contribute to MH-susceptibility may have a more subtle phenotypic change than increased channel activity in response to an agonist. That is, strategies that examine the EC coupling pathway may be more desirable than the current standard of directly activating RyR1 and measuring the resulting Ca^{2+} release. Variants may be examined in a whole-cell context by measurement of alterations to EC coupling under patch-clamp recording conditions.[383] This technique has been used in a range of skeletal muscle cells including primary human myotubes to analyse ion conductance from channels other than RyR1 such as those across the plasma membrane.[384,385]

Experimental strategies may also include the measurement of RyR1 channel activity in the context of artificial lipid bilayers created from SR vesicles—an experimental system that has been used extensively in ion channel research.[386] For example, the mechanical interaction between the DHPR β subunit and RyR1 has been examined in several studies by means of RyR1 channel activity in planar lipid bilayers in the presence of small, mutant peptides from the DHPR β subunit.[131,132] Experimental strategies such as these may also enable variants of unknown significance in genes other than *RYR1* to be analysed. For example, transient receptor potential vanilloid 1 variants have been linked to adverse reactions to anaesthesia and are therefore implicated in MH-susceptibility; however, the link is yet to be investigated experimentally.[25] Because of the theoretical ability to target any gene, the development of gene editing will greatly benefit research into complex neuromuscular disorders.

4.4.3.4 Engineering muscle tissue in vitro

The ability to grow and manipulate human muscle cells with specific genetic variants may lead to greater opportunities than the simple analysis of differentiated myotubes. One such opportunity is the engineering of skeletal muscle tissue for *ex vivo* functional

testing—either in an extracellular matrix contained within a scaffold or on a microfluidic platform. This technique would enable neuromuscular disease to be examined in an environment that embodies the complexity of mature skeletal muscle architecture. The growth of muscle bundles can be adapted for the experimental requirements; for example, muscle tissue has been successfully grown from a range of starting cells including human pluripotent stem cells and myoblasts of rat, mouse, and human origin.[387-391] There are many experimental opportunities for use with engineered muscle fibres, such as observing structural changes by electron microscopy and monitoring biophysical properties in response to different stimuli.

The ability to directly test the effects of drugs by use of this method was reported in a study in which tissue was engineered from myoblast cells extracted from an individual with Duchenne muscular dystrophy.[391] This established a disease model in which different treatments may be trialled for their efficacy, removing the need for animal experiments that do not reflect human physiology. A functional analysis of human muscle bundles engineered from primary myoblasts was recently reported in which both Ca^{2+} transients and the contractile force of the muscle were measured in response to either electrical stimulus or the neurotransmitter acetylcholine.[390] Because this method can mimic the skeletal muscle environment, any variant that disrupts or alters EC coupling may be characterised by measuring muscle tension in response to stimuli. The growth and manipulation of tissue-engineered muscle is yet to be automated—or even standardised—but this field is rapidly progressing and may provide a powerful tool for physiological studies of muscular disorders.

Future studies dedicated to the understanding of the functional consequences of variants associated with MH-susceptibility hold enormous potential for both MH-related research and the larger field of neuromuscular disorders. Sequencing technologies are constantly advancing, leading to the detection of more variants of unknown significance. The identification of variants in individuals with a disease phenotype is essential; however, there is little use for that information in the absence of appropriate functional testing to determine the clinical implications of those variants. The limitations of the experimental system such as the use of recombinant techniques with non-muscle cells have restricted

the research of complex genetic disease. The gene editing technique of CRISPR/Cas9 may be modified to target any gene for the creation of specific variants, and as such, has been used successfully in many cell types. Gene editing, therefore, has considerable implications in the study of disorders that are genetically heterogeneous such as MH-susceptibility.

5 Reference list

1. Rosenberg H, Sambuughin N, Riazi S, Dirksen R. Malignant Hyperthermia Susceptibility. 2003 [Updated 2013]. In: GeneReviews [Internet]. Seattle (WA): University of Washington, Seattle. Available from: https://www.ncbi.nlm.nih.gov/books/NBK1146/.

2. Glahn KPE, Ellis FR, Halsall PJ, Müller CR, Snoeck MMJ, Urwyler A, *et al.* Recognizing and managing a malignant hyperthermia crisis: Guidelines from the European Malignant Hyperthermia Group. British Journal of Anaesthesia. 2010;105(4):417-20.

3. Gupta PK, Hopkins PM. Diagnosis and management of malignant hyperthermia. British Journal of Anaesthesia. 2017;17(7):249-54.

4. Wang R, Zhong X, Meng X, Koop A, Tian X, Jones PP, *et al.* Localization of the dantrolene-binding sequence near the FK506-binding protein-binding site in the three-dimensional structure of the ryanodine receptor. Journal of Biological Chemistry. 2011;286(14):12202-12.

5. Choi RH, Koenig X, Launikonis BS. Dantrolene requires Mg^{2+} to arrest malignant hyperthermia. Proceedings of the National Academy of Sciences. 2017;114(18):4811-5.

6. Kolb ME, Horne ML, Martz R. Dantrolene in human malignant hyperthermia. Anesthesiology. 1982;56(4):254-62.

7. Krause T, Gerbershagen MU, Fiege M, Weisshorn R, Wappler F. Dantrolene - a review of its pharmacology, therapeutic use and new developments. Anaesthesia. 2004;59(4):364-73.

8. Kim D-C. Malignant hyperthermia. Korean Journal of Anesthesiology. 2012;63(5):391-401.

9. Larach MG, Gronert GA, Allen GC, Brandom BW, Lehman EB. Clinical presentation, treatment, and complications of malignant hyperthermia in North America from 1987 to 2006. Anesthesia and Analgesia. 2010;110(2):498-507.

10. Utili R, Boitnott JK, Zimmerman HJ. Dantrolene-associated hepatic injury. Incidence and character. Gastroenterology. 1977;72(4 Pt 1):610-6.

11. Chan CH. Dantrolene sodium and hepatic injury. Neurology. 1990;40(9):1427-32.

12. Larach MG, Localio AR, Allen GC, Denborough MA, Ellis FR, Gronert GA, *et al.* A clinical grading scale to predict malignant hyperthermia susceptibility. Anesthesiology. 1994;80(4):771-9.

13. Tautz TJ, Urwyler A, Antognini JF, Riou B. Case scenario: Increased end-tidal carbon dioxide: A diagnostic dilemma. Anesthesiology. 2010;112(2):440-6.

14. von Breunig F, Wappler F, Hagel C, von Richthofen V, Fiege M, Weisshorn R, *et al.* Histomorphologic examination of skeletal muscle preparations does not differentiate between malignant hyperthermia-susceptible and -normal patients. Anesthesiology. 2004;100(4):789-94.

15. Ording H, Brancadoro V, Cozzolino S, Ellis FR, Glauber V, Gonano EF, *et al. In vitro* contracture test for diagnosis of malignant hyperthermia following the protocol of the European MH Group: Results of testing patients surviving fulminant MH and unrelated low-risk subjects. The European Malignant Hyperthermia Group. Acta Anaesthesiologica Scandinavica. 1997;41(8):955-66.

16. Hopkins PM, Ruffert H, Snoeck MM, Girard T, Glahn KP, Ellis FR, *et al.* European Malignant Hyperthermia Group guidelines for investigation of malignant hyperthermia susceptibility. British Journal of Anaesthesia. 2015;115(4):531-9.

17. Brandt A, Schleithoff L, Jurkat-Rott K, Klingler W, Baur C, Lehmann-Horn F. Screening of the ryanodine receptor gene in 105 malignant hyperthermia families: Novel mutations and concordance with the *in vitro* contracture test. Human Molecular Genetics. 1999;8(11):2055-62.

18. McCarthy TV, Healy JM, Heffron JJ, Lehane M, Deufel T, Lehmann-Horn F, *et al.* Localization of the malignant hyperthermia susceptibility locus to human chromosome 19q12-13.2. Nature. 1990;343(6258):562-4.

19. Levitt RC, Olckers A, Meyers S, Fletcher JE, Rosenberg H, Isaacs H, *et al.* Evidence for the localization of a malignant hyperthermia susceptibility locus (MHS2) to human chromosome 17q. Genomics. 1992;14(3):562-6.

20. Iles DE, Lehmann-Horn F, Scherer SW, Tsui LC, Olde Weghuis D, Suijkerbuijk RF, *et al.* Localization of the gene encoding the alpha 2/delta-subunits of the L-type voltage-dependent calcium channel to chromosome 7q and analysis of the segregation of flanking markers in malignant hyperthermia susceptible families. Human Molecular Genetics. 1994;3(6):969-75.

21. Sudbrak R, Procaccio V, Klausnitzer M, Curran JL, Monsieurs K, van Broeckhoven C, *et al.* Mapping of a further malignant hyperthermia susceptibility locus to chromosome 3q13.1. The American Journal of Human Genetics. 1995;56(3):684-91.

22. Robinson RL, Monnier N, Wolz W, Jung M, Reis A, Nuernberg G, *et al.* A genome wide search for susceptibility loci in three European malignant hyperthermia pedigrees. Human Molecular Genetics. 1997;6(6):953-61.

23. Carsana A. Exercise-induced rhabdomyolysis and stress-induced malignant hyperthermia events, association with malignant hyperthermia susceptibility, and *RYR1* gene sequence variations. The Scientific World Journal. 2013;2013:531465.

24. Perez CF, Eltit JM, Lopez JR, Bodnár D, Dulhunty AF, Aditya S, *et al.* Functional and structural characterization of a novel malignant hyperthermia-susceptible variant of DHPR-β_{1a} subunit (CACNB1). American Journal of Physiology - Cell Physiology. 2018;314(3):C323-C33.

25. Linsley JW, Hsu I-U, Groom L, Yarotskyy V, Lavorato M, Horstick EJ, *et al.* Congenital myopathy results from misregulation of a muscle Ca^{2+} channel by mutant Stac3. Proceedings of the National Academy of Sciences. 2017;114(2):E228-E36.

26. Abeele FV, Lotteau S, Ducreux S, Dubois C, Monnier N, Hanna A, *et al.* TRPV1 variants impair intracellular Ca^{2+} signaling and may confer susceptibility to malignant hyperthermia. Genetics in Medicine. 2019;21(2):441-50.

27. Ording H. Incidence of malignant hyperthermia in Denmark. Anesthesia and Analgesia. 1985;64(7):700-4.

28. Monnier N, Krivosic-Horber R, Payen J-F, Kozak-Ribbens G, Nivoche Y, Adnet P, *et al.* Presence of two different genetic traits in malignant hyperthermia families: Implication for genetic analysis, diagnosis, and incidence of malignant hyperthermia susceptibility. Anesthesiology. 2002;97(5):1067-74.

29. Halsall PJ, Cain PA, Ellis FR. Retrospective analysis of anaesthetics received by patients before susceptibility to malignant hyperexia was recognized. British Journal of Anaesthesia. 1979;51(10):949-54.

30. Rosenberg H, Pollock N, Schiemann A, Bulger T, Stowell K. Malignant hyperthermia: A review. Orphanet Journal of Rare Diseases. 2015;10:93.

31. Denborough MA, Forster JF, Lovell RR, Maplestone PA, Villiers JD. Anaesthetic deaths in a family. British Journal of Anaesthesia. 1962;34:395-6.

32. Harrison GG. Porcine malignant hyperthermia—The saga of the "hot" pig. In: Britt BA, editor. Malignant Hyperthermia. Boston, MA: Springer US; 1987. p. 103-36.

33. Klein L, Rosenberg H. Malignant hyperthermia in animals other than swine. In: Britt BA, editor. Malignant Hyperthermia. Boston, MA: Springer US; 1987. p. 137-54.

34. Fujii J, Otsu K, Zorzato F, de Leon S, Khanna VK, Weiler JE, *et al.* Identification of a mutation in porcine ryanodine receptor associated with malignant hyperthermia. Science. 1991;253(5018):448-51.

35. Fletcher JE, Calvo PA, Rosenberg H. Phenotypes associated with malignant hyperthermia susceptibility in swine genotyped as homozygous or heterozygous for the ryanodine receptor mutation. British Journal of Anaesthesia. 1993;71(3):410-7.

36. Hong TT, Shaw RM. Ion channel trafficking. In: Conn PM, editor. Ion Channels in Health and Disease. Boston: Academic Press; 2016. p. 25-51.

37. Blausen.com staff. Medical gallery of Blausen Medical 2014. WikiJournal of Medicine2014.

38. Berchtold MW, Brinkmeier H, Müntener M. Calcium ion in skeletal muscle: Its crucial role for muscle function, plasticity, and disease. Physiological Reviews. 2000;80(3):1215-65.

39. Eisenberg BR. Quantitative ultrastructure of mammalian skeletal muscle. Comprehensive physiology. 1983.

40. Robb-Gaspers LD, Burnett P, Rutter GA, Denton RM, Rizzuto R, Thomas AP. Integrating cytosolic calcium signals into mitochondrial metabolic responses. The EMBO Journal. 1998;17(17):4987-5000.

41. Kavanagh NI, Ainscow EK, Brand MD. Calcium regulation of oxidative phosphorylation in rat skeletal muscle mitochondria. Biochimica Et Biophysica Acta. 2000;1457(1-2):57-70.

42. Santo-Domingo J, Demaurex N. Calcium uptake mechanisms of mitochondria. Biochimica Et Biophysica Acta. 2010;1797(6):907-12.

43. Hoth M, Button DC, Lewis RS. Mitochondrial control of calcium-channel gating: A mechanism for sustained signaling and transcriptional activation in T lymphocytes. Proceedings of the National Academy of Sciences. 2000;97(19):10607-12.

44. Montero M, Alonso MT, Carnicero E, Cuchillo-Ibanez I, Albillos A, Garcia AG, *et al.* Chromaffin-cell stimulation triggers fast millimolar mitochondrial Ca^{2+} transients that modulate secretion. Nature Cell Biology. 2000;2(2):57-61.

45. Yi J, Ma C, Li Y, Weisleder N, Rios E, Ma J, *et al.* Mitochondrial calcium uptake regulates rapid calcium transients in skeletal muscle during excitation-contraction (E-C) coupling. Journal of Biological Chemistry. 2011;286(37):32436-43.

46. Mishra P, Varuzhanyan G, Pham AH, Chan DC. Mitochondrial dynamics is a distinguishing feature of skeletal muscle fiber types and regulates organellar compartmentalization. Cell metabolism. 2015;22(6):1033-44.

47. Ervasti JM, Strand MA, Hanson TP, Mickelson JR, Louis CF. Ryanodine receptor in different malignant hyperthermia-susceptible porcine muscles. American Journal of Physiology. 1991;260(1 Pt 1):C58-66.

48. Gehlert S, Bloch W, Suhr F. Ca^{2+}-dependent regulations and signaling in skeletal muscle: From electro-mechanical coupling to adaptation. International Journal of Molecular Sciences. 2015;16(1):1066-95.

49. Melzer W, Herrmann-Frank A, Lüttgau HC. The role of Ca^{2+} ions in excitation-contraction coupling of skeletal muscle fibres. Biochimica Et Biophysica Acta. 1995;1241(1):59-116.

50. Marx SO, Ondrias K, Marks AR. Coupled gating between individual skeletal muscle Ca^{2+} release channels (ryanodine receptors). Science. 1998;281(5378):818-21.

51. Porta M, Diaz-Sylvester PL, Neumann JT, Escobar AL, Fleischer S, Copello JA. Coupled gating of skeletal muscle ryanodine receptors is modulated by Ca^{2+}, Mg^{2+}, and ATP. American Journal of Physiology. 2012;303(6):C682-97.

52. Martonosi AN. The structure and interactions of Ca^{2+}-ATPase. Bioscience Reports. 1995;15(5):263-81.

53. Griffiths EJ, Rutter GA. Mitochondrial calcium as a key regulator of mitochondrial ATP production in mammalian cells. Biochimica Et Biophysica Acta. 2009;1787(11):1324-33.

54. Nakai J, Dirksen RT, Nguyen HT, Pessah IN, Beam KG, Allen PD. Enhanced dihydropyridine receptor channel activity in the presence of ryanodine receptor. Nature. 1996;380(6569):72-5.

55. Stiber J, Hawkins A, Zhang Z-S, Wang S, Burch J, Graham V, *et al.* STIM1 signalling controls store-operated calcium entry required for development and contractile function in skeletal muscle. Nature Cell Biology. 2008;10(6):688-97.

56. Mancarella S, Potireddy S, Wang Y, Gao H, Gandhirajan RK, Autieri M, *et al.* Targeted STIM deletion impairs calcium homeostasis, NFAT activation, and growth of smooth muscle. The FASEB Journal. 2013;27(3):893-906.

57. Liou J, Kim ML, Heo WD, Jones JT, Myers JW, Ferrell JE, *et al.* STIM is a Ca^{2+} sensor essential for Ca^{2+}-store-depletion-triggered Ca^{2+} influx. Current Biology. 2005;15(13):1235-41.

58. Penna A, Demuro A, Yeromin AV, Zhang SL, Safrina O, Parker I, *et al.* The CRAC channel consists of a tetramer formed by Stim-induced dimerization of Orai dimers. Nature. 2008;456(7218):116-20.

59. Ahn MK, Lee KJ, Cai C, Huang M, Cho C-H, Ma J, *et al.* Mitsugumin 53 regulates extracellular Ca^{2+} entry and intracellular Ca^{2+} release via Orai1 and RyR1 in skeletal muscle. Scientific Reports. 2016;6:36909.

60. Pan Z, Yang D, Nagaraj RY, Nosek TA, Nishi M, Takeshima H, *et al.* Dysfunction of store-operated calcium channel in muscle cells lacking mg29. Nature Cell Biology. 2002;4(5):379-83.

61. Eltit JM, Ding X, Pessah IN, Allen PD, Lopez JR. Nonspecific sarcolemmal cation channels are critical for the pathogenesis of malignant hyperthermia. The FASEB Journal. 2013;27(3):991-1000.

62. Cho C-H, Woo JS, Perez CF, Lee EH. A focus on extracellular Ca^{2+} entry into skeletal muscle. Experimental & Molecular Medicine. 2017;49(9):e378.

63. Cherednichenko G, Hurne AM, Fessenden JD, Lee EH, Allen PD, Beam KG, *et al.* Conformational activation of Ca^{2+} entry by depolarization of skeletal myotubes. Proceedings of the National Academy of Sciences. 2004;101(44):15793-8.

64. Lyfenko AD, Dirksen RT. Differential dependence of store-operated and excitation-coupled Ca^{2+} entry in skeletal muscle on STIM1 and Orai1. The Journal of Physiology. 2008;586(20):4815-24.

65. Bannister RA, Pessah IN, Beam KG. The skeletal L-type Ca^{2+} current is a major contributor to excitation-coupled Ca^{2+} entry. The Journal of General Physiology. 2009;133(1):79-91.

66. Díaz ME, Trafford AW, O'Neill SC, Eisner DA. Measurement of sarcoplasmic reticulum Ca^{2+} content and sarcolemmal Ca^{2+} fluxes in isolated rat ventricular myocytes during spontaneous Ca^{2+} release. The Journal of Physiology. 1997;501(Pt 1):3-16.

67. Lakatta EG. Functional implications of spontaneous sarcoplasmic reticulum Ca^{2+} release in the heart. Cardiovascular Research. 1992;26(3):193-214.

68. Trafford AW, Sibbring GC, Diaz ME, Eisner DA. The effects of low concentrations of caffeine on spontaneous Ca release in isolated rat ventricular myocytes. Cell Calcium. 2000;28(4):269-76.

69. Jiang D, Chen W, Xiao J, Wang R, Kong H, Jones PP, *et al.* Reduced threshold for luminal Ca^{2+} activation of RyR1 underlies a causal mechanism of porcine malignant hyperthermia. Journal of Biological Chemistry. 2008;283(30):20813-20.

70. Jiang D, Xiao B, Yang D, Wang R, Choi P, Zhang L, *et al.* RyR2 mutations linked to ventricular tachycardia and sudden death reduce the threshold for store-overload-induced Ca^{2+} release (SOICR). Proceedings of the National Academy of Sciences. 2004;101(35):13062-7.

71. Liu N, Rizzi N, Boveri L, Priori SG. Ryanodine receptor and calsequestrin in arrhythmogenesis: What we have learnt from genetic diseases and transgenic mice. Journal of molecular and cellular cardiology. 2009;46(2):149-59.

72. Jones PP, Jiang D, Bolstad J, Hunt DJ, Zhang L, Demaurex N, *et al.* Endoplasmic reticulum Ca^{2+} measurements reveal that the cardiac ryanodine receptor mutations linked to cardiac arrhythmia and sudden death alter the threshold for store-overload-induced Ca^{2+} release. Biochemical Journal. 2008;412(1):171-8.

73. Liu Y, Kimlicka L, Hiess F, Tian X, Wang R, Zhang L, *et al.* The CPVT-associated RyR2 mutation G230C enhances store overload-induced Ca^{2+} release and destabilizes the N-terminal domains. Biochemical Journal. 2013;454(1):123-31.

74. Dainese M, Quarta M, Lyfenko AD, Paolini C, Canato M, Reggiani C, *et al.* Anesthetic- and heat-induced sudden death in calsequestrin-1-knockout mice. The FASEB Journal. 2009;23(6):1710-20.

75. MacLennan DH, Chen SRW. Store overload-induced Ca^{2+} release as a triggering mechanism for CPVT and MH episodes caused by mutations in RYR and CASQ genes. The Journal of Physiology. 2009;587(Pt 13):3113-5.

76. Cully TR, Edwards JN, Launikonis BS. Activation and propagation of Ca^{2+} release from inside the sarcoplasmic reticulum network of mammalian skeletal muscle. The Journal of Physiology. 2014;592(Pt 17):3727-46.

77. Kong H, Jones PP, Koop A, Zhang L, Duff HJ, Wayne Chen SR. Caffeine induces Ca^{2+} release by reducing the threshold for luminal Ca^{2+} activation of the ryanodine receptor. Biochemical Journal. 2008;414(3):441-52.

78. Chen W, Koop A, Liu Y, Guo W, Wei J, Wang R, *et al.* Reduced threshold for store overload-induced Ca^{2+} release is a common defect of RyR1 mutations associated with malignant hyperthermia and central core disease. Biochemical Journal. 2017;474(16):2749-61.

79. Takeshima H, Nishimura S, Matsumoto T, Ishida H, Kangawa K, Minamino N, *et al.* Primary structure and expression from complementary DNA of skeletal muscle ryanodine receptor. Nature. 1989;339(6224):439-45.

80. Otsu K, Willard HF, Khanna VK, Zorzato F, Green NM, MacLennan DH. Molecular cloning of cDNA encoding the Ca^{2+} release channel (ryanodine receptor) of rabbit cardiac muscle sarcoplasmic reticulum. Journal of Biological Chemistry. 1990;265(23):13472-83.

81. Hakamata Y, Nakai J, Takeshima H, Imoto K. Primary structure and distribution of a novel ryanodine receptor/calcium release channel from rabbit brain. FEBS Lett. 1992;312(2-3):229-35.

82. Tribe RM. Unravelling the role of the ryanodine receptor type 3 in smooth muscle. The Journal of Physiology. 2002;538(Pt 3):673-.

83. Tarroni P, Rossi D, Conti A, Sorrentino V. Expression of the ryanodine receptor type 3 calcium release channel during development and differentiation of mammalian skeletal muscle cells. Journal of Biological Chemistry. 1997;272(32):19808-13.

84. Dietze B, Bertocchini F, Barone V, Struk A, Sorrentino V, Melzer W. Voltage-controlled Ca^{2+} release in normal and ryanodine receptor type 3 (RyR3)-deficient mouse myotubes. The Journal of Physiology. 1998;513(1):3-9.

85. Fessenden JD, Wang Y, Moore RA, Chen SR, Allen PD, Pessah IN. Divergent functional properties of ryanodine receptor types 1 and 3 expressed in a myogenic cell line. Biophysical Journal. 2000;79(5):2509-25.

86. Bers DM. Cardiac excitation-contraction coupling. Nature. 2002;415(6868):198-205.

87. Yan Z, Bai X-C, Yan C, Wu J, Li Z, Xie T, *et al.* Structure of the rabbit ryanodine receptor RyR1 at near-atomic resolution. Nature. 2015;517(7532):50-5.

88. Kimlicka L, Lau K, Tung C-C, Van Petegem F. Disease mutations in the ryanodine receptor N-terminal region couple to a mobile intersubunit interface. Nature Communications. 2013;4:1506.

89. Bai X-C, Yan Z, Wu J, Li Z, Yan N. The Central domain of RyR1 is the transducer for long-range allosteric gating of channel opening. Cell Research. 2016;26(9):995-1006.

90. Samsó M, Wagenknecht T, Allen PD. Internal structure and visualization of transmembrane domains of the RyR1 calcium release channel by cryo-EM. Nature structural & molecular biology. 2005;12(6):539-44.

91. Lee JM, Rho S-H, Shin DW, Cho C, Park WJ, Eom SH, *et al.* Negatively charged amino acids within the intraluminal loop of ryanodine receptor are involved in the interaction with triadin. Journal of Biological Chemistry. 2004;279(8):6994-7000.

92. Gillespie D, Xu L, Meissner G. Selecting ions by size in a calcium channel: The ryanodine receptor case study. Biophysical Journal. 2014;107(10):2263-73.

93. Zalk R, Clarke OB, des Georges A, Grassucci RA, Reiken S, Mancia F, *et al.* Structure of a mammalian ryanodine receptor. Nature. 2015;517(7532):44-9.

94. Perez CF, Voss A, Pessah IN, Allen PD. RyR1/RyR3 chimeras reveal that multiple domains of RyR1 are involved in skeletal-type E-C coupling. Biophysical Journal. 2003;84(4):2655-63.

95. Yin CC, Blayney LM, Lai FA. Physical coupling between ryanodine receptor-calcium release channels. J Mol Biol. 2005;349(3):538-46.

96. Samsó M. A guide to the 3D structure of the ryanodine receptor type 1 by cryoEM. Protein Science. 2017;26(1):52-68.

97. Yuchi Z, Lau K, Van Petegem F. Disease mutations in the ryanodine receptor central region: Crystal structures of a phosphorylation hot spot domain. Structure. 2012;20(7):1201-11.

98. Reiken S, Lacampagne A, Zhou H, Kherani A, Lehnart SE, Ward C, *et al.* PKA phosphorylation activates the calcium release channel (ryanodine receptor) in skeletal muscle: Defective regulation in heart failure. Journal of Cell Biology. 2003;160(6):919-28.

99. Yuchi Z, Yuen SMWK, Lau K, Underhill AQ, Cornea RL, Fessenden JD, *et al.* Crystal structures of ryanodine receptor SPRY1 and tandem-repeat domains reveal a critical FKBP12 binding determinant. Nature Communications. 2015;6:7947.

100. Leong P, MacLennan DH. A 37-amino acid sequence in the skeletal muscle ryanodine receptor interacts with the cytoplasmic loop between domains II and III in the skeletal muscle dihydropyridine receptor. Journal of Biological Chemistry. 1998;273(14):7791-4.

101. Cui Y, Tae HS, Norris NC, Karunasekara Y, Pouliquin P, Board PG, *et al.* A dihydropyridine receptor alpha1s loop region critical for skeletal muscle contraction is intrinsically unstructured and binds to a SPRY domain of the type 1 ryanodine receptor. The International Journal of Biochemistry & Cell Biology. 2009;41(3):677-86.

102. Lau K, Van Petegem F. Crystal structures of wild type and disease mutant forms of the ryanodine receptor SPRY2 domain. Nature Communications. 2014;5:5397.

103. Clarke OB, Hendrickson WA. Structures of the colossal RyR1 calcium release channel. Current opinion in structural biology. 2016;39:144-52.

104. Laver DR, Lenz GK, Lamb GD. Regulation of the calcium release channel from rabbit skeletal muscle by the nucleotides ATP, AMP, IMP and adenosine. The Journal of Physiology. 2001;537(Pt 3):763-78.

105. Gaburjakova M, Gaburjakova J. Insight towards the identification of cytosolic Ca^{2+}-binding sites in ryanodine receptors from skeletal and cardiac muscle. Acta Physiologica. 2017;219(4):757-67.

106. Chen Y, Xue S, Zou J, Lopez JR, Yang JJ, Perez CF. Myoplasmic resting Ca^{2+} regulation by ryanodine receptors is under the control of a novel Ca^{2+}-binding region of the receptor. Biochemical Journal. 2014;460(2):261-71.

107. Meissner G. Ryanodine receptor/Ca^{2+} release channels and their regulation by endogenous effectors. Annual Review of Physiology. 1994;56:485-508.

108. Meissner G, Darling E, Eveleth J. Kinetics of rapid Ca^{2+} release by sarcoplasmic reticulum. Effects of Ca^{2+}, Mg^{2+}, and adenine nucleotides. Biochemistry. 1986;25(1):236-44.

109. Laver DR, O'Neill ER, Lamb GD. Luminal Ca^{2+}-regulated Mg^{2+} inhibition of skeletal RyRs reconstituted as isolated channels or coupled clusters. The Journal of General Physiology. 2004;124(6):741-58.

110. Laver DR, Baynes TM, Dulhunty AF. Magnesium inhibition of ryanodine-receptor calcium channels: Evidence for two independent mechanisms. The Journal of Membrane Biology. 1997;156(3):213-29.

111. Bhat MB, Zhao J, Takeshima H, Ma J. Functional calcium release channel formed by the carboxyl-terminal portion of ryanodine receptor. Biophysical Journal. 1997;73(3):1329-36.

112. Balshaw D, Gao L, Meissner G. Luminal loop of the ryanodine receptor: A pore-forming segment? Proceedings of the National Academy of Sciences. 1999;96(7):3345-7.

113. Ranatunga KM, Chen SR, Ruest L, Welch W, Williams AJ. Quantification of the effects of a ryanodine receptor channel mutation on interaction with a ryanoid. Mol Membr Biol. 2007;24(3):185-93.

114. Nagasaki K, Fleischer S. Ryanodine sensitivity of the calcium release channel of sarcoplasmic reticulum. Cell Calcium. 1988;9(1):1-7.

115. Fessenden JD, Perez CF, Goth S, Pessah IN, Allen PD. Identification of a key determinant of ryanodine receptor type 1 required for activation by 4-chloro-*m*-cresol. Journal of Biological Chemistry. 2003;278(31):28727-35.

116. Fessenden JD, Feng W, Pessah IN, Allen PD. Amino acid residues Gln4020 and Lys4021 of the ryanodine receptor type 1 are required for activation by 4-chloro-*m*-cresol. Journal of Biological Chemistry. 2006;281(30):21022-31.

117. Perni S, Lavorato M, Beam KG. *De novo* reconstitution reveals the proteins required for skeletal muscle voltage-induced Ca^{2+} release. Proceedings of the National Academy of Sciences. 2017;114(52):13822-7.

118. Dulhunty AF, Wei-LaPierre L, Casarotto MG, Beard NA. Core skeletal muscle ryanodine receptor calcium release complex. Clinical and Experimental Pharmacology and Physiology. 2017;44(1):3-12.

119. Bannister RA, Beam KG. $Ca_V1.1$: The atypical prototypical voltage-gated Ca^{2+} channel. Biochimica Et Biophysica Acta. 2013;1828(7):1587-97.

120. Wu J, Yan Z, Li Z, Yan C, Lu S, Dong M, *et al.* Structure of the voltage-gated calcium channel $Ca_V1.1$ complex. Science. 2015;350(6267).

121. Carbonneau L, Bhattacharya D, Sheridan DC, Coronado R. Multiple loops of the dihydropyridine receptor pore subunit are required for full-scale excitation-contraction coupling in skeletal muscle. Biophysical Journal. 2005;89(1):243-55.

122. Papadopoulos S, Leuranguer V, Bannister RA, Beam KG. Mapping sites of potential proximity between the dihydropyridine receptor and RyR1 in muscle using a cyan fluorescent protein-Yellow fluorescent protein tandem as a fluorescence resonance energy transfer probe. Journal of Biological Chemistry. 2004;279(42):44046-56.

123. Polster A, Ohrtman JD, Beam KG, Papadopoulos S. Fluorescence resonance energy transfer (FRET) indicates that association with the type I ryanodine receptor (RyR1) causes reorientation of multiple cytoplasmic domains of the dihydropyridine receptor (DHPR) α(1S) subunit. Journal of Biological Chemistry. 2012;287(49):41560-8.

124. Eltit JM, Bannister RA, Moua O, Altamirano F, Hopkins PM, Pessah IN, *et al.* Malignant hyperthermia susceptibility arising from altered resting coupling between the skeletal muscle L-type Ca^{2+} channel and the type 1 ryanodine receptor. Proceedings of the National Academy of Sciences. 2012;109(20):7923-8.

125. Pirone A, Schredelseker J, Tuluc P, Gravino E, Fortunato G, Flucher BE, *et al.* Identification and functional characterization of malignant hyperthermia mutation T1354S in the outer pore of the $Ca_V\alpha1S$-subunit. American Journal of Physiology-Cell Physiology. 2010;299(6):C1345-C54.

126. Weiss RG, O'Connell KMS, Flucher BE, Allen PD, Grabner M, Dirksen RT. Functional analysis of the R1086H malignant hyperthermia mutation in the DHPR reveals an unexpected influence of the III-IV loop on skeletal muscle EC coupling. American Journal of Physiology-Cell Physiology. 2004;287(4):C1094-C102.

127. Hu Z, Liang CM, Soong WT. Alternative splicing of L-type $Ca_V1.2$ calcium channels: Implications in cardiovascular diseases. Genes. 2017;8(12).

128. Neuhuber B, Gerster U, Döring F, Glossmann H, Tanabe T, Flucher BE. Association of calcium channel α(1S) and β(1a) subunits is required for the targeting of β(1a) but not of α(1S) into skeletal muscle triads. Proceedings of the National Academy of Sciences. 1998;95(9):5015-20.

129. Gregg RG, Messing A, Strube C, Beurg M, Moss R, Behan M, *et al.* Absence of the β subunit (cchb1) of the skeletal muscle dihydropyridine receptor alters expression of the α_1 subunit and eliminates excitation-contraction coupling. Proceedings of the National Academy of Sciences. 1996;93(24):13961-6.

130. Strube C, Beurg M, Powers PA, Gregg RG, Coronado R. Reduced Ca^{2+} current, charge movement, and absence of Ca^{2+} transients in skeletal muscle deficient in dihydropyridine receptor beta 1 subunit. Biophysical Journal. 1996;71(5):2531-43.

131. Rebbeck RT, Karunasekara Y, Gallant EM, Board PG, Beard NA, Casarotto MG, *et al.* The β(1a) subunit of the skeletal DHPR binds to skeletal RyR1 and activates the channel via Its 35-Residue C-terminal tail. Biophysical Journal. 2011;100(4):922-30.

132. Karunasekara Y, Rebbeck RT, Weaver LM, Board PG, Dulhunty AF, Casarotto MG. An α-helical C-terminal tail segment of the skeletal L-type Ca^{2+} channel β1a subunit activates ryanodine receptor type 1 via a hydrophobic surface. The FASEB Journal. 2012;26(12):5049-59.

133. Jayaraman T, Brillantes AM, Timerman AP, Fleischer S, Erdjument-Bromage H, Tempst P, *et al.* FK506 binding protein associated with the calcium release channel (ryanodine receptor). Journal of Biological Chemistry. 1992;267(14):9474-7.

134. Williams AJ, West DJ, Sitsapesan R. Light at the end of the Ca^{2+}-release channel tunnel: Structures and mechanisms involved in ion translocation in ryanodine receptor channels. Quarterly Reviews of Biophysics. 2001;34(1):61-104.

135. MacMillan D. FK506 binding proteins: Cellular regulators of intracellular Ca^{2+} signalling. Eur J Pharmacol. 2013;700(1-3):181-93.

136. Samsó M, Shen X, Allen PD. Structural characterization of the RyR1-FKBP12 interaction. J Mol Biol. 2006;356(4):917-27.

137. Girgenrath T, Mahalingam M, Svensson B, Nitu FR, Cornea RL, Fessenden JD. N-terminal and central segments of the type 1 ryanodine receptor mediate its interaction with FK506-binding proteins. Journal of Biological Chemistry. 2013;288(22):16073-84.

138. MacKrill JJ. Protein-protein interactions in intracellular Ca^{2+}-release channel function. Biochemical Journal. 1999;337 (Pt 3):345-61.

139. Venturi E, Galfré E, O'Brien F, Pitt Samantha J, Bellamy S, Sessions Richard B, *et al.* FKBP12.6 activates RyR1: Investigating the amino acid residues critical for channel modulation. Biophysical Journal. 2014;106(4):824-33.

140. Horstick EJ, Linsley JW, Dowling JJ, Hauser MA, McDonald KK, Ashley-Koch A, *et al.* Stac3 is a component of the excitation-contraction coupling machinery and mutated in Native American myopathy. Nature Communications. 2013;4:1952.

141. Polster A, Nelson BR, Olson EN, Beam KG. Stac3 has a direct role in skeletal muscle-type excitation-contraction coupling that is disrupted by a myopathy-causing mutation. Proceedings of the National Academy of Sciences. 2016;113(39):10986-91.

142. Cong X, Doering J, Grange RW, Jiang H. Defective excitation-contraction coupling is partially responsible for impaired contractility in hindlimb muscles of Stac3 knockout mice. Scientific Reports. 2016;6:26194.

143. Polster A, Perni S, Bichraoui H, Beam KG. Stac adaptor proteins regulate trafficking and function of muscle and neuronal L-type Ca^{2+} channels. Proceedings of the National Academy of Sciences. 2015;112(2):602-6.

144. Campiglio M, Flucher BE. STAC3 stably interacts through its C1 domain with $Ca_V1.1$ in skeletal muscle triads. Scientific Reports. 2017;7:41003.

145. Wu F, Quinonez M, DiFranco M, Cannon SC. Stac3 enhances expression of human $Ca_V1.1$ in Xenopus oocytes and reveals gating pore currents in HypoPP mutant channels. The Journal of General Physiology. 2018;150(3):475-89.

146. Polster A, Nelson BR, Papadopoulos S, Olson EN, Beam KG. Stac proteins associate with the critical domain for excitation-contraction coupling in the II-III loop of $Ca_V1.1$. The Journal of General Physiology. 2018;150(4):613-24.

147. Nelson BR, Wu F, Liu Y, Anderson DM, McAnally J, Lin W, *et al.* Skeletal muscle-specific T-tubule protein STAC3 mediates voltage-induced Ca^{2+} release and contractility. Proceedings of the National Academy of Sciences. 2013;110(29):11881-6.

148. Sanchez EJ, Lewis KM, Danna BR, Kang C. High-capacity Ca^{2+} binding of human skeletal calsequestrin. Journal of Biological Chemistry. 2012;287(14):11592-601.

149. Györke S, Terentyev D. Modulation of ryanodine receptor by luminal calcium and accessory proteins in health and cardiac disease. Cardiovascular Research. 2008;77(2):245-55.

150. Zima AV, Bovo E, Bers DM, Blatter LA. Ca^{2}+ spark-dependent and -independent sarcoplasmic reticulum Ca^{2}+ leak in normal and failing rabbit ventricular myocytes. The Journal of Physiology. 2010;588(23):4743-57.

151. Manno C, Figueroa LC, Gillespie D, Fitts R, Kang C, Franzini-Armstrong C, *et al.* Calsequestrin depolymerizes when calcium is depleted in the sarcoplasmic reticulum of working muscle. Proceedings of the National Academy of Sciences. 2017;114(4):E638-E47.

152. Protasi F, Paolini C, Dainese M. Calsequestrin-1: A new candidate gene for malignant hyperthermia and exertional/environmental heat stroke. The Journal of Physiology. 2009;587(13):3095-100.

153. Sztretye M, Yi J, Figueroa L, Zhou J, Royer L, Allen P, *et al.* Measurement of RyR permeability reveals a role of calsequestrin in termination of SR Ca^{2+} release in skeletal muscle. The Journal of General Physiology. 2011;138(2):231-47.

154. Song L, Alcalai R, Arad M, Wolf CM, Toka O, Conner DA, *et al.* Calsequestrin 2 (CASQ2) mutations increase expression of calreticulin and ryanodine receptors, causing catecholaminergic polymorphic ventricular tachycardia. Journal of Clinical Investigation. 2007;117(7):1814-23.

155. Beard NA, Dulhunty AF. C-terminal residues of skeletal muscle calsequestrin are essential for calcium binding and for skeletal ryanodine receptor inhibition. Skeletal Muscle. 2015;5:6.

156. Knudson CM, Stang KK, Moomaw CR, Slaughter CA, Campbell KP. Primary structure and topological analysis of a skeletal muscle-specific junctional sarcoplasmic reticulum glycoprotein (triadin). Journal of Biological Chemistry. 1993;268(17):12646-54.

157. Wei L, Gallant EM, Dulhunty AF, Beard NA. Junctin and triadin each activate skeletal ryanodine receptors but junctin alone mediates functional interactions with calsequestrin. The International Journal of Biochemistry & Cell Biology. 2009;41(11):2214-24.

158. Boncompagni S, Thomas M, Lopez JR, Allen PD, Yuan Q, Kranias EG, *et al.* Triadin/Junctin double null mouse reveals a differential role for Triadin and Junctin in anchoring CASQ to the jSR and regulating Ca^{2+} homeostasis. PloS One. 2012;7(7):e39962.

159. Goonasekera SA, Beard NA, Groom L, Kimura T, Lyfenko AD, Rosenfeld A, *et al.* Triadin binding to the C-terminal luminal loop of the ryanodine receptor is important for skeletal muscle excitation contraction coupling. The Journal of General Physiology. 2007;130(4):365-78.

160. Wium E, Dulhunty AF, Beard NA. A skeletal muscle ryanodine receptor interaction domain in triadin. PloS One. 2012;7(8):e43817.

161. Li L, Mirza S, Richardson SJ, Gallant EM, Thekkedam C, Pace SM, *et al.* A new cytoplasmic interaction between junctin and ryanodine receptor Ca²⁺ release channels. Journal of Cell Science. 2015;128(5):951.

162. Groh S, Marty I, Ottolia M, Prestipino G, Chapel A, Villaz M, *et al.* Functional interaction of the cytoplasmic domain of triadin with the skeletal ryanodine receptor. Journal of Biological Chemistry. 1999;274(18):12278-83.

163. Wang Y, Li X, Duan H, Fulton TR, Eu JP, Meissner G. Altered stored calcium release in skeletal myotubes deficient of triadin and junctin. Cell Calcium. 2009;45(1):29-37.

164. Shen X, Franzini-Armstrong C, Lopez JR, Jones LR, Kobayashi YM, Wang Y, *et al.* Triadins modulate intracellular Ca^{2+} homeostasis but are not essential for excitation-contraction coupling in skeletal muscle. Journal of Biological Chemistry. 2007;282(52):37864-74.

165. Chopra N, Knollmann BC. Triadin regulates cardiac muscle couplon structure and microdomain Ca^{2+} signalling: A path towards ventricular arrhythmias. Cardiovascular Research. 2013;98(2):187-91.

166. Kiewitz R, Acklin C, Schafer BW, Maco B, Uhrik B, Wuytack F, *et al.* Ca^{2+}-dependent interaction of S100A1 with the sarcoplasmic reticulum Ca^{2+}-ATPase2a and phospholamban in the human heart. Biochem Biophys Res Commun. 2003;306(2):550-7.

167. Tripathy A, Xu L, Mann G, Meissner G. Calmodulin activation and inhibition of skeletal muscle Ca^{2+} release channel (ryanodine receptor). Biophysical Journal. 1995;69(1):106-19.

168. Prosser BL, Hernandez-Ochoa EO, Schneider MF. S100A1 and calmodulin regulation of ryanodine receptor in striated muscle. Cell Calcium. 2011;50(4):323-31.

169. Prosser BL, Wright NT, Hernandez-Ochoa EO, Varney KM, Liu Y, Olojo RO, *et al.* S100A1 binds to the calmodulin-binding site of ryanodine receptor and modulates skeletal muscle excitation-contraction coupling. Journal of Biological Chemistry. 2008;283(8):5046-57.

170. Wagenknecht T, Radermacher M, Grassucci R, Berkowitz J, Xin HB, Fleischer S. Locations of calmodulin and FK506-binding protein on the three-dimensional architecture of the skeletal muscle ryanodine receptor. Journal of Biological Chemistry. 1997;272(51):32463-71.

171. Cornea RL, Nitu F, Gruber S, Kohler K, Satzer M, Thomas DD, *et al.* FRET-based mapping of calmodulin bound to the RyR1 Ca^{2+} release channel. Proceedings of the National Academy of Sciences. 2009;106(15):6128-33.

172. Moore CP, Rodney G, Zhang JZ, Santacruz-Toloza L, Strasburg G, Hamilton SL. Apocalmodulin and Ca^{2+} calmodulin bind to the same region on the skeletal muscle Ca^{2+} release channel. Biochemistry. 1999;38(26):8532-7.

173. Rebbeck RT, Nitu FR, Rohde D, Most P, Bers DM, Thomas DD, *et al.* S100A1 protein does not compete with calmodulin for ryanodine receptor binding but structurally Alters the ryanodine receptor-calmodulin complex. Journal of Biological Chemistry. 2016;291(30):15896-907.

174. Komazaki S, Ito K, Takeshima H, Nakamura H. Deficiency of triad formation in developing skeletal muscle cells lacking junctophilin type 1. FEBS Lett. 2002;524(1-3):225-9.

175. Takeshima H, Hoshijima M, Song L-S. Ca^{2+} microdomains organized by junctophilins. Cell Calcium. 2015;58(4):349-56.

176. Murphy RM, Dutka TL, Horvath D, Bell JR, Delbridge LM, Lamb GD. Ca^{2+}-dependent proteolysis of junctophilin-1 and junctophilin-2 in skeletal and cardiac muscle. The Journal of Physiology. 2013;591(Pt 3):719-29.

177. Hirata Y, Brotto M, Weisleder N, Chu Y, Lin P, Zhao X, *et al.* Uncoupling store-operated Ca^{2+} entry and altered Ca^{2+} release from sarcoplasmic reticulum through silencing of junctophilin genes. Biophysical Journal. 2006;90(12):4418-27.

178. Phimister AJ, Lango J, Lee EH, Ernst-Russell MA, Takeshima H, Ma J, *et al.* Conformation-dependent stability of junctophilin 1 (JP1) and ryanodine receptor type 1 (RyR1) channel complex is mediated by their hyper-reactive thiols. Journal of Biological Chemistry. 2007;282(12):8667-77.

179. Golini L, Chouabe C, Berthier C, Cusimano V, Fornaro M, Bonvallet R, *et al.* Junctophilin 1 and 2 proteins interact with the L-type Ca^{2+} channel dihydropyridine receptors (DHPRs) in skeletal muscle. Journal of Biological Chemistry. 2011;286(51):43717-25.

180. Nakada T, Kashihara T, Komatsu M, Kojima K, Takeshita T, Yamada M. Physical interaction of junctophilin and the $Ca_V1.1$ C terminus is crucial for skeletal muscle contraction. Proceedings of the National Academy of Sciences. 2018;115(17):4507-12.

181. Shoshan-Barmatz V, Orr I, Weil S, Meyer H, Varsanyi M, Heilmeyer LM. The identification of the phosphorylated 150/160-kDa proteins of sarcoplasmic reticulum, their kinase and their association with the ryanodine receptor. Biochimica Et Biophysica Acta. 1996;1283(1):89-100.

182. Arvanitis DA, Vafiadaki E, Sanoudou D, Kranias EG. Histidine-rich calcium binding protein: The new regulator of sarcoplasmic reticulum calcium cycling. Journal of molecular and cellular cardiology. 2011;50(1):43-9.

183. Lee HG, Kang H, Kim DH, Park WJ. Interaction of HRC (histidine-rich Ca^{2+}-binding protein) and triadin in the lumen of sarcoplasmic reticulum. Journal of Biological Chemistry. 2001;276(43):39533-8.

184. Sacchetto R, Damiani E, Turcato F, Nori A, Margreth A. Ca^{2+}-dependent interaction of triadin with histidine-rich Ca^{2+}-binding protein carboxyl-terminal region. Biochem Biophys Res Commun. 2001;289(5):1125-34.

185. Orr I, Shoshan-Barmatz V. Modulation of the skeletal muscle ryanodine receptor by endogenous phosphorylation of 160/150-kDa proteins of the sarcoplasmic reticulum. Biochimica Et Biophysica Acta. 1996;1283(1):80-8.

186. Arvanitis DA, Vafiadaki E, Fan GC, Mitton BA, Gregory KN, Del Monte F, *et al.* Histidine-rich Ca-binding protein interacts with sarcoplasmic reticulum Ca-ATPase. American Journal of Physiology. 2007;293(3):H1581-9.

187. Anderson AA, Treves S, Biral D, Betto R, Sandona D, Ronjat M, *et al.* The novel skeletal muscle sarcoplasmic reticulum JP-45 protein. Molecular cloning, tissue distribution, developmental expression, and interaction with alpha 1.1 subunit of the voltage-gated calcium channel. Journal of Biological Chemistry. 2003;278(41):39987-92.

188. Mosca B, Eckhardt J, Bergamelli L, Treves S, Bongianino R, De Negri M, *et al.* Role of the JP45-calsequestrin complex on calcium entry in slow twitch skeletal muscles. Journal of Biological Chemistry. 2016;291(28):14555-65.

189. Gouadon E, Schuhmeier RP, Ursu D, Anderson AA, Treves S, Zorzato F, *et al.* A possible role of the junctional face protein JP-45 in modulating Ca^{2+} release in skeletal muscle. The Journal of Physiology. 2006;572(Pt 1):269-80.

190. Anderson AA, Altafaj X, Zheng Z, Wang Z-M, Delbono O, Ronjat M, *et al.* The junctional SR protein JP-45 affects the functional expression of the voltage-dependent Ca2+ channel $Ca_V1.1$. Journal of Cell Science. 2006;119(Pt 10):2145-55.

191. Delbono O, Xia J, Treves S, Wang Z-M, Jimenez-Moreno R, Payne AM, *et al.* Loss of skeletal muscle strength by ablation of the sarcoplasmic reticulum protein JP45. Proceedings of the National Academy of Sciences. 2007;104(50):20108-13.

192. Althobiti M, Booms P, Fiszer D, Halsall PJ, Shaw MA, Hopkins PM. Sequencing the JSPR1 gene in patients susceptible to malignant hyperthermia and identification of two novel genetic variants. British Journal of Anaesthesia. 2009;103(2):321-.

193. Yasuda T, Delbono O, Wang Z-M, Messi ML, Girard T, Urwyler A, *et al.* JP-45/JSRP1 variants affect skeletal muscle excitation-contraction coupling by decreasing the sensitivity of the dihydropyridine receptor. Human Mutation. 2013;34(1):184-90.

194. Lynch PJ, Tong J, Lehane M, Mallet A, Giblin L, Heffron JJ, *et al.* A mutation in the transmembrane/luminal domain of the ryanodine receptor is associated with abnormal Ca^{2+} release channel function and severe central core disease. Proceedings of the National Academy of Sciences. 1999;96(7):4164-9.

195. Monnier N, Romero NB, Lerale J, Nivoche Y, Qi D, MacLennan DH, *et al.* An autosomal dominant congenital myopathy with cores and rods is associated with a neomutation in the *RYR1* gene encoding the skeletal muscle ryanodine receptor. Human Molecular Genetics. 2000;9(18):2599-608.

196. Shy GM, Magee KR. A new congenital non-progressive myopathy. Brain: A Journal of Neurology. 1956;79(4):610-21.

197. Dubowitz V, Brooke MH. Muscle Biopsy: A Modern Approach: W. B. Saunders; 1973 1973. 458 p.

198. McCarthy TV, Quane KA, Lynch PJ. Ryanodine receptor mutations in malignant hyperthermia and central core disease. Human Mutation. 2000;15(5):410-7.

199. Wu S, Ibarra MCA, Malicdan MCV, Murayama K, Ichihara Y, Kikuchi H, *et al.* Central core disease is due to *RYR1* mutations in more than 90% of patients. Brain: A Journal of Neurology. 2006;129(6):1470-80.

200. Jungbluth H, Müller CR, Halliger-Keller B, Brockington M, Brown SC, Feng L, *et al.* Autosomal recessive inheritance of *RYR1* mutations in a congenital myopathy with cores. Neurology. 2002;59(2):284-7.

201. Monnier N, Marty I, Faure J, Castiglioni C, Desnuelle C, Sacconi S, *et al.* Null mutations causing depletion of the type 1 ryanodine receptor (*RYR1*) are commonly associated with recessive structural congenital myopathies with cores. Human Mutation. 2008;29(5):670-8.

202. Halsall PJ, Bridges LR, Ellis FR, Hopkins PM. Should patients with central core disease be screened for malignant hyperthermia? Journal of Neurology, Neurosurgery, and Psychiatry. 1996;61(1):119-21.

203. Fujimura-Kiyono C, Racz G, Nishino I. Myotubular/centronuclear myopathy and central core disease. Neurology India. 2008;56(3):325-32.

204. Ferreiro A, Estournet B, Chateau D, Romero NB, Laroche C, Odent S, *et al.* Multi-minicore disease–searching for boundaries: Phenotype analysis of 38 cases. Annals of Neurology. 2000;48(5):745-57.

205. Engel AG, Gomez MR, Groover RV. Multicore disease. A recently recognized congenital myopathy associated with multifocal degeneration of muscle fibers. Mayo Clinic Proceedings. 1971;46(10):666-81.

206. Jungbluth H. Multi-minicore disease. Orphanet Journal of Rare Diseases. 2007;2:31-.

207. Monnier N, Ferreiro A, Marty I, Labarre-Vila A, Mezin P, Lunardi J. A homozygous splicing mutation causing a depletion of skeletal muscle *RYR1* is associated with multi-minicore disease congenital myopathy with ophthalmoplegia. Human Molecular Genetics. 2003;12(10):1171-8.

208. Ferreiro A, Quijano-Roy S, Pichereau C, Moghadaszadeh B, Goemans N, Bonnemann C, *et al.* Mutations of the selenoprotein N gene, which is implicated in rigid spine muscular dystrophy, cause the classical phenotype of multiminicore disease: Reassessing the nosology of early-onset myopathies. The American Journal of Human Genetics. 2002;71(4):739-49.

209. Marino M, Stoilova T, Giorgi C, Bachi A, Cattaneo A, Auricchio A, *et al.* SEPN1, an endoplasmic reticulum-localized selenoprotein linked to skeletal muscle pathology, counteracts hyperoxidation by means of redox-regulating SERCA2 pump activity. Human Molecular Genetics. 2015;24(7):1843-55.

210. Osada H, Masuda K, Seki K, Sekiya S. Multi-minicore disease with susceptibility to malignant hyperthermia in pregnancy. Gynecologic and Obstetric Investigation. 2004;58(1):32-5.

211. Koch BM, Bertorini TE, Eng GD, Boehm R. Severe multicore disease associated with reaction to anesthesia. Archives of Neurology. 1985;42(12):1204-6.

212. King JO, Denborough MA. Anesthetic-induced malignant hyperpyrexia in children. J Pediatr. 1973;83(1):37-40.

213. D'Arcy CE, Bjorksten A, Yiu EM, Bankier A, Gillies R, McLean CA, *et al.* King-denborough syndrome caused by a novel mutation in the ryanodine receptor gene. Neurology. 2008;71(10):776-7.

214. Dowling JJ, Lillis S, Amburgey K, Zhou H, Al-Sarraj S, Buk SJA, *et al.* King-Denborough syndrome with and without mutations in the skeletal muscle ryanodine receptor (*RYR1*) gene. Neuromuscular disorders. 2011;21(6):420-7.

215. Joseph MR, Theroux MC, Mooney JJ, Falitz S, Brandom BW, Byler DL. Intraoperative presentation of malignant hyperthermia (confirmed by *RYR1* gene mutation, c.7522C>T; p.R2508C) leads to diagnosis of King-Denborough syndrome in a child with hypotonia and dysmorphic features: A case report. A & A Case Reports. 2017;8(3):55-7.

216. Isaacs H, Badenhorst ME. Dominantly inherited malignant hyperthermia (MH) in the King–Denborough Syndrome. Muscle & Nerve. 1992;15(6):740-2.

217. Stamm DS, Aylsworth AS, Stajich JM, Kahler SG, Thorne LB, Speer MC, *et al.* Native American myopathy: Congenital myopathy with cleft palate, skeletal anomalies, and susceptibility to malignant hyperthermia. The American Journal of Human Genetics. 2008;146A(14):1832-41.

218. Grzybowski M, Schanzer A, Pepler A, Heller C, Neubauer BA, Hahn A. Novel STAC3 mutations in the first non-Amerindian patient with Native American myopathy. Neuropediatrics. 2017;48(6):451-5.

219. Stewart CR, Kahler SG, Gilchrist JM. Congenital myopathy with cleft palate and increased susceptibility to malignant hyperthermia: King syndrome? Pediatric Neurology. 1988;4(6):371-4.

220. Thomas J, Crowhurst T. Exertional heat stroke, rhabdomyolysis and susceptibility to malignant hyperthermia. Internal Medicine Journal. 2013;43(9):1035-8.

221. Muldoon S, Deuster P, Voelkel M, Capacchione J, Bunger R. Exertional heat illness, exertional rhabdomyolysis, and malignant hyperthermia: Is there a link? Current Sports Medicine Reports. 2008;7(2):74-80.

222. Groom L, Muldoon SM, Tang ZZ, Brandom BW, Bayarsaikhan M, Bina S, *et al.* Identical *de novo* mutation in the type 1 ryanodine receptor gene associated with fatal, stress-induced malignant hyperthermia in two unrelated families. Anesthesiology. 2011;115(5):938-45.

223. Kochling A, Wappler F, Winkler G, Schulte am Esch JS. Rhabdomyolysis following severe physical exercise in a patient with predisposition to malignant hyperthermia. Anaesth Intensive Care. 1998;26(3):315-8.

224. Capacchione JF, Muldoon SM. The relationship between exertional heat illness, exertional rhabdomyolysis, and malignant hyperthermia. Anesthesia and Analgesia. 2009;109(4):1065-9.

225. Poussel M, Guerci P, Kaminsky P, Heymonet M, Roux-Buisson N, Faure J, *et al.* Exertional heat stroke and susceptibility to malignant hyperthermia in an athlete: Evidence for a link? Journal of Athletic Training. 2015;50(11):1212-4.

226. Tobin JR, Jason DR, Challa VR, Nelson TE, Sambuughin N. Malignant hyperthermia and apparent heat stroke. JAMA. 2001;286(2):168-9.

227. Poels PJ, Joosten EM, Sengers RC, Stadhouders AM, Veerkamp JH, Benders AA. *In vitro* contraction test for malignant hyperthermia in patients with unexplained recurrent rhabdomyolysis. J Neurol Sci. 1991;105(1):67-72.

228. Wappler F, Fiege M, Steinfath M, Agarwal K, Scholz J, Singh S, *et al.* Evidence for susceptibility to malignant hyperthermia in patients with exercise-induced rhabdomyolysis. Anesthesiology. 2001;94(1):95-100.

229. Kraeva N, Sapa A, Dowling JJ, Riazi S. Malignant hyperthermia susceptibility in patients with exertional rhabdomyolysis: A retrospective cohort study and updated systematic review. Canadian Journal of Anesthesia. 2017;64(7):736-43.

230. Müller C. Criteria for gene mutations to be used in genetic testing of Malignant Hyperthermia susceptibility. European Malignant Hyperthermia Group; 2003.

231. Robinson R, Carpenter D, Shaw M-A, Halsall J, Hopkins P. Mutations in *RYR1* in malignant hyperthermia and central core disease. Human Mutation. 2006;27(10):977-89.

232. Bjorksten AR, Gillies RL, Hockey BM, Du Sart D. Sequencing of genes involved in the movement of calcium across human skeletal muscle sarcoplasmic reticulum: Continuing the search for genes associated with malignant hyperthermia. Anaesth Intensive Care. 2016;44(6):762-8.

233. Lu JT, Campeau PM, Lee BH. Genotype-phenotype correlation--promiscuity in the era of next-generation sequencing. The New England Journal of Medicine. 2014;371(7):593-6.

234. Gonsalves SG, Ng D, Johnston JJ, Teer JK, Stenson PD, Cooper DN, *et al.* Using exome data to identify malignant hyperthermia susceptibility mutations. Anesthesiology. 2013;119(5):1043-53.

235. Bell CJ, Dinwiddie DL, Miller NA, Hateley SL, Ganusova EE, Mudge J, *et al.* Carrier testing for severe childhood recessive diseases by next-generation sequencing. Science Translational Medicine. 2011;3(65):65ra4.

236. Cline MS, Karchin R. Using bioinformatics to predict the functional impact of SNVs. Bioinformatics. 2011;27(4):441-8.

237. Thusberg J, Olatubosun A, Vihinen M. Performance of mutation pathogenicity prediction methods on missense variants. Human Mutation. 2011;32(4):358-68.

238. O'Brien JJ, Feng W, Allen PD, Chen SRW, Pessah IN, Beam KG. Ca^{2+} activation of RyR1 is not necessary for the initiation of skeletal-type excitation-contraction coupling. Biophysical Journal. 2002;82(5):2428-35.

239. Mickelson JR, Litterer LA, Jacobson BA, Louis CF. Stimulation and inhibition of [3H]ryanodine binding to sarcoplasmic reticulum from malignant hyperthermia susceptible pigs. Archives of Biochemistry and Biophysics. 1990;278(1):251-7.

240. Sato K, Pollock N, Stowell KM. Functional studies of *RYR1* mutations in the skeletal muscle ryanodine receptor using human *RYR1* complementary DNA. Anesthesiology. 2010;112(6):1350-4.

241. Gschwend MH, Rüdel R, Brinkmeier H, Taylor SR, Föhr KJ. A transient and a persistent calcium release are induced by chlorocresol in cultivated mouse myotubes. Pflügers Archiv: European Journal of Physiology. 1999;438(1):101-6.

242. Tong J, Oyamada H, Demaurex N, Grinstein S, McCarthy TV, MacLennan DH. Caffeine and halothane sensitivity of intracellular Ca^{2+} release is altered by 15 calcium release channel (ryanodine receptor) mutations associated with malignant hyperthermia and/or central core disease. Journal of Biological Chemistry. 1997;272(42):26332-9.

243. Sato K, Roesl C, Pollock N, Stowell KM. Skeletal muscle ryanodine receptor mutations associated with malignant hyperthermia showed enhanced intensity and sensitivity to triggering drugs when expressed in human embryonic kidney cells. Anesthesiology. 2013;119(1):111-8.

244. Tong J, Du GG, Chen SR, MacLennan DH. HEK-293 cells possess a carbachol- and thapsigargin-sensitive intracellular Ca^{2+} store that is responsive to stop-flow medium changes and insensitive to caffeine and ryanodine. Biochemical Journal. 1999;343(1):39-44.

245. Avila G, O'Brien JJ, Dirksen RT. Excitation--contraction uncoupling by a human central core disease mutation in the ryanodine receptor. Proceedings of the National Academy of Sciences. 2001;98(7):4215-20.

246. Yang T, Ta TA, Pessah IN, Allen PD. Functional defects in six ryanodine receptor isoform-1 (RyR1) mutations associated with malignant hyperthermia and their impact on skeletal excitation-contraction coupling. Journal of Biological Chemistry. 2003;278(28):25722-30.

247. Yarotskyy V, Protasi F, Dirksen RT. Accelerated activation of SOCE current in myotubes from two mouse models of anesthetic- and heat-induced sudden death. PloS One. 2013;8(10):e77633.

248. Yang T, Riehl J, Esteve E, Matthaei KI, Goth S, Allen PD, *et al.* Pharmacologic and functional characterization of malignant hyperthermia in the R163C RyR1 knock-in mouse. Anesthesiology. 2006;105(6):1164-75.

249. Chelu MG, Goonasekera SA, Durham WJ, Tang W, Lueck JD, Riehl J, *et al.* Heat- and anesthesia-induced malignant hyperthermia in an RyR1 knock-in mouse. The FASEB Journal. 2006;20(2):329-30.

250. Barrientos GC, Feng W, Truong K, Matthaei KI, Yang T, Allen PD, *et al.* Gene dose influences cellular and calcium channel dysregulation in heterozygous and homozygous T4826I-*RYR1* malignant hyperthermia-susceptible muscle. Journal of Biological Chemistry. 2012;287(4):2863-76.

251. Loy RE, Orynbayev M, Xu L, Andronache Z, Apostol S, Zvaritch E, *et al.* Muscle weakness in Ryr1 I4895T/WT knock-in mice as a result of reduced ryanodine receptor Ca^{2+} ion permeation and release from the sarcoplasmic reticulum. The Journal of General Physiology. 2011;137(1):43-57.

252. Lopez JR, Kaura V, Diggle CP, Hopkins PM, Allen PD. Malignant hyperthermia, environmental heat stress, and intracellular calcium dysregulation in a mouse model expressing the p.G2435R variant of *RYR1*. British Journal of Anaesthesia. 2018;121(4):953-61.

253. Zorzato F. Characterisation of a novel mouse model carrying a non-sense mutation in *RYR1* EX36. Biophysical Journal. 2018;114(3):469a.

254. Davis EE, Katsanis N. The ciliopathies: A transitional model into systems biology of human genetic disease. Current Opinion in Genetics & Development. 2012;22(3):290-303.

255. Robinson RL, Anetseder MJ, Brancadoro V, van Broekhoven C, Carsana A, Censier K, *et al.* Recent advances in the diagnosis of malignant hyperthermia susceptibility: How confident can we be of genetic testing? European Journal of Human Genetics. 2003;11(4):342-8.

256. Fortunato G, Carsana A, Tinto N, Brancadoro V, Canfora G, Salvatore F. A case of discordance between genotype and phenotype in a malignant hyperthermia family. European Journal of Human Genetics. 1999;7(4):415-20.

257. Fagerlund TH, Ording H, Bendixen D, Islander G, Ranklev Twetman E, Berg K. Discordance between malignant hyperthermia susceptibility and *RYR1* mutation C1840T in two Scandinavian MH families exhibiting this mutation. Clinical Genetics. 1997;52(6):416-21.

258. Abràmoff MD, Magalhães PJ, Ram SJ. Image processing with ImageJ. Biophotonics International. 2004;11(7):36-42.

259. Richards S, Aziz N, Bale S, Bick D, Das S, Gastier-Foster J, *et al.* Standards and guidelines for the interpretation of sequence variants: A joint consensus recommendation of the American College of Medical Genetics and Genomics and the Association for Molecular Pathology. Genetics in Medicine. 2015;17(5):405-24.

260. Thomas P, Smart TG. HEK293 cell line: A vehicle for the expression of recombinant proteins. Journal of Pharmacological and Toxicological Methods. 2005;51(3):187-200.

261. Ooi A, Wong A, Esau L, Lemtiri-Chlieh F, Gehring C. A Guide to transient expression of membrane proteins in HEK-293 cells for functional characterization. Frontiers in Physiology. 2016;7:300.

262. Sauer B. Site-specific recombination: Developments and applications. Current Opinion in Biotechnology. 1994;5(5):521-7.

263. Craig NL. The mechanism of conservative site-specific recombination. Annual Review of Genetics. 1988;22:77-105.

264. Parker R, Schiemann AH, Langton E, Bulger T, Pollock N, Bjorksten A, *et al.* Functional characterization of C-terminal ryanodine receptor 1 variants associated with central core disease or malignant hyperthermia. J Neuromuscul Dis. 2017;4(2):147-58.

265. Merritt A, Booms P, Shaw MA, Miller DM, Daly C, Bilmen JG, *et al.* Assessing the pathogenicity of *RYR1* variants in malignant hyperthermia. British Journal of Anaesthesia. 2017;118(4):533-43.

266. Monnier N, Kozak-Ribbens G, Krivosic-Horber R, Nivoche Y, Qi D, Kraev N, *et al.* Correlations between genotype and pharmacological, histological, functional, and clinical phenotypes in malignant hyperthermia susceptibility. Human Mutation. 2005;26(5):413-25.

267. Kossugue PM, Paim JF, Navarro MM, Silva HC, Pavanello RCM, Gurgel-Giannetti J, *et al.* Central core disease due to recessive mutations in *RYR1* gene: Is it more common than described? Muscle & Nerve. 2007;35(5):670-4.

268. Sambuughin N, Holley H, Muldoon S, Brandom BW, de Bantel AM, Tobin JR, *et al.* Screening of the entire ryanodine receptor type 1 coding region for sequence variants associated with malignant hyperthermia susceptibility in the north american population. Anesthesiology. 2005;102(3):515-21.

269. Broman M, Heinecke K, Islander G, Schuster F, Glahn K, Bodelsson M, *et al.* Screening of the ryanodine 1 gene for malignant hyperthermia causative mutations by high resolution melt curve analysis. Anesthesia and Analgesia. 2011;113(5):1120-8.

270. Monnier N, Romero NB, Lerale J, Landrieu P, Nivoche Y, Fardeau M, *et al.* Familial and sporadic forms of central core disease are associated with mutations in the C-terminal domain of the skeletal muscle ryanodine receptor. Human Molecular Genetics. 2001;10(22):2581-92.

271. Walters-Sen LC, Hashimoto S, Thrush DL, Reshmi S, Gastier-Foster JM, Astbury C, *et al.* Variability in pathogenicity prediction programs: Impact on clinical diagnostics. Molecular Genetics & Genomic Medicine. 2015;3(2):99-110.

272. Pejaver V, Urresti J, Lugo-Martinez J, Pagel KA, Lin GN, Nam H-J, *et al.* MutPred2: Inferring the molecular and phenotypic impact of amino acid variants. bioRxiv. 2017.

273. Choi Y, Sims GE, Murphy S, Miller JR, Chan AP. Predicting the functional effect of amino acid substitutions and indels. PloS One. 2012;7(10):e46688.

274. Shihab HA, Gough J, Cooper DN, Stenson PD, Barker GL, Edwards KJ, *et al.* Predicting the functional, molecular, and phenotypic consequences of amino acid substitutions using hidden Markov models. Human Mutation. 2013;34(1):57-65.

275. Takahashi A, Camacho P, Lechleiter JD, Herman B. Measurement of intracellular calcium. Physiological Reviews. 1999;79(4):1089-125.

276. Ma J. Block by ruthenium red of the ryanodine-activated calcium release channel of skeletal muscle. The Journal of General Physiology. 1993;102(6):1031-56.

277. Yue C, White KL, Reed WA, Bunch TD. The existence of inositol 1,4,5-trisphosphate and ryanodine receptors in mature bovine oocytes. Development. 1995;121(8):2645-54.

278. Sampieri A, Santoyo K, Asanov A, Vaca L. Association of the IP3R to STIM1 provides a reduced intraluminal calcium microenvironment, resulting in enhanced store-operated calcium entry. Scientific Reports. 2018;8(1):13252.

279. Levano S, Vukcevic M, Singer M, Matter A, Treves S, Urwyler A, *et al.* Increasing the number of diagnostic mutations in malignant hyperthermia. Human Mutation. 2009;30(4):590-8.

280. Brandom BW, Bina S, Wong CA, Wallace T, Visoiu M, Isackson PJ, *et al.* Ryanodine receptor type 1 gene variants in the malignant hyperthermia-susceptible population of the United States. Anesthesia and Analgesia. 2013;116(5):1078-86.

281. Ibarra M Carlos A, Wu S, Murayama K, Minami N, Ichihara Y, Kikuchi H, *et al.* Malignant hyperthermia in Japan - mutation screening of the entire ryanodine receptor type 1 gene coding region by direct sequencing. Anesthesiology. 2006;104(6):1146-54.

282. Tung C-C, Lobo PA, Kimlicka L, Van Petegem F. The amino-terminal disease hotspot of ryanodine receptors forms a cytoplasmic vestibule. Nature. 2010;468:585.

283. Zhong X, Liu Y, Zhu L, Meng X, Wang R, Van Petegem F, *et al.* Conformational dynamics inside amino-terminal disease hotspot of ryanodine receptor. Structure. 2013;21(11):2051-60.

284. Lobo PA, Van Petegem F. Crystal structures of the N-terminal domains of cardiac and skeletal muscle ryanodine receptors: Insights into disease mutations. Structure. 2009;17(11):1505-14.

285. Gillies RL, Bjorksten AR, Davis M, Du Sart D. Identification of genetic mutations in Australian malignant hyperthermia families using sequencing of *RYR1* hotspots. Anaesth Intensive Care. 2008;36(3):391-403.

286. Shepherd S, Ellis F, Halsall J, Hopkins P, Robinson R. RYR1 mutations in UK central core disease patients: More than just the C-terminal transmembrane region of the RYR1 gene. Journal of Medical Genetics. 2004;41(3):e33.

287. Sharma P, Ishiyama N, Nair U, Li W, Dong A, Miyake T, *et al.* Structural determination of the phosphorylation domain of the ryanodine receptor. The FEBS journal. 2012;279(20):3952-64.

288. Brown RL, Pollock AN, Couchman KG, Hodges M, Hutchinson DO, Waaka R, *et al.* A novel ryanodine receptor mutation and genotype-phenotype correlation in a large malignant hyperthermia New Zealand Maori pedigree. Human Molecular Genetics. 2000;9(10):1515-24.

289. Diaz-Sylvester PL, Porta M, Copello JA. Halothane modulation of skeletal muscle ryanodine receptors: Dependence on Ca^{2+}, Mg^{2+}, and ATP. American Journal of Physiology Cell Physiology. 2008;294(4):1103-12.

290. Steele DS, Duke AM. Defective Mg^{2+} regulation of RyR1 as a causal factor in malignant hyperthermia. Archives of Biochemistry and Biophysics. 2007;458(1):57-64.

291. Dirksen RT, Avila G. Distinct effects on Ca^{2+} handling caused by malignant hyperthermia and central core disease mutations in RyR1. Biophysical Journal. 2004;87(5):3193-204.

292. Sei Y, Brandom BW, Bina S, Hosoi E, Gallagher KL, Wyre HW, *et al.* Patients with malignant hyperthermia demonstrate an altered calcium control mechanism in B lymphocytes. Anesthesiology. 2002;97(5):1052-8.

293. Schiemann AH, Paul N, Parker R, Pollock N, Bulger TF, Stowell KM. Functional characterization of 2 known ryanodine receptor mutations causing malignant hyperthermia. Anesthesia and Analgesia. 2014;118(2):375-80.

294. Tilgen N, Zorzato F, Halliger-Keller B, Muntoni F, Sewry C, Palmucci LM, *et al.* Identification of four novel mutations in the C-terminal membrane spanning domain of the ryanodine receptor 1: Association with central core disease and alteration of calcium homeostasis. Human Molecular Genetics. 2001;10(25):2879-87.

295. Zorzato F, Yamaguchi N, Xu L, Meissner G, Müller CR, Pouliquin P, *et al.* Clinical and functional effects of a deletion in a COOH-terminal lumenal loop of the skeletal muscle ryanodine receptor. Human Molecular Genetics. 2003;12(4):379-88.

296. Marks AR, Priori S, Memmi M, Kontula K, Laitinen PJ. Involvement of the cardiac ryanodine receptor/calcium release channel in catecholaminergic polymorphic ventricular tachycardia. Journal of Cellular Physiology. 2002;190(1):1-6.

297. Xu L, Wang Y, Yamaguchi N, Pasek DA, Meissner G. Single Channel Properties of Heterotetrameric Mutant RyR1 Ion Channels Linked to Core Myopathies. The Journal of Biological Chemistry. 2008;283(10):6321-9.

298. Rossi D, De Smet P, Lyfenko A, Galli L, Lorenzini S, Franci D, *et al.* A truncation in the *RYR1* gene associated with central core lesions in skeletal muscle fibres. Journal of Medical Genetics. 2007;44(2):e67-e.

299. Zhang JZ, McLay JC, Jones PP. The arrhythmogenic human HRC point mutation S96A leads to spontaneous Ca^{2+} release due to an impaired ability to buffer store Ca^{2+}. Journal of molecular and cellular cardiology. 2014;74:22-31.

300. Eltit JM, Li H, Ward CW, Molinski T, Pessah IN, Allen PD, *et al.* Orthograde dihydropyridine receptor signal regulates ryanodine receptor passive leak. Proceedings of the National Academy of Sciences. 2011;108(17):7046-51.

301. Bagchi S, Fredriksson R, Wallen-Mackenzie A. *In situ* proximity ligation assay (PLA). Methods in Molecular Biology. 2015;1318:149-59.

302. Ruigrok HJ, Shahid G, Goudeau B, Poulletier de Gannes F, Poque-Haro E, Hurtier A, *et al.* Full-spectral multiplexing of bioluminescence resonance energy transfer in three TRPV channels. Biophysical Journal. 2017;112(1):87-98.

303. Jones JL, Reynolds DF, Lai FA, Blayney LM. Ryanodine receptor binding to FKBP12 is modulated by channel activation state. Journal of Cell Science. 2005;118(Pt 20):4613-9.

304. Cheng W, Altafaj X, Ronjat M, Coronado R. Interaction between the dihydropyridine receptor Ca^{2+} channel β-subunit and ryanodine receptor type 1 strengthens excitation-contraction coupling. Proceedings of the National Academy of Sciences of the United States of America. 2005;102(52):19225-30.

305. Henderson MJ, Baldwin HA, Werley CA, Boccardo S, Whitaker LR, Yan X, *et al.* A low affinity GCaMP3 variant (GCaMPer) for imaging the endoplasmic reticulum calcium store. PloS One. 2015;10(10):e0139273.

306. Ziman AP, Ward CW, Rodney GG, Lederer WJ, Bloch RJ. Quantitative measurement of Ca^{2+} in the sarcoplasmic reticulum lumen of mammalian skeletal muscle. Biophysical Journal. 2010;99(8):2705-14.

307. Palmer AE, Jin C, Reed JC, Tsien RY. Bcl-2-mediated alterations in endoplasmic reticulum Ca^{2+} analyzed with an improved genetically encoded fluorescent sensor. Proceedings of the National Academy of Sciences of the United States of America. 2004;101(50):17404-9.

308. Kim SW, Lee JH, Park BC, Park TS. Myotube differentiation in clustered regularly interspaced short palindromic repeat/Cas9-mediated MyoD knockout quail myoblast cells. Asian-Australas J Anim Sci. 2017;30(7):1029-36.

309. Lattanzi A, Duguez S, Moiani A, Izmiryan A, Barbon E, Martin S, *et al.* Correction of the exon 2 duplication in DMD myoblasts by a single CRISPR/Cas9 system. Molecular Therapy Nucleic Acids. 2017;7:11-9.

310. Shahar OD, Raghu Ram EV, Shimshoni E, Hareli S, Meshorer E, Goldberg M. Live imaging of induced and controlled DNA double-strand break formation reveals extremely low repair by homologous recombination in human cells. Oncogene. 2012;31(30):3495-504.

311. Ducreux S, Zorzato F, Müller C, Sewry C, Muntoni F, Quinlivan R, *et al.* Effect of ryanodine receptor mutations on interleukin-6 release and intracellular calcium homeostasis in human myotubes from malignant hyperthermia-susceptible individuals and patients affected by central core disease. Journal of Biological Chemistry. 2004;279(42):43838-46.

312. Girard T, Treves S, Censier K, Mueller CR, Zorzato F, Urwyler A. Phenotyping malignant hyperthermia susceptibility by measuring halothane-induced changes in myoplasmic calcium concentration in cultured human skeletal muscle cells. British Journal of Anaesthesia. 2002;89(4):571-9.

313. Klingler MDW, Baur MDC, Georgieff MDM, Lehmann-Horn MDF, Melzer PDW. Detection of proton release from cultured human myotubes to identify malignant hyperthermia susceptibility. Anesthesiology. 2002;97(5):1059-66.

314. Wehner M, Rueffert H, Koenig F, Olthoff D. Functional characterization of malignant hyperthermia-associated RyR1 mutations in exon 44, using the human myotube model. Neuromuscular disorders. 2004;14(7):429-37.

315. Thorley M, Duguez S, Mazza EMC, Valsoni S, Bigot A, Mamchaoui K, *et al.* Skeletal muscle characteristics are preserved in hTERT/cdk4 human myogenic cell lines. Skeletal Muscle. 2016;6(1):43-.

316. Rokach O, Ullrich ND, Rausch M, Mouly V, Zhou H, Muntoni F, *et al.* Establishment of a human skeletal muscle-derived cell line: Biochemical, cellular and electrophysiological characterization. Biochemical Journal. 2013;455(2):169-77.

317. Arnold A-S, Laporte V, Dumont S, Appert-Collin A, Erbacher P, Coupin G, *et al.* Comparing reagents for efficient transfection of human primary myoblasts: FuGENE 6, Effectene and ExGen 500. Fundamental & Clinical Pharmacology. 2005;20(1):81-9.

318. Mars T, Strazisar M, Mis K, Kotnik N, Pegan K, Lojk J, *et al.* Electrotransfection and lipofection show comparable efficiency for *in vitro* gene delivery of primary human myoblasts. The Journal of Membrane Biology. 2015;248(2):273-83.

319. Campeau P, Chapdelaine P, Seigneurin-Venin S, Massie B, Tremblay JP. Transfection of large plasmids in primary human myoblasts. Gene Therapy. 2001;8:1387.

320. Zhu F, Gamboa M, Farruggio AP, Hippenmeyer S, Tasic B, Schule B, *et al.* DICE, an efficient system for iterative genomic editing in human pluripotent stem cells. Nucleic Acids Research. 2014;42(5):e34.

321. Maurisse R, De Semir D, Emamekhoo H, Bedayat B, Abdolmohammadi A, Parsi H, *et al.* Comparative transfection of DNA into primary and transformed mammalian cells from different lineages. BMC Biotechnology. 2010;10(1):9.

322. Jackson MF, Hoversten KE, Powers JM, Trobridge GD, Rodgers BD. Genetic manipulation of myoblasts and a novel primary myosatellite cell culture system: Comparing and optimizing approaches. The FEBS journal. 2013;280(3):827-39.

323. Certo MT, Ryu BY, Annis JE, Garibov M, Jarjour J, Rawlings DJ, *et al.* Tracking genome engineering outcome at individual DNA breakpoints. Nat Methods. 2011;8(8):671-6.

324. Farazmandfar T, Khanahmad Shahreza H, Haghshenas MR, Janbabai G, Azadeh H, Mansour Samaei N. Use of integrase-minus lentiviral vector for transient expression. Cell Journal. 2012;14(2):76-81.

325. Qamar Saeed M, Dufour N, Bartholmae C, Sieranska U, Knopf M, Thierry E, *et al.* Comparison between several integrase-defective lentiviral vectors reveals increased integration of an HIV vector bearing a D167H mutant. Molecular Therapy Nucleic Acids. 2014;3(12):e213.

326. Cong L, Ran FA, Cox D, Lin S, Barretto R, Habib N, *et al.* Multiplex genome engineering using CRISPR/Cas systems. Science. 2013;339(6121):819-23.

327. Mali P, Yang L, Esvelt KM, Aach J, Guell M, DiCarlo JE, *et al.* RNA-guided human genome engineering via Cas9. Science. 2013;339(6121):823-6.

328. Horvath P, Barrangou R. CRISPR/Cas, the immune system of bacteria and archaea. Science. 2010;327(5962):167-70.

329. Bryson TE, Anglin CM, Bridges PH, Cottle RN. Nuclease-mediated gene therapies for inherited metabolic diseases of the liver. The Yale journal of biology and medicine. 2017;90(4):553-66.

330. Wyvekens N, Tsai SQ, Joung JK. Genome editing in human cells using CRISPR/Cas nucleases. Current Protocols in Molecular Biology. 2015;112:31 3 1-18.

331. Jinek M, Chylinski K, Fonfara I, Hauer M, Doudna JA, Charpentier E. A programmable dual-RNA-guided DNA endonuclease in adaptive bacterial immunity. Science. 2012;337(6096):816-21.

332. Nishimasu H, Ran FA, Hsu PD, Konermann S, Shehata SI, Dohmae N, *et al.* Crystal structure of Cas9 in complex with guide RNA and target DNA. Cell. 2014;156(5):935-49.

333. Bibikova M, Golic M, Golic KG, Carroll D. Targeted chromosomal cleavage and mutagenesis in Drosophila using zinc-finger nucleases. Genetics. 2002;161(3):1169-75.

334. Parnas O, Jovanovic M, Eisenhaure TM, Herbst RH, Dixit A, Ye CJ, *et al.* A genome-wide CRISPR screen in primary immune cells to dissect regulatory networks. Cell. 2015;162(3):675-86.

335. Swiech L, Heidenreich M, Banerjee A, Habib N, Li Y, Trombetta J, *et al.* In vivo interrogation of gene function in the mammalian brain using CRISPR-Cas9. Nature Biotechnology. 2015;33(1):102-6.

336. Zhou Y, Zhu S, Cai C, Yuan P, Li C, Huang Y, *et al.* High-throughput screening of a CRISPR/Cas9 library for functional genomics in human cells. Nature. 2014;509(7501):487-91.

337. The nonprofit plasmid repository [Internet]. 2018. Available from: https://www.addgene.org/crispr/guide/.

338. Yin H, Xue W, Chen S, Bogorad RL, Benedetti E, Grompe M, *et al.* Genome editing with Cas9 in adult mice corrects a disease mutation and phenotype. Nature Biotechnology. 2014;32(6):551-3.

339. Irion U, Krauss J, Nusslein-Volhard C. Precise and efficient genome editing in zebrafish using the CRISPR/Cas9 system. Development. 2014;141(24):4827-30.

340. Platt RJ, Chen S, Zhou Y, Yim MJ, Swiech L, Kempton HR, *et al.* CRISPR-Cas9 knockin mice for genome editing and cancer modeling. Cell. 2014;159(2):440-55.

341. Bibikova M, Beumer K, Trautman JK, Carroll D. Enhancing gene targeting with designed zinc finger nucleases. Science. 2003;300(5620):764.

342. Cohen J. In dogs, CRISPR fixes a muscular dystrophy. Science. 2018;361(6405):835.

343. Pennisi E. The CRISPR craze. Science. 2013;341(6148):833-6.

344. Yoshimi K, Kaneko T, Voigt B, Mashimo T. Allele-specific genome editing and correction of disease-associated phenotypes in rats using the CRISPR-Cas platform. Nature Communications. 2014;5:4240.

345. Hsu PD, Scott DA, Weinstein JA, Ran FA, Konermann S, Agarwala V, *et al.* DNA targeting specificity of RNA-guided Cas9 nucleases. Nature Biotechnology. 2013;31(9):827-32.

346. Fu Y, Foden JA, Khayter C, Maeder ML, Reyon D, Joung JK, *et al.* High-frequency off-target mutagenesis induced by CRISPR-Cas nucleases in human cells. Nature Biotechnology. 2013;31(9):822-6.

347. Wu X, Scott DA, Kriz AJ, Chiu AC, Hsu PD, Dadon DB, *et al.* Genome-wide binding of the CRISPR endonuclease Cas9 in mammalian cells. Nature Biotechnology. 2014;32(7):670-6.

348. Zheng T, Hou Y, Zhang P, Zhang Z, Xu Y, Zhang L, *et al.* Profiling single-guide RNA specificity reveals a mismatch sensitive core sequence. Scientific Reports. 2017;7:40638.

349. Ran FA, Hsu PD, Lin C-Y, Gootenberg JS, Konermann S, Trevino A, *et al.* Double nicking by RNA-guided CRISPR Cas9 for enhanced genome editing specificity. Cell. 2013;154(6):1380-9.

350. Guilinger JP, Thompson DB, Liu DR. Fusion of catalytically inactive Cas9 to FokI nuclease improves the specificity of genome modification. Nature Biotechnology. 2014;32(6):577-82.

351. Slaymaker IM, Gao L, Zetsche B, Scott DA, Yan WX, Zhang F. Rationally engineered Cas9 nucleases with improved specificity. Science. 2016;351(6268):84-8.

352. Kleinstiver BP, Pattanayak V, Prew MS, Tsai SQ, Nguyen NT, Zheng Z, *et al.* High-fidelity CRISPR-Cas9 nucleases with no detectable genome-wide off-target effects. Nature. 2016;529(7587):490-5.

353. Fu Y, Sander JD, Reyon D, Cascio VM, Joung JK. Improving CRISPR-Cas nuclease specificity using truncated guide RNAs. Nature Biotechnology. 2014;32(3):279-84.

354. Zhang J-P, Li X-L, Neises A, Chen W, Hu L-P, Ji G-Z, *et al.* Different Effects of sgRNA Length on CRISPR-mediated Gene Knockout Efficiency. Scientific Reports. 2016;6:28566.

355. Optimized CRISPR Design [Internet]. 2013. Available from: http://crispr.mit.edu/.

356. Salsman J, Dellaire G. Precision genome editing in the CRISPR era. Biochemistry and Cell Biology. 2016;95(2):187-201.

357. Heckman KL, Pease LR. Gene splicing and mutagenesis by PCR-driven overlap extension. Nature Protocols. 2007;2(4):924-32.

358. Miyaoka Y, Berman JR, Cooper SB, Mayerl SJ, Chan AH, Zhang B, *et al.* Systematic quantification of HDR and NHEJ reveals effects of locus, nuclease, and cell type on genome-editing. Scientific Reports. 2016;6:23549.

359. Rong Z, Zhu S, Xu Y, Fu X. Homologous recombination in human embryonic stem cells using CRISPR/Cas9 nickase and a long DNA donor template. Protein & Cell. 2014;5(4):258-60.

360. Grievink H, Stowell KM. Identification of ryanodine receptor 1 single-nucleotide polymorphisms by high-resolution melting using the LightCycler 480 System. Anal Biochem. 2008;374(2):396-404.

361. Wehner M, Rueffert H, Koenig F, Olthoff D. Calcium release from sarcoplasmic reticulum is facilitated in human myotubes derived from carriers of the ryanodine receptor type 1 mutations Ile2182Phe and Gly2375Ala. Genet Test. 2003;7(3):203-11.

362. Roesl C, Sato K, Schiemann A, Pollock N, Stowell KM. Functional characterisation of the R2452W ryanodine receptor variant associated with malignant hyperthermia susceptibility. Cell Calcium. 2014;56(3):195-201.

363. Bialk P, Rivera-Torres N, Strouse B, Kmiec EB. Regulation of gene editing activity directed by single-stranded oligonucleotides and CRISPR/Cas9 systems. PloS One. 2015;10(6):e0129308.

364. Inui M, Miyado M, Igarashi M, Tamano M, Kubo A, Yamashita S, *et al.* Rapid generation of mouse models with defined point mutations by the CRISPR/Cas9 system. Scientific Reports. 2014;4:5396.

365. Paquet D, Kwart D, Chen A, Sproul A, Jacob S, Teo S, *et al.* Efficient introduction of specific homozygous and heterozygous mutations using CRISPR/Cas9. Nature. 2016;533:125.

366. Sanjana NE, Shalem O, Zhang F. Improved vectors and genome-wide libraries for CRISPR screening. Nat Methods. 2014;11(8):783-4.

367. Chakiath CS, Esposito D. Improved recombinational stability of lentiviral expression vectors using reduced-genome Escherichia coli. Biotechniques. 2007;43(4):466-70.

368. Sancak Y, Peterson TR, Shaul YD, Lindquist RA, Thoreen CC, Bar-Peled L, *et al.* The Rag GTPases bind raptor and mediate amino acid signaling to mTORC1. Science. 2008;320(5882):1496-501.

369. Lonza. Cell List - Integrated Solutions for Primary Cells and Transfection. BioResearch [Internet]. 2015.

370. Lonza. Fine Tuning Matrix. Available from: https://bioscience.lonza.com/lonza_bs/CH/en/download/content/asset/31152.

371. Stewart SA, Dykxhoorn DM, Palliser D, Mizuno H, Yu EY, An DS, *et al.* Lentivirus-delivered stable gene silencing by RNAi in primary cells. Rna. 2003;9(4):493-501.

372. Corsini J, Maxwell F, Maxwell IH. Storage of various cell lines at -70 degrees C or -80 degrees C in multi-well plates while attached to the substratum. Biotechniques. 2002;33(1):42, 4, 6.

373. Harrison MA, Rae IF. General techniques of cell culture. Cambridge: Cambridge University Press; 1997.

374. Miyaoka Y, Chan AH, Judge LM, Yoo J, Huang M, Nguyen TD, *et al.* Isolation of single-base genome-edited human iPS cells without antibiotic selection. Nat Methods. 2014;11(3):291-3.

375. Hindson BJ, Ness KD, Masquelier DA, Belgrader P, Heredia NJ, Makarewicz AJ, *et al.* High-throughput droplet digital PCR system for absolute quantitation of DNA copy number. Anal Chem. 2011;83(22):8604-10.

376. Lin S, Staahl BT, Alla RK, Doudna JA. Enhanced homology-directed human genome engineering by controlled timing of CRISPR/Cas9 delivery. Elife. 2014;3:e04766.

377. Doyon Y, Choi VM, Xia DF, Vo TD, Gregory PD, Holmes MC. Transient cold shock enhances zinc-finger nuclease–mediated gene disruption. Nat Methods. 2010;7:459.

378. Guo Q, Mintier G, Ma-Edmonds M, Storton D, Wang X, Xiao X, *et al.* 'Cold shock' increases the frequency of homology directed repair gene editing in induced pluripotent stem cells. Scientific Reports. 2018;8(1):2080.

379. Vanoye CG, Desai RR, Fabre KL, Gallagher SL, Potet F, DeKeyser J-M, *et al.* High-throughput functional evaluation of KCNQ1 decrypts variants of unknown significance. Circulation: Genomic and Precision Medicine. 2018;11(11):e002345.

380. Matsa E, Dixon JE, Medway C, Georgiou O, Patel MJ, Morgan K, *et al.* Allele-specific RNA interference rescues the long-QT syndrome phenotype in human-induced pluripotency stem cell cardiomyocytes. Eur Heart J. 2014;35(16):1078-87.

381. Christie KA, Courtney DG, DeDionisio LA, Shern CC, De Majumdar S, Mairs LC, *et al.* Towards personalised allele-specific CRISPR gene editing to treat autosomal dominant disorders. Scientific Reports. 2017;7(1):16174.

382. Pingjuan L, P. KB, Y. LM, S. PM, Daniel N-G, H. GS, *et al.* Allele-specific CRISPR-Cas9 genome editing of the single-base P23H mutation for rhodopsin-associated dominant retinitis rigmentosa. The CRISPR Journal. 2018;1(1):55-64.

383. Armstrong DL, Erxleben C, White JA. Patch clamp methods for studying calcium channels. Methods Cell Biol. 2010;99:183-97.

384. Ullrich ND, Fischer D, Kornblum C, Walter MC, Niggli E, Zorzato F, *et al.* Alterations of excitation-contraction coupling and excitation coupled Ca^{2+} entry in human myotubes carrying CAV3 mutations linked to rippling muscle. Human Mutation. 2011;32(3):309-17.

385. Calderón-Rivera A, Vega AV, Avila G. Creatine supplementation upregulates excitation-contraction coupling in C2C12 myotubes. Journal of Receptor, Ligand and Channel Research. 2010;3:63-71.

386. Maher J, Allen M. Planar lipid bilayers in recombinant ion channel research. Methods. 2018;147:206-12.

387. Juhas M, Engelmayr GC, Fontanella AN, Palmer GM, Bursac N. Biomimetic engineered muscle with capacity for vascular integration and functional maturation in vivo. Proceedings of the National Academy of Sciences. 2014;111(15):5508-13.

388. Agrawal G, Aung A, Varghese S. Skeletal muscle-on-a-chip: An in vitro model to evaluate tissue formation and injury. Lab on a chip. 2017;17(20):3447-61.

389. Rao L, Qian Y, Khodabukus A, Ribar T, Bursac N. Engineering human pluripotent stem cells into a functional skeletal muscle tissue. Nature Communications. 2018;9(1):126-.

390. Madden L, Juhas M, Kraus WE, Truskey GA, Bursac N. Bioengineered human myobundles mimic clinical responses of skeletal muscle to drugs. Elife. 2015;4:e04885-e.

391. Gholobova D, Gerard M, Decroix L, Desender L, Callewaert N, Annaert P, *et al.* Human tissue-engineered skeletal muscle: A novel 3D in vitro model for drug disposition and toxicity after intramuscular injection. Scientific Reports. 2018;8(1):12206.

6 Appendices

Appendix A Oligonucleotide sequences

Appendix A.1 Primer pairs used for polymerase chain reaction

Target	Primer	Sequence (5' – 3')	Annealing temperature
RyR1 p.Thr4826Ile HRM analysis	forward	ACTTCTTCTTTGCTGCC	65 °C
	reverse	GGTGACAGAGGACAGGAT	65 °C
FT-293 expression line transgene	forward	CGCAAATGGGCGGTAGGCGTG	60 °C
	reverse (pcFT)	TAGAAGGCACAGTCGAGG	60 °C
	reverse (*RYR1*)	ATAGAATGACACCTACTCAGA	60 °C
RyR1 p.Thr4826Ile RT1 overlap extension PCR	forward (A)	CCAAACAGAGCTGGCAC	65 °C
	reverse (A)	CAGAGGACAGGATGATGCGCAGCG TCTTG	65 °C
	forward (B)	CAAGACGCTGCGCATCATCCTGTCC TCTG	65 °C
	reverse (B)	GTTGAAGGCCACTACAGTATACAGG TAGACG	65 °C
	forward (C)	CGTCTACCTGTATACTGTAGTGGCC TTCAAC	68 °C
	reverse (C)	TGGGATTGCAGGCTGGA	68 °C
RyR1 p.Thr4826Ile RT2 overlap extension PCR	forward (A)	GCCCTTAGATTGCCAGATTAT	55 °C
	reverse (A)	CAGAGGACAGGATGATGCGCAG CGTCTTG	55 °C

(continued)

Target	Primer	Sequence (5' – 3')	Annealing temperature
RyR1 p.Thr4826Ile RT2 overlap extension PCR	forward (B)	CAAGACGCTGCGCATCATCCTGTCC TCTG	72 °C
	reverse (B)	GACGACCACCGCCAGCAATCCCACG GTCATCACC	72 °C
	forward (C)	GGTGATGACCGTGGGATTGCTGGCG GTGGTCGTC	60 °C
	reverse (C)	TATTAACTCCTTCAACAGATGCGA	60 °C
RyR1 p.Thr4826Ile RT3 overlap extension PCR	forward (A)	CCCTACCCTCCAGAGTG	65 °C
	reverse (A)	CAGAGGACAGGATGATGCGCAGCG TCTTG	65 °C
	forward (B)	CAAGACGCTGCGCATCATCCTGTCC TCTG	68 °C
	reverse (B)	CATGCTGGGTCCTGGTACAAGTTCA GTCCCTGTGG	68 °C
	forward (C)	CCACAGGGACTGAACTTGTACCAGG ACCCAGCATG	65 °C
	reverse (C)	TAGAACTTGCGGAAGAAGTTGAA	65 °C
RYR1 exon 27 deletion	forward	CTACCTCCTCCCCTCGGCT	66 °C
	reverse	GGAAGGAAGGAGCTTTGGAG	66 °C
Tet repressor gene	forward	ACAACCCGTAAACTCGCC	56 °C
	reverse	TTCCAATACGCAACCTAAAG	56 °C
T7 endonuclease 1 assay	forward	TGACCTGGCCCCATCCT	60 °C
	reverse	CTCATCCTCGCTCTTGTTG	60 °C

Appendix A.2 Primers used for Sanger sequencing

Target	Direction	Sequence (5' – 3')
pcDNA™5/FRT/TO insert	forward	CGCAAATGGGCGGTAGGCGTG
	reverse	TAGAAGGCACAGTCGAGG
ftRYR1 AvrII ligation site	reverse	CTAGAGAATAGGAACTTCGGAA
RYR1 c.14477C>T (RyR1 p.Thr4826Ile) cDNA	forward	GAACCCGCCCTGCGGTGTCTG
RYR1 c.38T>G (RyR1 p.Leu13Arg) cDNA	reverse	GGATGACTCCACGCCAGCCTC
RYR1 c.1390C>A (RyR1 p.Gln464Lys) cDNA	reverse	TGCTTGTCCAGGAGGGAAGATG
RYR1 c.1615T>C (RyR1 p.Phe539Leu) cDNA	forward	CTCTCCATGGTCCTGAATTGCATAGAC
RYR1 c.5119C>T (RyR1 p.Arg1707Cys) cDNA	reverse	TCACATCCTCATCGCCAAAGA
RYR1 c.8378C>T (RyR1 p.Pro2793Leu) cDNA	forward	AAATACGACCCGGAGCTGTA

Appendix A.3 Oligonucleotide pair used in pcFT creation

Target	Direction	Sequence (5' – 3')
pcDNA™5/FRT/TO multiple cloning site	forward	AGCTTATAGCTAGCTTAGGTACCA AGGGCGCGCCTATCCTAGGAATG
	reverse	GATCCATTCCTAGGATAGGCGCGC CCTTGGTACCTAAGCTAGCTATA

Appendix A.4 Oligonucleotide pairs for guide RNA creation

Target	Direction	Sequence (5' – 3')
Guide sequence 1	forward	CACCGGGTCGTCTACCTGTACACCG
	reverse	AAACCGGTGTACAGGTAGACGACCC
Guide sequence 2	forward	CACCGTCTGGCGGTGGTCGTCTACC
	reverse	AAACGGTAGACGACCACCGCCAGAC
Guide sequence 3	forward	CACCGGAGCCACAGGGACTGAACCG
	reverse	AAACCGGTTCAGTCCCTGTGGCTCC

Appendix B Vector maps

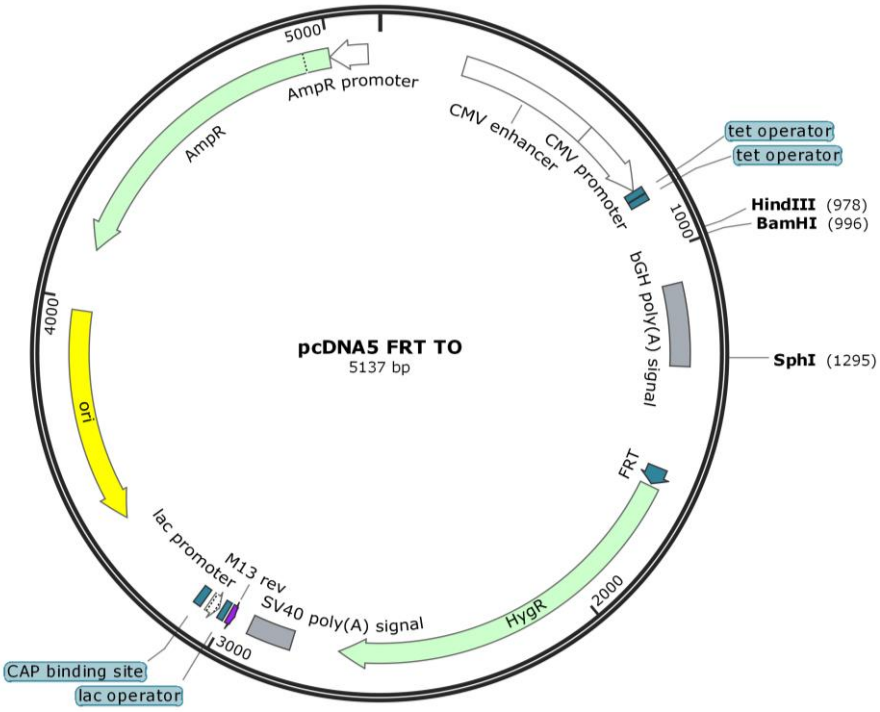

Appendix B.1 Vector map of pcDNA™5/FRT/TO

Detailed vector map of pcDNA™5/FRT/TO used in cloning for creation of the ftRYR1 expression vector. Locations of restriction sites are shown. Flippase recombination target (FRT) site is shown as a blue arrow and two tetracycline (tet) operator sites are shown as blue blocks. Ampicillin (AmpR) and hygromycin (HygR) resistance genes (green); origin of replication (ori; yellow); and associated gene expression components (white, grey, and blue) are shown. *Created with SnapGene software (GSL Biotech).*

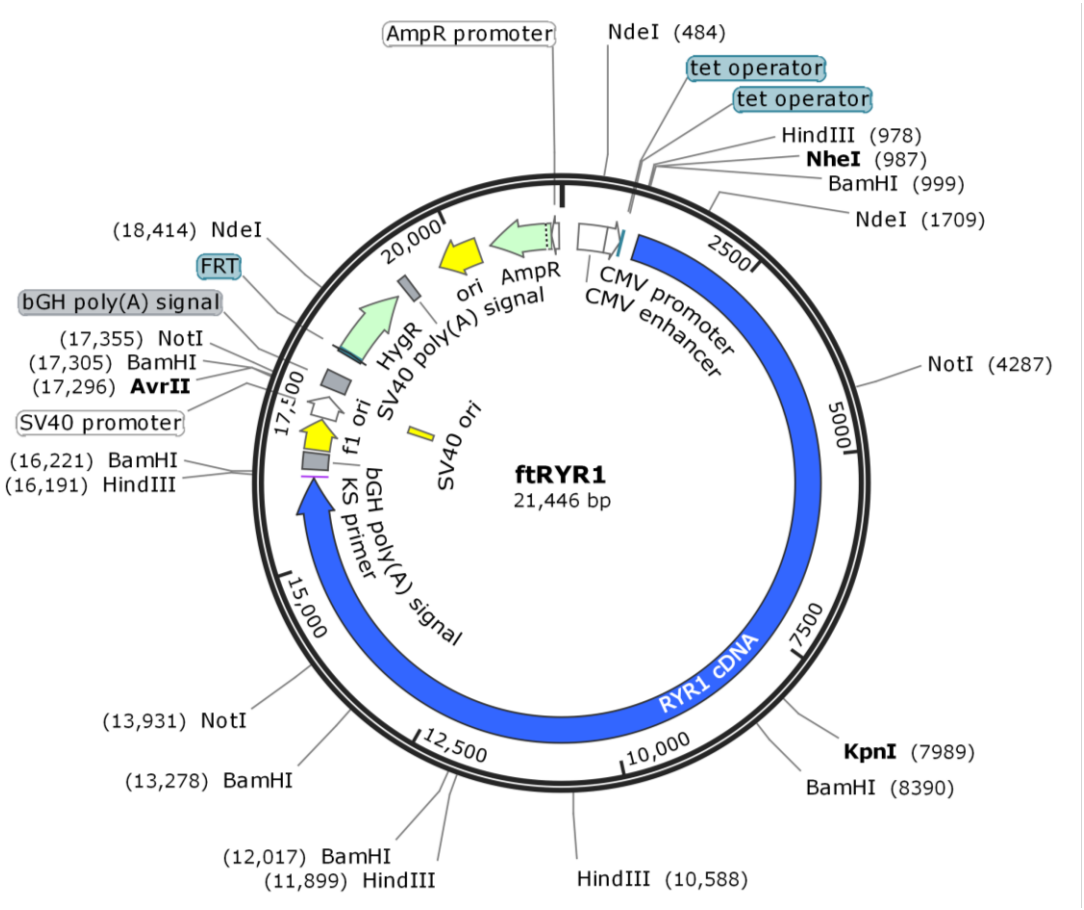

Appendix B.2 Vector map of ftRYR1

Detailed vector map of ftRYR1 used for creation of stable expression cell lines. Ryanodine receptor 1 complementary DNA (*RYR1* cDNA) is indicated by a blue arrow. Locations of restriction sites are shown. Locations of flippase recombination target (FRT) site and two tetracycline (tet) operator sites are shown. Ampicillin (AmpR) and hygromycin (HygR) resistance genes (green); origin of replication (ori; yellow); and associated gene expression components (white, grey, and blue) are shown. *Created with SnapGene software (GSL Biotech).*

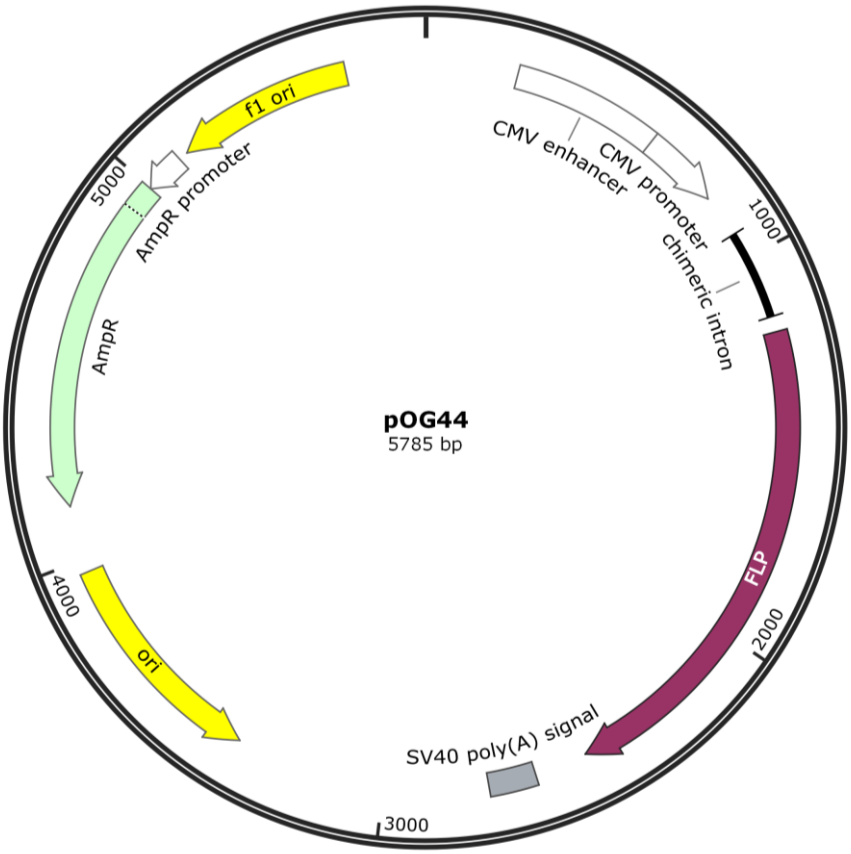

Appendix B.3 Vector map of pOG44

Detailed vector map of pOG44 used for creation of stable expression cell lines. Flippase enzyme gene (FLP) is shown as a purple arrow. Ampicillin resistance gene (AmpR; green); origins of replication (ori; yellow); and associated gene expression components (white and grey) are shown. *Created with SnapGene software (GSL Biotech).*

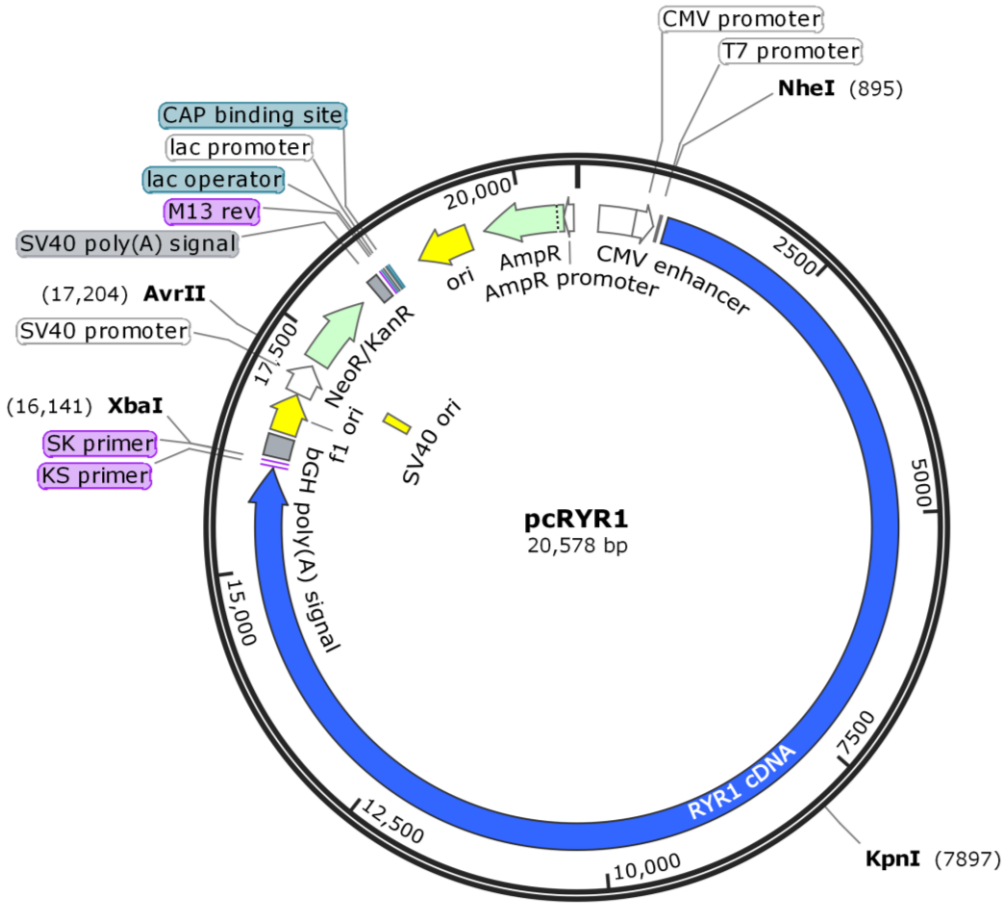

Appendix B.4 Vector map of pcRYR1

Detailed vector map of pcRYR1 used in cloning for creation of the ftRYR1 expression vector. Ryanodine receptor 1 complementary DNA (*RYR1* cDNA) is indicated by a blue arrow. Locations of restriction sites are shown. Ampicillin (AmpR) and neomycin/kanamycin (NeoR/KanR) resistance genes (green); origins of replication (ori; yellow); and associated gene expression components (white, grey, purple, and blue) are shown. *Created with SnapGene software (GSL Biotech).*

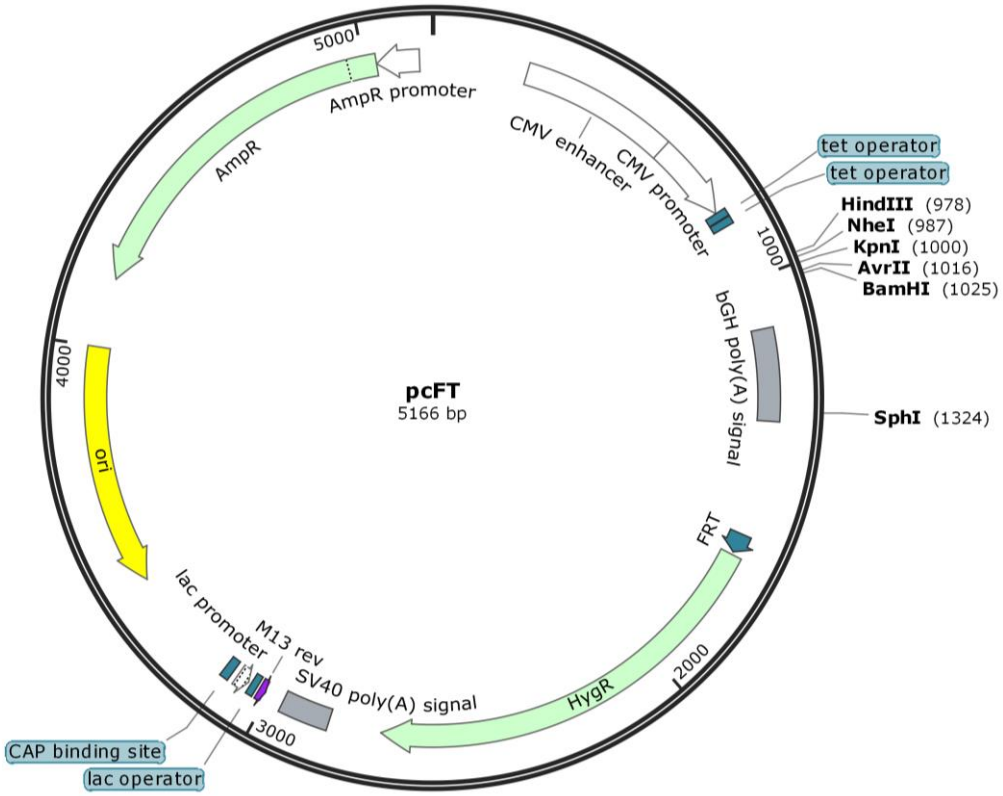

Appendix B.5 Vector map of pcFT

Detailed vector map of pcFT for creation of pcFT stable expression cell line. Locations of restriction sites are shown. Locations of restriction endonuclease recognition sites are shown. Locations of flippase recombination target (FRT) site and two tetracycline (tet) operator sites are shown. Ampicillin (AmpR) and hygromycin (HygR) resistance genes (green); origin of replication (ori; yellow); and associated gene expression components (white, grey, purple, and blue) are shown. *Created with SnapGene software (GSL Biotech).*

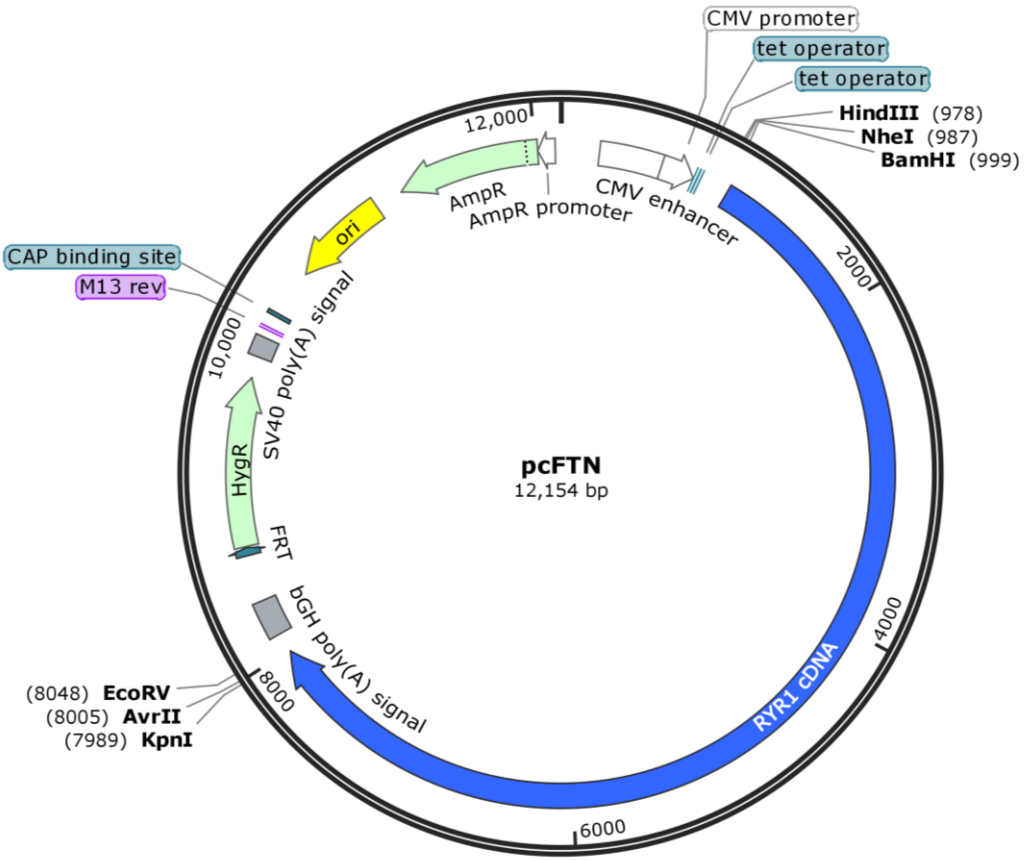

Appendix B.6 Vector map of pcFTN

Detailed vector map of pcFTN used in cloning for creation of the ftRYR1 expression vector. Portion of ryanodine receptor 1 complementary DNA (*RYR1* cDNA) is indicated by a blue arrow. Locations of restriction sites are shown. Locations of flippase recombination target (FRT) site and two tetracycline (tet) operator sites are shown. Ampicillin (AmpR) and hygromycin (HygR) resistance genes (green); origin of replication (ori; yellow); and associated gene expression components (white, grey, purple, and blue) are shown. *Created with SnapGene software (GSL Biotech).*

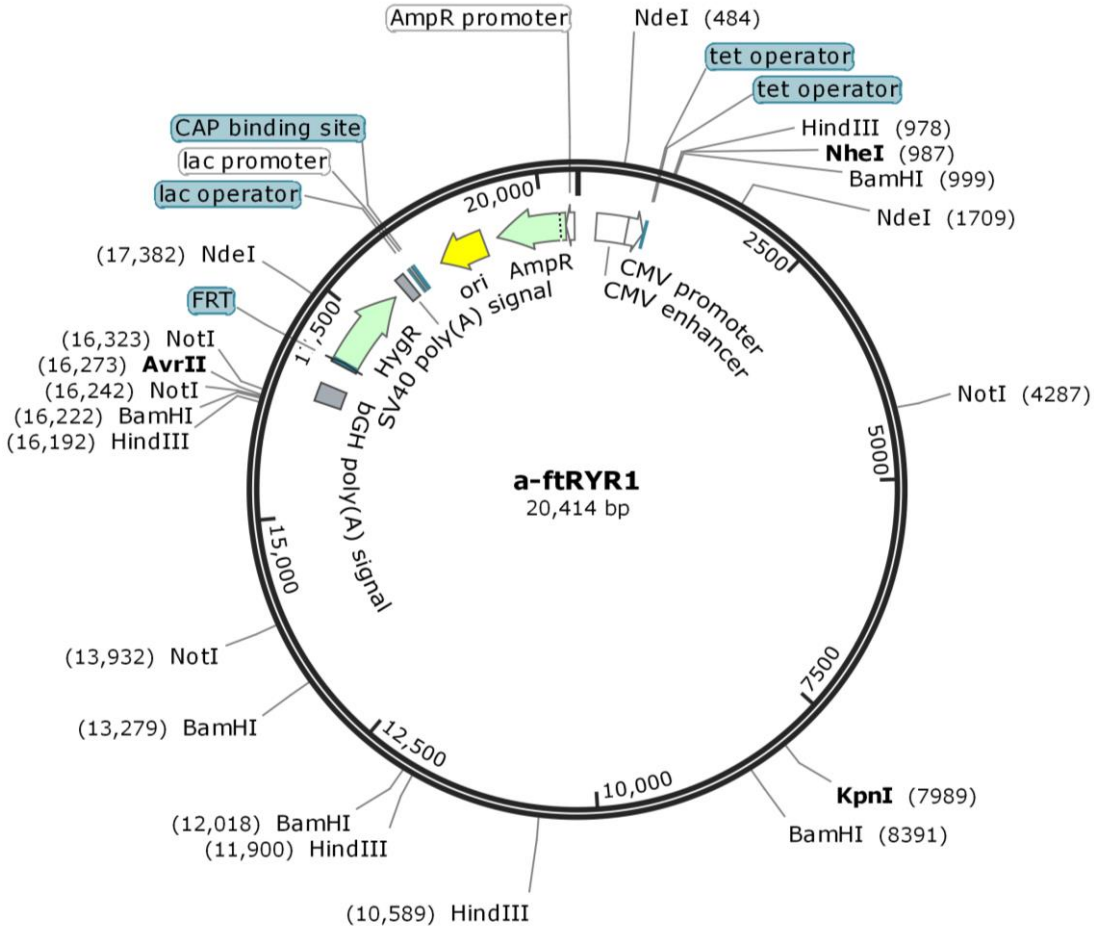

Appendix B.7 Vector map of a-ftRYR1

Detailed vector map of a-ftRYR1 used for creation of a stable expression cell line. Ryanodine receptor 1 complementary DNA (*RYR1* cDNA) is indicated by a blue arrow. Locations of restriction sites are shown. Locations of flippase recombination target (FRT) site and two tetracycline (tet) operator sites are shown. Ampicillin (AmpR) and hygromycin (HygR) resistance genes (green); origin of replication (ori; yellow); and associated gene expression components (white, grey, and blue) are shown. *Created with SnapGene software (GSL Biotech).*

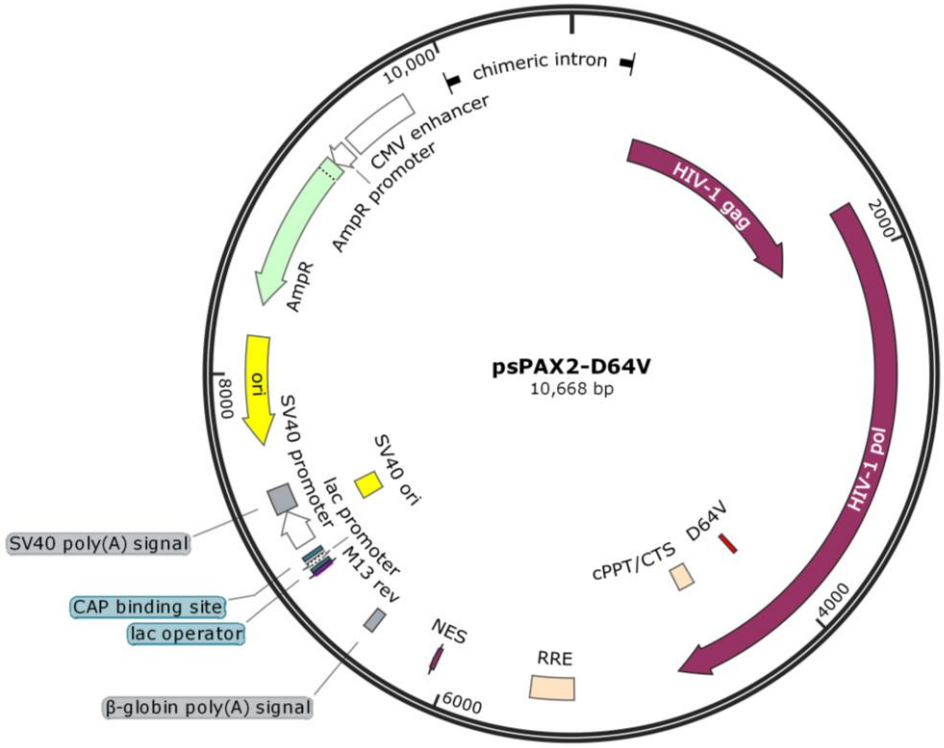

Appendix B.8 Vector map of psPAX2-D64V

Detailed vector map of psPAX2-D64V (Addgene) which was used in the production of lentivirus. Lentiviral genes are shown as purple arrows. Ampicillin resistance gene (AmpR; green); origins of replication (ori; yellow); and associated gene expression components (white, grey, and blue) are shown. *Created with SnapGene software (GSL Biotech).*

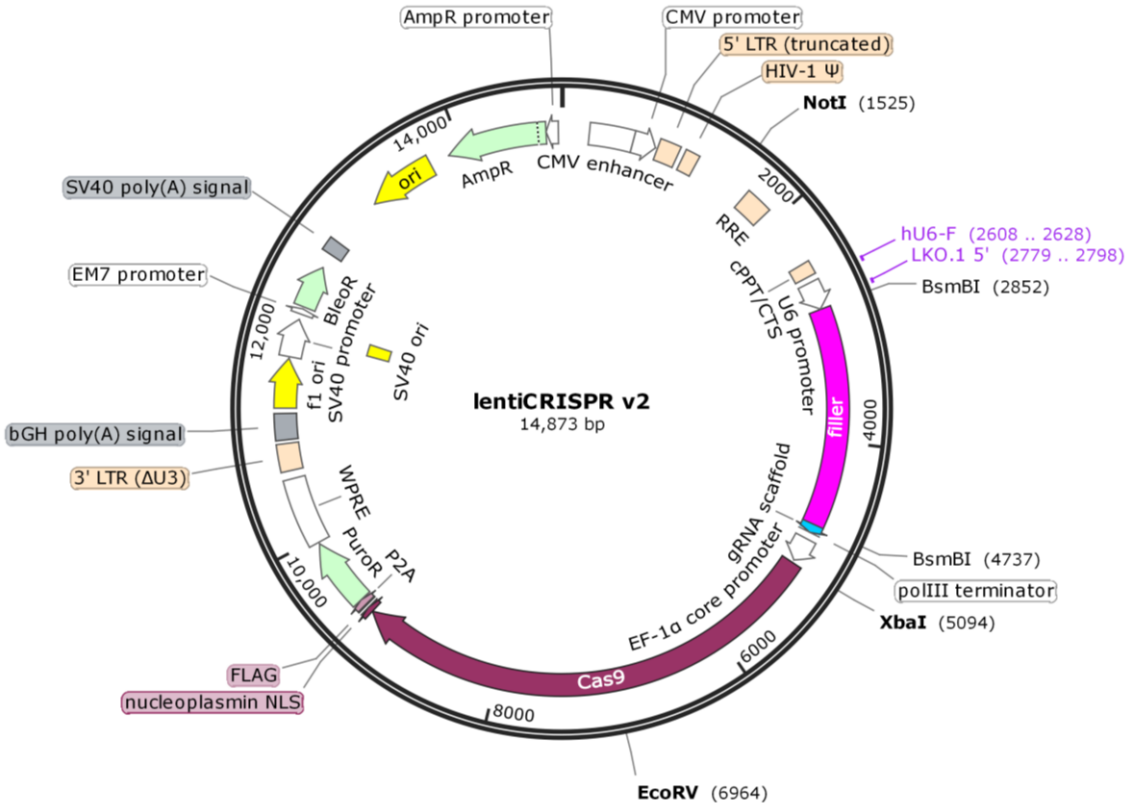

Appendix B.9 Vector map of lentiCRISPR v2

Detailed vector map of lentiCRISPR v2 (Addgene) which was used for cloning of LentiGuides. The 2 kilobase DNA filler (pink) and the guide RNA (gRNA) scaffold (blue) are shown flanked by BsmBI restriction sites. Cas9 coding sequence is shown as a purple arrow and lentiviral components are shown in orange. Ampicillin (AmpR), bleomycin (BleoR), and puromycin (PuroR) resistance genes (green); origins of replication (ori; yellow); and associated gene expression components (white, grey, and blue) are shown. *Created with SnapGene software (GSL Biotech).*

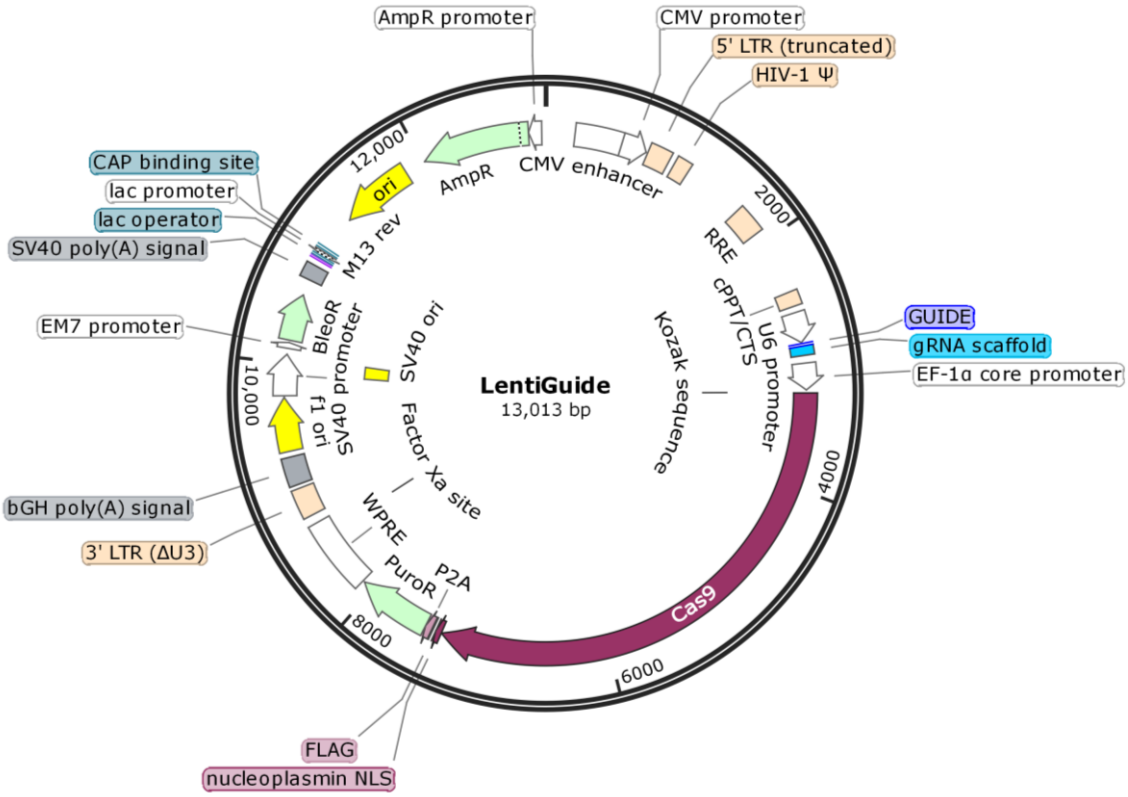

Appendix B.10 Vector map of LentiGuide

Detailed vector map of a representative LentiGuide plasmid which was used in gene editing. The guide sequence (dark blue) and the guide RNA (gRNA) scaffold (light blue) are shown. Cas9 coding sequence is shown as a purple arrow and lentiviral components are shown in orange. Ampicillin (AmpR), bleomycin (BleoR), and puromycin (PuroR) resistance genes (green); origins of replication (ori; yellow); and associated gene expression components (white, grey, and blue) are shown. *Created with SnapGene software (GSL Biotech).*

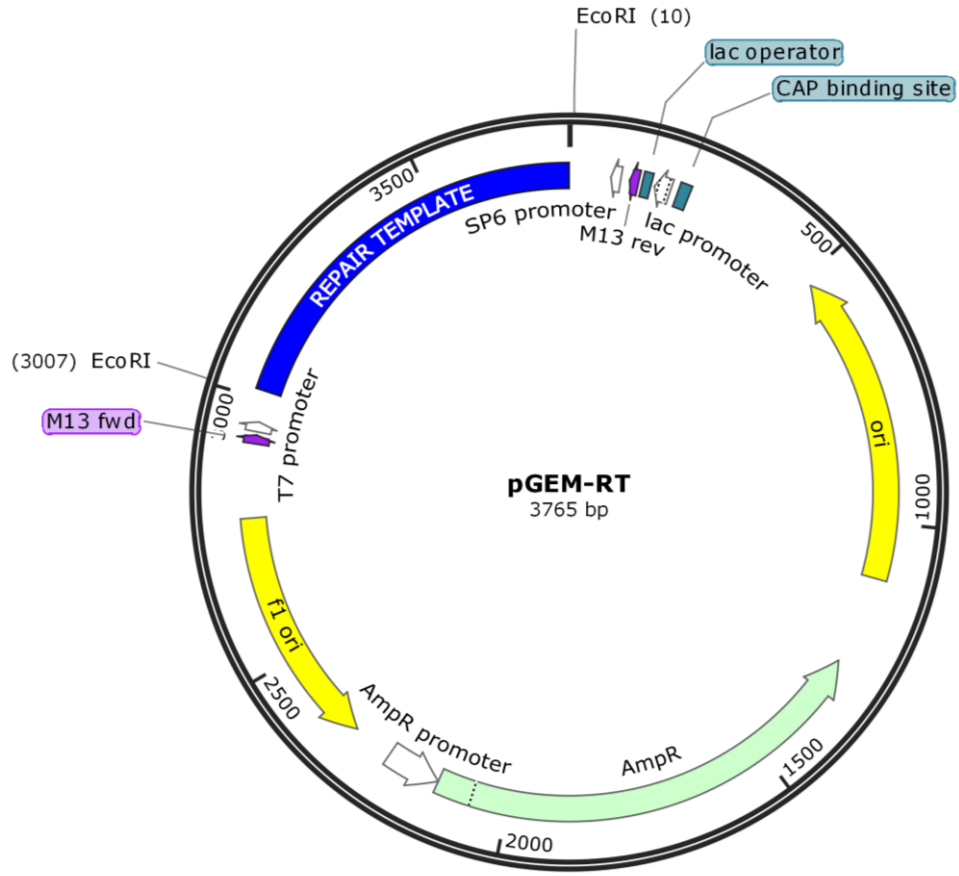

Appendix B.11 Vector map of pGEM-RT

Detailed vector map of a representative pGEM-RT (pGEM-RT1) plasmid which was used in gene editing. The repair template sequence is shown in dark blue. Ampicillin resistance gene (AmpR; green); origins of replication (ori; yellow); and associated gene expression components (white, grey, purple, and blue) are shown. *Created with SnapGene software (GSL Biotech).*

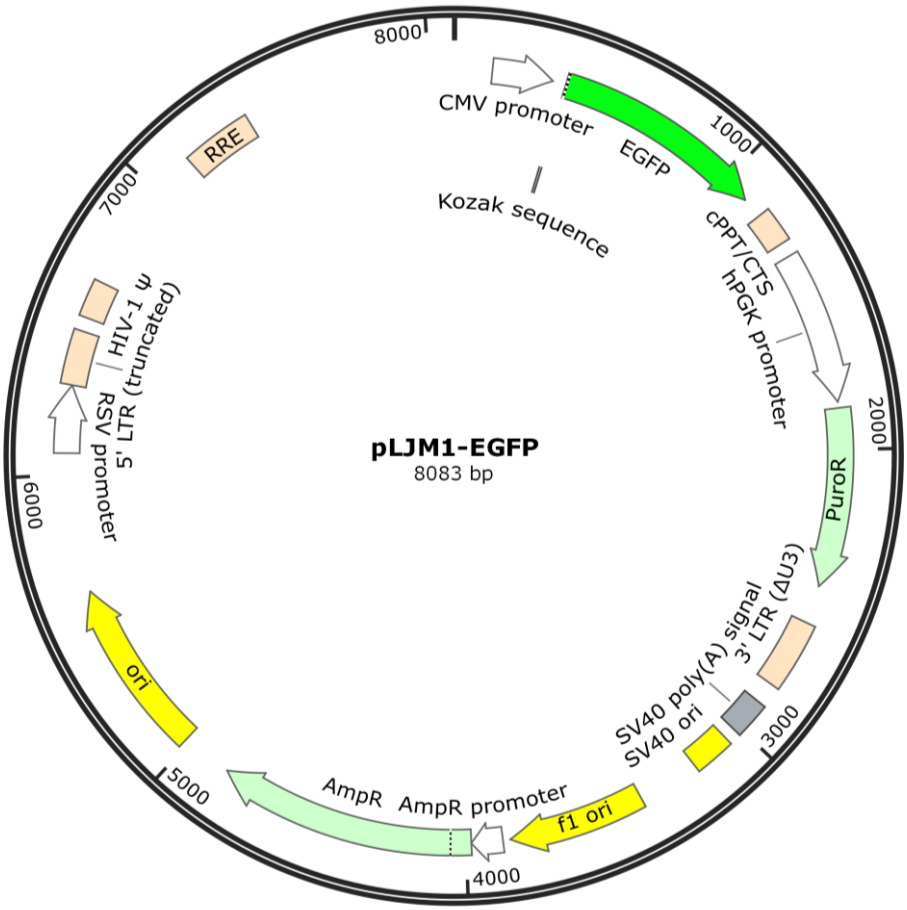

Appendix B.12 Vector map of pLJM1-EGFP

Detailed vector map of pLJM1-EGFP (Addgene) which was used for production of lentivirus and cloning Lenti-RT plasmids. The green fluorescent protein (eGFP) gene is shown in bright green and lentiviral components are shown in orange. Ampicillin (AmpR) and puromycin (PuroR) resistance genes (pale green); origins of replication (ori; yellow); and associated gene expression components (white and grey) are shown. *Created with SnapGene software (GSL Biotech).*

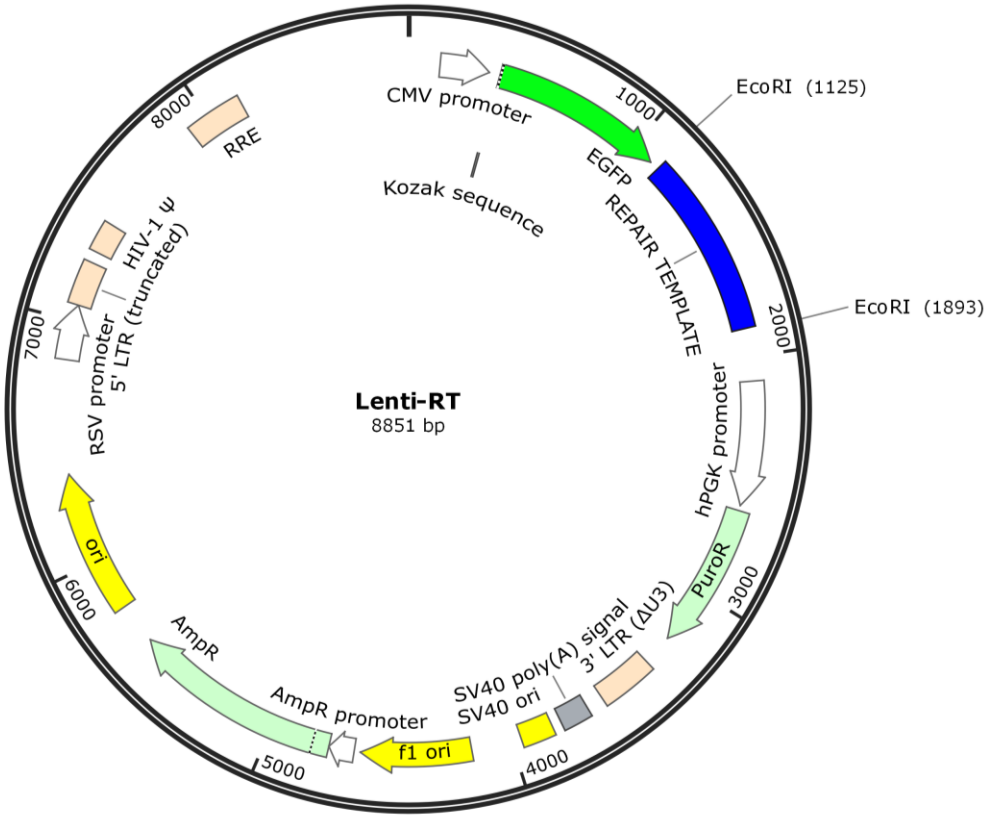

Appendix B.13 Vector map of Lenti-RT

Detailed vector map of a representative Lenti-RT plasmid used in gene editing. The repair template sequence (blue), green fluorescent protein (eGFP) gene (bright green), and lentiviral components (orange) are shown. Ampicillin (AmpR) and puromycin (PuroR) resistance genes (green); origins of replication (ori; yellow); and associated gene expression components (white and grey) are shown. *Created with SnapGene software (GSL Biotech).*

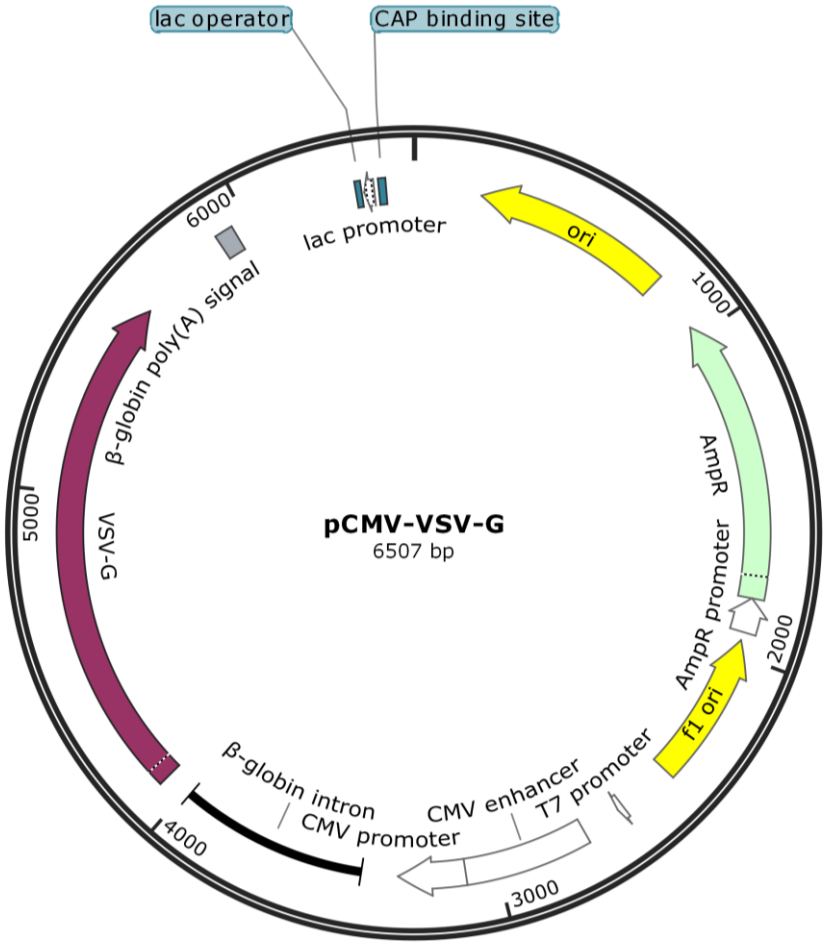

Appendix B.14 Vector map of pCMV-VSV-G

Detailed vector map of pCMV-VSV-G (Addgene) which was used for production of lentivirus. The lentiviral gene is shown in purple. Ampicillin resistance gene (AmpR; green); origins of replication (ori; yellow); and associated gene expression components (white, grey, and blue) are shown. *Created with SnapGene software (GSL Biotech).*

Appendix C DNA electrophoresis

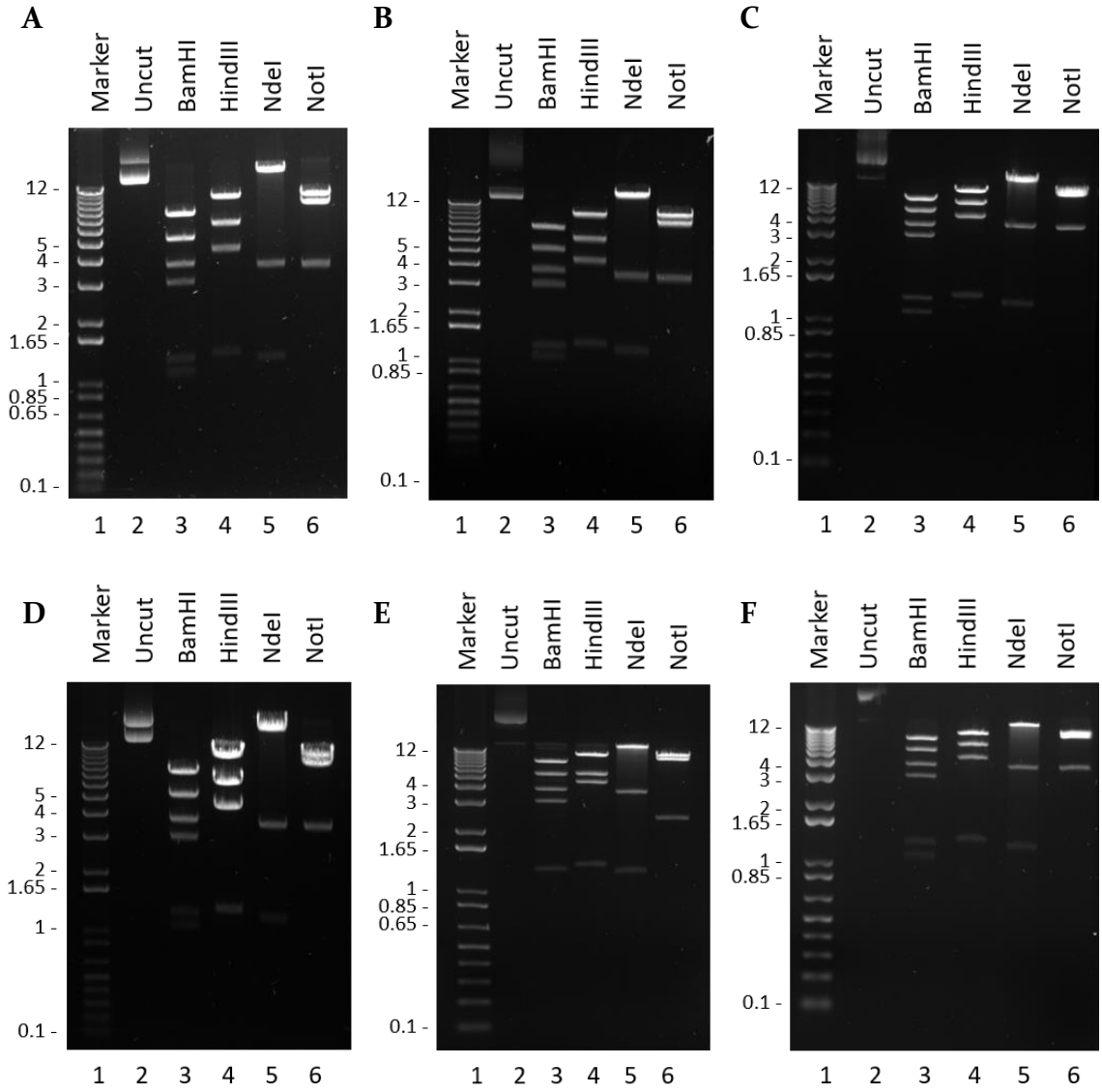

Appendix C.1 Restriction digestion of full-length *RYR1* variants

Restriction endonuclease digestion of the full-length Flp-In™ T-REx™ 293 expression vectors with BamHI, HindIII, NdeI, and NotI enzymes (Section 2.2.4) separated by gel electrophoresis in 0.8% agarose gels containing ethidium bromide (Section 2.2.3) alongside a representative uncut control in lane 2. Lane 1 contains 1 Kb Plus DNA Ladder with the length of each fragment indicated in kb. **A** *RYR1* c.14477C>T (RyR1 p.Thr4826Ile) ftRYR1. **B** *RYR1* c.38T>G (RyR1 p.Leu13Arg) ftRYR1. **C** *RYR1* c.1390C>A (RyR1 p.Gln464Lys) ftRYR1. **D** *RYR1* c.1615T>C (RyR1 p.Phe539Leu) ftRYR1. **E** *RYR1* c.5119C>T (RyR1 p.Arg1707Cys) ftRYR1. **F** *RYR1* c.8378C>T (RyR1 p.Pro2793Leu) a-ftRYR1.

Appendix C.2 Expected results of restriction digestion of expression vectors

Restriction endonuclease	ftRYR1 fragment lengths (kb)†	a-ftRYR1 fragment lengths (kb)†
BamHI	1.1, 1.3, 2.9, 3.6, 5.1, 7.4	1.3, 2.9, 3.6, 5.2, 7.4
HindIII	1.3, 4.3, 6.2, 9.6	1.3, 4.3, 5.2, 9.6
NdeI	1.2, 3.5, 16.7	1.2, 3.5, 15.7
NotI	3.4, 8.4, 9.6	0.1, 2.3, 9.6, 8.4

† Rounded to the nearest 100 base pairs.

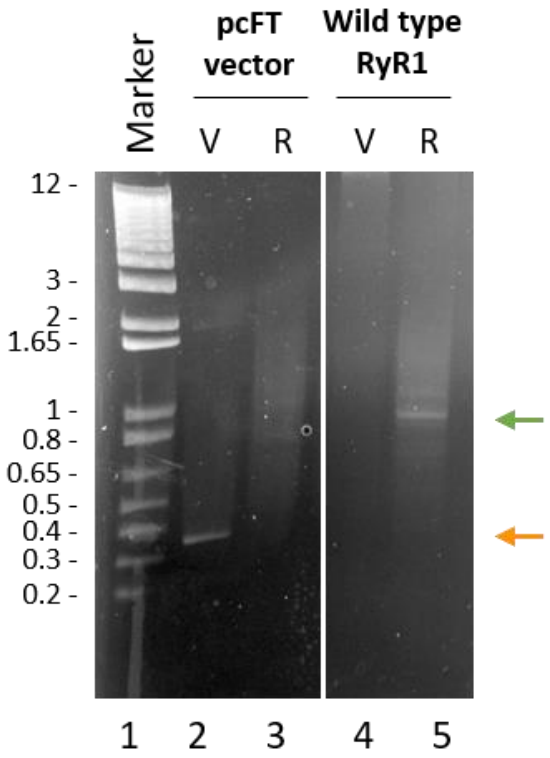

Appendix C.3 Preliminary confirmation of transgene integration

Transgene integration was confirmed by PCR amplification (Section 2.2.6) of the genomic DNA from the pcFT vector and wild-type (WT) ryanodine receptor 1 (RyR1) stable expression lines and visualised by gel electrophoresis in a 2% agarose gel containing ethidium bromide (Section 2.2.3). Migration of the 365 bp PCR product amplified from the vector is indicated with an orange arrow and migration of the 792 bp PCR product amplified from the *RYR1* complementary DNA (cDNA) is indicated with a green arrow. Lanes 2 and 4 are labelled with 'V' to indicate that the vector reverse primer was used PCR and lanes 3 and 5 are labelled with 'R' to indicate that the *RYR1* cDNA reverse primer was used. Lane 1 contains 1 Kb Plus DNA Ladder as a size control with the length of each fragment indicated in kb.

Appendix D Example of raw calcium release data

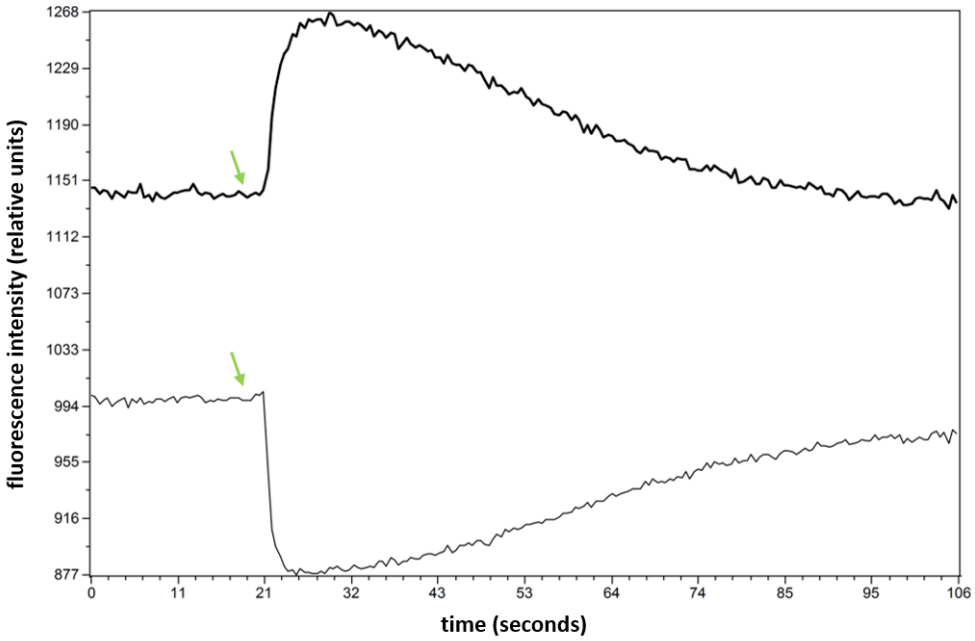

Appendix D.1 Raw calcium release data after agonist addition

Increase in cytoplasmic [Ca^{2+}] in the wild-type ftRYR1 stable expression line after addition of 1000 µM 4-chloro-*m*-cresol (green arrows) measured in relative fluorescence units. The trace in bold represents the increase in Ca^{2+}-bound Fura-2 by fluorescence emission at 510 nm after excitation at 340 nm. The thin trace represents the decrease in unbound Fura-2 by fluorescence emission at 510 nm after excitation at 380 nm.

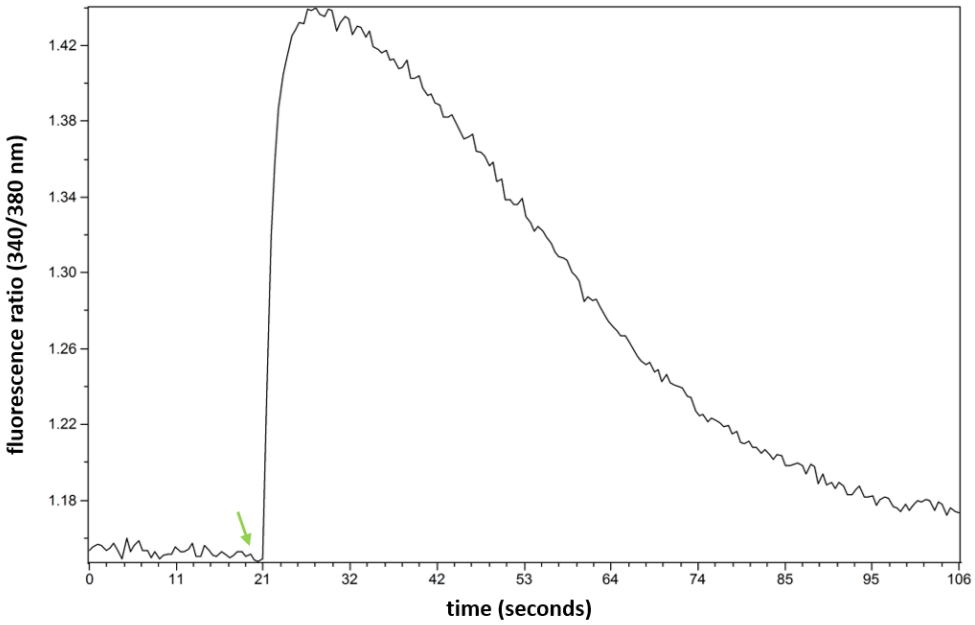

Appendix D.2 Calcium release from stores after agonist addition

Increase in cytoplasmic [Ca^{2+}] in the wild-type ftRYR1 stable expression line after addition of 1000 µM 4-chloro-*m*-cresol (green arrow). Represents the increase in Ca^{2+}-bound Fura-2 in the cytoplasm paired with a decrease in unbound Fura-2. Measured as a ratio of fluorescence emission at 510 nm after excitation at 340 nm over 380 nm.

Appendix E Alignments of Sanger sequencing

```
Genome assembly                                                 TCCTCGTGT GTCCCTGCCT 146250
HMCL-7304                                                       ......... .......... 19
Genome assembly TCCCCCTGAC CCCTGGCCCT GTGTGCCCAC AGTCCTTCCT GTACCTGGGC 146300
HMCL-7304       .......... .......... .......... .......... .......... 69
Genome assembly TGGTATATGG TGATGTCCCT CTTGGGACAC TACAACAACT TCTTCTTTGC 146350
HMCL-7304       .......... .......... .......... .......... .......... 119
Genome assembly TGCCCATCTC CTGGACATCG CCATGGGGGT CAAGACGCTG CGCACCATCC 146400
HMCL-7304       .......... .......... .......... .......... .......... 169
Genome assembly TGTCCTCTGT CACCCACAAT GGGAAACAGG TGTGGGGAGG ACCTGGCTGT 146450
HMCL-7304       .......... .......... .......... .......... .......... 219
Genome assembly GGGGCGTGGG CCAGCAGGGA CCAGCGTGGC AGTGGGTGGT GAAGGGATAA 146500
HMCL-7304       .......... .......... .......... .......... .......... 269
Genome assembly GGGCCGGGCA GCTGGGCTGA GGAGGGGCAA GGCCAGGTGC GCTGAGCCGG 146550
HMCL-7304       .......... .......... .......... .......... .......... 319
Genome assembly GGGTGTGTGG GGCAGCAAGG TAGAGCCACA GGGACTGAAC CGGGGCCAGG 146600
HMCL-7304       .......... .......... .......... .......... .......... 369
Genome assembly ACCCAGCATG GGCAGGGTGG GGGGAGGGCA AGCCCAGGGC GGAGCTGACC 146650
HMCL-7304       .......... .......... .......... .......... .......... 419
Genome assembly TGGCCCCATC CTGCCCCCAG CTGGTGATGA CCGTGGGCCT TCTGGCGGTG 146700
HMCL-7304       .......... .......... .......... .......... .......... 469
Genome assembly GTCGTCTACC TGTACACCGT GGTGGCCTTC AACTTCTTCC GCAAGTTCTA 146750
HMCL-7304       .......... .......... .......... .......... .......... 519
Genome assembly CAACAAGAGC GAGGATGAGG ATGAACCTGA CATGAAGTGT GATGACATGA 146800
HMCL-7304       .......... .......... .......... .......... .......... 569
Genome assembly TGACGGTGAG CCCCTCCCCT AGCACTCTGG GACCCTTCCT TCTCGCATCT 146850
HMCL-7304       .......... .......... .......... .......... .......... 619
Genome assembly GTTGAAGGAG TTAATAATGG TACCTCCAGG CCGGGCGTGG TGCCTCCAGC 146900
HMCL-7304       .......... .......... .......... .......... .......... 669
Genome assembly CTGCAATCCC AGTGCGTCGG GAGGCCGAGG CGGGACGATT ACTTGAGTCC 146950
HMCL-7304       .......... .......... .......... .......... .......... 719
Genome assembly AGGAGTTGGA AACCAGCCTG GGCAACAAAG CAAAAATCCT GTCTCTATAA 147000
HMCL-7304       .......... .......... .......... .......... .......... 769
Genome assembly AAAAAAATTT A                                           147050
HMCL-7304       .......... .                                           780
```

Appendix E.1 Sequence alignment of HMCL-7304 genome

Alignment of HMCL-7304 genome sequence and the hg38 human genome assembly in genomic region surrounding the *RYR1* c.14477C>T (RyR1 p.Thr4826Ile) mutation. Nucleotide number at end of each line. Consensus sequence shown as dots.

Appendix E.2 Sequence alignment of repair template 1

Alignment of the hg38 human genome assembly and repair template 1. The *RYR1* c.14477C>T (RyR1 p.Thr4826Ile) mutation is shown and the three clustered changes to guide sequence 1. Nucleotide number at end of each line. Consensus sequence shown as dots and changed residues shown in red.

Appendix E.3 Sequence alignment of repair template 2

Alignment of the hg38 human genome assembly and repair template 2. The *RYR1* c.14477C>T (RyR1 p.Thr4826Ile) mutation is shown and the three clustered changes to guide sequence 2. Nucleotide number at end of each line. Consensus sequence shown as dots and changed residues shown in red.

Appendix E.4 Sequence alignment of repair template 3

Alignment of the hg38 human genome assembly and repair template 3. The *RYR1* c.14477C>T (RyR1 p.Thr4826Ile) mutation is shown and the four clustered changes to guide sequence 3. Nucleotide number at end of each line. Consensus sequence shown as dots and changed residues shown in red.

Appendix F Titration of viral stocks for gene editing

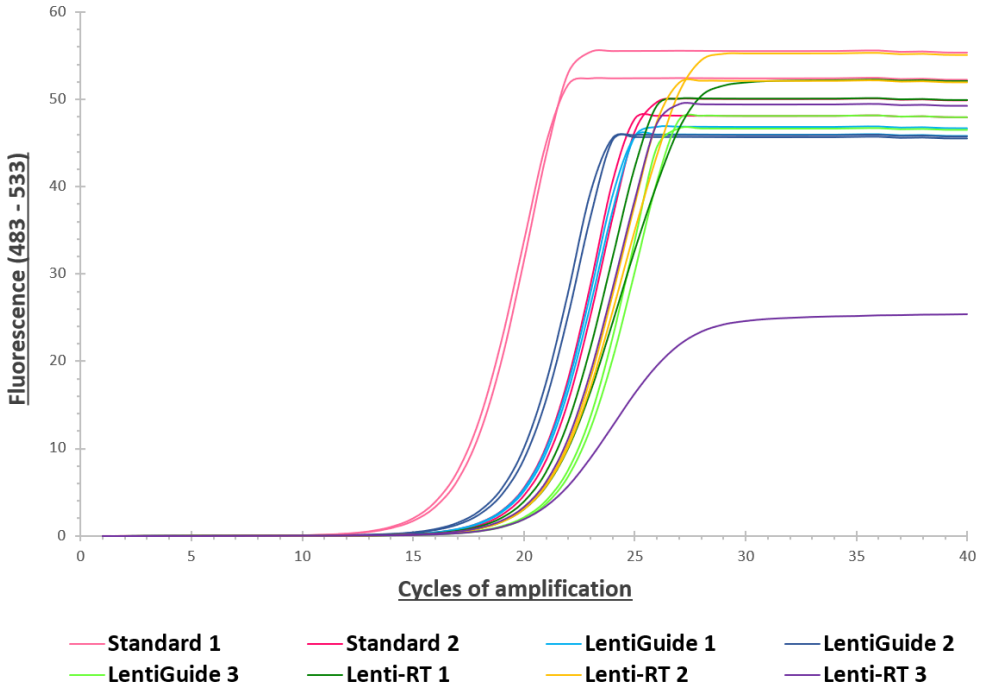

Appendix F.1 Kinetics of amplification for viral titration

The preparations of lentiviral stocks were analysed in duplicate by titration with reverse transcription quantitative PCR and compared with two internal RNA standards provided with the titration kit (Section 2.3.6). Numbers of viral genomes were measured as the increase in double-stranded DNA bound to the fluorescent dye over successive cycles of amplification by the increase in fluorescence between 483 – 533 nm wavelengths.

Appendix F.2 Concentrations of prepared viral samples

Sample	Viral titre (viral particles per millilitre)
LentiGuide 1	6.79×10^7
LentiGuide 2	1.26×10^8
LentiGuide 3	2.47×10^7
Lenti-RT 1	3.61×10^7
Lenti-RT 2	3.06×10^7
Lenti-RT 3	3.77×10^7